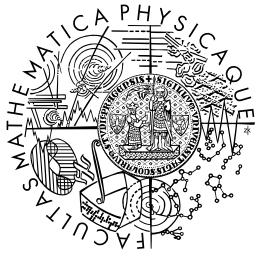

FACULTY
OF MATHEMATICS
AND PHYSICS
Charles University

DOCTORAL THESIS

Adam Janečka

Implicitly constituted fluids and their flows in complicated geometries

Mathematical Institute of Charles University

Supervisor of the doctoral thesis:	Mgr. Vít Průša, Ph.D.
Study programme:	Physics
Study branch:	Mathematical and Computer Modelling

Prague 2018

I declare that I carried out this doctoral thesis independently, and only with the cited sources, literature and other professional sources.

I understand that my work relates to the rights and obligations under the Act No. 121/2000 Sb., the Copyright Act, as amended, in particular the fact that the Charles University has the right to conclude a license agreement on the use of this work as a school work pursuant to Section 60 subsection 1 of the Copyright Act.

In Prague on May 30, 2018 Adam Janečka

Title: Implicitly constituted fluids and their flows in complicated geometries

Author: Adam Janečka

Institute: Mathematical Institute of Charles University

Supervisor: Mgr. Vít Průša, Ph.D., Mathematical Institute of Charles University

Abstract: We study behavior of incompressible non-Newtonian fluids with a relation between the shear stress and the shear rate given by a non-monotone S-shaped curve. These fluids are described with a special class of implicit constitutive relations that may be derived in a thermodynamically consistent manner using the entropy production maximization principle or gradient dynamics. In the latter approach, the constitutive relation is given as the derivative of a non-convex dissipation potential. The concept of dissipation potential allows us to discuss stability of the constitutive relation and explain the experimentally observed response discontinuities. We are also concerned with hydrodynamic stability of flows of implicitly constituted fluids. Finally, we propose a numerical scheme for simulation of transient flows of fluids with a specific non-monotone constitutive relation. We employ the numerical scheme in a simulation of two-dimensional Taylor–Couette flow and the numerical results confirm our theoretical observations concerning the admissible flow states.

Keywords: implicit constitutive relations, non-equilibrium thermodynamics, hydrodynamic stability, finite element method

Firstly, I would like to sincerely thank my supervisor, Dr. Vít Průša, for his patient guidance, motivation and advice he has always been willing to provide. Further, I am very grateful to Prof. Josef Málek for his continuous support and I also want to thank Dr. Michal Pavelka for being a great co-author.

Moreover, I would like to express many thanks to Prof. Kumbakonam R. Rajagopal for the unique chance to work with him and for many fruitful discussions we had together. Without a doubt, this would not have been possible without the support of the Fulbright Fellowship Program and I feel most honored to be given such an exceptional opportunity.

Furthermore, both my studies and the work on this thesis were supported by the ERC-CZ project LL1202 "MOdelling REvisited + MOdel REduction (MORE)" and by the University Centre of Excellence "Mathematical Modelling, Analysis and Computation (MathMAC)". I would also like to thank all other colleagues for always being very helpful. Particularly, I would like to recognize the help of Martin Řehoř, Jan Blechta, Dr. Ondřej Souček and Dr. Jaroslav Hron.

I also truly appreciate the unconditional support and understanding of my loved ones.

Contents

1. Introduction

The thesis is concerned with behavior of a special class of incompressible non-Newtonian fluids. We provide insight into mathematical and physical description of these fluids. With the proposed models we can then explain particular experimentally observed phenomena and investigate crucial question of the hydrodynamic stability. Furthermore, the proposed models are subsequently used in numerical simulations. The work is organized as follows.

First, in Chapter 2, we introduce the concept of **implicit constitutive relations**. This novel approach can be used to describe particular non-standard material responses – something the classical constitutive theories might be short of. We show that the implicit constitutive relations can be developed in a sound thermodynamic way within the framework of entropy production maximization. Specially, this method can be adopted to model fluids with a relation between the shear stress and the shear rate given by a non-monotone S-shaped curve. Models of this type are in the spotlight throughout the remainder of the thesis.

Models displaying the constitutive S-shape dependence can be also described by means of gradient dynamics where a part of the constitutive relation is given as the derivative of a **non-convex dissipation potential**. Note that unlike in the similar setting of phase transitions with a non-convex energy, in this case, the non-convexity is purely in the dissipative response. Therefore, we call it dissipative phase transition. This is discussed in Chapter 3. There, we also elucidate the experimentally observed phenomenon that the variation of the shear stress yields a continuous response, while varying the shear rate, the response exhibits a jump. These discontinuities can lead to a hysteretic behavior between different branches of the non-monotone constitutive relation. To this end, we introduce the concept of *CR-stability* explaining various regimes of the dynamics with respect to perturbations of the constitutive relation. Additionally, we remark the phenomenon of critical heat flux as another physical example that can be clarified by a non-convex dissipation potential.

In Chapter 4, we turn our attention to the concept of **hydrodynamic stability of flows of incompressible fluids described by the implicit type models**. Assuming the plane Poiseuille channel flow, we derive the unidirectional steady base flow solution. Then, in a simple setting, we demonstrate that flows within a regime of decreasing constitutive curve as a function of either the shear rate or the shear stress are unconditionally unstable. Further, we formulate the counterpart of the standard Reynolds–Orr energy equation and deduce stability criteria for a fluid at rest and the channel Poiseuille flow. The latter case is consequently studied in the context of linearized hydrodynamic stability. The results again confirm the instability of flow states occupying the decreasing part of the constitutive relation.

Finally in Chapter 5, we study flow of fluids characterized by a non-monotone constitutive relation. We propose a **numerical scheme for simulation of transient flows of incompressible non-Newtonian fluids characterized in the preceding chapters**. The proposed numerical scheme is based on reformulation of the governing equations as a system for the triple pressure-velocity-apparent viscosity, where the apparent viscosity is given by a scalar implicit equation. The

reformulated system is discretized using the finite element method and the final numerical scheme is implemented in FEniCS Project software. Using the developed code, we numerically study flow of fluid with a non-monotone constitutive relation in two dimensional Taylor–Couette geometry. In order to investigate the dynamical behavior implied by the non-monotone constitutive relations, we also present a reduced problem that can be understood as an implicit variant of Fourier's law of heat conduction.

We mention other models capable of capturing the non-monotone relation between the shear stress and the shear rate in Chapter 6, and then we conclude the thesis by summarizing all of our findings in the last chapter.

The thesis contains results from the following publications:

- Janečka, A. and V. Průša (2015): Perspectives on using implicit type constitutive relations in the modelling of the behaviour of non-Newtonian fluids. *AIP Conference Proceedings* **1662**.
- Janečka, A. and M. Pavelka (2018): Non-convex dissipation potentials in multiscale non-equilibrium thermodynamics. *Continuum Mechanics and Thermodynamics* (online).
- Janečka, A., J. Málek, V. Průša, and G. Tierra (2018): Numerical scheme for simulation of transient flows of non-Newtonian fluids characterised by a non-monotone relation between the symmetric part of the velocity gradient and the Cauchy stress tensor. *In preparation.*

The following papers are also explicitly mentioned in the text:

- Janečka, A., V. Průša, and K. R. Rajagopal (2016): Euler–Bernoulli type beam theory for elastic bodies with nonlinear response in the small strain range. *Archives of Mechanics* **68**(1): 3–25.
- Janečka, A. and M. Pavelka (2018): Gradient dynamics and entropy production maximization. *Journal of Non-Equilibrium Thermodynamics* **43**(1): 1–19.

2. Implicit constitutive relations for non-Newtonian fluids

Rajagopal (2003, 2006) introduced the concept of the so-called implicit type constitutive relations, which provides a novel approach to the phenomenological theory of constitutive relations, especially in the description of behavior of non-Newtonian fluids. Here, we introduce this approach in the context of thermodynamics of non-Newtonian fluids and we investigate its benefits contrary to the classical theory of constitutive relations. We mainly focus on the mathematical modeling of fluids in which the relation between the shear stress and the shear rate is given by a non-monotone S-shaped curve.

We also discuss a thermodynamical framework of entropy production maximization that allows to consistently develop implicit constitutive relations, see Rajagopal and Srinivasa (2000, 2004, 2008)

This chapter is based on previous work published in Janečka and Průša (2015).

2.1 Implicit constitutive models

In the classical phenomenological approach to describing an incompressible fluid, one provides a constitutive relation for the Cauchy stress $\mathbb{T}$ in terms of the pressure p and the symmetric part of the velocity gradient $\mathbb{D} =_{\text{def}} \frac{1}{2}\left(\nabla \boldsymbol{v} + \nabla \boldsymbol{v}^{\mathsf{T}}\right)$ as

$$\mathbb{T} = -p\mathbb{I} + \mathfrak{g}(\mathbb{D}), \tag{2.1}$$

where $\mathbb{I}$ is the identity tensor and $\mathfrak{g}$ is a tensorial function. For incompressible fluids, the pressure p is the indeterminate part of the stress due to the constraint of incompressibility and the function $\mathfrak{g}$ is determined only up to an arbitrary tensor function that is a scalar multiple of $\mathbb{I}$. Thus we require the extra stress $\mathfrak{g}(\mathbb{D})$ to be traceless

$$\operatorname{Tr}\mathfrak{g}(\mathbb{D}) = 0, \tag{2.2}$$

see Truesdell and Noll (2004). Taking the trace of (2.1), we see that the pressure p is the mean normal stress

$$p = -\frac{1}{3}\operatorname{Tr}\mathbb{T}, \tag{2.3}$$

see Rajagopal (2015) for more details concerning the pressure and its notion. The extra stress $\mathfrak{g}(\mathbb{D})$ corresponds to the deviatoric part of the Cauchy stress $\mathbb{T}_\delta =_{\text{def}} \mathbb{T} - \left(\frac{1}{3}\operatorname{Tr}\mathbb{T}\right)\mathbb{I}$

$$\mathbb{T}_\delta = \mathfrak{g}(\mathbb{D}). \tag{2.4}$$

Constitutive relation (2.1) can be further generalized within the concept of simple fluid with an assumption that the "present stress is determined by the history of the gradient of the deformation function", see Truesdell and Noll (1965). The general constitutive relation expressing that the value of the Cauchy stress $\mathbb{T}$ at time t depends on all previous deformation states is

$$\mathbb{T} = -p\mathbb{I} + \mathfrak{F}_{s=0}^{+\infty}(\mathbb{C}_t(t-s)), \tag{2.5}$$

where $\mathbb{C}_t(t-s)$ is the relative right Cauchy–Green tensor and $\mathfrak{F}_{s=0}^{+\infty}$ denotes the functional acting on the history of the relative Cauchy–Green tensor.

The classical incompressible Navier–Stokes fluid model

$$\mathbb{T} = -p\mathbb{I} + 2\mu\mathbb{D}, \tag{2.6}$$

as some exact models used in the mechanics of non-Newtonian fluids, falls into the class of models of type (2.5). It can be also shown that the standard differential type models can be interpreted as approximations of the general type model (2.5) for "slow motions". Therefore, constitutive relation (2.5) is often interpreted as the most general constitutive relation for incompressible non-Newtonian fluids, see for example Hutter and Jöhnk (2004), Müller (1985) and Haupt (2000).

2.1.1 S-shaped curves

The problem with constitutive relations (2.1) and (2.5) is that they both express the Cauchy stress as a function (or functional) of other quantities. Therefore, despite their substantive generality, they are not capable to describe some experimental data. In Figure 2.1, we reproduce plots of the viscosity μ and the shear stress σ versus the shear rate $\dot{\gamma}$ for some fluids. Clearly, there exists a certain range of shear rates where the stress is multivalued and we say that the shear stress versus shear rate dependence is an *S-shaped curve*.

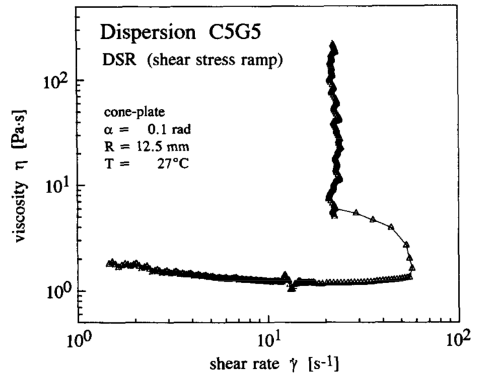

(a) Viscosity function for polymer dispersion C5G5 (styren/ethyl acrylate copolymer particles in glycol) in a shear stress ramp experiment (reprinted from Laun (1994)).

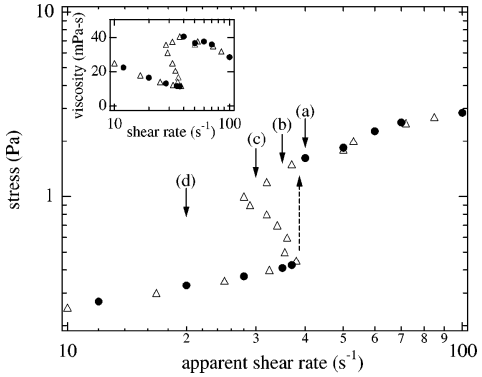

(b) Steady-state stress/shear–rate behavior obtained under constant applied shear stress (Δ) and constant applied shear rate (•) for a 7.5/7.5 mM TTAA/NaSal solution (reprinted from Boltenhagen et al. (1997)).

Figure 2.1: Experimental data for some fluids.

The S-shaped curves appear in many other experimental works focused on materials ranging from long polymer chain suspensions to granular suspensions, see Perlácová and Průša (2015) for references.

The S-shaped curves can also arise from microscopic level theories. In a pivotal paper, de Gennes (1974) discussed abrupt unwinding of dilute, long, flexible polymer coils in extensional flows. He argued that this coil–stretch transition could lead to the S-shaped curves for single molecules and as a consequence the existence of hysteresis. This concept was independently introduced by Hinch

(1974, 1977) and further elaborated by Tanner (1975). Even though Fan et al. (1985) claimed that the S-shape curves are a result of the used approximations, the effects were indeed experimentally observed on a molecular level (single DNA molecules) by Schroeder et al. (2003). As it has long been conjectured, the hysteresis seems to be present also on the macroscopic level (bulk shear stress versus shear rate) as suggest the results by François et al. (2009). For more experimental data showing S-shaped curves see Sridhar et al. (2007) and Prakash (2009).

Based on phenomenological Landau theory for shear flow of dry granular particles for frictional systems, Grob et al. (2014) introduced phenomenological constitutive relation able to describe the S-shape curve between macroscopic variables $\dot{\gamma}$ and σ

$$\dot{\gamma}(\sigma) = \alpha\sigma^{\frac{1}{2}} - \beta\sigma + \delta\sigma^2, \tag{2.7}$$

where α, β and δ are material coefficients. This model is in a very good agreement with experimental results obtained by Bi et al. (2011). The same class of constitutive relations can be derived either from microstructural evolution equation, see Olmsted (2008), or from mode-coupling approaches, see Holmes et al. (2005). For a review of an experimental study of a closely related effect of particle jamming, i.e., discontinuous transition towards a more viscous flow, see Hébraud (2009).

Other models apt for describing some of the macroscopic experimental S-shaped curves can be found in Perlácová and Průša (2015). One of the phenomenological constitutive relations is

$$\dot{\gamma}(\sigma) = \left[a\left(1 + b\sigma^2\right)^n + c\right]\sigma, \tag{2.8}$$

where a, b, c, and n are material parameters. This is an one-dimensional version of the constitutive relation proposed by Le Roux and Rajagopal (2013), which we will study in the following chapters.

2.1.2 Generalization of the classical constitutive theory

The aim is to provide a constitutive theory adequate to describe the experimental data discussed above. To this end, we need to generalize the classical constitutive theory that is only able to yield constitutive relations of the type (2.4) or (2.5). In particular, the desired theory must be able to recognize phenomenological relations of type (2.7) and (2.8) just as special instances of some general constitutive relation.

As reported by Rajagopal (2003, 2006), due to the incompressibility condition $\operatorname{Tr}\mathbb{D} = \operatorname{div}\boldsymbol{v} = 0$, the constitutive relation for the Navier–Stokes fluid (2.6) can be rewritten as

$$\mathbb{T} = \left(\frac{1}{3}\operatorname{Tr}\mathbb{T}\right)\mathbb{I} + 2\mu\mathbb{D}, \tag{2.9}$$

which can be further formulated as

$$\mathbb{T}_\delta - 2\mu\mathbb{D} = \mathbb{0}, \tag{2.10}$$

with $\mathbb{T}_\delta =_{\text{def}} \mathbb{T} - \left(\frac{1}{3}\operatorname{Tr}\mathbb{T}\right)\mathbb{I}$ denoting the traceless part of the Cauchy stress tensor. In order to obtain nonlinear relations between the Cauchy stress tensor and the symmetric part of the velocity gradient, we can generalize (2.10) as

$$\mathfrak{h}\left(\mathbb{T}_\delta, \mathbb{D}\right) = \mathbb{0}, \tag{2.11}$$

where $\mathfrak{h}$ is a tensorial function. Now, instead of an explicit relation, we have an *implicit relation* between $\mathbb{T}_\delta$ and $\mathbb{D}$.

A special class of the general constitutive relations (2.11) is

$$\mathbb{D} = \mathfrak{f}(\mathbb{T}_\delta), \tag{2.12}$$

with a typical representative, the stress power-law constitutive relation

$$\mathbb{D} = \left[a\left(1 + b|\mathbb{T}_\delta|^2\right)^n + c\right]\mathbb{T}_\delta, \tag{2.13}$$

which reduces to (2.8) in the simple shear flow, see Málek et al. (2010) and Le Roux and Rajagopal (2013) for comprehensive discussion of the properties of models of type (2.13).[1] Further, Narayan and Rajagopal (2013) studied the counterparts of Stokes' first and second problems using the model (2.13) with $c = 0$ and Srinivasan and Karra (2015) employed it for the flow in an orthogonal rheometer. Other examples of constitutive models that naturally fit into the class (2.12) are piezoviscous fluids, for example Barus (1893), or viscoplastic fluids that exhibit yield stress behavior, typically Bingham model, Oldroyd (1947), and its generalization, Herschel–Bulkley model, Herschel and Bulkley (1926). Note that already Bingham (1922) plotted his results as the shear rate versus the shear stress, i.e., in the form (2.12).

Following the implicit type approach (2.11), we can also generalize the concept of simple fluid (2.5) by a implicit type formula

$$\mathfrak{H}_{s=0}^{+\infty}\left(\mathbb{T}(t-s), \mathbb{C}_t(t-s)\right) = \mathbb{0}, \tag{2.14}$$

that relates the histories of the stress tensor and the relative right Cauchy–Green tensor, see Průša and Rajagopal (2012).

Since, in a particular setting, the phenomenological constitutive relation (2.8) is an one-dimensional version of the fully three-dimensional relation (2.13), the implicit constitutive theory is the sought appropriate generalization of the classical framework able to provide description of the experimental data reviewed in Section 2.1.1.

Implicit constitutive models are by no means limited to modeling of fluids. They can be very well employed in nonlinear elasticity. Rajagopal (2010, 2013) proposed several models that are able to exhibit nonlinear response even in the small strain range. For numerical results we refer, for example, to Kulvait et al. (2013); Janečka et al. (2016).

Implicit constitutive relations of type (2.11) or (2.14) enable the description of complex rheological properties of some materials. This cannot be achieved by the standard approach (2.4) or within the concept of simple fluid (2.5) in general. Even though macroscopic constitutive relations of type (2.7) and (2.8) can be obtained using the approaches based on detailed investigation of the microscopic structure of the given material, the phenomenological approach is irreplaceable when modeling the material as a single continuous medium[2] and when solely

[1] Even though the name suggests a relation to the classical Ostwald–de Waele power-law model, de Waele (1923); Ostwald (1925), the constitutive relation is, in fact, a counterpart to the Carreau A model, Carreau (1972).

[2] That is, ignoring the fact that the material is in fact a dispersion or, in general, a mixture.

the macroscopic properties of the given material are of concern. As the macroscopic quantities are often the only quantities of interest and the microstructure is irrelevant, the relative simplicity of the phenomenological approach is highly appreciated.[3] Neither the phenomenological macroscopic theory nor the detailed microscopic theory can be free of various assumptions. If the macroscopic behavior is of interest, it is favorable to make the assumptions directly on the macroscopic level rather than to make them on the microscopic level and then try to trace back their impact to the macroscopic behavior. The self evident drawback of the phenomenological approach is that it is inapplicable if the microstructure is of real interest.

The relative simplicity of the phenomenological approach allows to easily develop constitutive relations that are *fully three-dimensional*, *thermodynamically consistent* and *readily coupled with other macroscopic physical quantities*. On top of that, the novel theory of *implicit constitutive relations* can also handle materials that exhibit the behavior shown in Figure 2.1. In other words, the implicit type constitutive relations provide, among others, a theoretical background for the modeling of materials where the stress (shear stress σ) is not a function of the kinematic variables (shear rate $\dot{\gamma}$). Therefore, the class of materials that can be described by phenomenological constitutive relations is greatly expanded.

2.1.3 Some properties of implicit constitutive relations

Determining the constitutive relation for a non-Newtonian fluid corresponds to providing the relation between *two tensorial quantities*, the Cauchy stress tensor $\mathbb{T}$ and the symmetric part of the velocity gradient $\mathbb{D}$. Knowing just the one-dimensional shear stress versus shear rate relation is, in general, insufficient to conclude something about the three-dimensional relation between the corresponding tensors. Some of the important characteristics of the non-Newtonian fluids, such as normal stress differences, see Truesdell and Noll (1965); Coleman et al. (1966) or Tanner and Walters (1998), are inherently of three-dimensional nature. Therefore, the structure concerning the relation between the tensorial quantities is of interest.

Modeling of normal stress differences

One of the implications of the concept of implicit constitutive relations closely related to applications is the capability of capturing the phenomenon of the normal stress differences. Perlácová and Průša (2015) have investigated algebraic implicit constitutive relations of the form

$$\mathfrak{h}\left(\mathbb{T}_\delta, \mathbb{D}\right) = \mathbb{0}, \tag{2.15}$$

with respect to the modeling of normal stress differences in *isotropic* incompressible homogeneous fluids.

Let us assume that the function $\mathfrak{h}$ in (2.15) is an *isotropic* tensorial function of $\mathbb{T}_\delta$ and $\mathbb{D}$, that is, for all orthogonal tensors $\mathbb{Q}$,

$$\mathfrak{h}\left(\mathbb{Q}\mathbb{T}_\delta\mathbb{Q}^\mathsf{T}, \mathbb{Q}\mathbb{D}\mathbb{Q}^\mathsf{T}\right) = \mathbb{Q}\mathfrak{h}\left(\mathbb{T}_\delta, \mathbb{D}\right)\mathbb{Q}^\mathsf{T}. \tag{2.16}$$

[3] Analogously, modeling the flow of water with Navier–Stokes type equations, there is no need to know anything about the water molecules and the modes of their interaction.

Then, the representation theorems for isotropic tensorial functions impose strong restrictions on the possible relation between $\mathbb{T}$ and $\mathbb{D}$, see Spencer (1971) for the standard theorems and Rajagopal (2006) for the theorems in the context of implicit constitutive relations.

In particular, to model an incompressible fluid with material coefficients independent of the pressure (the mean normal stress), it then follows from the representation theorem that the general constitutive relation (2.15) can be reformulated as

$$\alpha_1 \mathbb{T}_\delta + \alpha_2 \mathbb{D} + \alpha_3 \left(\mathbb{T}_\delta^2\right)_\delta + \alpha_4 \left(\mathbb{D}^2\right)_\delta + \alpha_5 (\mathbb{T}_\delta \mathbb{D} + \mathbb{D}\mathbb{T}_\delta)_\delta + \alpha_6 \left(\mathbb{T}_\delta^2 \mathbb{D} + \mathbb{D}\mathbb{T}_\delta^2\right)_\delta + \alpha_7 \left(\mathbb{T}_\delta \mathbb{D}^2 + \mathbb{D}^2 \mathbb{T}_\delta\right)_\delta + \alpha_8 \left(\mathbb{T}_\delta^2 \mathbb{D}^2 + \mathbb{D}^2 \mathbb{T}_\delta^2\right)_\delta = \mathbb{0}, \quad (2.17)$$

where $\mathbb{A}_\delta =_{\text{def}} \mathbb{A} - \frac{1}{3} (\operatorname{Tr} \mathbb{A}) \mathbb{I}$ denotes the traceless part of the corresponding tensor and $\{\alpha_i\}_{i=0}^{8}$ are functions of combined invariants of $\mathbb{T}_\delta$ and $\mathbb{D}$

$$\operatorname{Tr} \mathbb{T}_\delta^2,\ \operatorname{Tr} \mathbb{D}^2,\ \operatorname{Tr} \mathbb{T}_\delta^3,\ \operatorname{Tr} \mathbb{D}^3,\ \operatorname{Tr} (\mathbb{T}_\delta \mathbb{D}),\ \operatorname{Tr} \left(\mathbb{T}_\delta^2 \mathbb{D}\right),\ \operatorname{Tr} \left(\mathbb{T}_\delta \mathbb{D}^2\right),\ \operatorname{Tr} \left(\mathbb{T}_\delta^2 \mathbb{D}^2\right),$$

where Tr denotes the trace of the corresponding tensor. Note that relation (2.17) immediately implies that the fluid is incompressible, $\operatorname{Tr} \mathbb{D} = 0$, and since there only appears the deviatoric part of the Cauchy stress $\mathbb{T}_\delta$, it suggests that the pressure is not present in the constitutive relation.

Using the representation formula (2.17), it is easy to investigate the behavior of the given material in the simple shear flow and analyze the possible three-dimensional effects (normal stress differences). Perlácová and Průša (2015) conjectured that the constitutive relations of type (2.17) can be used to model both normal stress differences N_1 and N_2. Furthermore, they have shown that the simple shear flow is *dynamically admissible* for some *specific* nontrivial implicit constitutive relation that exhibits nonzero normal stress difference N_2. Moreover, the given constitutive relation has been found to be *thermodynamically admissible*.[4] This result indicates that the class of implicit models (2.15) contains interesting models that go beyond the standard setting and are worth of investigation.

Materials with fading memory

Another possible way how to obtain some specific fully three-dimensional implicit type constitutive relations is the generalization of the classical concept of fading memory to the implicit type setting, see Průša and Rajagopal (2012). One can start with a general implicit type relation between the histories of the Cauchy stress tensor and the right Cauchy–Green tensor,

$$\mathfrak{H}_{s=0}^{+\infty} \left(\mathbb{T}(t-s), \mathbb{C}_t(t-s)\right) = \mathbb{0}, \quad (2.18)$$

and then combine the ideas of Oldroyd (1950) and Coleman and Noll (1960) to conclude something about the behavior of this general constitutive relation in

[4] Dynamical admissibility means that the simple shear flow is a solution to the complete set of governing equations for the given constitutive relation. Thermodynamical admissibility means that the constitutive relation does not violate the second law of thermodynamics.

"slow" processes. For example, considering slow processes in an isotropic incompressible homogeneous fluid, the "first order" *approximation* of (2.18) is

$$\mathbb{T} = -p\mathbb{I} + \mathbb{S}, \tag{2.19a}$$

and the evolution equation for the extra stress $\mathbb{S}$ reads

$$b_0 \left(\operatorname{Tr}\mathbb{S}\right)\mathbb{I} + b_1\mathbb{S} + 2b_3\mathbb{D} + b_4\left(\operatorname{Tr}\overset{\triangledown}{\mathbb{S}}\right)\mathbb{I} + b_5\overset{\triangledown}{\mathbb{S}} = \mathbb{O}, \tag{2.19b}$$

where $\{b_i\}_{i=0}^5$ are constants, and $\overset{\triangledown}{\mathbb{S}} =_{\text{def}} \frac{\mathrm{d}\mathbb{S}}{\mathrm{d}t} - \mathbb{L}\mathbb{S} - \mathbb{S}\mathbb{L}^\top$ denotes the upper convected time derivative of $\mathbb{S}$.

This statement in fact says that for any relation between the stress and kinematics, the viscoelastic type model with suitably chosen (possibly zero) coefficients $\{b_i\}_{i=0}^5$ can provide a reasonable description of the behavior of the given material in "slow" motions. Constitutive relation (2.19) can be considered as the Taylor expansion of the general constitutive relation (2.18). Using a higher order expansion, see Průša and Rajagopal (2012), it can be shown that the Maxwell, Oldroyd-B, Rivlin–Ericksen and other popular fluid models fit into the implicit framework in the sense that they are good approximations of the hypothetical complex constitutive relation (2.18). This shows that the implicit constitutive theory provides a very robust and general framework to describe fluid response.

2.2 Thermodynamics

In the classical theory of constitutive relations, it must be assured that the given constitutive relation is *thermodynamically admissible*, that is, it obeys the second law of thermodynamics. For example, in the context of isothermal processes of incompressible fluids, the second law is satisfied if the product $\mathbb{T} : \mathbb{D}$ is non-negative.[5] Below we show, that the product $\mathbb{T} : \mathbb{D}$ is in fact tantamount to the local entropy production of the fluid.

In some cases, the thermodynamical admissibility is easy to show. The constitutive relation for the incompressible Navier–Stokes fluid $\mathbb{T} = -p\mathbb{I} + 2\mu\mathbb{D}$ yields in virtue of the incompressibility restriction $\operatorname{Tr}\mathbb{D} = \operatorname{div}\boldsymbol{v} = 0$

$$\mathbb{T} : \mathbb{D} = 2\mu\mathbb{D} : \mathbb{D} = 2\mu\left|\mathbb{D}\right|^2. \tag{2.20}$$

Hence, the product $\mathbb{T} : \mathbb{D}$ is non-negative provided that the viscosity is non-negative.

Similarly, for the implicit constitutive relation (2.13), we obtain

$$\mathbb{T} : \mathbb{D} = \left[a\left(1 + b\left|\mathbb{T}_\delta\right|^2\right)^n + c\right]\mathbb{T}_\delta : \mathbb{T}_\delta = \left[a\left(1 + b\left|\mathbb{T}_\delta\right|^2\right)^n + c\right]\left|\mathbb{T}_\delta\right|^2. \tag{2.21}$$

In this case, the product $\mathbb{T} : \mathbb{D}$ is non-negative for example if $a \geq 0$ and $c \geq 0$. Clearly, if one wants to study thermodynamical consistency of more complex constitutive relations such as (2.17) or (2.19) the issue gets more complicated.

[5] The scalar product on the space of matrices is defined as $\mathbb{A} : \mathbb{B} =_{\text{def}} \operatorname{Tr}\left(\mathbb{A}\mathbb{B}^\top\right)$ and the corresponding norm is given by $|\mathbb{A}| =_{\text{def}} \left(\mathbb{A} : \mathbb{A}\right)^{\frac{1}{2}}$.

The advantage of the approach developed by Rajagopal and Srinivasa (2000, 2004, 2011) is that it reverses the standard workflow. Instead of specifying the constitutive relation between $\mathbb{T}$ and $\mathbb{D}$ and then investigating the non-negativity of their product (the entropy production), one starts with the specification of the constitutive relation for the entropy production and then derives the constitutive relation between $\mathbb{T}$ and $\mathbb{D}$. As the starting point of the whole procedure is the specification of the entropy production, the established constitutive relations are naturally thermodynamically consistent and obey the second law of thermodynamics. It is also much easier and transparent to specify a formula for a single scalar quantity, the entropy production, than to directly specify the relation between the two tensorial quantities. Moreover, the idea of implicit constitutive relations discussed in the previous section can be seamlessly integrated into this framework.

In what follows, we will show derivation of models (2.6) and (2.13) within this thermodynamical framework. Although these models have been already shown to be thermodynamically consistent and using such advanced thermodynamical framework is not necessary, our aim is to demonstrate the procedure in a simple setting. Concerning the applications of this method in more complex settings we refer the reader to Rajagopal and Srinivasa (2000, 2004, 2008, 2011). In real-life scenarios, this approach was used, for example, to derive a model of vulcanization of rubber, see Kannan and Rajagopal (2011), or to design a constitutive relation for asphalt binder, see Málek et al. (2015).

2.2.1 Preliminaries

The continuous medium is governed by the evolution equations for the density ρ, the velocity $\boldsymbol{v}$ and the total energy[6] e_{tot}. In the Eulerian description, they read

$$\frac{\mathrm{d}\rho}{\mathrm{d}t} + \rho \operatorname{div} \boldsymbol{v} = 0, \tag{2.22a}$$

$$\rho \frac{\mathrm{d}\boldsymbol{v}}{\mathrm{d}t} = \operatorname{div} \mathbb{T} + \rho \boldsymbol{b}, \tag{2.22b}$$

$$\rho \frac{\mathrm{d}e_{\mathrm{tot}}}{\mathrm{d}t} = \operatorname{div} (\mathbb{T}\boldsymbol{v}) - \operatorname{div} \boldsymbol{j}_q + \rho \boldsymbol{b} \cdot \boldsymbol{v}, \tag{2.22c}$$

where $\boldsymbol{b}$ denotes the body force and $\boldsymbol{j}_q$ is the heat flux. Symbol $\frac{\mathrm{d}}{\mathrm{d}t}$ stands for the convective derivative $\frac{\mathrm{d}}{\mathrm{d}t} =_{\mathrm{def}} \frac{\partial}{\partial t} + \boldsymbol{v} \cdot \nabla$. The epitome of the second law of thermodynamics is the classical Clausius inequality, see Clausius (1879). Its continuous counterpart is the Clausius–Duhem inequality

$$\rho \frac{\mathrm{d}\eta}{\mathrm{d}t} + \operatorname{div}\left(\frac{\boldsymbol{j}_q}{\theta}\right) = \xi \geq 0, \tag{2.23}$$

where θ denotes the temperature, η the specific entropy and ξ the entropy production per unit volume.

[6] More precisely, e_{tot} denotes the density of specific energy, that is the total energy per unit mass, $[e] = \mathrm{J/kg}$. We will frequently omit the adjective "specific", and we will simply talk about total energy. Similar omission will also hold for the specific body force, specific entropy, specific entropy production and so on.

Since the total energy $e_{\mathrm{tot}} =_{\mathrm{def}} e + \frac{1}{2}\boldsymbol{v}\cdot\boldsymbol{v}$ is the sum of the internal energy e and the kinetic energy $\frac{1}{2}\boldsymbol{v}\cdot\boldsymbol{v}$, multiplying (2.22b) by $\boldsymbol{v}$ and then subtracting from (2.22c) leads to the evolution equation for the internal energy

$$\rho\frac{\mathrm{d}e}{\mathrm{d}t} = \mathbb{T} : \mathbb{D} - \operatorname{div}\boldsymbol{j}_q, \tag{2.24}$$

where we also exploited the symmetricity of the Cauchy stress tensor $\mathbb{T} = \mathbb{T}^{\intercal}$. Using the assumption that the internal energy is a function of the entropy and the density[7], $e = e(\rho, \eta)$, we can *identify* the corresponding entropy production ξ in the Clausius–Duhem inequality (2.23). Direct differentiation of $e = e(\rho, \eta)$ with respect to time yields

$$\frac{\mathrm{d}e}{\mathrm{d}t} = \frac{\partial e}{\partial \rho}\frac{\mathrm{d}\rho}{\mathrm{d}t} + \frac{\partial e}{\partial \eta}\frac{\mathrm{d}\eta}{\mathrm{d}t}. \tag{2.25}$$

The time derivatives of the density and the internal energy are already known from (2.22a) and (2.24) respectively. Substituting them into (2.25) and using the definition of the thermodynamic temperature $\theta =_{\mathrm{def}} \frac{\partial e}{\partial \eta}$, after some manipulation, we arrive at

$$\rho\frac{\mathrm{d}\eta}{\mathrm{d}t} + \operatorname{div}\left(\frac{\boldsymbol{j}_q}{\theta}\right) = \frac{1}{\theta}\left[\mathbb{T}_\delta : \mathbb{D}_\delta + \left(\frac{1}{3}\operatorname{Tr}\mathbb{T} + \rho^2\frac{\partial e}{\partial \rho}\right)\operatorname{div}\boldsymbol{v} - \frac{1}{\theta}\boldsymbol{j}_q\cdot\nabla\theta\right]. \tag{2.26}$$

Comparison of (2.26) and (2.23) yields the sought formula for the entropy production

$$\xi =_{\mathrm{def}} \frac{1}{\theta}\left[\mathbb{T}_\delta : \mathbb{D}_\delta + \left(\frac{1}{3}\operatorname{Tr}\mathbb{T} + \rho^2\frac{\partial e}{\partial \rho}\right)\operatorname{div}\boldsymbol{v} - \frac{1}{\theta}\boldsymbol{j}_q\cdot\nabla\theta\right]. \tag{2.27}$$

In the special case of incompressible fluid incapable of heat conduction, we have $e =_{\mathrm{def}} e(\eta)$, $\operatorname{div}\boldsymbol{v} = 0$ and $\boldsymbol{j}_q =_{\mathrm{def}} \boldsymbol{0}$, and the entropy production simplifies to

$$\xi =_{\mathrm{def}} \frac{1}{\theta}\mathbb{T}_\delta : \mathbb{D}_\delta. \tag{2.28}$$

In virtue of the incompressibility condition $\operatorname{Tr}\mathbb{D} = 0$, the last formula can be also rewritten as $\xi =_{\mathrm{def}} \frac{1}{\theta}\mathbb{T} : \mathbb{D}$. Note that everything that has been said so far holds independently of the particular formula for the Cauchy stress tensor $\mathbb{T}$.

Let us now discuss how to employ the formula for the entropy production in the development of constitutive relations. Concerning the constitutive relations for incompressible heat non-conducting fluids, we want to find a relation between $\mathbb{T}$ and $\mathbb{D}$ in such a way that $\mathbb{T} : \mathbb{D}$ is non-negative. In order to assure this, we shall first fix a non-negative entropy production $\xi \geq 0$ in such a way that it vanishes at rest. Then we need to find the corresponding constitutive relation between $\mathbb{T}$ and $\mathbb{D}$. The link between the stress, the symmetric part of the velocity gradient and the entropy production is equation (2.28). From here, the chosen entropy production ξ must be equal to the product $\frac{1}{\theta}\mathbb{T} : \mathbb{D}$.

The problem is that (2.28) is a *single scalar equation* from which we would like to conclude the relations between the six independent components of the stress tensor and the six independent components of the symmetric part of the velocity

[7] Note that the assumption on the specific form of the energy as a function of the density and entropy is in fact our *first constitutive assumption* concerning the given material.

gradient. Obviously, another physical assumption needs to be made, otherwise there is no chance to reasonably specify the relation between the corresponding tensors.

We shall adopt the assumption on the maximization of the entropy production in the form developed by Rajagopal and Srinivasa (2004). Provided that all restrictions concerning the material behavior, such as incompressibility, are satisfied, the premise is that the choice between possible competing constitutive relations for the given material should be made in such a way that the material response is the one that maximizes the entropy production.[8]

Therefore, we can identify the constitutive relation by maximizing the entropy production over the possible values of independent variables. In other words, we specify the entropy production ξ as a function of $\mathbb{D}$ and we fix the value of the stress $\mathbb{T}$. Then we should maximize the entropy production ξ with respect to $\mathbb{D}$ subject to constraint $\xi - \frac{1}{\theta}\mathbb{T} : \mathbb{D} = 0$ and other possible constraints such as the incompressibility. The value of $\mathbb{D}$ that leads to the maximal value of ξ is declared as the value of the $\mathbb{D}$ that corresponds to the given $\mathbb{T}$.[9] For more details about this procedure in continuum thermodynamics of fluids, see Málek and Průša (2017),

Apparently, there are more than one possible thermodynamically consistent approaches for modeling dissipative processes and developing constitutive relations. Closely related framework to the entropy production maximization is the *steepest entropy ascent*, see Beretta (2014). Another approach is the *gradient dynamics* which is crucial in the GENERIC framework, see Grmela and Öttinger (1997); Öttinger and Grmela (1997). In Chapter 3, we give a primer of the GENERIC framework and study constitutive relation (2.13) within the gradient dynamics. For a comparison of the gradient dynamics and the entropy production maximization, we refer to Janečka and Pavelka (2018a).

2.2.2 Incompressible Navier–Stokes fluid and incompressible power-law type non-Newtonian fluid

We shall now demonstrate the outlined procedure in the context of isothermal incompressible heat non-conducting Navier–Stokes fluid and power-law type non-Newtonian fluid.

As stated before, in the case of incompressible heat non-conducting fluids, the energetic state equation can be chosen as $e = e(\eta)$. We already know, see above, that the corresponding entropy production in the system of interest is identified as

$$\xi = \frac{1}{\theta}\mathbb{T} : \mathbb{D}. \tag{2.29}$$

Then, we need to decide what are the free variables. We can choose between the symmetric part of the velocity gradient $\mathbb{D}$ and the Cauchy stress tensor $\mathbb{T}$.

[8] This should not be confused with the classical Onsager (1931a,b) minimum entropy production theorem. The minimum entropy production theorem talks about the behavior of a particular material with fixed constitutive relation in the vicinity of a steady state. Here we talk about the choice between possible constitutive models, see Rajagopal and Srinivasa (2004) for details.

[9] It would be very well possible to proceed in an opposite way, that is, specify the entropy production as a function of $\mathbb{T}$, fix the value of $\mathbb{D}$ and maximize with respect to $\mathbb{T}$, see Section 2.2.3.

Now, our choice is the symmetric part of the velocity gradient. Hence, the Cauchy stress tensor $\mathbb{T}$ is arbitrary, but it is fixed, and we search for the corresponding $\mathbb{D}$. The temperature θ is fixed and is of no interest.

Further, we must make a constitutive assumption upon a specific form for the entropy production ξ as a function of the free variable. The entropy production ξ must be non-negative and vanishing at rest. A rather general option is

$$\xi =_{\text{def}} \frac{\varphi(|\mathbb{D}|^2)}{\theta}, \tag{2.30}$$

where φ is a smooth function. In particular, think of $\varphi =_{\text{def}} 2\mu |\mathbb{D}|^2$ for incompressible Navier–Stokes fluid or $\varphi =_{\text{def}} 2\mu(1+\beta |\mathbb{D}|^2)^n |\mathbb{D}|^2$ for incompressible power-law type fluid. In both cases, μ is a positive constant (viscosity).

Since we are interested in an incompressible material, we require an additional restriction on the free variable

$$\operatorname{Tr} \mathbb{D} = 0. \tag{2.31}$$

Now, we maximize the entropy production (2.30) with respect to $\mathbb{D}$ for fixed $\mathbb{T}$ due to the constraints (2.29) and (2.31). The Lagrange function $L(\mathbb{D})$ for the constrained maximization procedure is

$$L(\mathbb{D}) =_{\text{def}} \xi + \lambda_1 \left(\xi - \frac{1}{\theta} \mathbb{T} : \mathbb{D} \right) + \lambda_2 \operatorname{Tr} \mathbb{D}, \tag{2.32}$$

λ_1 and λ_2 being the Lagrange multipliers. The condition on the extremum, the requirement on zero value of the derivative of L with respect to $\mathbb{D}$, reads

$$\frac{\partial \xi}{\partial \mathbb{D}} + \lambda_1 \left(\frac{\partial \xi}{\partial \mathbb{D}} - \frac{1}{\theta} \mathbb{T} \right) + \lambda_2 \mathbb{I} = \mathbb{0}, \tag{2.33}$$

which must be solved with respect to $\mathbb{D}$ ($\mathbb{T}$ is fixed). Rearranging (2.33) yields

$$\frac{1}{\theta} \mathbb{T} = \frac{\lambda_2}{\lambda_1} \mathbb{I} + \frac{1+\lambda_1}{\lambda_1} \frac{\partial \xi}{\partial \mathbb{D}}, \tag{2.34}$$

and now, we need to eliminate the Lagrange multiplies. If we denote the square of the norm of the symmetric part of the velocity gradient $s =_{\text{def}} \mathbb{D} : \mathbb{D} = |\mathbb{D}|^2$, from (2.30), the chain rule implies $\frac{\partial \xi}{\partial \mathbb{D}} = \frac{1}{\theta} \frac{\partial \varphi}{\partial s} 2\mathbb{D}$. Therefore, equation (2.34) can be rewritten as

$$\frac{1}{\theta} \mathbb{T} = \frac{\lambda_2}{\lambda_1} \mathbb{I} + 2 \frac{1+\lambda_1}{\lambda_1} \frac{1}{\theta} \frac{\partial \varphi}{\partial s} \mathbb{D}. \tag{2.35}$$

Since $\mathbb{I} : \mathbb{D} = \operatorname{Tr} \mathbb{D} = 0$, multiplication of (2.35) with $\mathbb{D}$ gives

$$\frac{1}{\theta} \mathbb{T} : \mathbb{D} = 2 \frac{1+\lambda_1}{\lambda_1} \frac{1}{\theta} \frac{\partial \varphi}{\partial s} |\mathbb{D}|^2 . \tag{2.36}$$

Further, we know that $\frac{1}{\theta} \mathbb{T} : \mathbb{D} = \xi$, hence (2.36) reduces to

$$\frac{\varphi}{|\mathbb{D}|^2} = 2 \frac{1+\lambda_1}{\lambda_1} \frac{\partial \varphi}{\partial s}, \tag{2.37}$$

which upon substitution back into (2.35) yields

$$\mathbb{T} = \theta \frac{\lambda_2}{\lambda_1} \mathbb{I} + \frac{\varphi}{|\mathbb{D}|^2} \mathbb{D}. \tag{2.38}$$

As the material is incompressible ($\operatorname{Tr}\mathbb{D} = 0$), taking the trace of (2.38) yields $\operatorname{Tr}\mathbb{T} = 3\frac{\lambda_2}{\lambda_1}\theta$, which allows us to identify the negative ratio of the Lagrange multipliers $-\frac{\lambda_2}{\lambda_1}\theta$ with the mean normal stress $p = -\frac{1}{3}\operatorname{Tr}\mathbb{T}$. In other words, equation (2.38) in fact reads

$$\mathbb{T}_\delta = \frac{\varphi}{|\mathbb{D}|^2}\mathbb{D}. \tag{2.39}$$

As a result, the complete formula for the Cauchy stress tensor is $\mathbb{T} = -p\mathbb{I} + \frac{\varphi}{|\mathbb{D}|^2}\mathbb{D}$, which for our particular choices of φ yields the well-known constitutive relation for the incompressible Navier–Stokes fluid

$$\mathbb{T} = -p\mathbb{I} + 2\mu\mathbb{D}, \tag{2.40a}$$

and the constitutive relation for incompressible power-law type non-Newtonian fluid

$$\mathbb{T} = -p\mathbb{I} + 2\mu\left(1 + \beta|\mathbb{D}|^2\right)^n\mathbb{D}, \tag{2.40b}$$

respectively.

The maximization procedure as shown above is, strictly speaking, valid only if the chosen function φ is a convex function. If it is not true, the situation is more complicated and we shall not go into the details here.

2.2.3 Incompressible stress power-law fluid

Now, we will use the maximization procedure to obtain the stress power-law fluid (2.13). We will exploit the fact that *the role of* $\mathbb{T}$ *and* $\mathbb{D}$ *in the maximization procedure can be completely reversed*.

As before, the energetic state equation is of the form $e = e(\eta)$ and from (2.28), the corresponding entropy production in the system of interest is

$$\xi = \frac{1}{\theta}\mathbb{T}_\delta : \mathbb{D}, \tag{2.41}$$

where we have used the incompressibility requirement $\operatorname{Tr}\mathbb{D} = \operatorname{div}\boldsymbol{v} = 0$ which provides the equality $\mathbb{D}_\delta = \mathbb{D}$.

Now, our choice of the free variable is the traceless part of the Cauchy stress tensor $\mathbb{T}_\delta$ and the symmetric part of the velocity gradient $\mathbb{D}$ is arbitrary but fixed. Again, the temperature θ is of no interest as it is fixed.

Besides being non-negative and vanishing at rest, the entropy production ξ must be clearly a function of the free variable. Our choice is analogous to (2.30)

$$\xi =_{\text{def}} \frac{\phi\left(|\mathbb{T}_\delta|^2\right)}{\theta}, \tag{2.42}$$

where ϕ is a smooth function. Specially consider $\phi =_{\text{def}} \left[a\left(1 + b|\mathbb{T}_\delta|^2\right)^n + c\right]|\mathbb{T}_\delta|^2$, where a and b are positive constants, c is non-negative and n is a real number.

As using $\mathbb{T}_\delta$ in (2.42) instead of $\mathbb{T}$ is sufficient to guarantee incompressibility, there are no further restrictions on the values of the free variable.

The entropy production (2.42) is maximized for fixed $\mathbb{D}$ over $\mathbb{T}_\delta$ with respect to the constraint (2.41). The Lagrange function $L(\mathbb{T}_\delta)$ for the constrained maximization is

$$L(\mathbb{T}_\delta) =_{\text{def}} \xi + \lambda\left(\xi - \frac{1}{\theta}\mathbb{T}_\delta : \mathbb{D}\right), \tag{2.43}$$

where λ is the Lagrange multiplier. The condition on the extremum reads

$$\frac{\partial \xi}{\partial \mathbb{T}_\delta} + \lambda \left(\frac{\partial \xi}{\partial \mathbb{T}_\delta} - \frac{1}{\theta} \mathbb{D} \right) = \mathbb{0}, \tag{2.44}$$

or, after rearranging

$$\frac{1}{\theta} \mathbb{D} = \frac{1+\lambda}{\lambda} \frac{\partial \xi}{\partial \mathbb{T}_\delta}. \tag{2.45}$$

This equation must be solved with respect to $\mathbb{T}_\delta$ ($\mathbb{D}$ is fixed). Again, if we denote the square of the norm of the free variable, i.e., the traceless part of the Cauchy stress tensor, $s =_{\text{def}} \mathbb{T}_\delta : \mathbb{T}_\delta = |\mathbb{T}_\delta|^2$, from (2.42), the chain rule implies $\frac{\partial \xi}{\partial \mathbb{T}_\delta} = \frac{1}{\theta} \frac{\partial \phi}{\partial s} 2 \mathbb{T}_\delta$. Therefore, equation (2.45) can be rewritten as

$$\mathbb{D} = 2 \frac{1+\lambda}{\lambda} \frac{\partial \phi}{\partial s} \mathbb{T}_\delta. \tag{2.46}$$

To eliminate the Lagrange multiplier, we multiply (2.46) with $\mathbb{T}_\delta$

$$\mathbb{D} : \mathbb{T}_\delta = 2 \frac{1+\lambda}{\lambda} \frac{\partial \phi}{\partial s} |\mathbb{T}_\delta|^2 . \tag{2.47}$$

Further, we know that $\frac{1}{\theta} \mathbb{T}_\delta : \mathbb{D} = \xi$, hence (2.47) reduces to

$$\frac{\phi}{|\mathbb{T}_\delta|^2} = 2 \frac{1+\lambda}{\lambda} \frac{\partial \phi}{\partial s}, \tag{2.48}$$

which upon substitution back into (2.46) yields

$$\mathbb{D} = \frac{\phi}{|\mathbb{T}_\delta|^2} \mathbb{T}_\delta. \tag{2.49}$$

Note that since $\operatorname{Tr} \mathbb{T}_\delta = 0$, we automatically have $\operatorname{Tr} \mathbb{D} = 0$ and the fluid is indeed incompressible. From our particular choice of ϕ then follows the constitutive relation in the form

$$\mathbb{D} = \left[a \left(1 + b |\mathbb{T}_\delta|^2 \right)^n + c \right] \mathbb{T}_\delta. \tag{2.50}$$

As we have already remarked in the previous case, the maximization procedure as shown above is valid only if the chosen function ϕ is a convex function. If it is not true, the situation is more complicated, we shall not go into the details here.

The entropy production (2.42) can be also rewritten in the form $\xi =_{\text{def}} \frac{\phi(\operatorname{Tr} \mathbb{T}_\delta^2)}{\theta}$, which means that the entropy production is a function of one of the invariants of $\mathbb{T}_\delta$. Other invariants can be used as well. In such a case, the final constitutive relation would be a special case of (2.17) and its thermodynamical admissibility would automatically hold.

2.2.4 Mathematical modeling

If the mechanical response of an incompressible heat non-conducting fluid is described by an implicit constitutive relation of type (2.15), the complete set of governing equations for the flow of the fluid reads

$$\rho \frac{\mathrm{d}\boldsymbol{v}}{\mathrm{d}t} = \operatorname{div} \mathbb{T} + \rho \boldsymbol{b}, \tag{2.51a}$$

$$\mathfrak{h} \left(\mathbb{T}_\delta, \mathbb{D} \right) = \mathbb{0}. \tag{2.51b}$$

Unlike in the standard setting, the constitutive relation (2.51b) might not be solvable for $\mathbb{T}_\delta$, hence one can not substitute for $\mathbb{T}$ back into (2.51a). In other words, the system must be solved in the form shown above.

Consequently, the nonstandard structure of the constitutive relations requires a revised mathematical approach to the modeling of non-Newtonian fluids. Several important steps have been already done in this direction, see Bulíček et al. (2012, 2009). Unfortunately, the theory cannot handle the case of constitutive relations that leads, for example, to the S-shaped curves. Besides the purely analytical considerations, there also exist works focused on numerical techniques for some systems of type (2.51), see Diening et al. (2013); Hron et al. (2017); Süli and Tscherpel (2018).

2.3 Conclusion

Certain types of complex rheological response of some fluids cannot be described using the classical phenomenological theory of constitutive relations. We have outlined the possible benefits of using implicit constitutive relations in describing such types of response. If the classical phenomenological theory of constitutive relations is insufficient and if the implicit constitutive relations provide its generalization, several important concepts in the theory of non-Newtonian fluids must be carefully reconsidered. In particular, the theory of viscometric functions, see for example Coleman et al. (1966) and Böhme (1987), should be carefully modified.

More importantly, the combination of the idea of implicit constitutive relations with the thermodynamical procedure introduced by Rajagopal and Srinivasa (2004) provides a very general theoretical framework for developing mathematical models for non-Newtonian fluids. In particular, one can think of developing thermodynamically consistent constitutive relations for viscoelastic materials with S-shaped type response in the shear stress/shear rate dependence in the simple steady shear flow. Using the idea of implicit constitutive relations beyond the purely mechanical setting, i.e., coupling with thermal effects, electromagnetic field or chemical reactions, is also possible, and it is currently subject of intense research activity.

3. Non-convex dissipation potentials in multiscale non-equilibrium thermodynamics

This chapter is motivated by the peculiar behavior of some fluids in the shear flow, see Boltenhagen et al. (1997). The common experimental setting is a non-Newtonian fluid contained in a gap between two concentric cylinders. The inner cylinder is fixed while the outer one is able to rotate. The outer cylinder is put in motion either by prescribing the rotational velocity or imposing the force. In this manner, either the shear rate or the shear stress can be controlled with the other quantity being measured.[1] When varying the shear stress, the response is continuous, whereas when varying the shear rate, shear stress exhibits a jump, see Figure 3.1.

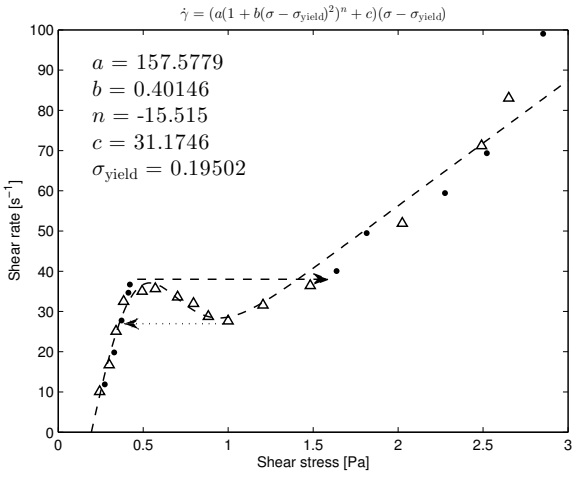

Figure 3.1: Steady-state stress/shear–rate behavior for a 7.5/7.5 mM TTAA/-NaSal solution from the controlled shear stress (Δ) and controlled shear rate ($\bullet$) experiments by Boltenhagen et al. (1997). The fit (- -) was obtained from the constant applied stress data using one-dimensional form of the constitutive relation (2.13). When increasing the shear stress, shear rate varies continuously (although not monotonically). On the other hand, when increasing the shear rate, shear stress exhibits a *discontinuity* and possibly hysteresis. The dashed arrow indicates the experimentally observed jump in the shear stress while the dotted arrow the predicted jump when lowering the shear rate, see Section 3.4.1.

Our aim is to describe the relation between the shear stress and the shear rate by means of a constitutive relation compatible with non-equilibrium thermodynamics and then try to explain the different behavior between the controlled shear rate and the controlled shear stress experiments.

First, we provide an introduction to the used thermodynamic framework in Section 3.1. Then, we choose an appropriate model to fit the experimental data

[1] We assume that the measured quantities correspond to the actual properties of the fluid within the gap.

and in Section 3.2, the constitutive relation is reformulated in terms of gradient dynamics as the derivative of a non-convex dissipation potential. In Section 3.2.1, we identify the conjugate representation using the multivalued conjugate dissipation potential. Subsequently, in Section 3.3, the dynamics is lifted to an extended state space and investigated in the context of mesoscopic multiscale thermodynamics. This enables us to discuss various regimes of the dynamics and its stability, metastability and instability with respect to perturbations of the constitutive relation (*CR-stability*) in Section 3.4.1, which is the focal point of this chapter. As a result, the interesting observed behavior of complex fluids in the shear flow can be explained as it is given a clear physical picture.

In Section 3.3.5, we also comment on more physically sound forms of the extension than the one studied throughout the majority of the chapter. Non-smooth dissipation potentials that can generate yield stress behavior are then mentioned in Section 3.5.

Moreover, we remark the phenomenon of critical heat flux in Section 3.6. As it can also be approached by the method of non-convex dissipation potentials, we are able to explain its behavior in the same manner as in the shear stress/rate case.

This chapter has been adapted from Janečka and Pavelka (2018b) and we refer there for more details.

3.1 GENERIC structure of hydrodynamics

Time evolution of state variables $\boldsymbol{x}$ can be split into its *reversible* and *irreversible* (dissipative) part

$$\frac{\partial \boldsymbol{x}}{\partial t} = \left(\frac{\partial \boldsymbol{x}}{\partial t}\right)_{\text{rev}} + \left(\frac{\partial \boldsymbol{x}}{\partial t}\right)_{\text{irr}}, \tag{3.1}$$

where the reversible part is invariant with respect to the time-reversal transformation. This means that without the irreversible part, reversing the course of time together with the velocities of all particles, the system would reach its initial state, see Pavelka et al. (2014). Within the GENERIC framework, Grmela and Öttinger (1997); Öttinger and Grmela (1997), the evolution equation (3.1) is given as

$$\frac{\partial \boldsymbol{x}}{\partial t} = \mathbf{L}\frac{\partial E}{\partial \boldsymbol{x}} + \left.\frac{\partial \Xi}{\partial \boldsymbol{x}^*}\right|_{\boldsymbol{x}^* = S_{\boldsymbol{x}}}, \tag{3.2}$$

where $\mathbf{L}$ is the Poisson bivector, Ξ the dissipation potential, E the energy and S the entropy of the system, and $\boldsymbol{x}^*$ are the conjugate variables.[2] If there is a field quantity among the state variables, the quantities are real functionals and the derivatives should be understood as functional derivatives. The Poisson bivector $\mathbf{L}$ satisfies

$$\{A, B\} = \left\langle \frac{\partial A}{\partial \boldsymbol{x}}, \mathbf{L}\frac{\partial B}{\partial \boldsymbol{x}} \right\rangle, \tag{3.3a}$$

$$\mathbf{L}\frac{\partial S}{\partial \boldsymbol{x}} = \mathbf{0}, \tag{3.3b}$$

[2] The shorthand subscript notation $S_{\boldsymbol{x}}$ stands for the (functional) derivative of S with respect to $\boldsymbol{x}$.

where $\{A, B\}$ is Poisson bracket[3] between any two functionals A and B, $\langle \bullet, \bullet \rangle$ being the L^2 scalar product. The dissipation potential Ξ must be sufficiently regular, zero at the origin and convex near the origin (equilibrium).

Then, the time evolution of an arbitrary functional of the state variables $A(\boldsymbol{x})$ is given by

$$\frac{\partial A}{\partial t} = \left\langle \frac{\partial A}{\partial \boldsymbol{x}}, \frac{\partial \boldsymbol{x}}{\partial t} \right\rangle = \underbrace{\left\langle \frac{\partial A}{\partial \boldsymbol{x}}, \mathbf{L} \frac{\partial E}{\partial \boldsymbol{x}} \right\rangle}_{\{A,E\}} + \left\langle \frac{\partial A}{\partial \boldsymbol{x}}, \frac{\partial \Xi}{\partial \boldsymbol{x}^*} \right\rangle. \tag{3.4}$$

The reversible evolution is Hamiltonian, as it is generated by the Poisson bracket. Of special interest is the evolution of the entropy

$$\frac{\partial S}{\partial t} = \{S, E\} + \left\langle \boldsymbol{x}^*, \frac{\partial \Xi}{\partial \boldsymbol{x}^*} \right\rangle. \tag{3.5}$$

The first term is zero due to (3.3b) and the antisymmetricity of the Poisson bracket. Exploiting the convexity of the dissipation potential near equilibrium, we can approximate it by a quadratic function. Consequently, the second term is positive, entropy rises and the system tends toward equilibrium. Apparently, when there is no dissipation (the second term), entropy is constant and the process is reversible.

3.1.1 Reversible part of the time evolution

In the classical hydrodynamics, the state variables are the mass density ρ, momentum density $\boldsymbol{u}$ and the entropy density s. The reversible evolution of a functional of the hydrodynamic state variables is

$$\frac{\partial A}{\partial t} = \{A, E\}^{(CH)}, \tag{3.6}$$

where the Poisson bracket of classical hydrodynamics, for example Arnold (1966), is, using the summation convention, given by

$$\begin{aligned} \{A, B\}^{(CH)} = & \int \rho \left(\partial_i A_\rho B_{u_i} - \partial_i B_\rho A_{u_i} \right) \mathrm{d}\boldsymbol{r} \\ & + \int u_i \left(\partial_j A_{u_i} B_{u_j} - \partial_j B_{u_i} A_{u_j} \right) \mathrm{d}\boldsymbol{r} \\ & + \int s \left(\partial_i A_s B_{u_i} - \partial_i B_s A_{u_i} \right) \mathrm{d}\boldsymbol{r}. \end{aligned} \tag{3.7}$$

The energy is given as a sum of the specific kinetic energy and the internal energy density $e(\rho, s)$ that depends on the density ρ and the entropy density s

$$E = \int \left(\frac{|\boldsymbol{u}|^2}{2\rho} + e(\rho, s) \right) \mathrm{d}\boldsymbol{r}. \tag{3.8}$$

So the particular derivatives appearing in (3.7) are

$$E_\rho = -\frac{|\boldsymbol{u}|^2}{2\rho^2} + e_\rho, \qquad E_{u_i} = \frac{u_i}{\rho}, \qquad E_s = e_s. \tag{3.9}$$

[3] That is, it is antisymmetric, $\{A, B\} = -\{B, A\}$, and it satisfies the Jacobi identity $\{A, \{B, C\}\} + \{B, \{C, A\}\} + \{C, \{A, B\}\} = 0$.

Rewriting the time derivative of the functional A as

$$\frac{\partial A}{\partial t} = \int \left(A_\rho \frac{\partial \rho}{\partial t} + A_{u_i} \frac{\partial u_i}{\partial t} + A_s \frac{\partial s}{\partial t} \right) \mathrm{d}\boldsymbol{r}, \tag{3.10}$$

we can compare the particular terms with (3.6). This yields the reversible parts of evolution equations for the hydrodynamic fields

$$\frac{\partial \rho}{\partial t} = -\partial_i(\rho E_{u_i}) = -\operatorname{div}(\rho \boldsymbol{v}), \tag{3.11a}$$

$$\frac{\partial u_i}{\partial t} = -\partial_j \left(u_i E_{u_j} \right) - \rho \partial_i E_\rho - u_j \partial_i E_{u_j} - s \partial_i E_s = -\partial_j \left(\rho v_i v_j \right) - \partial_i p, \tag{3.11b}$$

$$\frac{\partial s}{\partial t} = -\partial_i(s E_{u_i}) = -\operatorname{div}(s \boldsymbol{v}), \tag{3.11c}$$

where $v_i =_{\mathrm{def}} u_i/\rho$ are the components of the velocity $\boldsymbol{v}$ and $p =_{\mathrm{def}} -e(\rho, s) + \rho e_\rho + s e_s$ is the pressure. The reversible evolution given by the Poisson bracket (3.7) with the energy (3.8) of the hydrodynamic fields $(\rho, \boldsymbol{u}, s)$ is, as expected, the compressible Euler equations for the inviscid fluid. To enforce incompressibility, see Janečka and Pavelka (2018a).

3.1.2 Irreversible part of the evolution

The dissipation of a fluid is caused by viscous, or generally other non-Newtonian, effects. Hence, we have to model the irreversible part of the momentum density evolution. Evolution of the momentum density $\boldsymbol{u}$ can be equivalently expressed in terms of what we call a *multiscale thermodynamic Lyapunov* (MTL) function $\Psi^{(CH \to E)}$ as

$$\frac{\partial \boldsymbol{u}}{\partial t} = \left(\frac{\partial \boldsymbol{u}}{\partial t} \right)_{\mathrm{rev}} + \Xi_{\boldsymbol{u}^*}\big|_{\boldsymbol{u}^* = \Psi^{(CH \to E)}_{\boldsymbol{u}}}, \tag{3.12}$$

where the reversible part is given by the Euler equations (3.11b). The MTL function driving classical hydrodynamics (CH) to equilibrium (E) is the negative of the thermodynamic potential[4] used by Grmela (2017), that is

$$\Psi^{(CH \to E)}(\rho, \boldsymbol{u}, e_{\mathrm{tot}}) =_{\mathrm{def}} S(\rho, \boldsymbol{u}, e_{\mathrm{tot}}) - \frac{1}{T_0} E(\rho, \boldsymbol{u}, e_{\mathrm{tot}}) + \frac{\mu_0}{T_0} M(\rho, \boldsymbol{u}, e_{\mathrm{tot}}), \tag{3.13}$$

where $e_{\mathrm{tot}} =_{\mathrm{def}} \frac{|\boldsymbol{u}|^2}{2\rho} + e$ is the total energy density (per volume). Since the MTL functions are the negatives of the thermodynamic potentials, everything that is valid for the thermodynamic potentials also holds for the MTL functions, only with an opposite sign. In particular, as the convex thermodynamic potential decreases toward equilibrium, the concave MTL function increases.

Further, total entropy is

$$S = \int s \left(\rho, e_{\mathrm{tot}} - \frac{|\boldsymbol{u}|^2}{2\rho} \right) \mathrm{d}\boldsymbol{r}, \tag{3.14}$$

where $s(\rho, e)$ denotes local equilibrium entropy density that depends on the density ρ and the internal energy density e, total energy is $E = \int e_{\mathrm{tot}} \, \mathrm{d}\boldsymbol{r}$ and

[4] Thermodynamic potential can be also interpreted as availability, see Waldram (1985), exergy or maximum work, see Landau and Lifshitz (1968) or the original idea introduced by Gibbs (1876, 1878)).

$M = \int \rho \, \mathrm{d}\boldsymbol{r}$ is the total mass. Constant T_0 is the temperature an isolated system would have after relaxation to equilibrium and constant μ_0 is the equilibrium chemical potential. Local temperature T is defined as the inverse of the derivative of the entropy with respect to the total energy density $T(\boldsymbol{r}) =_{\mathrm{def}} \left(S_{e(\boldsymbol{r})}\right)^{-1}$. The derivative of the MTL function with respect to the momentum $\boldsymbol{u}$ is the conjugate momentum $\boldsymbol{u}^*$

$$\boldsymbol{u}^* = \left(\frac{\partial \Psi^{(CH\to E)}}{\partial \boldsymbol{u}}\right)_{\rho,s} = S_{\boldsymbol{u}} = -\frac{1}{T}\frac{\boldsymbol{u}}{\rho}, \tag{3.15}$$

which is, under isothermal conditions, proportional to the velocity $\boldsymbol{v} = \boldsymbol{u}/\rho$.

The dissipation potential is often a function of thermodynamic forces $\mathbf{X}$ which are expressed as (linear) operators acting on the conjugate variables $\mathbf{X} = \Gamma(\boldsymbol{x}^*)$, Γ being a operator. In our case, we are interested in the momentum density evolution and so the dissipation potential is in the form

$$\Xi = \Xi\left(\Gamma(\boldsymbol{u}^*)\right). \tag{3.16}$$

Particularly, from

$$\Gamma(\bullet) = -\frac{1}{2}\left(\nabla \bullet + (\nabla \bullet)^{\mathsf{T}}\right), \tag{3.17}$$

follows that the force associated with the conjugate momentum is the symmetric part of the velocity gradient $\Gamma(\boldsymbol{u}^*)_{\boldsymbol{u}^*=\Psi_{\boldsymbol{u}}^{(CH\to E)}} = \frac{1}{T_0}\mathbb{D}$, where the constant prefactor T_0 is going to be ignored for the sake of simplicity. In a slightly overloaded notation, we then have

$$\Xi_{\boldsymbol{u}^*} = \left\langle \Xi_{\mathbb{D}}, \frac{\partial \mathbb{D}}{\partial \boldsymbol{u}^*} \right\rangle = \left\langle \Xi_{\mathbb{D}}, \frac{\partial \Gamma(\boldsymbol{u}^*)}{\partial \boldsymbol{u}^*} \right\rangle = \Gamma^{\mathsf{T}}\left(\Xi_{\mathbb{D}}\right), \tag{3.18}$$

where the adjoint operator Γ^{T} is defined by

$$\langle \mathbb{A}, \Gamma(\boldsymbol{a})\rangle = \langle \Gamma^{\mathsf{T}}(\mathbb{A}), \boldsymbol{a}\rangle, \qquad \forall \text{ symmetric tensors } \mathbb{A} \text{ and vectors } \boldsymbol{a}. \tag{3.19}$$

For the operator (3.17), we have $\Gamma^{\mathsf{T}}(\bullet) = \mathrm{div}(\bullet)$ and the evolution equation for momentum density (3.12) becomes

$$\frac{\partial \boldsymbol{u}}{\partial t} = \left(\frac{\partial \boldsymbol{u}}{\partial t}\right)_{\mathrm{rev}} + \mathrm{div}(\Xi_{\mathbb{D}}). \tag{3.20}$$

This is the standard evolution equation for the momentum density in fluid dynamics, derived purely from the GENERIC structure (3.2). Choosing the dissipation potential as

$$\Xi\left(\mathbb{D}\right) = \int \mu \left|\mathbb{D}\right|^2 \mathrm{d}\boldsymbol{r}, \tag{3.21}$$

from the second term of (3.20), we recover the classical Newtonian viscous contribution.

Since the pressure is already contained in the reversible part of (3.20), it is tempting to denote the derivative of the dissipation potential as the deviatoric part of the Cauchy stress $\mathbb{T}_\delta = \Xi_{\mathbb{D}}$. In the next section, we will show that it is indeed justifiable to do so as $\mathbb{T}_\delta$ is the thermodynamic flux conjugate to the thermodynamic force $\mathbb{D}$.

3.2 Gradient dynamics

The experimental dependence of shear rate on shear stress in Figure 3.1 can be described by a non-Newtonian fluid model (2.13)

$$\mathbb{D} = \left[a\left(1 + b|\mathbb{T}_\delta|^2\right)^n + c\right]\mathbb{T}_\delta. \tag{3.22}$$

It is a special case of the general implicit constitutive relation (2.11)

$$\mathfrak{h}(\mathbb{T}_\delta, \mathbb{D}) = \mathbb{0}, \tag{3.23}$$

where $\mathfrak{h}$ is a tensorial function. Nevertheless, it is not clear whether the fully implicit case brings any advantage and whether it is physically substantiated. On the other hand, the special case $\mathbb{D} = \mathfrak{f}(\mathbb{T}_\delta)$ has a sound thermodynamic meaning and practical advantages, see Section 3.3 and Perlácová and Průša (2015).

Note that since only the deviatoric part of the stress tensor $\mathbb{T}_\delta$ is taken into account, the fluid is considered to be effectively incompressible. It is possible that abandoning the constraint of incompressibility could lead to different interesting behavior but for our purposes, it is sufficient to keep this constraint.

Constitutive relation (3.22) can be also regarded as a consequence of gradient dynamics which is a cornerstone of the GENERIC framework where it generates the dissipative evolution, see Section 3.1. Gradient dynamics has strong connection to the principle of large deviations, see Mielke et al. (2016), and it can be related to other techniques associated with the maximization of entropy production, see Janečka and Pavelka (2018a). Öttinger (2005) and Hütter and Svendsen (2013) favor an alternative non-potential version of GENERIC. Although it is more general as it allows for antisymmetric dissipative coupling, it is not clear whether such coupling is necessary and correct, see Grmela (2010). We prefer the potential version of GENERIC because reversibility and irreversibility are clearly distinguished, see Pavelka et al. (2014), and because we can employ Legendre transformations. Legendre transformations, or their generalizations, see Appendix A, are crucial in obtaining our results.

Let the dissipation potential Ξ be a differentiable function of the thermodynamic force $\mathbf{X}$, then the conjugate disssipation potential Ξ^* as a function of the thermodynamic flux $\mathbf{J}$ is given by the Legendre transformation

$$\frac{\partial}{\partial \mathbf{X}}\left(\langle \mathbf{J}, \mathbf{X}\rangle - \Xi(\mathbf{X})\right) = \mathbb{0}. \tag{3.24}$$

This implies that the thermodynamic flux $\mathbf{J}$ is the derivative of the dissipation potential Ξ

$$\mathbf{J} = \frac{\partial \Xi}{\partial \mathbf{X}}, \tag{3.25}$$

giving the dependence $\mathbf{X} = \tilde{\mathbf{X}}(\mathbf{J})$. Then, the explicit formula for the conjugate dissipation potential Ξ^* reads

$$\Xi^*(\mathbf{J}) = \left\langle \mathbf{J}, \tilde{\mathbf{X}}(\mathbf{J})\right\rangle - \Xi\left(\tilde{\mathbf{X}}(\mathbf{J})\right). \tag{3.26}$$

Analogously, one would obtain from the backward Legendre transformation that the thermodynamic force $\mathbf{X}$ is the derivative of the conjugate dissipation potential Ξ^*

$$\mathbf{X} = \frac{\partial \Xi^*}{\partial \mathbf{J}}. \tag{3.27}$$

In our case, the symmetric part of the velocity gradient $\mathbb{D}$ is the thermodynamic force and the deviatoric part of the Cauchy stress $\mathbb{T}_\delta$ is the thermodynamic flux. From (3.27) then follows

$$\mathbb{D} = \frac{\partial \Xi^*}{\partial \mathbb{T}_\delta}, \tag{3.28}$$

or alternatively, from the conjugate form (3.25)

$$\mathbb{T}_\delta = \frac{\partial \Xi}{\partial \mathbb{D}}. \tag{3.29}$$

The dissipation potential Ξ depends on $\mathbb{D}$ and is conjugate to Ξ^* by means of the Legendre transformation, see Section 3.2.1 for more details.

From (3.28), the conjugate dissipation potential corresponding to the constitutive relation (3.22) is

$$\Xi^*\left(\mathbb{T}_\delta\right) = \begin{cases} \frac{a}{2b(n+1)}\left[\left(1+b\left|\mathbb{T}_\delta\right|^2\right)^{n+1}-1\right] + \frac{c}{2}\left|\mathbb{T}_\delta\right|^2, & n \neq -1, \\ \frac{a}{2b}\ln\left(1+b\left|\mathbb{T}_\delta\right|^2\right) + \frac{c}{2}\left|\mathbb{T}_\delta\right|^2, & n = -1, \end{cases} \tag{3.30}$$

and is plotted in Figure 3.2. The dissipation potential Ξ that generates $\mathbb{T}_\delta$ in (3.29) is then specified in Section 3.2.1.

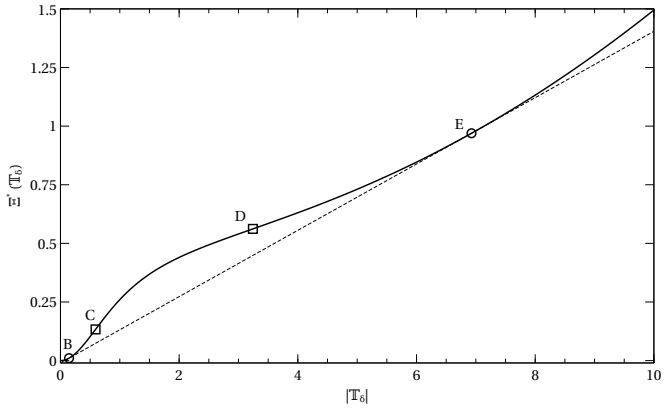

Figure 3.2: Dissipation potential $\Xi^*\left(\mathbb{T}_\delta\right)$ corresponding to the constitutive relation (3.22) with parameter values $a = 1$, $b = 1$, $c = 0.02$ and $n = -2$. The segment $C - D$ is not convex, thereby the dissipation potential is not CR-stable in this region. The dashed tangent line $B - E$ indicates the convex hull of the potential and coincides with the Maxwell lever rule construction. The segments $B - C$ and $D - E$ correspond to the CR-metastable regions (compare with Figure 3.4).

The important feature of the dissipation potential (3.30) is that it is convex in the vicinity of zero while non-convex for higher stresses. Convexity is consequently regained for even higher values of the stress. By analogy with equilibrium thermodynamics, see Callen (1985), we expect that the convex parts generate CR-stable or CR-metastable evolution while the non-convex parts are CR-unstable. This is indeed so, as discussed in Sections 3.3 and 3.4.1.

Convexity and the second law of thermodynamics

Assume for a moment that the dissipation potential $\Xi(\mathbb{D})$ is smooth and convex. It is positive everywhere except in the thermodynamic equilibrium as it is zero at

the origin. The origin is also the only point where the derivative of the dissipation potential is zero, $\mathbb{T}_\delta = \Xi_\mathbb{D}|_{\mathbb{D}=\mathbb{0}} = \mathbb{0}$. The conjugate dissipation potential $\Xi^*(\mathbb{T}_\delta)$ formed by Legendre transformation is also convex and zero at the origin. Then we can immediately see from the Fenchel–Young's equality, e.g., (Roubíček, 2005, p. 267)

$$\langle \mathbb{D}, \mathbb{T}_\delta \rangle = \underbrace{\Xi(\mathbb{D})}_{\geq 0} + \underbrace{\Xi^*(\mathbb{T}_\delta)}_{\geq 0} \geq 0, \tag{3.31}$$

that the entropy production, given as a product of thermodynamic forces and fluxes, see (2.28), is positive. Convexity of the dissipation potential thus implies compatibility with the second law of thermodynamics.

Non-convexity and the second law of thermodynamics

Convexity of the dissipation potential is a sufficient, not a necessary, condition for compatibility with the second law of thermodynamics. The second law is fulfilled if and only if the dissipation potential generates non-negative entropy production[5]

$$\langle \mathbb{D}, \Xi_\mathbb{D} \rangle \geq 0 \qquad \text{or} \qquad \langle \mathbb{T}_\delta, \Xi^*_{\mathbb{T}_\delta} \rangle \geq 0. \tag{3.32}$$

Typically, this condition is required to hold only locally (not after integration over the whole system) in non-equilibrium thermodynamics. If we further consider the dissipation potential to depend only on the norm of the thermodynamic force or flux, the local version of the condition (3.32)

$$0 \leq \mathbb{T}_\delta : \Xi^*_{\mathbb{T}_\delta} = |\mathbb{T}_\delta| \frac{\mathbb{T}_\delta}{|\mathbb{T}_\delta|} : \Xi^*_{|\mathbb{T}_\delta|} \frac{\partial |\mathbb{T}_\delta|}{\partial \mathbb{T}_\delta} = |\mathbb{T}_\delta| \frac{\mathbb{T}_\delta}{|\mathbb{T}_\delta|} : \Xi^*_{|\mathbb{T}_\delta|} \frac{\mathbb{T}_\delta}{|\mathbb{T}_\delta|} = |\mathbb{T}_\delta| \, \Xi^*_{|\mathbb{T}_\delta|}, \tag{3.33}$$

is satisfied if the function $\Xi^*(|\mathbb{T}_\delta|)$ is monotonous, see Fig. 3.2. In this sense, a non-convex dissipation potential which is monotonous as a function of $|\mathbb{T}_\delta|$ respects the second law of thermodynamics. Generalization to dissipation potentials that are not necessarily simple functions of the norm of the forces or fluxes can be found for instance in (Bulíček et al., 2017, Eq. 28–30).

It should be also recognized that condition (3.32) expresses non-negativity of the entropy production only if the thermodynamic potential whose derivatives generate the thermodynamic forces is convex. Therefore, we always assume that the entropy is a concave function of state variables and that the thermodynamic potential is convex.

The experimental observations can be presumably understood also without non-convex dissipation potentials but on more detailed levels of description. Non-convex dissipation potential is a result of a reduction from a more detailed level of description equipped with a convex dissipation potential. However, it is not clear what is the more detailed level of description. Perhaps a further extension in the sense of internal variables (that can be often seen as a CR-extension) could generate the same results using a convex dissipation potential. Unless such extension is known, we shall proceed with non-convex dissipation potentials.

Convexity of the dissipation potential near equilibrium is in tight relation with stability of the equilibrium state. Apart from convexity of the dissipation

[5] $\Xi_\mathbb{D} = \mathbb{T}_\delta$ from (3.29) and $\Xi^*_{\mathbb{T}_\delta} = \mathbb{D}$ from (3.28).

potential, convexity of the energy plays a crucial role in stability analysis as well. When these two requirements are satisfied, the equilibrium state is stable with respect to small fluctuations, as can be seen, for example, from the analysis of the spectrum of the linearized GENERIC formulation near equilibrium, see Pavelka et al. (2014), or as discussed in the paper by Matolcsi (1992). Thermodynamic equilibrium is stable if the dissipation potential is convex and the entropy concave near equilibrium.

On the other hand, although convexity (or monotonicity) implies increase of the entropy from condition (3.32), it does not make up for an exact mathematical proof of the existence of solutions and of the approach to equilibrium from arbitrarily far-from-equilibrium states. However, it is the main ingredient from both the physical and the mathematical point of view. This can be well illustrated in the case of the Boltzmann equation where the exact mathematics has been done.

Boltzmann equation is an illustration of GENERIC with a non-quadratic but convex dissipation potential, see Grmela and Öttinger (1997). The proof of the global existence of solutions has been done by DiPerna and Lions (1991), for which the latter author received the Fields Medal. The Boltzmann H-theorem is not sufficient but plays an crucial role in the proof. The approach to the equilibrium state was also shown by Desvillettes and Villani (2005), where again the Boltzmann H-theorem does not suffice but plays an essential role.

To sum up, the increase of the entropy, as implied by monotonicity of the dissipation potential, does not immediately assure all the mathematical rigor in the proofs of the existence of solutions and the approach to the equilibrium from any far-from-equilibrium state, but it is an essential ingredient in these proofs (that have been done only for a few mesoscopic time evolution equations so far).

Nevertheless, it is possible to interpret the $\mathbb{D} = \mathfrak{f}(\mathbb{T}_\delta)$ dependence in Figure 3.1 (open triangles) in terms of gradient dynamics. For each $\mathbb{T}_\delta$, there is a unique value of $\mathbb{D}$, which is the slope of the function Ξ^* at the particular value of $\mathbb{T}_\delta$. In the next section, we try to answer how to interpret this dependence.

Before we proceed with the details on the conjugate dissipation potential, let us briefly comment on the relation to the shear banding phenomena reviewed by Fielding (2007) and Olmsted (2008). Shear banding is usually experimentally observed in the cylindrical Couette flow, where instabilities in form of (visible) bands might develop. If the bands develop in the radial direction, the phenomenon is referred to as *gradient banding* while if they develop in the direction of the rotational axis, the phenomenon is referred to as *vorticity banding*.

Gradient banding is usually connected to a shear stress/rate dependence where multiple shear rates correspond to a single shear stress while vorticity banding is linked to the existence of the S-shaped curves, see Section 2.1.1. Although this is a typical distinction between these two phenomena, it is not always accurate, see Olmsted (2008). In the case of gradient banding, crossing the domain of unstable shear rates, the region of higher shear rates is usually characterized by a lower effective viscosity, i.e., the fluid is shear thinning. On the other hand, vorticity banding is often observed in flows of shear thickening fluids (higher viscosity). However, there have been reported experiments where such distinction was not valid, Olmsted (2008).

Since it is difficult to characterize the gradient/vorticity banding in the terms of the shear stress/rate dependence or shear thinning/thickening fluids, we shall

discuss some particular examples. There are several models that lead to the shear stress/rate dependency with multiple shear rates for a single shear stress. To name a few, the Johnson–Segalman model, Johnson and Segalman (1977), or rather its weakly non-local variant, Olmsted et al. (2000), models in the framework of thermodynamics with internal variables, Verhás (1997); Asszonyi et al. (2015), viscoelastic models undergoing scission of polymeric chains, Grmela et al. (2010), or viscoelastic models with relaxation of internal structure, Rajabian et al. (2005); Germann et al. (2013). In Chapter 6, we introduce several models in more detail but the literature is rather vast and we do not attempt to make the list of references complete. Interested reader could consult, for example, recent special issue of the Journal of Rheology, Fielding (2016). Most of the models exhibit shear thinning and it is believed that shear thickening should be captured by constitutive relations with a non-linear dependence of the shear rate on the shear stress, Radulescu et al. (1999). This is a motivation for the constitutive relation (3.22) that can describe the shear thickening S-shaped curves, typically suggesting vorticity banding.

Connection to entropy production maximization

Besides the entropy production maximization illustrated in Chapter 2, gradient dynamics is another possible method for modeling dissipative processes. Both methods are analogous in the way that they require a similar physical input of how energy (or entropy) is stored and how it is dissipated in the considered material. Entropy production maximization is widely used and it provides a lot of insight into modeling of complex materials. Gradient dynamics is also a practical method for generating constitutive relations. It can be further applied for reductions onto less detailed levels of description. Janečka and Pavelka (2018a) reviewed and compared both approaches in detail. They identified the cases when the resulting constitutive relations provided by both methods coincide and when they differ. For a deeper discussion, we refer to the mentioned paper.

3.2.1 Conjugate representation

The purpose of this section is to present details on the Legendre duality between the dissipation potential Ξ and its conjugate Ξ^*. Consequence of the non-convexity of Ξ^* is that Ξ is multivalued, i.e., there are multiple stresses corresponding to a certain velocity gradient. The velocity gradients that correspond to multiple stresses then constitute the CR-metastable and CR-unstable regions of the dynamics and are discussed in Section 3.4.1. Note also that the Legendre transformation can be regarded as a constrained extremization of the generating potential, which is often a practical method, see e.g. Junker et al. (2014).

From (3.20), (3.11b) and (3.29), the balance of linear momentum $\boldsymbol{u}$ reads[6]

$$\frac{\partial \boldsymbol{u}}{\partial t} = \underbrace{-\operatorname{div}\left(\frac{\boldsymbol{u}\otimes\boldsymbol{u}}{\rho}\right) - \nabla p}_{\text{reversible terms}} + \operatorname{div}\mathbb{T}_\delta, \tag{3.34}$$

[6]Strictly speaking, evolution equation (3.34) is in the entropic representation with variables $(\rho, \boldsymbol{u}, e_{\text{tot}})$ while (3.11b) is in the energetic representation with variables $(\rho, \boldsymbol{u}, s)$ and one should thus perform transformation from the latter representation to the former, see Öttinger (2005).

The irreversible part of this evolution equation is in the form of divergence of the thermodynamic flux $\mathbb{T}_\delta$ and the reversible terms are the gradient of the pressure p and the divergence of the convective terms, see Section. 3.1.1.

Since we assume that the fluid is incompressible and isothermal, only the momentum density acts as a state variable. Carrying out the CR-extension in Section 3.3.1, the conjugate stress tensor becomes a state variable as well.

Denoting the solutions to (3.28) by $\tilde{\mathbb{T}}_\delta(\mathbb{D})$, it can be rewritten as

$$\frac{\partial}{\partial \mathbb{T}_\delta}\left(\langle \mathbb{T}_\delta, \mathbb{D}\rangle - \Xi^*(\mathbb{T}_\delta)\right)\Big|_{\mathbb{T}_\delta=\tilde{\mathbb{T}}_\delta(\mathbb{D})} = \mathbb{0}, \tag{3.35}$$

This leads to the formulation of the dissipation potential Ξ conjugate to Ξ^*

$$\Xi(\mathbb{D}) =_{\text{def}} \left\langle \tilde{\mathbb{T}}_\delta(\mathbb{D}), \mathbb{D}\right\rangle - \Xi^*\left(\tilde{\mathbb{T}}_\delta(\mathbb{D})\right), \tag{3.36}$$

a reciprocal definition to (3.26). Note that we do not require the solution $\tilde{\mathbb{T}}_\delta(\mathbb{D})$ to be unique, which means that we do not interpret it as a function, but rather as a graph in the $(\mathbb{D}, \mathbb{T}_\delta)$ plane or as a collection of functions. Therefore, the dissipation potential Ξ can be multivalued as is the case for the non-convex dissipation potential (3.30), see Figure 3.3. Although the dissipation potential is multivalued, it is uniquely determined and the generalized (multivalued) Legendre transformation is invertible[7], see Dorst and Van den Boomgaard (1993, 1994).

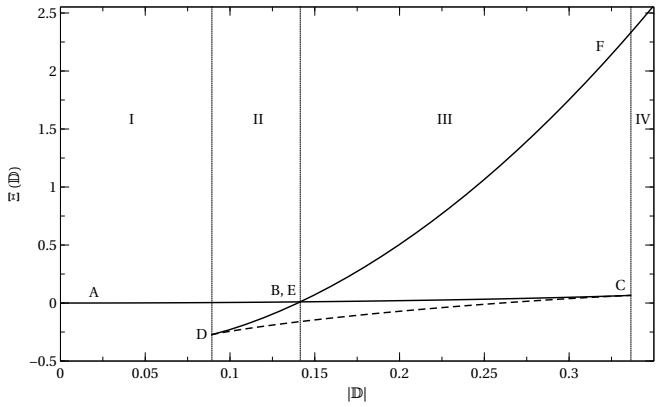

Figure 3.3: Conjugate dissipation potential $\Xi(\mathbb{D})$ corresponding to the constitutive relation (3.22) is obtained from the dissipation potential $\Xi^*(\mathbb{T}_\delta)$ (Figure 3.2) using the generalized Legendre transformation (3.36). In regions II and III, the potential is multivalued. The dashed line $C-D$ is the CR-unstable branch, lines $B-C$ and $D-E$ are CR-metastable branches, and the curve $A-B$, $E-F$ is globally CR-stable and corresponds to the convex hull of the dissipation potential Ξ^*. See Section 3.4.1 for detailed explanation.

Likewise, solutions of (3.29) are denoted by $\tilde{\mathbb{D}}(\mathbb{T}_\delta)$. These solutions compose the same graph in the $(\mathbb{D}, \mathbb{T}_\delta)$ plane as the solutions $\tilde{\mathbb{T}}_\delta(\mathbb{D})$. An example of such graph expressing simply the one-dimensional constitutive relation (3.22) is plotted

[7]Invertible in the sense that the backward Legendre transformation restores the original function (or rather graph).

in Figure 3.4. Employing the solutions $\tilde{\mathbb{D}}(\mathbb{T}_\delta)$ in (3.26) leads back to the original dissipation potential

$$\Xi^*(\mathbb{T}_\delta) = \left\langle \mathbb{T}_\delta, \tilde{\mathbb{D}}(\mathbb{T}_\delta) \right\rangle - \Xi\left(\tilde{\mathbb{D}}(\mathbb{T}_\delta)\right), \tag{3.37}$$

whose derivative gives (3.29). We have thus performed the Legendre transformation from Ξ^* to Ξ and back. For generalizations of the Legendre transformation, see Appendix A.

In Figure 3.4, there is also indicated the Maxwell lever rule known from equilibrium thermodynamics, see Callen (1985). On one hand, we have

$$\int_{|\mathbb{T}_\delta(B)|}^{|\mathbb{T}_\delta(E)|} |\mathbb{D}(T)| \, \mathrm{d}T = \int_{|\mathbb{T}_\delta(B)|}^{|\mathbb{T}_\delta(E)|} \left|\Xi^*_{\mathbb{T}_\delta}(T)\right| \, \mathrm{d}T = \Xi^*(|\mathbb{T}_\delta(E)|) - \Xi^*(|\mathbb{T}_\delta(B)|), \tag{3.38}$$

while on the other hand, it is clear from Figure 3.2 that

$$\frac{\Xi^*(|\mathbb{T}_\delta(E)|) - \Xi^*(|\mathbb{T}_\delta(B)|)}{|\mathbb{T}_\delta(E)| - |\mathbb{T}_\delta(B)|} = \left|\Xi^*_{\mathbb{T}_\delta}(E)\right| = \left|\Xi^*_{\mathbb{T}_\delta}(B)\right|. \tag{3.39}$$

Combining these two results leads to

$$\int_{|\mathbb{T}_\delta(B)|}^{|\mathbb{T}_\delta(E)|} |\mathbb{D}(T)| \, \mathrm{d}T = (|\mathbb{T}_\delta(E)| - |\mathbb{T}_\delta(B)|) \underbrace{|\mathbb{D}(|\mathbb{T}_\delta(E)|)|}_{|\mathbb{D}(|\mathbb{T}_\delta(B)|)|}, \tag{3.40}$$

which means that the shaded areas in Figure 3.4 are equal.

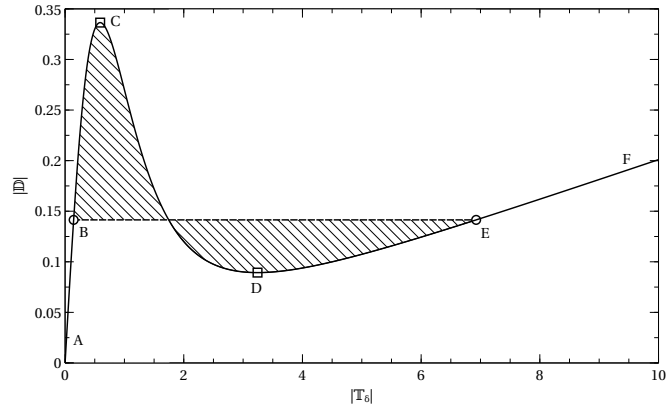

Figure 3.4: Flow curve (the constitutive relation) given by (3.22) with parameter values $a = 1$, $b = 1$, $c = 0.02$ and $n = -2$. The line $B - E$ is constructed using the Maxwell lever rule so that the shaded areas are equal. Since the segment $C - D$ corresponds to the region where the dissipation potential Ξ^* loses convexity, it is CR-unstable, as commented in Section 3.4.1. The lines $B - C$ and $D - E$ are CR-metastable as they coincide with the lower CR-stable branches of the dissipation potential Ξ, see Figure 3.3.

In the case of the non-convex dissipation potential, we expect an analogical behavior as in equilibrium phase transitions where the system evolves along the straight Maxwell line for large fluctuations. If the fluctuations are sufficiently small, hysteresis is observed.

Having the Legendre duality between Ξ as a function of the thermodynamic forces and Ξ^* as a function of the thermodynamic fluxes is often beneficial as one of the forms might be more accessible. For example, the former choice was used in chemical kinetics by Grmela (2012) while Mielke (2003) used the latter one in plasticity modeling.

Stability of the constitutive relation

By CR-stability of constitutive relations generated by non-convex dissipation potentials, we mean whether the constitutive relation is CR-stable with respect to perturbations. If the dissipation potential is convex everywhere, the dual (Legendre conjugate) dissipation potential is convex as well and for each value of the thermodynamic force there is only one value of the flux. On the other hand, if the potential is non-convex, the dual dissipation potential is multivalued and for some values of the thermodynamic force (or flux) there are several possible values of the flux (or force). The graph of the constitutive relation then has several branches as in Figure 3.3. In regions with multiple admissible fluxes (or forces), perturbation of the flux (or force) can cause evolution of the system toward another branch. The region is said to be *CR-unstable* if any perturbation leads to selection of a different branch, *CR-metastable* if only large enough perturbations switch the system to a different branch and *CR-stable* if the current branch of the constitutive relation is unaffected by any perturbation.

3.3 Extended hydrodynamics

In this section, the set of hydrodynamic state variables[8] is expanded by promoting the thermodynamic flux $\mathbb{T}_\delta$ to an independent state variable, hence the name *extended hydrodynamics* (EH). The idea of extending the set of state variables is ubiquitous in non-equilibrium thermodynamics. For example, it occurs in the Extended Irreversible Thermodynamics (EIT), Jou et al. (2010), or in thermodynamics with internal variables, Berezovski and Ván (2017).

For simplicity, we consider only the isothermal setting. Then, the isothermal hydrodynamic evolution is enriched to a form of extended hydrodynamics and the extra state variable has its own evolution equation. It will be shown that the extra evolution is determined by the derivative of another MTL function with respect to the conjugate of the extra state variable, see Section 3.3.4. The extra state variable evolves toward the maxima of the MTL function. The figures in Section 3.4.1 show the dependence of the MTL function on the thermodynamic force $\mathbb{D}$ and the consequent evolution of the extra state variable. This gives a graphical representation of the CR-stability analysis of the system.

Dissipation potential Ξ^* is convex near equilibrium and for high values of the stress, but it loses convexity in the intermediate range. Convexity leads to existence of the Lyapunov functional, see e.g. Grmela and Öttinger (1997), and to validity of the Braun–Le Chatelier principle, see Pavelka and Grmela (2016), that guarantees stability. Instability can be thus anticipated in the non-convex regions.

[8]The state variables are $(\rho, \boldsymbol{u}, s)$ in the energetic representation or $(\rho, \boldsymbol{u}, e_{\mathrm{tot}})$ in the entropic representation.

The aim is to study non-equilibrium thermodynamic description of stability, metastability and instability. The analysis is formulated within a recent framework of *Constitutive Relation thermodynamics* (CR-thermodynamics) developed by Grmela (2017), which is a form of mesoscopic multiscale thermodynamics. Compared to the original paper by Grmela (2017), we use the MTL functions instead of the thermodynamic potentials for we can then consistently use the same form of the Legendre transformation. Another difference is that the extra variable is denoted by $\mathbb{T}_\delta^*$ instead of $\mathbb{T}_\delta$ so that the usual meaning of the flux is kept.

3.3.1 Promoting conjugate stress to a new state variable

The goal is to promote the thermodynamic flux $\mathbb{T}_\delta$ to an independent state variable. Since we want to preserve the form of the evolution equation for the momentum density (3.34) so that $\mathbb{T}_\delta$ remains on the right-hand side, we cannot promote $\mathbb{T}_\delta$ itself. If we did so, there would be some conjugate quantity in a form of a derivative of a potential with respect to $\mathbb{T}_\delta$ as is obvious from (3.2). For that reason, conjugate flux $\mathbb{T}_\delta^*$ (conjugate stress) is chosen as the new variable.

As is usual in non-equilibrium thermodynamics, see Grmela et al. (2015), the dissipation can be moved onto a higher (more detailed) level of description, i.e., into the evolution equation for the extra state variable. Dissipative evolution of the momentum density can be then recovered by letting the extra variable relax. The reversible coupling between the original state variables and the extra state variable is required to be antisymmetric in order to fulfill the Onsager–Casimir reciprocal relations, see Casimir (1945); Öttinger (2005); Pavelka et al. (2014). Following Grmela (2017), we write the evolution equations for the extended hydrodynamics of (3.34) as

$$\frac{\partial \boldsymbol{u}}{\partial t} = \left(\frac{\partial \boldsymbol{u}}{\partial t}\right)_{\text{rev}} + \Gamma^\intercal\left(\mathbb{T}_\delta^{**}\right), \tag{3.41a}$$

$$\frac{\partial \mathbb{T}_\delta^*}{\partial t} = -\Gamma(\boldsymbol{u}^*) + \Xi^*_{\mathbb{T}_\delta^{**}}. \tag{3.41b}$$

To close the evolution equations, we must supply new MTL function $\Psi^{(EH\to E)}$ that drives the evolution of the extended hydrodynamics toward equilibrium. Specification of the MTL function $\Psi^{(EH\to E)}$ determines the conjugate variables as the corresponding derivatives, i.e., $\boldsymbol{u}^* = \Psi_{\boldsymbol{u}}^{(EH\to E)}$ and $\mathbb{T}_\delta^{**} = \mathbb{T}_\delta = \Psi_{\mathbb{T}_\delta^*}^{(EH\to E)}$. We can identify $\mathbb{T}_\delta^{**}$ with $\mathbb{T}_\delta$ because the generalized Legendre transformation is idempotent (second application of the transformation restores the original functional). Evolution equations (3.41) represent evolution on the extended level of hydrodynamics. Alternatively, the extra evolution equation (3.41b) can be interpreted as a numerical scheme for the constitutive relation (3.22).

Furthermore, the parity of $\mathbb{T}_\delta$ with respect to the time reversal has changed, see Pavelka et al. (2014) for the notion of parity in this context. In the original (non-extended) time evolution (3.34), $\mathbb{T}_\delta$ was odd as it generated the irreversible evolution. Now, the time evolution (3.41) has another Hamiltonian part

$$\begin{pmatrix} 0 & \Gamma^\intercal \\ -\Gamma & 0 \end{pmatrix}\begin{pmatrix} \boldsymbol{u}^* \\ \mathbb{T}_\delta \end{pmatrix},$$

generated by a skew-symmetric operator.[9] Since Hamiltonian dynamics is reversible, $\mathbb{T}_\delta^{**}$ and consequently $\mathbb{T}_\delta$ are both even. MTL functions and dissipation potentials are assumed to be even with respect to the time reversal so $\mathbb{T}_\delta^*$ is also even as it is conjugate with respect to them. Therefore, in contrast with (3.34), evolution equation (3.41a) is now reversible. The physical reason is that we now have a more detailed description of the stress. Additionally, the dissipation was indeed moved to (3.41b) as the first term is reversible and the second one irreversible. This means that by moving to a more detailed level of description, parity of the quantity promoted to an extra state variable may change. The quantity becomes independent and is no longer enslaved by the constitutive relation valid before the promotion. As a result, irreversible terms may become reversible.

3.3.2 Specification of the MTL function

The conjugate stress $\mathbb{T}_\delta^*$ will be now specified more precisely. The relation between $\mathbb{T}_\delta$ and $\mathbb{T}_\delta^*$ is a Legendre transformation which can be expressed as

$$\mathbb{T}_\delta = \Psi^{(EH\to E)}_{\mathbb{T}_\delta^*}, \qquad \text{or} \qquad \frac{\partial}{\partial \mathbb{T}_\delta^*}\left(\langle \mathbb{T}_\delta, \mathbb{T}_\delta^*\rangle - \Psi^{(EH\to E)}\right) = \mathbb{0}. \tag{3.42}$$

The transformation is carried out with respect to the MTL function

$$\Psi^{(EH\to E)} =_{\text{def}} S^{(EH\to E)} - \frac{1}{T_0}E^{(EH\to E)} + \frac{\mu_0}{T_0}M^{(EH\to E)}, \tag{3.43}$$

that drives the extended hydrodynamics toward equilibrium. All quantities with the $(EH \to E)$ superscript depend on the hydrodynamic fields $\boldsymbol{x}^{(CH)} =_{\text{def}} (\rho, \boldsymbol{u}, e_{\text{tot}})$ and on the conjugate stress tensor $\mathbb{T}_\delta^*$. Quantities $E^{(EH\to E)}$, $S^{(EH\to E)}$ and $M^{(EH\to E)}$, which have been left undetermined so far, are the building blocks of the corresponding MTL function and they reflect the particular nature of the physical system.

Let us consider at least one possible choice of $\Psi^{(EH\to E)}$. Within the kinetic theory, see de Groot and Mazur (1984), kinetic energy of particles is equal to the sum of kinetic energy of the overall motion $|\boldsymbol{u}|^2/(2\rho)$ and pressure. Thus, the deviatoric part of the stress tensor does not contribute to the energy (when neglecting long-range pair interactions). On the other hand, additional knowledge expressed as the extra state variable reduces the entropy and the entropy on the (EH) level is therefore lower than the entropy on the level of classical hydrodynamics (CH). The first approximation of the (EH) entropy then is

$$S^{(EH\to E)} =_{\text{def}} S^{(CH\to E)} - \frac{1}{2}\int \beta\,|\mathbb{T}_\delta^*|^2\,\mathrm{d}\boldsymbol{r} = \int s\left(\rho, e_{\text{tot}} - \frac{|\boldsymbol{u}|^2}{2\rho}\right) - \frac{1}{2}\beta\,|\mathbb{T}_\delta^*|^2\,\mathrm{d}\boldsymbol{r}, \tag{3.44}$$

similarly as in the Extended Irreversible Thermodynamics, see Jou et al. (2010). Coefficient β is positive so that the entropy is concave. Energy and mass on the (EH) level are the same as on the (CH) level, thus the MTL function driving evolution of the extended hydrodynamics toward equilibrium is

$$\Psi^{(EH\to E)}\left(\rho, \boldsymbol{u}, e_{\text{tot}}, \mathbb{T}_\delta^*\right) =_{\text{def}} \Psi^{(CH\to E)}\left(\rho, \boldsymbol{u}, e_{\text{tot}}\right) - \frac{1}{2}\int \beta\,|\mathbb{T}_\delta^*|^2\,\mathrm{d}\boldsymbol{r}, \tag{3.45}$$

[9] The corresponding Poisson bracket does not have to satisfy the Jacobi identity for every Γ, see Grmela (2017) for details.

from which follows that

$$\mathbb{T}_\delta = \Psi^{(EH\to E)}_{\mathbb{T}^*_\delta} = -\beta\mathbb{T}^*_\delta. \tag{3.46}$$

In summary, for the particular choice of the entropy (3.44), the conjugate stress tensor $\mathbb{T}^*_\delta$ is proportional to the standard stress tensor $\mathbb{T}_\delta$ and the evolution equations (3.41) for the constitutive relation (3.22) and the operator Γ defined by (3.17) read

$$\frac{\partial \boldsymbol{u}}{\partial t} = -\operatorname{div}\left(\frac{\boldsymbol{u}\otimes\boldsymbol{u}}{\rho}\right) - \nabla p + \operatorname{div}\mathbb{T}_\delta, \tag{3.47a}$$

$$-\frac{1}{\beta}\frac{\partial \mathbb{T}_\delta}{\partial t} = -\mathbb{D} + \left[a(1+b|\mathbb{T}_\delta|^2)^n + c\right]\mathbb{T}_\delta. \tag{3.47b}$$

The second equation can be apparently interpreted as the time derivative regularization of the original constitutive relation.

Note that the MTL function $\Psi^{(EH\to E)}$ plays a role closely related to the entropy production as can be seen from

$$\dot\Psi^{(EH\to E)} = \left\langle \Psi^{(EH\to E)}_{\mathbb{T}^*_\delta}, \left(\frac{\partial \mathbb{T}^*_\delta}{\partial t}\right)_{\text{irr}} \right\rangle = \left\langle \mathbb{T}_\delta, \Xi^*_{\mathbb{T}_\delta} \right\rangle, \tag{3.48}$$

where we used (3.41b). For monotonous dissipation potential Ξ^*, the expression is non-negative and the second law of thermodynamics is satisfied.

3.3.3 Duality between $\mathbb{T}_\delta$ and $\mathbb{T}^*_\delta$

Omitting the density and the energy as the arguments, the conjugate MTL function $\Psi^{*,(EH\to E)}$ can be constructed as

$$\Psi^{*,(EH\to E)}(\boldsymbol{u}^*, \mathbb{T}_\delta) = \langle \mathbb{T}^*_\delta(\mathbb{T}_\delta), \mathbb{T}_\delta\rangle - \Psi^{(EH\to E)}\left(\boldsymbol{u}, \mathbb{T}^*_\delta(\mathbb{T}_\delta)\right) \tag{3.49}$$

where $\mathbb{T}^*_\delta(\mathbb{T}_\delta)$ is the solution to (3.42), i.e., the relation (3.46) for the particular choice of entropy (3.44). Conversely, the Legendre transformation

$$\mathbb{T}^*_\delta = \Psi^{*,(EH\to E)}_{\mathbb{T}_\delta}, \qquad \text{or} \qquad \frac{\partial}{\partial \mathbb{T}_\delta}\left(\langle \mathbb{T}_\delta, \mathbb{T}^*_\delta\rangle - \Psi^{*,(EH\to E)}\right) = \mathbb{0} \tag{3.50}$$

leads back to the original MTL function,

$$\Psi^{(EH\to E)}(\boldsymbol{u}, \mathbb{T}^*_\delta) = \langle \mathbb{T}_\delta(\mathbb{T}^*_\delta), \mathbb{T}^*_\delta\rangle - \Psi^{*,(EH\to E)}\left(\boldsymbol{u}^*, \mathbb{T}_\delta(\mathbb{T}^*_\delta)\right), \tag{3.51}$$

where $\mathbb{T}_\delta(\mathbb{T}^*_\delta)$ is the solution to (3.50). The Legendre duality between $\mathbb{T}_\delta$ and $\mathbb{T}^*_\delta$ has been thereby established.

3.3.4 Fast reducing evolution

The thermodynamic extension allows us to identify the reducing evolution of $\mathbb{T}^*_\delta$ that leads back to the classical hydrodynamics, that is, the fast evolution that reduces to the original hydrodynamic evolution of variables $\boldsymbol{x}^{(CH)}$. Equation (3.41b) can be rewritten as

$$\frac{\partial \mathbb{T}^*_\delta}{\partial t} = -\frac{\partial}{\partial \mathbb{T}_\delta}\left(\langle \Gamma(\boldsymbol{u}^*), \mathbb{T}_\delta\rangle - \Xi^*(\mathbb{T}_\delta)\right)\Big|_{\boldsymbol{u}^*=\Psi^{(EH\to E)}_{\boldsymbol{u}};\, \mathbb{T}_\delta=\Psi^{(EH\to E)}_{\mathbb{T}^*_\delta}} = -\Psi^{(EH\to CH)}_{\mathbb{T}_\delta}, \tag{3.52}$$

where we defined the MTL function driving evolution from extended hydrodynamics to classical hydrodynamics

$$\Psi^{(EH\to CH)}(\mathbb{D},\mathbb{T}_\delta) =_{\text{def}} \langle \mathbb{D},\mathbb{T}_\delta\rangle - \Xi^*(\mathbb{T}_\delta), \tag{3.53}$$

with $\mathbb{D} = \Gamma(\boldsymbol{u}^*)$, and it will be referred to as the *reducing MTL function*. Equation (3.52) means that the conjugate stress $\mathbb{T}^*_\delta$ evolves in the direction of steepest descent of $\Psi^{(EH\to CH)}$. MTL function (3.53) generates the Legendre transformation from Ξ^* to Ξ as

$$\Psi^{(EH\to CH)}_{\mathbb{T}_\delta} = \mathbb{0}, \tag{3.54}$$

which is equivalent to (3.35). The constitutive relation is thus recovered after the extra variable $\mathbb{T}^*_\delta$ has relaxed to a state enslaved by the slow variable $\boldsymbol{u}$.

Since $\mathbb{T}_\delta = \Psi^{(EH\to E)}_{\mathbb{T}^*_\delta}$ and using (3.52), the reducing evolution can be alternatively formulated as

$$\frac{\partial \mathbb{T}_\delta}{\partial t} = -\left\langle \Psi^{(EH\to E)}_{\mathbb{T}^*_\delta\mathbb{T}^*_\delta}, \Psi^{(EH\to CH)}_{\mathbb{T}_\delta}\right\rangle. \tag{3.55}$$

Further, compatibility of the reducing evolution (3.52) with the second law of thermodynamics is guaranteed by concavity of $\Psi^{(EH\to E)}$

$$\dot\Psi^{(EH\to CH)} = -\int \Psi^{(EH\to CH)}_{\mathbb{T}_\delta} : \Psi^{(EH\to E)}_{\mathbb{T}^*_\delta\mathbb{T}^*_\delta}\Psi^{(EH\to CH)}_{\mathbb{T}_\delta}\,\mathrm{d}\boldsymbol{r} \geq 0. \tag{3.56}$$

Note that only derivatives with respect to the fast variable are taken into account because only evolution of the fast variable is considered in the reducing evolution.

On the other hand, dissipation potentials Ξ and Ξ^* are not convex, hence

$$\dot\Psi^{(CH\to E)} = \left\langle \Psi^{(CH\to E)}_{\boldsymbol{u}}, \Xi^*_{\boldsymbol{u}^*}\big|_{\boldsymbol{u}^*=\Psi^{(CH\to E)}_{\boldsymbol{u}}}\right\rangle = \langle \boldsymbol{u}^*, \Gamma^\mathsf{T}(\Xi_\mathbb{D})\rangle = \langle \mathbb{D},\Xi_\mathbb{D}\rangle, \tag{3.57}$$

does not need to have a definite sign and the evolution on the hydrodynamic level can have apparent negative entropy production, compare with (3.48). Indeed, the slope of Ξ^* could be negative for positive values of $|\mathbb{D}|$. The way out of such a problem is the lift to extended hydrodynamics, where the entropy production keeps its positivity. In other words, apparent negative entropy production indicates evolution of instability (phase transition) and can be regarded as an invitation to a higher (more detailed) level of description.

After having demonstrated how the constitutive relation can be interpreted as a consequence of a more detailed evolution, study of behavior of the more detailed evolution gives information about the CR-stability of the constitutive relation itself. The constitutive relation is stable if any perturbation decreases in time, it is metastable if only small perturbations decrease in time, and it is unstable if no perturbation decreases in time. The relation between CR-stability and the usual mathematical concept of stability is discussed in Section 3.4.2.

3.3.5 Alternative forms of the extension

Even though evolution equations (3.41) are relatively simple and useful for qualitative analysis of CR-stability carried out in Section 3.4.1, they are not objective due to the presence of (non-objective) partial time derivative of the conjugate stress $\mathbb{T}^*_\delta$. Moreover, the Jacobi identity is not satisfied for this system of equations, which was checked using the program by Kröger and Hütter (2010). Hence,

the evolution equations have to be regarded rather as a toy model useful for explaining the construction of the extension and the CR-stability implications.

The extension can be made more physically sound by choosing a better operator Γ. Such a choice, however, must be accompanied by another choice of the quantity to be promoted to an extra state variable. For example, the choice[10]

$$\Gamma^\top(\mathbb{c}^*) = -T_0[(\nabla\mathbb{c})^\top]\mathbb{c}^* - T_0\,\mathrm{div}\,(\mathbb{c}^*\mathbb{c}^\top) - T_0\,\mathrm{div}\,((\mathbb{c}^*)^\top\mathbb{c})\,, \tag{3.58}$$

with the conformation tensor $\mathbb{c}$ being the new variable leads to the adjoint operator

$$\Gamma(\boldsymbol{u}^*) = -T_0[\nabla\mathbb{c}]\boldsymbol{u}^* + T_0(\nabla\boldsymbol{u}^*)\mathbb{c} + T_0\mathbb{c}(\nabla\boldsymbol{u}^*)^\top. \tag{3.59}$$

It should be stressed that this extension is considered in the energetic representation, where the entropy density s is among the state variables instead of the total energy density e_{tot}. We shall refer to this extension as to the *conformation tensor* (CT) level.

Analogously to (3.41), the evolution equation for the extra variable is

$$\frac{\partial\mathbb{c}}{\partial t} = -\Gamma(\boldsymbol{u}^*) + \frac{\partial\Xi^*}{\partial\mathbb{c}^*} = T_0[\nabla\mathbb{c}]\boldsymbol{u}^* - T_0(\nabla\boldsymbol{u}^*)\mathbb{c} - T_0\mathbb{c}(\nabla\boldsymbol{u}^*)^\top + \frac{\partial\Xi^*}{\partial\mathbb{c}^*}. \tag{3.60}$$

In the energetic representation, total entropy depends only on the entropy density, so the conjugate momentum $\boldsymbol{u}^*$ given by the corresponding derivative of MTL function (3.43) is

$$\boldsymbol{u}^* = \Psi_{\boldsymbol{u}}^{(CT\to E)} = -\frac{1}{T_0}E_{\boldsymbol{u}} = -\frac{1}{T_0}\frac{\boldsymbol{u}}{\rho} = -\frac{1}{T_0}\boldsymbol{v}. \tag{3.61}$$

The evolution equation (3.60) then becomes

$$\overset{\triangledown}{\mathbb{c}} = \frac{\partial\Xi^*}{\partial\mathbb{c}^*}, \tag{3.62}$$

where $\overset{\triangledown}{\mathbb{c}} =_{\mathrm{def}} \frac{\partial\mathbb{c}}{\partial t} + [\nabla\mathbb{c}]\boldsymbol{v} - \mathbb{L}\mathbb{c} - \mathbb{c}\mathbb{L}^\top$ is the upper convected (Oldroyd) derivative, $\mathbb{L} =_{\mathrm{def}} \nabla\boldsymbol{v}$ being the velocity gradient. Note that the upper convected derivative is generated by the reversible part of the evolution equation (3.60). Due to this derivative the extended evolution is objective. It also fulfills the Jacobi identity, hence is Hamiltonian, see Grmela (1993). It seems that objectivity is in tight relation with the validity of the Jacobi identity. Evolution equation (3.62) is the analogue of (3.41).

Equivalently as in Section 3.2.1, from the Legendre transformation

$$\frac{\partial}{\partial\boldsymbol{u}^*}\left(\langle\boldsymbol{u}^*, \Gamma^\top(\mathbb{c}^*)\rangle - \Xi(\boldsymbol{u}^*)\right) = \mathbb{0}, \tag{3.63}$$

we can find the solution $\boldsymbol{u}^* = \tilde{\boldsymbol{u}}^*(\mathbb{c}^*)$ and then define the conjugate dissipation potential Ξ^*

$$\Xi^*(\mathbb{c}^*) =_{\mathrm{def}} \left\langle\Gamma(\tilde{\boldsymbol{u}}^*(\mathbb{c}^*)), \mathbb{c}^*\right\rangle - \Xi\left(\tilde{\boldsymbol{u}}^*(\mathbb{c}^*)\right). \tag{3.64}$$

The relation between $\mathbb{c}$ and $\mathbb{c}^*$ can be obtained through the Legendre transformation with respect to the MTL function $\Psi^{(CT\to E)}$, see Section 3.3.3. Analogously

[10] Transposition of a third-order tensor $\mathcal{S}$ is defined as $\boldsymbol{v}\cdot\mathcal{S}^\top\mathbb{A} = \mathcal{S}\boldsymbol{v} : \mathbb{A}$.

to (3.43), the particular MTL function would be constructed from entropy, energy and total mass, see Sarti and Marrucci (1973); Grmela (1993), and it would depend on the class of materials under consideration.

Defining reducing MTL function

$$\Psi^{(CT\to CH)} =_{\text{def}} \langle \Gamma(\boldsymbol{u}^*), \mathbb{c}^* \rangle - \Xi^*(\mathbb{c}^*), \tag{3.65}$$

evolution equation (3.60) can be rewritten as

$$\frac{\partial \mathbb{c}}{\partial t} = -\frac{\partial}{\partial \mathbb{c}^*} \Psi^{(CT\to CH)}, \tag{3.66}$$

and the analysis of the second law of thermodynamics could proceed exactly as in Section 3.3.4.

This alternative extension is closer to the common modeling of the the shear banding as viscoelastic models are usually employed, see the discussion in Section 3.2. Choosing a different operator Γ, one can also derive evolution equations for Reynolds stress or weakly non-local vorticity, that can be found in Grmela et al. (2004); Pavelka et al. (2016). For simplicity, we shall however stick to the extension where the extra state variable is the conjugate stress tensor $\mathbb{T}^*_\delta$.

3.4 Interpretation of CR-stability

3.4.1 Thermodynamic interpretation

The reducing MTL function $\Psi^{(EH\to CH)}$ is plotted in Figure 3.5 for several values of $|\mathbb{D}|$.

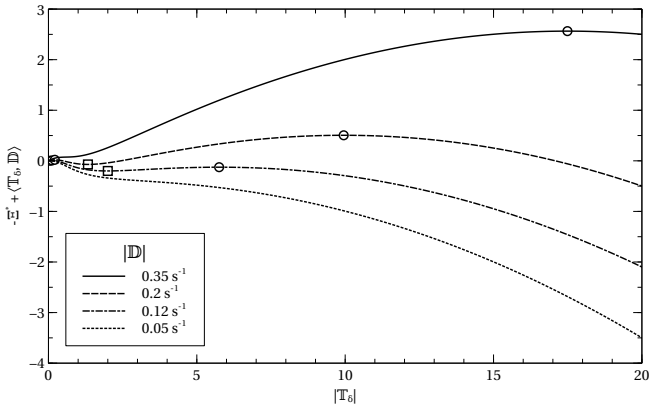

Figure 3.5: Reducing MTL function $\Psi^{(EH\to CH)}$ given by (3.53). For low values of the thermodynamic force $|\mathbb{D}|$, the function has only one local maximum near the origin $|\mathbb{T}_\delta| = 0\,\text{Pa}$. As $|\mathbb{D}|$ increases, a second local maximum develops in region with higher stress $|\mathbb{T}_\delta|$. For even higher values, the second maximum becomes higher than the first maximum and eventually, the first maximum disappears. Local maxima are indicated by circles ($\circ$) while local minima by squares ($\square$).

The curves plotted in the figure correspond to the following different regimes of the reducing evolution, indicated also in Figure 3.3.

I For low values of $|\mathbb{D}|$ (Regime I in Figure 3.3), there is only one local maximum near the origin $|\mathbb{T}_\delta| = 0\,\mathrm{Pa}$, as the curve for $|\mathbb{D}| = 0.05\,\mathrm{s}^{-1}$ indicates. Since $\Psi^{(EH\to E)}$ has to be chosen concave, see (3.56), from (3.55) follows then that the stress evolves in the direction of the derivative of the reducing MTL function $\Psi^{(EH\to CH)}$. In other words, if the derivative is positive, the stress increases, and if it is negative, it decreases. Thus, if $|\mathbb{T}_\delta|$ is initially to the left of the local maximum, the derivative is positive and it tends to the local maximum. On the other hand, if it is to the right, the derivative is negative, and again it tends to the maximum. Consequently, the evolution is CR-stable as $|\mathbb{T}_\delta|$ is always attracted to the local (and global) maximum.

II As $|\mathbb{D}|$ increases (Regime II), another local maximum appears for some higher stress (curve for $|\mathbb{D}| = 0.12\,\mathrm{s}^{-1}$). Similarly as in Regime I, this new local maximum attracts $|\mathbb{T}_\delta|$ from its neighborhood. However, since the first maximum is higher, settling of $|\mathbb{T}_\delta|$ in the second maximum can be seen as a CR-metastable state. With a sufficient fluctuation, $|\mathbb{T}_\delta|$ will end up in the first (higher) maximum. Moreover, a local minimum appears between the two local maxima. The local minimum corresponds to a CR-unstable state since $|\mathbb{T}_\delta|$ is attracted to the local maxima. This can be seen from (3.55) and from the signs of the derivative of the reducing MTL function to the left and to the right of the local minimum.

III For even higher values of $|\mathbb{D}|$ (Regime III and curve $|\mathbb{D}| = 0.2\,\mathrm{s}^{-1}$), the second maximum becomes higher than the first one. The first maximum thus becomes CR-metastable while the second becomes CR-stable. The local minimum is still located between the maxima, and although it is a stationary point ($\dot{\mathbb{T}}_\delta = \mathbb{0}$), it is CR-unstable since any arbitrarily small fluctuation would attract the stress toward one of the maxima. Note that the transient state between Regimes II and III, when the two local maxima have the same height, corresponds to the value of $|\mathbb{D}|$ selected by the Maxwell lever rule, see Section 3.2.

IV Finally, the first local maximum disappears (as well as the local minimum) for even higher values of $|\mathbb{D}|$ (Regime IV and curve $|\mathbb{D}| = 0.35\,\mathrm{s}^{-1}$) and the second maximum becomes the globally CR-stable state.

The just described dynamics of the stress tensor can be also seen in Figure 3.3. Regime I (low values of $|\mathbb{D}|$) corresponds to the part of curve $A-B$ left of point D where only one $\mathbb{T}_\delta = \Xi_{\mathbb{D}}$ is possible. Regime II (one CR-stable, one CR-unstable and one CR-metastable state) is indicated in the figure as well. The upper solid curve is the CR-stable state, the lower solid curve is the CR-metastable state and the dashed curve is the CR-unstable state. Regime III (one CR-metastable, one CR-unstable and one CR-stable) is described analogically. Finally, Regime IV has only one CR-stable state, right of point C in the figure. The reducing evolution (3.55) can therefore distinguish CR-stable, CR-metastable and CR-unstable states in Figure 3.3. The analysis is similar to the treatment of phase transitions in equilibrium thermodynamics, see Landau and Lifshitz (1968); Callen (1985). For that reason, we can refer to our case as to a kind of *dissipative phase transition.*

Let us now return to the experimental data in Figure 3.1 and to the question why the stress is discontinuous. We start in Regime I, where the stress is determined uniquely. After passing to Regime II, another possible state appears. The stress still evolves continuously as it occurs in the CR-stable state that belongs to the global maximum of the reducing MTL function $\Psi^{(EH\to CH)}$. Progressing further to Regime III, the CR-stable state becomes CR-metastable. If the experiment is conducted carefully enough and the fluctuations are small, the stress might be still found on the metastable branch $B-C$ in Figure 3.3. Once past point C, the first local maximum disappears, and the stress does not have any other option than to jump to the CR-stable state and that is why it evolves *discontinuously*.

Moreover, it might be expected that when coming back from high shear rates, shear stress can go as low as to point D in Figure 3.3. Then, it would jump to the CR-stable branch. One should thus observe *hysteresis* indicated in Figure 3.1. We are not aware of such a backward experiment having been carried out, but modeling of hysteresis by means of introducing a new evolution equation is common, see Kubin and Poirier (1988). Of course, if the fluctuations arising from the experiment are large, only the CR-stable state would be selected and the dynamics would follow the Maxwell lever rule without any hysteresis.

On the other hand, when slowly varying $|\mathbb{T}_\delta|$, there is always a unique value of $|\mathbb{D}|$ determined by the slope of the dissipation potential Ξ^* in Figure 3.2. Since the slope varies continuously, *no jump of the shear rate* is observed in the experiment.

3.4.2 Regularized constitutive relation stability

The same dynamical behavior can be concluded directly from the stability of the regularized constitutive relation (3.47b). Its one-dimensional counterpart with a general conjugate dissipation potential Ξ^* reads

$$\frac{1}{\beta}\frac{\partial|\mathbb{T}_\delta|}{\partial t} = |\mathbb{D}| - \Xi^*_{|\mathbb{T}_\delta|}\left(|\mathbb{T}_\delta|\right). \tag{3.67}$$

In the shear rate controlled experiment, we assume that $|\mathbb{D}| = |\mathbb{D}|\,(t)$ is given. Equation (3.67) is then a non-autonomous ordinary differential equation with stationary points $|\mathbb{D}| - \Xi^*_{|\mathbb{T}_\delta|}\left(|\mathbb{T}_\delta|\right)$. It can equivalently written as an extended autonomous system

$$\frac{\partial|\mathbb{T}_\delta|}{\partial t} = \beta\left[|\mathbb{D}|\,(\tau) - \Xi^*_{|\mathbb{T}_\delta|}\left(|\mathbb{T}_\delta|\right)\right], \tag{3.68a}$$

$$\frac{\partial\tau}{\partial t} = 1. \tag{3.68b}$$

From this system, we can deduce the phase field in the $|\mathbb{D}|$–$|\mathbb{T}_\delta|$ plane. In Figure 3.6, we show the phase field for the particular choice of the dual dissipation potential (3.30). We can easily see that the solutions are quickly (depending on the parameter β) attracted toward the increasing parts of the constitutive relation and repelled from the decreasing part. In other words, the decreasing part is unstable while the increasing parts are asymptotically stable in the usual mathematical sense. This leads to the jumps (and possibly hysteresis) in the values of the stress $|\mathbb{T}_\delta|$ when changing $|\mathbb{D}|$.

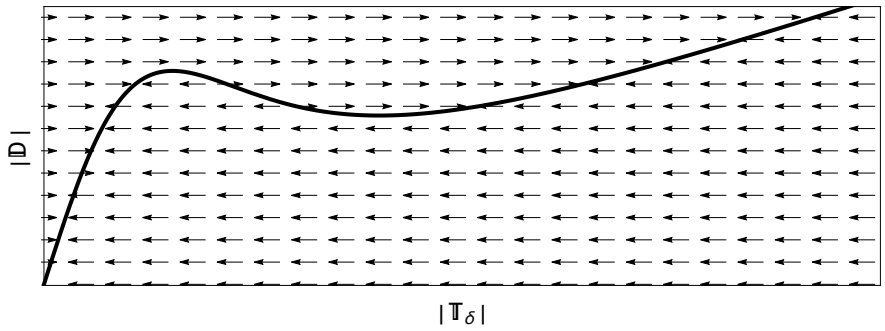

Figure 3.6: Constitutive relation generated by the dual dissipation potential (3.30) with parameters $a = 1$, $b = 1$, $c = 0.12$ and $n = -2$, and the corresponding phase field. Vectors are rescaled to have uniform size.

On the other hand, if we prescribe $|\mathbb{T}_\delta| = |\mathbb{T}_\delta|(t)$ (shear stress controlled experiment) and we further assume that its time derivative is small enough, (3.67) reduces back to the original constitutive relation. In this case, there are no jumps.

In this case, the CR-stability analysis leads to the same conclusions as the usual stability analysis for ordinary differential equations provided the evolution of the extra state variable (here, the conjugate stress) is assumed much faster than the evolution of the remaining variables.

3.5 Non-smooth dissipation potentials

This section addresses yield stress behavior instead of S-shaped curves. It is included because we believe that non-smoothness of dissipation potentials might be a natural addition to the discussion of non-convexity.

Inspired by Rajagopal and Srinivasa (2004), dissipation potential that exhibits the presence of *yield stress* (activation criterion) is, for example,

$$\Xi(\mathbb{D}) = \int \left(\alpha |\mathbb{D}| + \frac{1}{2}\beta |\mathbb{D}|^2 \right) \mathrm{d}\boldsymbol{r}, \tag{3.69}$$

where α and β are positive constants, see Figure 3.7a. Coefficient α corresponds to the value of the yield stress. For stresses lower than the yield stress, there is no corresponding $|\mathbb{D}|$. More exactly, the only value of $|\mathbb{D}|$ matching these stresses is zero.

Dissipation potential (3.69) is not smooth at $|\mathbb{D}| = 0$, where it has no derivative. Therefore, Legendre transformation to Ξ has to be generalized by means of subdifferentials, see e.g. Roubíček (2005),

$$\mathbb{T}_\delta \in \partial\Xi, \tag{3.70}$$

where $\partial\Xi$ is the set of slopes of all hyperplanes touching Ξ at a point $\mathbb{D}$. When constructing the subdifferential we assume that Ξ is convex and continuous in a neighborhood of the point of non-smoothness. Continuity then guarantees that the set is non-empty as a consequence of the Hahn–Banach theorem, as commented in Roubíček (2005). Non-smoothness in non-convex regions can be handled as in Remark 5.8 in Roubíček (2005). When Ξ is smooth, i.e., it has standard functional derivative, inclusion (3.70) becomes equality and the Legendre transformation restores its usual form (3.29).

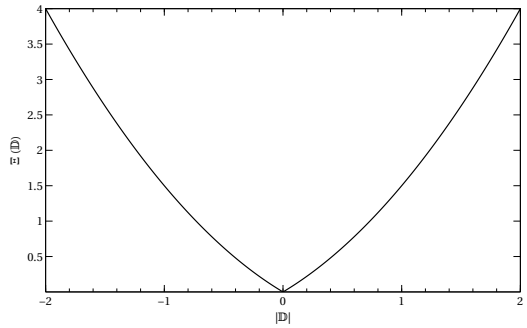

(a) Dissipation potential Ξ exhibiting yield stress. The potential is not differentiable at $|\mathbb{D}| = 0$.

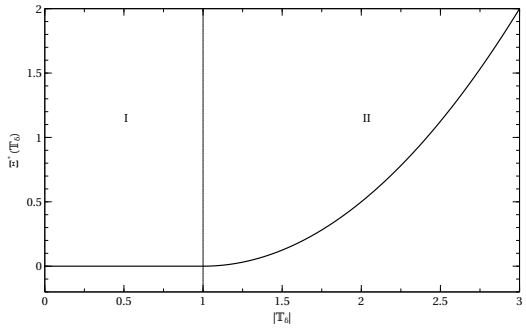

(b) Conjugate dissipation potential Ξ^* obtained by Legendre transformation using subdifferentials from (3.69). Note that it is smooth everywhere in contrast to Ξ. It is flat near the origin and grows for higher stresses.

Figure 3.7: Dissipation potential (3.69) and its conjugate, $\alpha = \beta = 1$.

Inclusion (3.70) can be interpreted as the following problem: For a given $\mathbb{T}_\delta$ find all $\mathbb{D}$ such that the inclusion is fulfilled. Solution to the problem is a graph $\mathbb{D}(\mathbb{T}_\delta)$. It can be seen in Figure 3.7a that for sufficiently high stresses (higher than the yield stress), there is always a non-zero $|\mathbb{D}|$ for which $\mathbb{T}_\delta = \Xi_{\mathbb{D}}$. However, only the set $\partial\Xi$ at $|\mathbb{D}| = 0$ contains the sub-critical stresses. This means that when the stress is lower than the yield stress, only $|\mathbb{D}| = 0$ is the solution to the problem. We will return to this point graphically later on.

The conjugate dissipation potential is defined as

$$\Xi^*(\mathbb{T}_\delta) = \langle \mathbb{D}(\mathbb{T}_\delta), \mathbb{T}_\delta \rangle - \Xi\left(\mathbb{D}(\mathbb{T}_\delta)\right), \tag{3.71}$$

and it is depicted in Figure 3.7b. Since the conjugate dissipation potential is smooth, the backward Legendre transformation is carried out with derivatives as usually.

Let us now have a look at these dissipation potentials from the perspective of the multiscale mesoscopic thermodynamics as in Section 3.3. The reducing MTL function is again $-\Xi^*(\mathbb{T}_\delta) + \langle \mathbb{T}_\delta, \mathbb{D} \rangle$ and it is plotted in Figure 3.8.

Again, the stress tends to the maximum of the MTL function for the given $|\mathbb{D}|$. When $|\mathbb{D}| = 0$, the absolute value of the stress can end up anywhere between 0 and 1 as the function is flat in that region. For higher values of $|\mathbb{D}|$, the maximum is located to the right of $|\mathbb{T}_\delta| = 1$. In other words, for non-zero $|\mathbb{D}|$, stress has to be higher than the threshold $|\mathbb{T}_\delta| = 1$. The material thus exhibits yield stress behavior and its irreversible evolution is CR-stable as could be expected since the dissipation potential Ξ is convex.

3.6 Critical heat flux

Nukiyama (1934) experimentally showed that by controlling the heat flux $\boldsymbol{q}$ from a hot platinum wire to boiling water, the temperature of the wire T jumps between the heating branch and the cooling branch and exhibits a hysteresis loop. Then, Drew and Mueller (1937) were able to control the temperature of the wire and

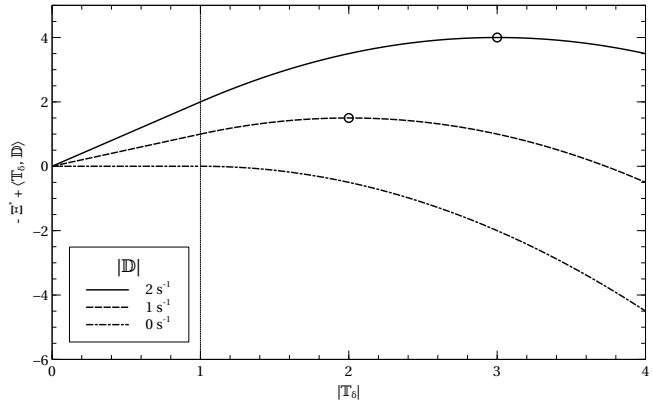

Figure 3.8: Reducing MTL function for the yield stress model with parameters $\alpha = \beta = 1$. Stress is attracted to the local maxima. For $|\mathbb{D}| = 0$, the region $0 \leq |\mathbb{T}_\delta| \leq 1$ is flat and the stress can be any of these values. For higher $|\mathbb{D}|$, there is a maximum above the yield stress value.

observed that the heat flux initially grows with the temperature, then decreases until it finally grows again. The boiling curve, heat flux versus temperature gradient (thermodynamic force) dependence, is then non-monotonous, see also Stosic (2005) and the book by Bergman et al. (2011). In Figure 3.9, we have plotted the experimental data by Nukiyama (1934) and fitted them with a relation of the form (3.22)

$$\boldsymbol{q} = \left[a \left(1 + b \left| \nabla T \right|^2 \right)^n + c \right] \nabla T, \tag{3.72}$$

with the temperature gradient ∇T being approximated as the difference between the temperature of the wire T and the temperature of the water T_{water}.

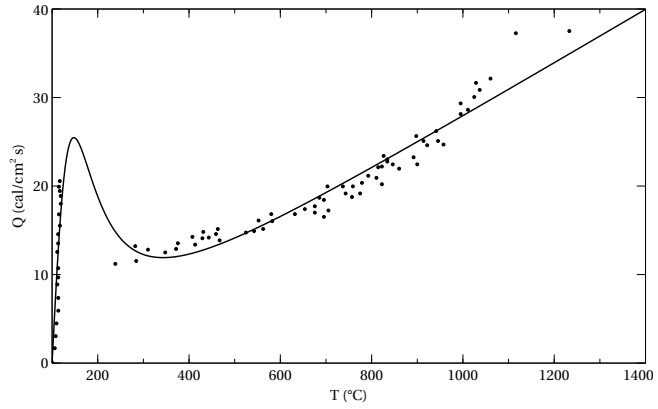

Figure 3.9: Boiling curve for a platinum wire of diameter $d = 0.14\,\text{mm}$ and boiling water $T_{\text{water}} = 100\,°\text{C}$ from Nukiyama (1934). The data were fitted with relation (3.72) with $a = 0.98$, $b = 0.00026$, $c = 0.03$ and $n = -1.41$.

As the flux–force relation can be described with an analogue of (3.22), it can be likewise generated by a non-convex dissipation potential. Such a formulation would then lead to implications on the CR-stability of the constitutive relation and the experimentally observed hysteresis. For instance, the CR-unstable part is inaccessible when controlling the heat flux while careful temperature variation

makes it available. This is analogous to the shear stress/rate behavior described in this paper. We hope to address this issue more explicitly in the near future.

3.7 Conclusion

The considered experimental data were fitted using the one-dimensional version of the constitutive relation (3.22), see Figure 3.1. The constitutive relation was then reformulated by means of dissipation potential $\Xi^*(\mathbb{T}_\delta)$ defined as (3.30). The dissipation potential is convex near equilibrium but loses convexity for higher stresses. Due to the loss of convexity the Legendre-like conjugate dissipation potential $\Xi(\mathbb{D})$ is multivalued. This reflects the observation in the shear flow experiment that the variation of the shear stress leads to a continuous evolution of the shear rate, $\mathbb{D} = \Xi^*_{\mathbb{T}_\delta}$ is determined uniquely. On the other hand, varying the shear rate leads to a jump, and possibly hysteresis, in the shear stress response, $\mathbb{T}_\delta = \Xi_{\mathbb{D}}$ is not unique. The phenomenon of critical heat flux can be addressed analogically.

Elevating the classical hydrodynamics to the extended hydrodynamics in Section 3.3, it can be shown which parts of the multivalued dissipation potential $\Xi(\mathbb{D})$ are CR-stable, CR-metastable or CR-unstable (with respect to perturbations of the constitutive relation). Then, it is also possible to identify between which branches of the dissipation potential the shear stress jumps, see Section 3.4.1. Our findings are compatible with the experimental data. In other words, instead of performing mathematical analysis of stability of the evolution equations with respect to the perturbations of the constitutive relation, we can simply construct dynamics of the fluctuations and then determine whether they grow or vanish.

4. Stability of implicitly constituted fluids

The area of *hydrodynamic stability* dates back to the late 19th century[1] when Reynolds (1883) conducted his famous experiment with steady Poiseuille flow in a circular pipe and Rayleigh (1879, 1887) studied the topic theoretically. Later, Orr (1907a,b) and Sommerfeld (1908) independently introduced an approach to explain the onset of turbulence and the fundamental equation of hydrodynamic stability, the *Orr–Sommerfeld equation*, was named after them. Another technique is the *energy method* developed by Reynolds (1895) and used by many others like Synge (1938), Kampé de Fériet (1949) or Serrin (1959), to name a few.

Considering inviscid fluid, plenty is known about its stability and there exist several criteria for determining if the flow is stable or not, see for example Reynolds (1883), Fjørtoft (1950) or Howard (1961). For a general review of the inviscid theory see for instance Drazin and Howard (1966). On the other hand, determining the stability in the viscous case is extremely difficult. The standard approach is to linearize the equations for the disturbance and then study their temporal evolution. This leads to the Orr–Sommerfeld equation that has to be solved numerically. Grosch and Salwen (1968) tackled the problem using expansions in orthogonal functions which proved very fruitful. Using expansions in the Chebyshev polynomials, Orszag (1971) was able to find the critical Reynolds number and also accurately computed first 32 least stable eigenvalues. Little known fact is, that he missed one eigenvalue which was later discovered by Dongarra et al. (1996). Contrary to this approach, Trefethen et al. (1993) argued for the usage of pseudospectra as the eigenvalue analysis is of no use in some types of flow.

There were also written several books on this topic and we refer to Lin (1955), Chandrasekhar (1961), Drazin and Reid (2004) or Schmid and Henningson (2001).

In this chapter, we are particularly interested in the stability of flows of implicitly constituted fluids of the type $\mathbb{D} = \mathfrak{f}(\mathbb{T}_\delta)$. First we derive the stationary Poiseuille base flow in a channel and then we conclude several results about the stability both theoretically and numerically. The central observation is that the decreasing part of the non-monotone flow curve always yields an unstable flow. This fact is in close agreement with the results obtained in Chapter 3 and we further support it with numerical simulations.

4.1 Plane Poiseuille flow

As already noted, we shall study counterpart of the plane Poiseuille flow, that is steady, fully developed flow due to constant pressure gradient in the z-direction between two fixed infinite parallel plates at $y = \pm L$, see Figure 4.1. On both plates, we shall impose the no-slip boundary condition.

[1] Certainly, people were fascinated by hydrodynamic stability and the consequent turbulence much earlier as it is clear, for example, from the sketches of Leonardo da Vinci.

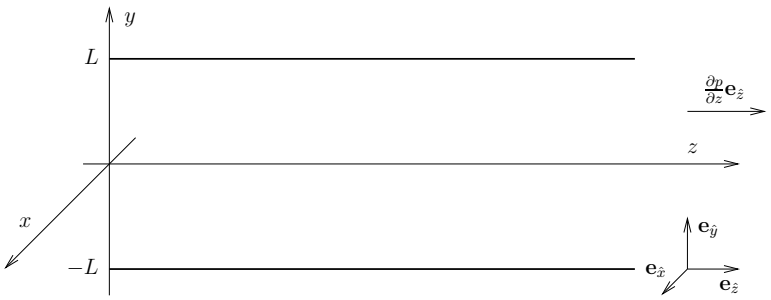

Figure 4.1: Problem geometry of the plane Poiseuille flow.

We are interested in flows of a fluids described by constitutive relation

$$\mathbb{D} = f\left(|\mathbb{T}_\delta|^2\right)\mathbb{T}_\delta, \tag{4.1}$$

where f is positive scalar function. This is a special subclass of constitutive relations of the type $\mathbb{D} = \mathfrak{f}(\mathbb{T}_\delta)$. The steady state solution will serve as the base flow for further stability investigation. In the derivation, we closely follow Málek et al. (2010).

Since the constitutive relation (4.1) automatically satisfies the incompressibility condition $\operatorname{Tr}\mathbb{D} = 0$, we do not need to enforce the balance of mass and the full system of governing equations in the absence of body forces reads

$$\rho\frac{\mathrm{d}\boldsymbol{v}}{\mathrm{d}t} = \operatorname{div}\mathbb{T}, \tag{4.2a}$$

$$\mathbb{D} = f\left(|\mathbb{T}_\delta|^2\right)\mathbb{T}_\delta, \tag{4.2b}$$

where ρ is the density and $\boldsymbol{v}$ is the velocity. Introducing dimensionless variables

$$\boldsymbol{x}^\star =_{\text{def}} \frac{\boldsymbol{x}}{L}, \qquad \boldsymbol{v}^\star =_{\text{def}} \frac{\boldsymbol{v}}{V}, \qquad t^\star =_{\text{def}} t\frac{V}{L}, \qquad \mathbb{T}^\star =_{\text{def}} \frac{\mathbb{T}}{T_{\text{char}}}, \qquad f^\star =_{\text{def}} \frac{f}{f_{\text{char}}},$$

where the characteristic velocity V, the characteristic stress T_{char} and the model-dependent characteristic value f_{char} need to be yet defined. Requiring further $\frac{f_{\text{char}}T_{\text{char}}L}{V} = 1$ leads to the non-dimensional version of the governing equations (4.2)

$$\frac{\mathrm{d}\boldsymbol{v}^\star}{\mathrm{d}t^\star} = \frac{1}{\mathcal{R}_1}\operatorname{div}\mathbb{T}^\star, \tag{4.3a}$$

$$\mathbb{D}^\star = f^\star\left(|\mathbb{T}^\star_\delta|^2\right)\mathbb{T}^\star_\delta, \tag{4.3b}$$

where $\mathcal{R}_1 =_{\text{def}} f_{\text{char}}\rho VL$ is the analogue of the Reynolds number. The characteristic stress is given by $T_{\text{char}} =_{\text{def}} \frac{V}{f_{\text{char}}L}$ and the characteristic velocity V will be specified later. Since we will only work with dimensionless quantities, we will omit the stars for the sake of simplicity.

We shall seek the stress field of the form

$$\mathbb{T}_\delta = T\left(\boldsymbol{e}_{\hat{z}}\otimes\boldsymbol{e}_{\hat{y}} + \boldsymbol{e}_{\hat{y}}\otimes\boldsymbol{e}_{\hat{z}}\right), \tag{4.4}$$

where $\boldsymbol{e}_{\hat{z}}$ and $\boldsymbol{e}_{\hat{y}}$ are unit vectors in the z and y coordinate directions, respectively, and $T = T(y)$ is a scalar function. Substituting (4.4) into (4.3b) yields

$$\mathbb{D} = f\left(2T^2\right)T\left(\boldsymbol{e}_{\hat{z}}\otimes\boldsymbol{e}_{\hat{y}} + \boldsymbol{e}_{\hat{y}}\otimes\boldsymbol{e}_{\hat{z}}\right), \tag{4.5}$$

and since T is a function of y only, velocity field consistent with the assumption (4.4) must have the form

$$\boldsymbol{v} = v^{\hat{z}}(y)\boldsymbol{e}_{\hat{z}}. \tag{4.6}$$

From (4.4), (4.6) and the balance of linear momentum (4.3a) then follows

$$0 = \frac{1}{\mathcal{R}_1}\frac{\partial}{\partial x}\left(\frac{1}{3}\operatorname{Tr}\mathbb{T}\right), \tag{4.7a}$$

$$0 = \frac{1}{\mathcal{R}_1}\frac{\partial}{\partial y}\left(\frac{1}{3}\operatorname{Tr}\mathbb{T}\right), \tag{4.7b}$$

$$0 = \frac{1}{\mathcal{R}_1}\left(\frac{\partial T}{\partial y} + \frac{\partial}{\partial z}\left(\frac{1}{3}\operatorname{Tr}\mathbb{T}\right)\right), \tag{4.7c}$$

which suggests

$$T(y) = Cy + E, \qquad \text{and} \qquad -\frac{\partial}{\partial z}\left(\frac{1}{3}\operatorname{Tr}\mathbb{T}\right) = C, \tag{4.8}$$

C and E being constants. Obviously, C is the dimensionless gradient of the mean normal stress (the pressure (2.3)) in the direction of the channel's axis

$$C = \frac{\partial p^\star}{\partial z^\star} = \frac{L}{T_{\text{char}}}\frac{\partial p}{\partial z} = \frac{f_{\text{char}}L^2}{V}\frac{\partial p}{\partial z}, \tag{4.9}$$

where the physical pressure gradient $\frac{\partial p}{\partial z} < 0$ is a given datum of the problem. Fixing $C = -1$ implies $V = f_{\text{char}}L^2\left|\frac{\partial p}{\partial z}\right|$ and it is one possibility how to specify the characteristic velocity V, see Málek et al. (2010).

From (4.6) we get

$$\mathbb{D} = \frac{1}{2}\frac{\mathrm{d}v^{\hat{z}}}{\mathrm{d}y}\left(\boldsymbol{e}_{\hat{z}}\otimes\boldsymbol{e}_{\hat{y}} + \boldsymbol{e}_{\hat{y}}\otimes\boldsymbol{e}_{\hat{z}}\right), \tag{4.10}$$

and comparing it with (4.5) results in

$$\frac{\mathrm{d}v^{\hat{z}}}{\mathrm{d}y} = 2f\left(2T^2\right)T. \tag{4.11}$$

Substituting (4.8) into the last expression leads to the following ordinary differential equation for the velocity

$$\frac{\mathrm{d}v^{\hat{z}}}{\mathrm{d}y} = 2f\left(2(Cy+E)^2\right)(Cy+E), \tag{4.12}$$

which also implies

$$\frac{\mathrm{d}^2v^{\hat{z}}}{\mathrm{d}y^2} = 2C\left[f\left(2(Cy+E)^2\right) + 4(Cy+E)^2\left.\frac{\mathrm{d}f}{\mathrm{d}s}\right|_{s=(2(Cy+E)^2)}\right]. \tag{4.13}$$

4.1.1 Classical Newtonian fluid

When $f \equiv 1$, the problem (4.12) reduces to the classical problem for the Newtonian fluid, and $v^{\hat{z}}(y)$ is given by $v^{\hat{z}}(y) = 2\left(\frac{C}{2}y^2 + Ey\right) + F$, F being a constant. Imposing the boundary conditions $v^{\hat{z}}(\pm 1) = 0$ leads to $E = 0$ and $F = -C$ so the velocity is

$$v^{\hat{z}}(y) = C\left(y^2 - 1\right). \tag{4.14}$$

4.1.2 Non-Newtonian fluid

In case of a non-Newtonian fluid, that is $f \not\equiv 1$, we can write the solution to (4.12) as

$$\begin{aligned} v^{\hat{z}}(y) &= 2\int_0^y f\left(2(C\eta+E)^2\right)(C\eta+E)\,\mathrm{d}\eta = \left|\xi = 2(C\eta+E)^2\right| \\ &= \frac{1}{2C}\int_{2E^2}^{2(Cy+E)^2} f(\xi)\,\mathrm{d}\xi = \frac{1}{2C}\mathcal{F}(2(Cy+E)^2) + F, \end{aligned} \tag{4.15}$$

where $\mathcal{F}$ is the primitive function of function f and F is a constant to be determined from the boundary conditions $v^{\hat{z}}(\pm 1) = 0$. Imposing the boundary conditions leads to the following system of equations for E and F

$$\frac{1}{2C}\mathcal{F}(2(-C+E)^2) + F = 0, \tag{4.16a}$$

$$\frac{1}{2C}\mathcal{F}(2(C+E)^2) + F = 0. \tag{4.16b}$$

The solution to (4.16) is $E = 0$, $F = -\frac{1}{2C}\mathcal{F}\left(2C^2\right)$. Substituting for E and F back into (4.15), (4.12) and (4.13) gives the formulae for the velocity and its derivatives

$$v^{\hat{z}}(y) = \frac{1}{2C}\left(\mathcal{F}(2C^2y^2) - \mathcal{F}(2C^2)\right), \tag{4.17a}$$

$$\frac{\mathrm{d}v^{\hat{z}}}{\mathrm{d}y} = 2Cyf\left(2C^2y^2\right), \tag{4.17b}$$

$$\frac{\mathrm{d}^2v^{\hat{z}}}{\mathrm{d}y^2} = 2C\left[f\left(2C^2y^2\right) + 4C^2y^2\left.\frac{\mathrm{d}f}{\mathrm{d}s}\right|_{s=2C^2y^2}\right]. \tag{4.17c}$$

Remark. Since $|\mathbb{T}_\delta| = \sqrt{2}\,|C|\,|y|$, the right-hand side of (4.17c) can be rewritten as $2C\left.\frac{\mathrm{d}}{\mathrm{d}s}\left[f(s^2)s\right]\right|_{s=\sqrt{2}|C||y|}$ which corresponds to the derivative of the flow curve (the shear rate/shear stress dependence). Thus, whenever there is a plateau on the flow curve, inflection points might occur in the velocity profile. Inflection points play, for example, a crucial role in the stability of flows of inviscid fluids, see Schmid and Henningson (2001).

Le Roux–Rajagopal model

For the model (2.13) introduced by Le Roux and Rajagopal (2013)

$$\mathbb{D} = \left[a\left(1 + b|\mathbb{T}_\delta|^2\right)^n + c\right]\mathbb{T}_\delta, \tag{4.18}$$

we can set $f_{\mathrm{char}} =_{\mathrm{def}} a$, so the other dimensionless quantities are $T_{\mathrm{char}} = \frac{V}{aL}$, $\mathcal{R}_2 = \frac{bV^2}{a^2L^2}$, $\mathcal{R}_3 = \frac{c}{a}$. Fixing $\mathcal{R}_2 = 1$ gives another possible way how to specify the characteristic velocity, that is $V =_{\mathrm{def}} \frac{aL}{\sqrt{b}}$. This is discussed in detail in the following section. The constitutive relation (4.18) in its general dimensionless form then reads

$$\mathbb{D} = \left[\left(1 + \mathcal{R}_2|\mathbb{T}_\delta|^2\right)^n + \mathcal{R}_3\right]\mathbb{T}_\delta. \tag{4.19}$$

Simple integration of $f(s) = (1 + \mathcal{R}_2 s)^n + \mathcal{R}_3$ leads to

$$\mathcal{F}(s) = \begin{cases} \frac{1}{(n+1)\mathcal{R}_2} (1 + \mathcal{R}_2 s)^{n+1} + \mathcal{R}_3 s, & n \neq -1, \\ \frac{1}{\mathcal{R}_2} \ln (1 + \mathcal{R}_2 s) + \mathcal{R}_3 s, & n = -1, \end{cases}$$

and from (4.17a), we can easily obtain formula for the velocity

$$v^{\hat{z}}(y) = \begin{cases} \frac{1}{2(n+1)C\mathcal{R}_2} \left[(1 + 2\mathcal{R}_2 C^2 y^2)^{n+1} - (1 + 2\mathcal{R}_2 C^2)^{n+1} \right] + C\mathcal{R}_3 (y^2 - 1), & n \neq -1, \\ \frac{1}{2C\mathcal{R}_2} \left[\ln (1 + 2\mathcal{R}_2 C^2 y^2) - \ln (1 + 2\mathcal{R}_2 C^2) \right] + C\mathcal{R}_3 (y^2 - 1), & n = -1. \end{cases} \tag{4.20}$$

Note that the velocity for the stress power-law model studied by Málek et al. (2010) can be recovered just by setting $\mathcal{R}_3 = 0$.

4.1.3 Choosing the characteristic velocity

As said before, we have at least two reasonable options how to choose the characteristic velocity V. Using the model (4.18) and setting $f_{\text{char}} = a$, we shall show the relationships between different dimensionless numbers in both these cases.

Málek et al. (2010) fixed the dimensionless pressure gradient $C = -1$, consequently specifying the characteristic velocity as

$$V =_{\text{def}} aL^2 \left| \frac{\partial p}{\partial z} \right|.$$

This choice yields for the counterpart of the Reynolds number $\mathcal{R}_1$ and the dimensionless number $\mathcal{R}_2$

$$\mathcal{R}_1 =_{\text{def}} a\rho V L = a^2 \rho L^3 \left| \frac{\partial p}{\partial z} \right|,$$
$$\mathcal{R}_2 =_{\text{def}} \frac{bV^2}{a^2 L^2} = bL^2 \left(\frac{\partial p}{\partial z} \right)^2.$$

The second way how to specify the characteristic velocity V is to fix $\mathcal{R}_2 = 1$, which gives

$$V =_{\text{def}} \frac{aL}{\sqrt{b}}.$$

In this case, the counterpart of the Reynolds number $\mathcal{R}_1$ and the dimensionless pressure gradient C are given by

$$\mathcal{R}_1 =_{\text{def}} a\rho V L = \frac{a^2 \rho L^2}{\sqrt{b}},$$
$$C =_{\text{def}} \frac{aL^2}{V} \frac{\partial p}{\partial z} = \sqrt{b} L \frac{\partial p}{\partial z}.$$

Since in the case of plane Poiseuille flow, the pressure gradient in the flow direction $\frac{\partial p}{\partial z}$ is the crucial quantity having effect on the flow, we prefer the latter specification of the characteristic velocity where the pressure gradient figures only in its dimensionless counterpart and does not influence the dimensionless constitutive relation as in the former case. From this reason, we shall use only the latter specification.

4.2 Instability of decreasing flow curve

Some constitutive relation can exhibit non-monotone flow curves, that is, there is a region where the flow curve decreases. In this section, we will show, that flows within a regime of the decreasing flow curve are unconditionally unstable. Among models that might display such behavior are, for example, classical power-law models, stress power-law models, see Málek et al. (2010), or model introduced by Le Roux and Rajagopal (2013).

Following Schmitt et al. (1995), we shall assume steady shear flow between two infinite parallel plates at $y = \pm 1$. The bottom plate is stationary while the upper plate moves at a constant speed V in the z-direction. On both plates, we require the no-slip boundary condition. Then the velocity is given by

$$\boldsymbol{v} = \dot{\gamma}(y+1)\boldsymbol{e}_{\hat{z}}, \tag{4.21}$$

where $\dot{\gamma} =_{\text{def}} \frac{V}{2}$ is the constant shear rate. From (4.21), we see that the symmetric part of the velocity gradient is

$$\mathbb{D} = \frac{\dot{\gamma}}{2}\left(\boldsymbol{e}_{\hat{z}} \otimes \boldsymbol{e}_{\hat{y}} + \boldsymbol{e}_{\hat{y}} \otimes \boldsymbol{e}_{\hat{z}}\right). \tag{4.22}$$

Since we will consider constitutive relation connecting the symmetric part of the velocity gradient $\mathbb{D}$ and the traceless part of the Cauchy stress $\mathbb{T}_\delta$, we shall assume the stress field of the form

$$\mathbb{T}_\delta = \sigma\left(\boldsymbol{e}_{\hat{z}} \otimes \boldsymbol{e}_{\hat{y}} + \boldsymbol{e}_{\hat{y}} \otimes \boldsymbol{e}_{\hat{z}}\right). \tag{4.23}$$

We suppose that the basic steady shear flow is disturbed with a small[2] velocity perturbation in the z-direction

$$\boldsymbol{v}'(y,t) = v'^{\hat{z}}(y,t)\boldsymbol{e}_{\hat{z}}, \tag{4.24}$$

and a small stress perturbation

$$\mathbb{T}'_\delta(y,t) = \sigma'(y,t)\left(\boldsymbol{e}_{\hat{z}} \otimes \boldsymbol{e}_{\hat{y}} + \boldsymbol{e}_{\hat{y}} \otimes \boldsymbol{e}_{\hat{z}}\right). \tag{4.25}$$

From (4.24), we see that the symmetric part of the velocity gradient of the disturbance is

$$\mathbb{D}'(y,t) = \frac{\dot{\gamma}'(y,t)}{2}\left(\boldsymbol{e}_{\hat{z}} \otimes \boldsymbol{e}_{\hat{y}} + \boldsymbol{e}_{\hat{y}} \otimes \boldsymbol{e}_{\hat{z}}\right), \tag{4.26}$$

where $\dot{\gamma}'(y,t) =_{\text{def}} \frac{\partial v'^{\hat{z}}}{\partial y}$ is the nonconstant shear rate of the disturbance.

Both the undisturbed and the disturbed flows must satisfy the balance of linear momentum in the absence of body forces (4.3a). Since the flow is driven by the velocity of the upper plate (Couette flow), we can assume the gradient of the mean normal stress (the pressure) to be zero, thus

$$\operatorname{div}\mathbb{T} = \operatorname{div}\mathbb{T}_\delta. \tag{4.27}$$

Subtracting the balance of linear momentum of the undisturbed flow from the balance of linear momentum of the disturbed flow yields

$$\frac{\partial v'^{\hat{z}}}{\partial t} = \frac{1}{\mathcal{R}_1}\frac{\partial \sigma'}{\partial y}. \tag{4.28}$$

In order to close the system, equation (4.28) must be supplemented by a constitutive relation between σ' and $\dot{\gamma}'$.

[2]With respect to the corresponding components of the undisturbed flow.

4.2.1 Classical models

First, we shall consider the classical approach when the stress is expressed in terms of the symmetric part of the velocity gradient in the form

$$\mathbb{T}_\delta = 2\hat{g}\left(|\mathbb{D}|\right)\mathbb{D}. \tag{4.29}$$

Assuming a shear flow with a constant shear rate $\dot{\gamma}$, the yz-component of (4.29) reads

$$\sigma = g\left(\dot{\gamma}\right)\dot{\gamma}, \tag{4.30}$$

where $\sigma =_{\text{def}} \mathrm{T}_\delta^{\prime\hat{y}\hat{z}}$ and $g\left(\dot{\gamma}\right) =_{\text{def}} \hat{g}\left(2^{-1/2}\dot{\gamma}\right)$. For the disturbed motion, relation (4.30) then reads

$$\sigma + \sigma' = g\left(\dot{\gamma} + \dot{\gamma}'\right)\left(\dot{\gamma} + \dot{\gamma}'\right). \tag{4.31}$$

Linearizing function g about the undisturbed flow, i.e., $g\left(\dot{\gamma} + \dot{\gamma}'\right) = g(\dot{\gamma}) + \frac{\mathrm{d}g}{\mathrm{d}s}\big|_{s=\dot{\gamma}}\dot{\gamma}'$, we arrive at

$$\sigma' = \left(g\left(\dot{\gamma}\right) + \left.\frac{\mathrm{d}g}{\mathrm{d}s}\right|_{s=\dot{\gamma}_0}\dot{\gamma}\right)\dot{\gamma}' = \left.\frac{\mathrm{d}\sigma}{\mathrm{d}s}\right|_{s=\dot{\gamma}}\dot{\gamma}', \tag{4.32}$$

where we neglected the nonlinear terms and used the fact that the undisturbed flow satisfies relation (4.30). Inserting (4.32) into (4.28) then yields the one-dimensional heat equation

$$\frac{\partial v'^{\hat{z}}}{\partial t} = \frac{1}{\mathcal{R}_1}\left.\frac{\mathrm{d}\sigma}{\mathrm{d}s}\right|_{s=\dot{\gamma}}\frac{\partial^2 v'^{\hat{z}}}{\partial y^2}. \tag{4.33}$$

If $\frac{\mathrm{d}\sigma}{\mathrm{d}s}\big|_{s=\dot{\gamma}} < 0$, we readily see that the instability will grow in time and the flow will be unstable. This result was also obtained for more general viscoelastic fluids by Yerushalmi et al. (1970).

4.2.2 Novel approach

Now, we shall consider implicit-type models

$$\mathbb{D} = \frac{1}{2}\hat{f}\left(|\mathbb{T}_\delta|\right)\mathbb{T}_\delta. \tag{4.34}$$

Assuming the same shear flow and using the notation as before, the yz-component of (4.34) reads

$$\dot{\gamma} = f\left(\sigma\right)\sigma, \tag{4.35}$$

where $f(\sigma) =_{\text{def}} \hat{f}(\sqrt{2}\sigma)$. Thus, we have for the disturbed flow

$$\dot{\gamma} + \dot{\gamma}' = f\left(\sigma + \sigma'\right)\left(\sigma + \sigma'\right). \tag{4.36}$$

Again, linearizing the function f about the undisturbed flow, i.e., $f\left(\sigma + \sigma'\right) = f(\sigma) + \frac{\mathrm{d}f}{\mathrm{d}s}\big|_{s=\sigma}\sigma'$, neglecting nonlinear terms and using (4.35) leads to

$$\dot{\gamma}' = \left(f\left(\sigma\right) + \left.\frac{\mathrm{d}f}{\mathrm{d}s}\right|_{s=\sigma}\sigma\right)\sigma' = \left.\frac{\mathrm{d}\dot{\gamma}}{\mathrm{d}s}\right|_{s=\sigma}\sigma'. \tag{4.37}$$

Inserting (4.37) into (4.28) gives a similar result as in the classical case, that is, if the the flow curve $\dot{\gamma}(\sigma)$ is decreasing, the flow is unstable.

We have thus shown that in the classical setting, at all values of the shear rate $\dot{\gamma}$ where the flow curve $\sigma(\dot{\gamma})$ is decreasing, the flow is unstable. Similarly, in the novel, implicit-like setting, the flow is unstable at all values of the shear stress σ where the flow curve $\dot{\gamma}(\sigma)$ is decreasing. Supposing local invertibility of the flow curves, both results are equivalent.

Even though we have not considered a fully three-dimensional disturbance of the basic flow, instability due to a one-dimensional disturbance means that the flow is unstable with respect to some initial disturbance and therefore unstable.

4.3 Reynolds–Orr energy equation

4.3.1 Energy equation for general flow

Consider a basic motion $\left(\bar{\boldsymbol{v}}, \bar{\mathbb{T}}_\delta\right)$ and a disturbed motion $\left(\bar{\boldsymbol{v}} + \boldsymbol{v}', \bar{\mathbb{T}}_\delta + \mathbb{T}'_\delta\right)$ of a fluid inside a region Ω, where Ω might be either bounded or unbounded. In case Ω is bounded, we shall require velocity to be zero on the boundary $\partial\Omega$. Since the disturbed motion must satisfy the same boundary condition as the basic flow, we can readily see that

$$\boldsymbol{v}'|_{\partial\Omega} = 0. \tag{4.38}$$

In case Ω is unbounded, we shall require the disturbance $\boldsymbol{v}'$ to be either spatially localized or periodic at each instant.

In order to investigate the problem of stability of the flow, we shall examine the temporal behavior of the kinetic energy of the disturbance

$$E =_{\text{def}} \frac{1}{2}\int_\Omega |\boldsymbol{v}'|^2 \,\mathrm{d}v. \tag{4.39}$$

Using the Reynolds transport theorem, the material time derivative of the disturbance energy can be expressed as

$$\frac{\mathrm{d}E}{\mathrm{d}t} = \frac{1}{2}\int_\Omega \frac{\partial|\boldsymbol{v}'|^2}{\partial t}\,\mathrm{d}v + \frac{1}{2}\int_{\partial\Omega} |\boldsymbol{v}'|^2\, \bar{\boldsymbol{v}}\cdot\boldsymbol{n}\,\mathrm{d}a, \tag{4.40}$$

where $\boldsymbol{n}$ is the unit outward normal vector. The stability criterion is given in the following definition.

Definition. *The flow is* monotonically stable *if for all disturbances* $\boldsymbol{v}'$

$$\frac{\mathrm{d}E}{\mathrm{d}t} < 0. \tag{4.41}$$

Subtracting the governing equation (4.3a) for the basic and the disturbed motions, we obtain the governing equation for the disturbance which together with the constitutive relation reads

$$\frac{\partial \boldsymbol{v}'}{\partial t} + \left[(\bar{\boldsymbol{v}} + \boldsymbol{v}')\cdot\nabla\right]\boldsymbol{v}' + (\boldsymbol{v}'\cdot\nabla)\bar{\boldsymbol{v}} = \frac{1}{\mathcal{R}_1}\left(-\nabla p' + \operatorname{div}\mathbb{T}'_\delta\right), \tag{4.42a}$$

$$\mathbb{D}' = f\left(|\mathbb{T}'_\delta|^2\right)\mathbb{T}'_\delta, \tag{4.42b}$$

where $p' =_{\text{def}} -\frac{1}{3}\operatorname{Tr}\mathbb{T}'$ is the disturbance of the pressure (mean normal stress). Note that the incompressibility of the disturbance $\operatorname{div}\boldsymbol{v}' = 0$ is automatically implied by equation (4.42b).

Scalar product of (4.42a) with $\boldsymbol{v}'$ leads to

$$\frac{1}{2}\frac{\partial|\boldsymbol{v}'|^2}{\partial t} = -\left(\boldsymbol{v}'\cdot\bar{\mathbb{D}}\boldsymbol{v}' + \frac{1}{\mathcal{R}_1}\mathbb{T}'_\delta : \nabla\boldsymbol{v}'\right) + \operatorname{div}\left(\frac{1}{\mathcal{R}_1}\mathbb{T}'^{\mathsf{T}}_\delta\boldsymbol{v}' - \frac{1}{\mathcal{R}_1}p'\boldsymbol{v}' - \frac{1}{2}|\boldsymbol{v}'|^2(\bar{\boldsymbol{v}}+\boldsymbol{v}')\right), \tag{4.43}$$

where we have used the following identities

$$\begin{aligned}
\frac{\partial\boldsymbol{v}'}{\partial t}\cdot\boldsymbol{v}' &= \frac{1}{2}\frac{\partial|\boldsymbol{v}'|^2}{\partial t},\\
\left[(\bar{\boldsymbol{v}}+\boldsymbol{v}')\cdot\nabla\right]\boldsymbol{v}'\cdot\boldsymbol{v}' &= (\nabla\boldsymbol{v}')^{\mathsf{T}}\boldsymbol{v}'\cdot(\bar{\boldsymbol{v}}+\boldsymbol{v}') = \frac{1}{2}\left(\nabla|\boldsymbol{v}'|^2\right)\cdot(\bar{\boldsymbol{v}}+\boldsymbol{v}')\\
&= \frac{1}{2}\operatorname{div}\left(|\boldsymbol{v}'|^2(\bar{\boldsymbol{v}}+\boldsymbol{v}')\right) - \frac{1}{2}|\boldsymbol{v}'|^2\underbrace{\operatorname{div}(\bar{\boldsymbol{v}}+\boldsymbol{v}')}_{=0},\\
(\boldsymbol{v}'\cdot\nabla)\bar{\boldsymbol{v}}\cdot\boldsymbol{v}' &= (\nabla\bar{\boldsymbol{v}}) : (\boldsymbol{v}'\otimes\boldsymbol{v}') = \bar{\mathbb{D}} : (\boldsymbol{v}'\otimes\boldsymbol{v}') = \boldsymbol{v}'\cdot\bar{\mathbb{D}}\boldsymbol{v}',\\
-\frac{1}{\mathcal{R}_1}\nabla p'\cdot\boldsymbol{v}' &= -\frac{1}{\mathcal{R}_1}\operatorname{div}(p'\boldsymbol{v}') + \frac{1}{\mathcal{R}_1}p'\underbrace{\operatorname{div}\boldsymbol{v}'}_{=0},\\
\frac{1}{\mathcal{R}_1}\operatorname{div}\mathbb{T}'_\delta\cdot\boldsymbol{v}' &= -\frac{1}{\mathcal{R}_1}\mathbb{T}'_\delta : \nabla\boldsymbol{v}' + \frac{1}{\mathcal{R}_1}\operatorname{div}\left(\mathbb{T}'^{\mathsf{T}}_\delta\boldsymbol{v}'\right).
\end{aligned}$$

From (4.40), (4.43) and the divergence theorem then follows

$$\frac{\mathrm{d}E}{\mathrm{d}t} = -\int_\Omega\left(\boldsymbol{v}'\cdot\bar{\mathbb{D}}\boldsymbol{v}' + \frac{1}{\mathcal{R}_1}\mathbb{T}'_\delta : \nabla\boldsymbol{v}'\right)\mathrm{d}v + \int_{\partial\Omega}\left(\frac{1}{\mathcal{R}_1}\mathbb{T}'^{\mathsf{T}}_\delta\boldsymbol{v}' - \frac{1}{\mathcal{R}_1}p'\boldsymbol{v}' - \frac{1}{2}|\boldsymbol{v}'|^2\boldsymbol{v}'\right)\cdot\boldsymbol{n}\,\mathrm{d}a. \tag{4.44}$$

The use of the divergence theorem for unbounded Ω can be justified by taking some bounded subdomain of Ω.[3] We can choose this subdomain so that the second term in (4.44) will vanish. For localized disturbance, we shall chose Ω such that $\operatorname{diam}\Omega$ is large. In case of periodic disturbance, considered mainly in Poiseuille and Couette flows, the region Ω can be chosen to cover exactly one period and the (generally non-zero) boundary integrals at each side of Ω will cancel out each other. If Ω is bounded, the second term in (4.44) will vanish immediately due to (4.38). In any case, vanishing of the boundary integral in (4.44) leads to the generalized version of the *Reynolds–Orr energy equation*

$$\frac{\mathrm{d}E}{\mathrm{d}t} = -\int_\Omega\left(\boldsymbol{v}'\cdot\bar{\mathbb{D}}\boldsymbol{v}' + \frac{1}{\mathcal{R}_1}\mathbb{T}'_\delta : \nabla\boldsymbol{v}'\right)\mathrm{d}v. \tag{4.45}$$

Note that in deriving (4.45), no linearization was used in the sense that higher order terms of $\boldsymbol{v}'$ would be neglected as in the case of linearized stability in Section 4.4.

Using the identity

$$\boldsymbol{v}'\cdot\bar{\mathbb{D}}\boldsymbol{v}' = \boldsymbol{v}'\cdot(\nabla\bar{\boldsymbol{v}})\boldsymbol{v}' = \operatorname{div}\left[(\boldsymbol{v}'\cdot\bar{\boldsymbol{v}})\boldsymbol{v}'\right] - \bar{\boldsymbol{v}}\cdot(\nabla\boldsymbol{v}')\boldsymbol{v}' - (\boldsymbol{v}'\cdot\bar{\boldsymbol{v}})\underbrace{\operatorname{div}\boldsymbol{v}'}_{=0}, \tag{4.46}$$

and the divergence theorem, (4.45) can be written in an alternative form

$$\frac{\mathrm{d}E}{\mathrm{d}t} = \int_\Omega\left(\bar{\boldsymbol{v}}\cdot(\nabla\boldsymbol{v}')\boldsymbol{v}' - \frac{1}{\mathcal{R}_1}\mathbb{T}'_\delta : \nabla\boldsymbol{v}'\right)\mathrm{d}v. \tag{4.47}$$

[3] Abusing the notation, this subdomain shall be also denoted Ω.

Further supposing that $\mathbb{T}'_\delta$ is symmetric, we can rewrite the second term in (4.45) as

$$-\frac{1}{\mathcal{R}_1}\int_\Omega \mathbb{T}'_\delta : \mathbb{D}'\,\mathrm{d}v, \tag{4.48}$$

and we can substitute for $\mathbb{D}'$ from (4.42b). Obviously, we can also substitute for $\mathbb{T}'_\delta$ but unless the constitutive relation (4.42b) is invertible, the expression will depend on both $\mathbb{T}'_\delta$ and $\mathbb{D}'$. In our case, $\mathbb{T}'_\delta$ is symmetric as can be readily seen from (4.42b), so the Reynolds–Orr energy equation (4.45) takes the form

$$\frac{\mathrm{d}E}{\mathrm{d}t} = -\int_\Omega \left(\boldsymbol{v}'\cdot\bar{\mathbb{D}}\boldsymbol{v}' + \frac{1}{\mathcal{R}_1} f\left(|\mathbb{T}'_\delta|^2\right)|\mathbb{T}'_\delta|^2\right)\mathrm{d}v. \tag{4.49}$$

In case of the classical Newtonian fluid, $\mathbb{T}'_\delta = \mathbb{D}'$ as $f \equiv 1$ and in (4.42b), we have

$$\mathbb{T}'_\delta : \nabla\boldsymbol{v}' = \frac{1}{2}\left[(\nabla\boldsymbol{v}') + (\nabla\boldsymbol{v}')^\top\right] : \nabla\boldsymbol{v}' = \frac{1}{2}\left[\nabla\boldsymbol{v}' : \nabla\boldsymbol{v}' + (\nabla\boldsymbol{v}')^\top : \nabla\boldsymbol{v}'\right]. \tag{4.50}$$

The second term disappears since it can be further rewritten as $\operatorname{div}\left[(\nabla\boldsymbol{v}')\boldsymbol{v}'\right] - \operatorname{div}\left[(\nabla\boldsymbol{v}')^\top\right]\cdot\boldsymbol{v}'$, where the former term vanishes due to the periodic/bounded character of the disturbance, while the later vanishes due to its incompressibility. Thus we arrive at the classical formula[4]

$$\frac{\mathrm{d}E}{\mathrm{d}t} = -\int_\Omega \left(\boldsymbol{v}'\cdot\bar{\mathbb{D}}\boldsymbol{v}' + \frac{1}{2\mathcal{R}_1}\nabla\boldsymbol{v}' : \nabla\boldsymbol{v}'\right)\mathrm{d}v, \tag{4.51}$$

as found, for example, in Serrin (1959).

Remark. Deriving (4.51), we also showed, as a by-product, a useful equality for incompressible disturbances with zero value on the boundary

$$\int_\Omega |\mathbb{D}'|^2\,\mathrm{d}v = \frac{1}{2}\int_\Omega |\nabla\boldsymbol{v}'|^2\,\mathrm{d}v, \qquad \forall\boldsymbol{v}' \in H^1_{0,\mathrm{div}}(\Omega), \tag{4.52}$$

where $H^1_{0,\mathrm{div}}(\Omega)$ is the standard Sobolev space containing divergence-free functions vanishing on the boundary (or being spatially periodic). In fact, (4.52) is a special case of Korn's inequality, see Horgan (1995).

4.3.2 Disturbing a fluid at rest

Let us consider a fluid at rest, i.e., $\bar{\boldsymbol{v}} \equiv \boldsymbol{0}$, contained in a bounded domain Ω. Disturbing the fluid at time $t = 0$, we investigate the kinetic energy of the disturbance E. Since the fluid is at rest, there is also no velocity gradient, that is $\bar{\mathbb{D}} = 0$ and the first term in (4.45) vanishes. As we assume the disturbance to be zero on the boundary $\partial\Omega$, we can exploit the so-called Friedrichs' inequality

$$\int_\Omega |\boldsymbol{v}'|^2\,\mathrm{d}v \le C_F\int_\Omega |\nabla\boldsymbol{v}'|\,\mathrm{d}v, \qquad \forall\boldsymbol{v}' \in H^1_0(\Omega), \tag{4.53}$$

where the positive constant C_F depends only on the domain Ω.

In case of the classical Newtonian fluid, combining (4.51) and (4.53) leads to the estimate

$$\frac{\mathrm{d}E}{\mathrm{d}t} = -\frac{1}{2\mathcal{R}_1}\int_\Omega (\nabla\boldsymbol{v}' : \nabla\boldsymbol{v}')\,\mathrm{d}v \le -\frac{1}{2\mathcal{R}_1 C_F}\int_\Omega |\boldsymbol{v}'|^2\,\mathrm{d}v = -\frac{E}{\mathcal{R}_1 C_F}, \tag{4.54}$$

[4]Note that the relation between the classical Reynolds number and its analogue is $\mathrm{Re} = 2\mathcal{R}_1$.

or

$$\frac{\mathrm{d}}{\mathrm{d}t}\left(E\mathrm{e}^{\frac{t}{\mathcal{R}_1 C_F}}\right) \leq 0. \tag{4.55}$$

Integrating from 0 to t then yields

$$E(t) \leq E_0 \mathrm{e}^{-\frac{t}{\mathcal{R}_1 C_F}}, \tag{4.56}$$

where E_0 is the initial kinetic energy of the disturbance. Therefore, the disturbance dies out as $t \to \infty$ and the fluid will return to rest.

Considering models of type (4.1), from (4.45) follows

$$\frac{\mathrm{d}E}{\mathrm{d}t} = -\frac{1}{\mathcal{R}_1}\int_\Omega \frac{1}{f\left(\left|\mathbb{T}'_\delta\right|^2\right)}\left|\mathbb{D}'\right|^2 \,\mathrm{d}v \leq -\frac{1}{\mathcal{R}_1}\frac{1}{\max f\left(\left|\mathbb{T}'_\delta\right|^2\right)}\int_\Omega \left|\mathbb{D}'\right|^2 \,\mathrm{d}v \tag{4.57}$$

$$= -\frac{1}{2\mathcal{R}_1}\frac{1}{\max f\left(\left|\mathbb{T}'_\delta\right|^2\right)}\int_\Omega |\nabla \boldsymbol{v}'|^2 \,\mathrm{d}v \leq -\frac{1}{2\mathcal{R}_1 C_F}\frac{1}{\max f\left(\left|\mathbb{T}'_\delta\right|^2\right)}\int_\Omega |\boldsymbol{v}'|^2 \,\mathrm{d}v \tag{4.58}$$

where we used the Korn's equality (4.52) and the Friedrichs' inequality (4.53). Again, integrating from 0 to t as in the previous case, we arrive at

$$E(t) \leq E_0 \mathrm{e}^{-\frac{t}{\mathcal{R}_1 C_F \max f}}. \tag{4.59}$$

Thus, when the fluid is at rest, we observe the same exponential decrease of the kinetic energy of the disturbance for fluids described by (4.7) as for the classical Newtonian fluid.

For example, for the Le Roux–Rajagopal model (4.19), the maximal value of the function f can be easily estimated from

$$f\left(|\mathbb{T}_\delta|^2\right) = \left[\left(1+|\mathbb{T}_\delta|^2\right)^n + \mathcal{R}_3\right] \in \begin{cases} (\mathcal{R}_3, 1+\mathcal{R}_3), & n \in (-\infty, 0), \\ 1+\mathcal{R}_3, & n = 0, \\ (1+\mathcal{R}_3, +\infty), & n \in (0, +\infty), \end{cases} \tag{4.60}$$

see Figure 4.2.

4.3.3 Poiseuille flow in a channel

Now, we shall consider the problem of plane Poiseuille flow as described in Section 4.1. We have shown that the base flow is in the form (4.6)

$$\bar{\boldsymbol{v}} = \bar{v}^{\hat{z}}(y)\boldsymbol{e}_{\hat{z}}.$$

At the fixed walls $y = \pm 1$, we assume velocity to be zero. Therefore, the imposed disturbance also vanishes at $y = \pm 1$ and furthermore, we shall assume it to be either spatially localized or periodic.

This time, the generalized Reynolds–Orr energy equation (4.45) cannot be further simplified as there is a nontrivial base flow and we have

$$\frac{\mathrm{d}E}{\mathrm{d}t} = -\int_\Omega \left(\boldsymbol{v}' \cdot \bar{\mathbb{D}}\boldsymbol{v}' + \frac{1}{\mathcal{R}_1}\mathbb{T}'_\delta : \mathbb{D}'\right) \mathrm{d}v. \tag{4.61}$$

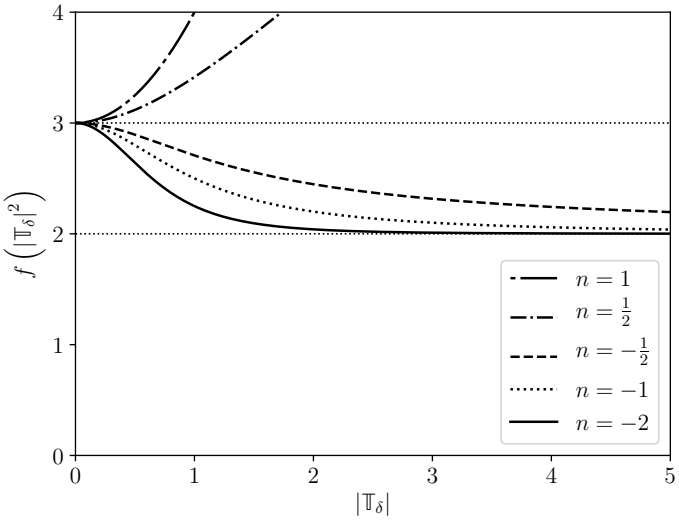

Figure 4.2: Function f corresponding to the Le Roux–Rajagopal model (4.19) for various values of the parameter n, $\mathcal{R}_3 = 2$.

Expressing the energy equation in terms of the velocity, we can estimate the particular terms, thus finding an universal stability criterion.

First, we shall consider the disturbance to be spatially localized in a subdomain $\Omega_0 =_{\text{def}} [0, L_1] \times [-1, 1] \times [0, L_2] \subset \Omega$ for all times $t \geq 0$ where L_1, L_2 are some large constants such that $\boldsymbol{v}'|_{\partial\Omega_0} = \mathbf{0}$. Then, the first term in equation (4.61) can be estimated as

$$-\int_\Omega \boldsymbol{v}' \cdot \bar{\mathbb{D}}\boldsymbol{v}' \,\mathrm{d}v \leq \max_{y\in[-1,1]} \left|\frac{\mathrm{d}\bar{v}^{\hat{z}}}{\mathrm{d}y}\right| \int_{\Omega_0} |\boldsymbol{v}'|^2 \,\mathrm{d}v. \tag{4.62}$$

Again, we can estimate the second term in (4.61) using the Korn's equality (4.52), Friedrichs' inequality (4.53) and exploiting the fact that function f is positive as

$$-\frac{1}{\mathcal{R}_1}\int_\Omega \mathbb{T}'_\delta : \mathbb{D}' \,\mathrm{d}v \leq -\frac{1}{2\mathcal{R}_1 C_F}\frac{1}{\max f\left(\left|\mathbb{T}'_\delta\right|^2\right)} \int_{\Omega_0} |\boldsymbol{v}'|^2 \,\mathrm{d}v. \tag{4.63}$$

From (4.62) and (4.63) then follows an estimate for (4.61)

$$\frac{\mathrm{d}E}{\mathrm{d}t} \leq \left(2 \max_{y\in[-1,1]} \left|\frac{\mathrm{d}\bar{v}^{\hat{z}}}{\mathrm{d}y}\right| - \frac{1}{\mathcal{R}_1 C_F}\frac{1}{\max f}\right) E. \tag{4.64}$$

As a consequence, we have once more the exponential time evolution of the energy of the disturbance

$$E(t) \leq E_0 \exp\left[\left(2 \max_{y\in[-1,1]} \left|\frac{\mathrm{d}\bar{v}^{\hat{z}}}{\mathrm{d}y}\right| - \frac{1}{\mathcal{R}_1 C_F}\frac{1}{\max f}\right) t\right]. \tag{4.65}$$

Note that for a Newtonian fluid when $f \equiv 1$, relation (4.64) reads

$$\frac{\mathrm{d}E}{\mathrm{d}t} \leq \left(2 \max_{y\in[-1,1]} \left|\frac{\mathrm{d}\bar{v}^{\hat{z}}}{\mathrm{d}y}\right| - \frac{1}{\mathcal{R}_1 C_F}\right) E, \tag{4.66}$$

which is the same result as obtained by Serrin (1959). In the original paper, the quantities are given by $m = \max\left|\frac{\mathrm{d}\bar{v}^{\hat{z}}}{\mathrm{d}y}\right|$, $\nu = \frac{1}{2\mathcal{R}_1}$ $C_F = \frac{d^2}{\alpha}$, where $d = \operatorname{diam}\Omega_0$ and α is a constant depending on the geometry of the flow region.

Now, we shall consider the disturbance to be periodic, in other words, we will assume the velocity and the stress of the disturbance in the form of a wave

$$\boldsymbol{v}'(x,y,z,t) = \hat{\boldsymbol{v}}'(y,t)\mathrm{e}^{i(\alpha z+\beta x)}, \qquad \mathbb{T}'_\delta(x,y,z,t) = \hat{\mathbb{T}}'_\delta(y,t)\mathrm{e}^{i(\alpha z+\beta x)}, \tag{4.67}$$

where $\alpha, \beta \geq 0$ denote the streamwise and spanwise wave numbers.[5] We will therefore choose the domain of interest to cover exactly one period in each direction, that is $\Omega_0 =_{\mathrm{def}} \left[0, \frac{2\pi}{\beta}\right] \times [-1,1] \times \left[0, \frac{2\pi}{\alpha}\right] \subset \Omega$.

The energy equation (4.61) can be seen as

$$\frac{\mathrm{d}E}{\mathrm{d}t} = -\left\langle \boldsymbol{v}', \bar{\mathbb{D}}\boldsymbol{v}'\right\rangle_{\Omega_0} - \frac{1}{\mathcal{R}_1}\left\langle \frac{1}{f\left(\left|\mathbb{T}'_\delta\right|^2\right)}\mathbb{D}', \mathbb{D}'\right\rangle_{\Omega_0}, \tag{4.68}$$

and

$$E = \frac{1}{2}\left\langle \boldsymbol{v}', \boldsymbol{v}'\right\rangle_{\Omega_0}, \tag{4.69}$$

where $\langle \bullet, \bullet\rangle_{\Omega_0}$ is an appropriate vector or tensor inner product. Following Salwen and Grosch (1972), we define the vector inner product as

$$\left\langle \boldsymbol{u}, \boldsymbol{v}\right\rangle_{\Omega_0} =_{\mathrm{def}} \int_{\Omega_0} \boldsymbol{u}\cdot\boldsymbol{v}^\star \,\mathrm{d}v = \int_{x=0}^{\frac{2\pi}{\beta}}\int_{y=-1}^{1}\int_{z=0}^{\frac{2\pi}{\alpha}} \hat{\boldsymbol{u}}\cdot\hat{\boldsymbol{v}}^\star \,\mathrm{d}z\,\mathrm{d}y\,\mathrm{d}x = \frac{4\pi^2}{\alpha\beta}\int_{y=-1}^{1}\hat{\boldsymbol{u}}\cdot\hat{\boldsymbol{v}}^\star\,\mathrm{d}y, \tag{4.70}$$

where the star denotes the complex conjugate.[6] In the same manner, we can define the inner product for tensors. Using these inner products, we can rewrite (4.68) as

$$\frac{\mathrm{d}E}{\mathrm{d}t} = -\int_{y=-1}^{1}\left(\hat{\boldsymbol{v}}'\cdot\bar{\mathbb{D}}\hat{\boldsymbol{v}}' + \frac{1}{\mathcal{R}_1 f\left(\left|\hat{\mathbb{T}}'_\delta\right|^2\right)}\left|\hat{\mathbb{D}}'\right|^2\right)\mathrm{d}y, \tag{4.71}$$

where $\hat{\mathbb{D}}' =_{\mathrm{def}} \frac{1}{2}\left[\hat{\nabla}\hat{\boldsymbol{v}}' + \left(\hat{\nabla}\hat{\boldsymbol{v}}'\right)^\top\right]$ and $\hat{\nabla} =_{\mathrm{def}} \begin{bmatrix} i\beta \\ \frac{\partial}{\partial y} \\ i\alpha \end{bmatrix}$. Equation (4.71) has the same structure as the original equation (4.61) so we can use exactly the same estimates as in the case of a spatially localized disturbance. The only difference is the value of the Friedrichs' constant C_F.

In the case of a periodic disturbance, we can exploit the one-dimensional version of the Friedrichs' inequality – the Wirtinger's inequality that states

$$\int_0^\pi |f(x)|^2\,\mathrm{d}x \leq \int_0^\pi \left|\frac{\mathrm{d}f}{\mathrm{d}x}\right|^2\,\mathrm{d}x,$$

for $f(0) = f(\pi) = 0$, $\frac{\mathrm{d}f}{\mathrm{d}x} \in L^2([0,\pi])$ with the equality only for $f(x) = A\sin x$, A being constant, see Hardy et al. (1952); Nečas (2012). By a simple change

[5] Here, we do not assume an exponential time-dependence as is done in Section 4.4.

[6] In case $\alpha = 0$ or $\beta = 0$, the integration with respect to z, respectively to x is omitted.

of variables, we obtain a modification of this inequality for an arbitrary interval $[a, b]$

$$\int_a^b |f(x)|^2 \, \mathrm{d}x \leq \left(\frac{b-a}{\pi}\right)^2 \int_a^b \left|\frac{\mathrm{d}f}{\mathrm{d}x}\right|^2 \mathrm{d}x. \tag{4.72}$$

So in our case, the Friedrichs' constant is given by $C_F = \left(\frac{2}{\pi}\right)^2 \simeq 0.41$. The inverse of this value is also the lowest eigenvalue of the Stokes operator for the classical incompressible Newtonian fluid, see Rummler (1997).

For a spatially localized disturbance, the value of the Friedrichs' constant is $C_F = \frac{2d^2}{(3+\sqrt{13})\pi^2} \simeq 0.03d^2$, where d is a edge of some cube that can contain the the domain Ω_0, i.e., $d = \max\{L_1, 2, L_2\}$, see Serrin (1959).

Base flow estimates

We can further estimate the terms in (4.64) using the formulae for the base flow. From (4.17b), we see that the relation for the absolute value of the derivative of the base flow velocity is

$$\left|\frac{\mathrm{d}\bar{v}^{\hat{z}}}{\mathrm{d}y}\right| = \sqrt{2}\,|s|\, f(s^2)\Big|_{s=\sqrt{2}Cy}. \tag{4.73}$$

Here we make an additional assumption that the flow curve represented by the expression $sf(s^2)$ is monotonically increasing as we know from Section 4.2 that decreasing flow curve causes instability. Then the maximum of $\left|\frac{\mathrm{d}\bar{v}^{\hat{z}}}{\mathrm{d}y}\right|$ is attained for a maximal s, in other words

$$\max_{y\in[-1,1]} \left|\frac{\mathrm{d}\bar{v}^{\hat{z}}}{\mathrm{d}y}\right| = \left|\frac{\mathrm{d}\bar{v}^{\hat{z}}}{\mathrm{d}y}\right|_{y=\pm 1} = 2\,|C|\, f\left(2C^2\right). \tag{4.74}$$

The maximum value is thus attained at the channel walls. This can be also seen from (4.17c) as the increasing flow curve generates parabolic-like velocity profile with no inflection points.

Employing (4.74) in (4.64) then yields

$$\frac{\mathrm{d}E}{\mathrm{d}t} \leq \left(4\,|C|\, f\left(2C^2\right) - \frac{1}{\mathcal{R}_1 C_F}\frac{1}{\max f}\right) E. \tag{4.75}$$

Therefore, in order the flow to be monotonically stable, the counterpart of the Reynolds number must satisfy

$$\mathcal{R}_1 < \frac{1}{4\,|C|\, f\left(2C^2\right) C_F \max f}. \tag{4.76}$$

In case of the Le Roux–Rajagopal model (4.19), the maximal value of the function f can estimated identically as in Section 4.3.2. Furthermore, we also have a condition on the monotonicity of the flow curve. For $n > -\frac{1}{2}$, it is always increasing while for $n < -\frac{1}{2}$ it is increasing if

$$2\left(\frac{2n-2}{2n+1}\right)^{n-1} \leq \mathcal{R}_3,$$

see Lemma 2.1 in Le Roux and Rajagopal (2013).

4.4 Orr–Sommerfeld–Squire system derivation

4.4.1 Normal velocity evolution equation

Again, we shall consider the counterpart of the plane Poiseuille flow between two fixed infinite parallel plates with the base flow of the form (4.6)

$$\bar{\boldsymbol{v}} = \bar{v}^{\hat{z}}(y)\boldsymbol{e}_{\hat{z}},$$

satisfying the system of governing equations in the absence of body forces (4.3)

$$\begin{aligned}\frac{\mathrm{d}\bar{\boldsymbol{v}}}{\mathrm{d}t} &= \frac{1}{\mathcal{R}_1}\operatorname{div}\bar{\mathbb{T}},\\ \bar{\mathbb{D}} &= f\left(\left|\bar{\mathbb{T}}_\delta\right|^2\right)\bar{\mathbb{T}}_\delta.\end{aligned}$$

Then, the *linearized* governing equations for infinitesimal disturbances read

$$\frac{\partial \boldsymbol{v}'}{\partial t} + (\bar{\boldsymbol{v}}\cdot\nabla)\boldsymbol{v}' + (\boldsymbol{v}'\cdot\nabla)\bar{\boldsymbol{v}} = \frac{1}{\mathcal{R}_1}\left(-\nabla p' + \operatorname{div}\mathbb{T}'_\delta\right), \tag{4.77a}$$

$$\mathbb{D}' = f\left(\left|\bar{\mathbb{T}}_\delta\right|^2\right)\mathbb{T}'_\delta + 2\left.\frac{\mathrm{d}f}{\mathrm{d}s}\right|_{s=\left|\bar{\mathbb{T}}_\delta\right|^2}\left(\mathbb{T}'_\delta : \bar{\mathbb{T}}_\delta\right)\bar{\mathbb{T}}_\delta. \tag{4.77b}$$

with the incompressibility condition $\operatorname{div}\boldsymbol{v}' = 0$ immediately following from the second equation.

Taking the divergence of (4.77a) and using the incompressibility of the disturbance together with

$$\operatorname{div}\left[(\bar{\boldsymbol{v}}\cdot\nabla)\boldsymbol{v}' + (\boldsymbol{v}'\cdot\nabla)\bar{\boldsymbol{v}}\right] = 2\nabla\boldsymbol{v}' : (\nabla\bar{\boldsymbol{v}})^{\mathsf{T}} = 2\frac{\partial v'^{\hat{y}}}{\partial z}\frac{\mathrm{d}\bar{v}^{\hat{z}}}{\mathrm{d}y},$$

yields an equation for the perturbation pressure

$$\Delta p' = \operatorname{div}\left(\operatorname{div}\mathbb{T}'_\delta\right) - 2\mathcal{R}_1\frac{\partial v'^{\hat{y}}}{\partial z}\frac{\mathrm{d}\bar{v}^{\hat{z}}}{\mathrm{d}y}. \tag{4.78}$$

This gives us a tool that can be used to eliminate the pressure from the governing equations. Applying the Laplace operator to (4.77a) gives

$$\Delta\left(\frac{\partial \boldsymbol{v}'}{\partial t} + (\bar{\boldsymbol{v}}\cdot\nabla)\boldsymbol{v}' + (\boldsymbol{v}'\cdot\nabla)\bar{\boldsymbol{v}}\right) = \frac{1}{\mathcal{R}_1}\left[-\nabla(\Delta p') + \Delta(\operatorname{div}\mathbb{T}'_\delta)\right], \tag{4.79}$$

which, exploiting (4.78), takes the form

$$\begin{aligned}\frac{\partial}{\partial t}\Delta\boldsymbol{v}' + \Delta\left[(\bar{\boldsymbol{v}}\cdot\nabla)\boldsymbol{v}' + (\boldsymbol{v}'\cdot\nabla)\bar{\boldsymbol{v}}\right] = \\ -\frac{1}{\mathcal{R}_1}\nabla\left(\operatorname{div}\left(\operatorname{div}\mathbb{T}'_\delta\right) - 2\mathcal{R}_1\frac{\partial v'^{\hat{y}}}{\partial z}\frac{\mathrm{d}\bar{v}^{\hat{z}}}{\mathrm{d}y}\right) + \frac{1}{\mathcal{R}_1}\Delta(\operatorname{div}\mathbb{T}'_\delta).\end{aligned}$$

The $\boldsymbol{e}_{\hat{y}}$ component of the last equation reads

$$\begin{aligned}\frac{\partial}{\partial t}\Delta v'^{\hat{y}} + \Delta\left[(\bar{\boldsymbol{v}}\cdot\nabla)\boldsymbol{v}' + (\boldsymbol{v}'\cdot\nabla)\bar{\boldsymbol{v}}\right]^{\hat{y}} = \\ -\frac{1}{\mathcal{R}_1}\frac{\partial}{\partial y}\left(\operatorname{div}\left(\operatorname{div}\mathbb{T}'_\delta\right) - 2\mathcal{R}_1\frac{\partial v'^{\hat{y}}}{\partial z}\frac{\mathrm{d}\bar{v}^{\hat{z}}}{\mathrm{d}y}\right) + \frac{1}{\mathcal{R}_1}\Delta(\operatorname{div}\mathbb{T}'_\delta)^{\hat{y}},\end{aligned}$$

and since $[(\bar{\boldsymbol{v}}\cdot\nabla)\boldsymbol{v}'+(\boldsymbol{v}'\cdot\nabla)\bar{\boldsymbol{v}}]^{\hat{y}}=\bar{v}^{\hat{z}}\frac{\partial v'^{\hat{y}}}{\partial z}$, it can be further rewritten as

$$\frac{\partial}{\partial t}\Delta v'^{\hat{y}}+\Delta\left(\bar{v}^{\hat{z}}\frac{\partial v'^{\hat{y}}}{\partial z}\right)=2\frac{\partial}{\partial y}\left(\frac{\partial v'^{\hat{y}}}{\partial z}\frac{\mathrm{d}\bar{v}^{\hat{z}}}{\mathrm{d}y}\right)-\frac{1}{\mathcal{R}_1}\frac{\partial}{\partial y}\left[\operatorname{div}\left(\operatorname{div}\mathbb{T}'_\delta\right)\right]+\frac{1}{\mathcal{R}_1}\Delta(\operatorname{div}\mathbb{T}'_\delta)^{\hat{y}}. \tag{4.80}$$

From the identity

$$\Delta\left(\bar{v}^{\hat{z}}\frac{\partial v'^{\hat{y}}}{\partial z}\right)=\bar{v}^{\hat{z}}\Delta\frac{\partial v'^{\hat{y}}}{\partial z}+2\frac{\partial^2 v'^{\hat{y}}}{\partial y\partial z}\frac{\mathrm{d}\bar{v}^{\hat{z}}}{\mathrm{d}y}+\frac{\partial v'^{\hat{y}}}{\partial z}\frac{\mathrm{d}^2\bar{v}^{\hat{z}}}{\mathrm{d}y^2},$$

and noting further that the first term on the right hand side of (4.80) reads

$$2\frac{\partial}{\partial y}\left(\frac{\partial v'^{\hat{y}}}{\partial z}\frac{\mathrm{d}\bar{v}^{\hat{z}}}{\mathrm{d}y}\right)=2\frac{\partial^2 v'^{\hat{y}}}{\partial y\partial z}\frac{\mathrm{d}\bar{v}^{\hat{z}}}{\mathrm{d}y}+2\frac{\partial v'^{\hat{y}}}{\partial z}\frac{\mathrm{d}^2\bar{v}^{\hat{z}}}{\mathrm{d}y^2},$$

we arrive at the evolution equation for the normal velocity $v'^{\hat{y}}$ of the disturbance

$$\frac{\partial}{\partial t}\Delta v'^{\hat{y}}+\bar{v}^{\hat{z}}\frac{\partial}{\partial z}\Delta v'^{\hat{y}}-\frac{\partial v'^{\hat{y}}}{\partial z}\frac{\mathrm{d}^2\bar{v}^{\hat{z}}}{\mathrm{d}y^2}=-\frac{1}{\mathcal{R}_1}\frac{\partial}{\partial y}\left(\operatorname{div}\left(\operatorname{div}\mathbb{T}'_\delta\right)\right)+\frac{1}{\mathcal{R}_1}\Delta(\operatorname{div}\mathbb{T}'_\delta)^{\hat{y}}. \tag{4.81}$$

4.4.2 Normal vorticity evolution equation

If one considers three-dimensional perturbations, then we need an additional equation in order to fully determine the perturbed velocity and the pressure. It is convenient to consider evolution equation for the normal vorticity of the disturbance[7]

$$\eta^{\hat{y}}=_{\mathrm{def}}\frac{\partial v'^{\hat{x}}}{\partial z}-\frac{\partial v'^{\hat{z}}}{\partial x}.$$

From (4.77a), the evolution equations for $v'^{\hat{x}}$ and $v'^{\hat{z}}$ read

$$\frac{\partial v'^{\hat{x}}}{\partial t}+\bar{v}^{\hat{z}}\frac{\partial v'^{\hat{x}}}{\partial z}=\frac{1}{\mathcal{R}_1}\left[-\frac{\partial p'}{\partial x}+(\operatorname{div}\mathbb{T}'_\delta)^{\hat{x}}\right], \tag{4.82a}$$

$$\frac{\partial v'^{\hat{z}}}{\partial t}+\bar{v}^{\hat{z}}\frac{\partial v'^{\hat{z}}}{\partial z}+v'^{\hat{y}}\frac{\mathrm{d}\bar{v}^{\hat{z}}}{\mathrm{d}y}=\frac{1}{\mathcal{R}_1}\left[-\frac{\partial p'}{\partial z}+(\operatorname{div}\mathbb{T}'_\delta)^{\hat{z}}\right]. \tag{4.82b}$$

Taking the x-derivative of (4.82b) and subtracting it from the z-derivative of (4.82a) leads to

$$\frac{\partial}{\partial t}\left(\frac{\partial v'^{\hat{x}}}{\partial z}-\frac{\partial v'^{\hat{z}}}{\partial x}\right)+\bar{v}^{\hat{z}}\frac{\partial}{\partial z}\left(\frac{\partial v'^{\hat{x}}}{\partial z}-\frac{\partial v'^{\hat{z}}}{\partial x}\right)-\frac{\partial v'^{\hat{y}}}{\partial x}\frac{\mathrm{d}\bar{v}^{\hat{z}}}{\mathrm{d}y}=\frac{1}{\mathcal{R}_1}\left[\frac{\partial}{\partial z}(\operatorname{div}\mathbb{T}'_\delta)^{\hat{x}}-\frac{\partial}{\partial x}(\operatorname{div}\mathbb{T}'_\delta)^{\hat{z}}\right],$$

or in terms of the normal vorticity $\eta^{\hat{y}}$, to

$$\frac{\partial\eta^{\hat{y}}}{\partial t}+\bar{v}^{\hat{z}}\frac{\partial\eta^{\hat{y}}}{\partial z}-\frac{\partial v'^{\hat{y}}}{\partial x}\frac{\mathrm{d}\bar{v}^{\hat{z}}}{\mathrm{d}y}=\frac{1}{\mathcal{R}_1}\left[\frac{\partial}{\partial z}(\operatorname{div}\mathbb{T}'_\delta)^{\hat{x}}-\frac{\partial}{\partial x}(\operatorname{div}\mathbb{T}'_\delta)^{\hat{z}}\right]. \tag{4.83}$$

[7]Sometimes, the normal vorticity is defined with the opposite sign.

4.4.3 The Orr–Sommerfeld and Squire type equations

Let us now assume wave-like disturbances of the form

$$\begin{aligned}\boldsymbol{v}'(x,y,z,t) &= \tilde{\boldsymbol{v}}'(y)\mathrm{e}^{\mathrm{i}(\alpha z+\beta x-\omega t)},\\ \eta^{\hat{y}}(x,y,z,t) &= \tilde{\eta}^{\hat{y}}(y)\mathrm{e}^{\mathrm{i}(\alpha z+\beta x-\omega t)},\\ \mathbb{T}'_\delta(x,y,z,t) &= \widetilde{\mathbb{T}}'_\delta(y)\mathrm{e}^{\mathrm{i}(\alpha z+\beta x-\omega t)},\end{aligned}$$

where $\alpha \geq 0$ is the streamwise wave number, $\beta \geq 0$ is the spanwise wave number and ω denotes the complex frequency. Then the Laplace operator transforms as

$$\Delta = \frac{\partial^2}{\partial x^2}+\frac{\partial^2}{\partial y^2}+\frac{\partial^2}{\partial z^2} \quad \longmapsto \quad \widetilde{\Delta} =_{\mathrm{def}} -\alpha^2-\beta^2+\frac{\mathrm{d}^2}{\mathrm{d}y^2} = \frac{\mathrm{d}^2}{\mathrm{d}y^2}-k^2,$$

where $k^2 =_{\mathrm{def}} \alpha^2+\beta^2$ is the wave number, and (4.81) and (4.83) reduce to

$$\begin{aligned}&\left[\left(-\mathrm{i}\omega+\mathrm{i}\alpha\bar{v}^{\hat{z}}\right)\left(\frac{\mathrm{d}^2}{\mathrm{d}y^2}-k^2\right)-\mathrm{i}\alpha\frac{\mathrm{d}^2\bar{v}^{\hat{z}}}{\mathrm{d}y^2}\right]\tilde{v}'^{\hat{y}} =\\ &\qquad -\frac{1}{\mathcal{R}_1}\frac{\mathrm{d}}{\mathrm{d}y}\left[\widetilde{\mathrm{div}}\left(\widetilde{\mathrm{div}}\,\widetilde{\mathbb{T}}'_\delta\right)\right]+\frac{1}{\mathcal{R}_1}\left(\frac{\mathrm{d}^2}{\mathrm{d}y^2}-k^2\right)\left(\widetilde{\mathrm{div}}\,\widetilde{\mathbb{T}}'_\delta\right)^{\hat{y}}, \quad (4.84a)\end{aligned}$$

$$\left(-\mathrm{i}\omega+\mathrm{i}\alpha\bar{v}^{\hat{z}}\right)\tilde{\eta}^{\hat{y}}-\mathrm{i}\beta\tilde{v}'^{\hat{y}}\frac{\mathrm{d}\bar{v}^{\hat{z}}}{\mathrm{d}y} = \frac{1}{\mathcal{R}_1}\left[\mathrm{i}\alpha\left(\widetilde{\mathrm{div}}\,\widetilde{\mathbb{T}}'_\delta\right)^{\hat{x}}-\mathrm{i}\beta\left(\widetilde{\mathrm{div}}\,\widetilde{\mathbb{T}}'_\delta\right)^{\hat{z}}\right], \quad (4.84b)$$

$\widetilde{\mathrm{div}}$ being the transformed divergence operator. The first equation for the normal velocity $\tilde{v}'^{\hat{y}}$ is a generalization of the Orr–Sommerfeld equation, Orr (1907a,b); Sommerfeld (1908), while the second equation for the normal vorticity $\tilde{\eta}^{\hat{y}}$ is a generalization of the Squire equation, Squire (1933). The whole system is closed with the linearized constitutive equation for the disturbance (4.77b). Note that (4.84) can be equivalently derived by taking the Fourier transform of (4.81) and (4.83) in the horizontal (x and z) directions.

The classical Orr–Sommerfeld and Squire equations can be easily derived from (4.84) by setting $f \equiv 1$. Indeed, in such a case, $\mathbb{D}' = \mathbb{T}'_\delta$ and we have from the incompressibility condition for the disturbance $\widetilde{\mathrm{div}}\,\widetilde{\mathbb{T}}'_\delta = \frac{1}{2}\widetilde{\Delta}\tilde{\boldsymbol{v}}'$. Thus

$$\widetilde{\mathrm{div}}\left(\widetilde{\mathrm{div}}\,\widetilde{\mathbb{T}}'_\delta\right) = 0, \qquad \mathrm{i}\alpha\left(\widetilde{\mathrm{div}}\,\widetilde{\mathbb{T}}'_\delta\right)^{\hat{x}}-\mathrm{i}\beta\left(\widetilde{\mathrm{div}}\,\widetilde{\mathbb{T}}'_\delta\right)^{\hat{z}} = \frac{1}{2}\widetilde{\Delta}\tilde{\eta}^{\hat{y}},$$

and we recover the classical homogeneous Orr–Sommerfeld equation and the classical Squire equation[8]

$$\left[\left(-\mathrm{i}\omega+\mathrm{i}\alpha\bar{v}^{\hat{z}}\right)\left(\frac{\mathrm{d}^2}{\mathrm{d}y^2}-k^2\right)-\mathrm{i}\alpha\frac{\mathrm{d}^2\bar{v}^{\hat{z}}}{\mathrm{d}y^2}-\frac{1}{2\mathcal{R}_1}\left(\frac{\mathrm{d}^2}{\mathrm{d}y^2}-k^2\right)^2\right]\tilde{v}'^{\hat{y}} = 0, \quad (4.85a)$$

$$\left[\left(-\mathrm{i}\omega+\mathrm{i}\alpha\bar{v}^{\hat{z}}\right)-\frac{1}{2\mathcal{R}_1}\left(\frac{\mathrm{d}^2}{\mathrm{d}y^2}-k^2\right)\right]\tilde{\eta}^{\hat{y}} = \mathrm{i}\beta\tilde{v}'^{\hat{y}}\frac{\mathrm{d}\bar{v}^{\hat{z}}}{\mathrm{d}y}. \quad (4.85b)$$

[8]Remember that the relation between the classical Reynolds number and its analogue is $\mathrm{Re} = 2\mathcal{R}_1$.

Solutions of the generalized Orr–Sommerfeld equation in two- and three-dimensions

We can show that to each three-dimensional solution of the generalized Orr–Sommerfeld equation (4.84a) corresponds a two-dimensional solution at a lower Reynolds number analogue $\mathcal{R}_1$. Following Schmid and Henningson (2001), we shall consider the complex phase speed c given by

$$\omega = \alpha c. \tag{4.86}$$

Then the generalized Orr–Sommerfeld equation (4.84a) can be rewritten as

$$\left[\left(\bar{v}^{\hat{z}} - c\right)\left(\frac{\mathrm{d}^2}{\mathrm{d}y^2} - k^2\right) - \frac{\mathrm{d}^2\bar{v}^{\hat{z}}}{\mathrm{d}y^2}\right]\tilde{v}'^{\hat{y}} = - \frac{1}{\mathrm{i}\alpha\mathcal{R}_1}\frac{\mathrm{d}}{\mathrm{d}y}\left[\widetilde{\mathrm{div}}\left(\widetilde{\mathrm{div}}\,\widetilde{\mathbb{T}}'_\delta\right)\right] + \frac{1}{\mathrm{i}\alpha\mathcal{R}_1}\left(\frac{\mathrm{d}^2}{\mathrm{d}y^2} - k^2\right)\left(\widetilde{\mathrm{div}}\,\widetilde{\mathbb{T}}'_\delta\right)^{\hat{y}}. \tag{4.87}$$

and it is to be compared with the two-dimensional ($\beta = 0$) generalized Orr–Sommerfeld equation

$$\left[\left(\bar{v}^{\hat{z}} - c\right)\left(\frac{\mathrm{d}^2}{\mathrm{d}y^2} - \alpha_{2D}^2\right) - \frac{\mathrm{d}^2\bar{v}^{\hat{z}}}{\mathrm{d}y^2}\right]\tilde{v}'^{\hat{y}} = - \frac{1}{\mathrm{i}\alpha_{2D}\mathcal{R}_1^{2D}}\frac{\mathrm{d}}{\mathrm{d}y}\left[\widetilde{\mathrm{div}}\left(\widetilde{\mathrm{div}}\,\widetilde{\mathbb{T}}'_\delta\right)\right] + \frac{1}{\mathrm{i}\alpha_{2D}\mathcal{R}_1^{2D}}\left(\frac{\mathrm{d}^2}{\mathrm{d}y^2} - \alpha_{2D}^2\right)\left(\widetilde{\mathrm{div}}\,\widetilde{\mathbb{T}}'_\delta\right)^{\hat{y}}. \tag{4.88}$$

Apparently, these two equations have the same solutions if the following Squire-like transformation holds

$$\alpha_{2D} = k = \sqrt{\alpha^2 + \beta^2}, \tag{4.89a}$$

$$\alpha_{2D}\mathcal{R}_1^{2D} = \alpha\mathcal{R}_1, \tag{4.89b}$$

and as a consequence

$$\mathcal{R}_1^{2D} = \mathcal{R}_1\frac{\alpha}{k} < \mathcal{R}_1. \tag{4.90}$$

Thus, if the flow is unstable due to a three-dimensional disturbance, instability due to a two-dimensional disturbance appears at a lower Reynolds number analogue.

4.4.4 Two-dimensional disturbances

Since we have just shown that three-dimensional disturbances cause instability at higher Reynolds numbers, we shall assume two-dimensional disturbances and consequently only two-dimensional flows. In this case, the disturbance has no $\boldsymbol{e}_{\hat{x}}$ component and does not depend on the x-coordinate, that is

$$v'^{\hat{x}} = 0, \qquad \boldsymbol{v}' = \boldsymbol{v}'(y,z,t) = \tilde{\boldsymbol{v}}'(y)\mathrm{e}^{\mathrm{i}(\alpha z - \omega t)}, \qquad k = \alpha.$$

Then just (4.84a) (together with the linearized constitutive law) is enough to fully determine the perturbed velocity and pressure fields. Indeed, the incompressibility condition

$$\frac{\mathrm{d}\tilde{v}'^{\hat{y}}}{\mathrm{d}y} + \mathrm{i}\alpha\tilde{v}'^{\hat{z}} = 0, \tag{4.91}$$

gives us a relation between $v'^{\hat{y}}$ and $v'^{\hat{z}}$ and the pressure can be reconstructed using (4.78).

Taking the y-derivative of (4.91) yields

$$\frac{\mathrm{d}\tilde{v}'^{\hat{z}}}{\mathrm{d}y} = \frac{\mathrm{i}}{\alpha}\frac{\mathrm{d}^2\tilde{v}'^{\hat{y}}}{\mathrm{d}y^2},$$

which can be used to express the symmetric part of the disturbance velocity gradient only in terms of $\tilde{v}'^{\hat{y}}$

$$\widetilde{\mathbb{D}}' = \begin{bmatrix} 0 & 0 & 0 \\ 0 & \frac{\mathrm{d}\tilde{v}'^{\hat{y}}}{\mathrm{d}y} & \frac{1}{2}\left(\mathrm{i}\alpha\tilde{v}'^{\hat{y}} + \frac{\mathrm{d}\tilde{v}'^{\hat{z}}}{\mathrm{d}y}\right) \\ 0 & \frac{1}{2}\left(\mathrm{i}\alpha\tilde{v}'^{\hat{y}} + \frac{\mathrm{d}\tilde{v}'^{\hat{z}}}{\mathrm{d}y}\right) & \mathrm{i}\alpha\tilde{v}'^{\hat{z}} \end{bmatrix} = \begin{bmatrix} 0 & 0 & 0 \\ 0 & \frac{\mathrm{d}\tilde{v}'^{\hat{y}}}{\mathrm{d}y} & \frac{\mathrm{i}}{2\alpha}\left(\alpha^2\tilde{v}'^{\hat{y}} + \frac{\mathrm{d}^2\tilde{v}'^{\hat{y}}}{\mathrm{d}y^2}\right) \\ 0 & \frac{\mathrm{i}}{2\alpha}\left(\alpha^2\tilde{v}'^{\hat{y}} + \frac{\mathrm{d}^2\tilde{v}'^{\hat{y}}}{\mathrm{d}y^2}\right) & -\frac{\mathrm{d}\tilde{v}'^{\hat{y}}}{\mathrm{d}y} \end{bmatrix}. \quad (4.92)$$

Assuming that the disturbance stress tensor is symmetric and exploiting that $\operatorname{Tr}\mathbb{T}'_\delta = 0$, we have

$$\widetilde{\mathbb{T}}'_\delta = \begin{bmatrix} 0 & 0 & 0 \\ 0 & \mathrm{T}'^{\hat{y}\hat{y}}_\delta & \mathrm{T}'^{\hat{y}\hat{z}}_\delta \\ 0 & \mathrm{T}'^{\hat{y}\hat{z}}_\delta & -\mathrm{T}'^{\hat{y}\hat{y}}_\delta \end{bmatrix},$$

and its divergence is

$$\widetilde{\operatorname{div}}\widetilde{\mathbb{T}}'_\delta = \begin{bmatrix} 0 \\ \frac{\mathrm{d}\tilde{\mathrm{T}}'^{\hat{y}\hat{y}}_\delta}{\mathrm{d}y} + \mathrm{i}\alpha\tilde{\mathrm{T}}'^{\hat{y}\hat{z}}_\delta \\ \frac{\mathrm{d}\tilde{\mathrm{T}}'^{\hat{y}\hat{z}}_\delta}{\mathrm{d}y} - \mathrm{i}\alpha\tilde{\mathrm{T}}'^{\hat{y}\hat{y}}_\delta \end{bmatrix}.$$

Now, we can compute for the quantity on the right-hand side of (4.84a)

$$\begin{aligned} -\frac{\mathrm{d}}{\mathrm{d}y}\left[\widetilde{\operatorname{div}}\left(\widetilde{\operatorname{div}}\widetilde{\mathbb{T}}'_\delta\right)\right] + \left(\frac{\mathrm{d}^2}{\mathrm{d}y^2} - \alpha^2\right)\left(\widetilde{\operatorname{div}}\widetilde{\mathbb{T}}'_\delta\right)^{\hat{y}} &= -\frac{\mathrm{d}}{\mathrm{d}y}\left[\frac{\mathrm{d}}{\mathrm{d}y}\left(\widetilde{\operatorname{div}}\widetilde{\mathbb{T}}'_\delta\right)^{\hat{y}} + \mathrm{i}\alpha\left(\widetilde{\operatorname{div}}\widetilde{\mathbb{T}}'_\delta\right)^{\hat{z}}\right] \\ &\quad + \left(\frac{\mathrm{d}^2}{\mathrm{d}y^2} - \alpha^2\right)\left(\widetilde{\operatorname{div}}\widetilde{\mathbb{T}}'_\delta\right)^{\hat{y}} \\ &= -\mathrm{i}\alpha\frac{\mathrm{d}}{\mathrm{d}y}\left(\widetilde{\operatorname{div}}\widetilde{\mathbb{T}}'_\delta\right)^{\hat{z}} - \alpha^2\left(\widetilde{\operatorname{div}}\widetilde{\mathbb{T}}'_\delta\right)^{\hat{y}} \\ &= -2\alpha^2\frac{\mathrm{d}\tilde{\mathrm{T}}'^{\hat{y}\hat{y}}_\delta}{\mathrm{d}y} - \mathrm{i}\alpha\left(\frac{\mathrm{d}^2}{\mathrm{d}y^2} + \alpha^2\right)\tilde{\mathrm{T}}'^{\hat{y}\hat{z}}_\delta. \end{aligned}$$

The basic stress tensor is assumed to be of the form (4.4), therefore

$$\widetilde{\mathbb{T}}'_\delta : \bar{\mathbb{T}}_\delta = \begin{bmatrix} 0 & 0 & 0 \\ 0 & \tilde{\mathrm{T}}'^{\hat{y}\hat{y}}_\delta & \tilde{\mathrm{T}}'^{\hat{y}\hat{z}}_\delta \\ 0 & \tilde{\mathrm{T}}'^{\hat{y}\hat{z}}_\delta & -\tilde{\mathrm{T}}'^{\hat{y}\hat{y}}_\delta \end{bmatrix} : \begin{bmatrix} 0 & 0 & 0 \\ 0 & 0 & T \\ 0 & T & 0 \end{bmatrix} = 2T\tilde{\mathrm{T}}'^{\hat{y}\hat{z}}_\delta.$$

The symmetric part of the disturbance velocity gradient must satisfy both the definition (4.92) and the linearized constitutive relation (4.77b), thus

$$\begin{bmatrix} \frac{\mathrm{d}\tilde{v}'^{\hat{y}}}{\mathrm{d}y} & \frac{\mathrm{i}}{2\alpha}\left(\alpha^2\tilde{v}'^{\hat{y}} + \frac{\mathrm{d}^2\tilde{v}'^{\hat{y}}}{\mathrm{d}y^2}\right) \\ \frac{\mathrm{i}}{2\alpha}\left(\alpha^2\tilde{v}'^{\hat{y}} + \frac{\mathrm{d}^2\tilde{v}'^{\hat{y}}}{\mathrm{d}y^2}\right) & -\frac{\mathrm{d}\tilde{v}'^{\hat{y}}}{\mathrm{d}y} \end{bmatrix} = \bar{f}\begin{bmatrix} \tilde{\mathrm{T}}'^{\hat{y}\hat{y}}_\delta & \tilde{\mathrm{T}}'^{\hat{y}\hat{z}}_\delta \\ \tilde{\mathrm{T}}'^{\hat{y}\hat{z}}_\delta & -\tilde{\mathrm{T}}'^{\hat{y}\hat{y}}_\delta \end{bmatrix} + 2\frac{\mathrm{d}\bar{f}}{\mathrm{d}s}\left(2T^2\tilde{\mathrm{T}}'^{\hat{y}\hat{z}}_\delta\right)\begin{bmatrix} 0 & 1 \\ 1 & 0 \end{bmatrix},$$

where we used the notation

$$\bar{f} =_{\text{def}} f\left(\left|\bar{\mathbb{T}}_\delta\right|^2\right), \qquad \frac{\mathrm{d}\bar{f}}{\mathrm{d}s} =_{\text{def}} \left.\frac{\mathrm{d}f}{\mathrm{d}s}\right|_{s=\left|\bar{\mathbb{T}}_\delta\right|^2}.$$

Term by term comparison leads to

$$\frac{\mathrm{d}\tilde{v}'^{\hat{y}}}{\mathrm{d}y} = f\left(\left|\bar{\mathbb{T}}_\delta\right|^2\right)\tilde{\mathrm{T}}_\delta'^{\hat{y}\hat{y}},$$
$$\frac{\mathrm{i}}{2\alpha}\left(\alpha^2\tilde{v}'^{\hat{y}} + \frac{\mathrm{d}^2\tilde{v}'^{\hat{y}}}{\mathrm{d}y^2}\right) = \left[f\left(\left|\bar{\mathbb{T}}_\delta\right|^2\right) + 4T^2\left.\frac{\partial f}{\partial s}\right|_{s=\left|\bar{\mathbb{T}}_\delta\right|^2}\right]\tilde{\mathrm{T}}_\delta'^{\hat{y}\hat{z}},$$

and so the complete system to be solved reads

$$\left[\left(-\mathrm{i}\omega + \mathrm{i}\alpha\bar{v}^{\hat{z}}\right)\left(\frac{\mathrm{d}^2}{\mathrm{d}y^2} - \alpha^2\right) - \mathrm{i}\alpha\frac{\mathrm{d}^2\bar{v}^{\hat{z}}}{\mathrm{d}y^2}\right]\tilde{v}'^{\hat{y}} = -\frac{2\alpha^2}{\mathcal{R}_1}\frac{\mathrm{d}\tilde{\mathrm{T}}_\delta'^{\hat{y}\hat{y}}}{\mathrm{d}y} - \frac{\mathrm{i}\alpha}{\mathcal{R}_1}\left(\frac{\mathrm{d}^2}{\mathrm{d}y^2} + \alpha^2\right)\tilde{\mathrm{T}}_\delta'^{\hat{y}\hat{z}}, \tag{4.93a}$$

$$\frac{\mathrm{d}\tilde{v}'^{\hat{y}}}{\mathrm{d}y} = f\left(\left|\bar{\mathbb{T}}_\delta\right|^2\right)\tilde{\mathrm{T}}_\delta'^{\hat{y}\hat{y}}, \tag{4.93b}$$

$$\frac{\mathrm{i}}{2\alpha}\left(\frac{\mathrm{d}^2}{\mathrm{d}y^2} + \alpha^2\right)\tilde{v}'^{\hat{y}} = \left[f\left(\left|\bar{\mathbb{T}}_\delta\right|^2\right) + 4T^2\left.\frac{\mathrm{d}f}{\mathrm{d}s}\right|_{s=\left|\bar{\mathbb{T}}_\delta\right|^2}\right]\tilde{\mathrm{T}}_\delta'^{\hat{y}\hat{z}}. \tag{4.93c}$$

This is a generalized eigenvalue problem for the frequency ω as the eigenvalue.

Exploiting the solution of the plane Poiseuille flow (4.17), the system (4.93) can be consequently written as

$$\left[\left(-\mathrm{i}\omega + \mathrm{i}\alpha\bar{v}^{\hat{z}}\right)\left(\frac{\mathrm{d}^2}{\mathrm{d}y^2} - \alpha^2\right) - \mathrm{i}\alpha\frac{\mathrm{d}^2\bar{v}^{\hat{z}}}{\mathrm{d}y^2}\right]\tilde{v}'^{\hat{y}} = -\frac{2\alpha^2}{\mathcal{R}_1}\frac{\mathrm{d}\tilde{\mathrm{T}}_\delta'^{\hat{y}\hat{y}}}{\mathrm{d}y} - \frac{\mathrm{i}\alpha}{\mathcal{R}_1}\left(\frac{\mathrm{d}^2}{\mathrm{d}y^2} + \alpha^2\right)\tilde{\mathrm{T}}_\delta'^{\hat{y}\hat{z}}, \tag{4.94a}$$

$$2Cy\frac{\mathrm{d}\tilde{v}'^{\hat{y}}}{\mathrm{d}y} = \frac{\mathrm{d}\bar{v}^{\hat{z}}}{\mathrm{d}y}\tilde{\mathrm{T}}_\delta'^{\hat{y}\hat{y}}, \tag{4.94b}$$

$$\frac{\mathrm{i}C}{\alpha}\left(\frac{\mathrm{d}^2}{\mathrm{d}y^2} + \alpha^2\right)\tilde{v}'^{\hat{y}} = \frac{\mathrm{d}^2\bar{v}^{\hat{z}}}{\mathrm{d}y^2}\tilde{\mathrm{T}}_\delta'^{\hat{y}\hat{z}}. \tag{4.94c}$$

4.4.5 Boundary conditions

The final system (4.94) must be also supplemented with set of boundary conditions. We shall consider the disturbance to be zero on the channel wall, i.e.,

$$\boldsymbol{v}'\big|_{y=\pm1} = \boldsymbol{0}. \tag{4.95}$$

In other words, this expresses the *no-slip* and the *no-penetration* boundary conditions for the disturbance. Relation (4.95) implies that

$$\tilde{\boldsymbol{v}}'\big|_{y=\pm1} = \begin{bmatrix} 0 \\ \tilde{v}'^{\hat{y}} \\ \tilde{v}'^{\hat{z}} \end{bmatrix}_{y=\pm1} = \boldsymbol{0}.$$

In virtue of the incompressibility condition (4.91), boundary condition for $\tilde{v}'^{\hat{z}}$ reads

$$\frac{\mathrm{d}\tilde{v}'^{\hat{y}}}{\mathrm{d}y}(\pm1) = 0.$$

Thus the complete set of boundary conditions is

$$\tilde{v}'^{\hat{y}}(\pm 1) = \frac{\mathrm{d}\tilde{v}'^{\hat{y}}}{\mathrm{d}y}(\pm 1) = 0. \tag{4.96}$$

4.5 Eigenvalue bounds

The complete system to be solved is (4.94) supplemented with the set of boundary conditions (4.96). As noted before, it is a generalized eigenvalue problem with the frequency ω being the eigenvalue. Here, we shall provide estimates on the eigenvalues closely following Joseph (1968).

Instead of the complex frequency ω, we will consider the complex phase speed $c = c_r + \mathrm{i}c_i$ given by (4.86). This results in slightly different version of (4.94)

$$\left[\left(\bar{v}^{\hat{z}} - c\right)\left(\frac{\mathrm{d}^2}{\mathrm{d}y^2} - \alpha^2\right) - \frac{\mathrm{d}^2\bar{v}^{\hat{z}}}{\mathrm{d}y^2}\right]\tilde{v}'^{\hat{y}} = \frac{2\mathrm{i}\alpha}{\mathcal{R}_1}\frac{\mathrm{d}\tilde{\mathrm{T}}_\delta'^{\hat{y}\hat{y}}}{\mathrm{d}y} - \frac{1}{\mathcal{R}_1}\left(\frac{\mathrm{d}^2}{\mathrm{d}y^2} + \alpha^2\right)\tilde{\mathrm{T}}_\delta'^{\hat{y}\hat{z}}. \tag{4.97}$$

Multiplying (4.97) with the complex conjugate of $\tilde{v}'^{\hat{y}}$ and integrating over the y-interval yields on the left hand side the following terms

$$\begin{aligned}
\int_{-1}^{1}\bar{v}^{\hat{z}}\frac{\mathrm{d}^2\tilde{v}'^{\hat{y}}}{\mathrm{d}y^2}\left(\tilde{v}'^{\hat{y}}\right)^*\mathrm{d}y &= -\int_{-1}^{1}\frac{\mathrm{d}\bar{v}^{\hat{z}}}{\mathrm{d}y}\frac{\mathrm{d}\tilde{v}'^{\hat{y}}}{\mathrm{d}y}\left(\tilde{v}'^{\hat{y}}\right)^*\mathrm{d}y - \int_{-1}^{1}\bar{v}^{\hat{z}}\left|\frac{\mathrm{d}\tilde{v}'^{\hat{y}}}{\mathrm{d}y}\right|^2\mathrm{d}y,\\
-\alpha^2\int_{-1}^{1}\bar{v}^{\hat{z}}\tilde{v}'^{\hat{y}}\left(\tilde{v}'^{\hat{y}}\right)^*\mathrm{d}y &= -\alpha^2\int_{-1}^{1}\bar{v}^{\hat{z}}\left|\tilde{v}'^{\hat{y}}\right|^2\mathrm{d}y,\\
-c\int_{-1}^{1}\frac{\mathrm{d}^2\tilde{v}'^{\hat{y}}}{\mathrm{d}y^2}\left(\tilde{v}'^{\hat{y}}\right)^*\mathrm{d}y &= c\int_{-1}^{1}\left|\frac{\mathrm{d}\tilde{v}'^{\hat{y}}}{\mathrm{d}y}\right|^2\mathrm{d}y = cI_1^2,\\
\alpha^2 c\int_{-1}^{1}\tilde{v}'^{\hat{y}}\left(\tilde{v}'^{\hat{y}}\right)^*\mathrm{d}y &= \alpha^2 c\int_{-1}^{1}\left|\tilde{v}'^{\hat{y}}\right|^2\mathrm{d}y = \alpha^2 cI_0^2,\\
-\int_{1}^{1}\frac{\mathrm{d}^2\bar{v}^{\hat{z}}}{\mathrm{d}y^2}\tilde{v}'^{\hat{y}}\left(\tilde{v}'^{\hat{y}}\right)^*\mathrm{d}y &= -\int_{1}^{1}\frac{\mathrm{d}^2\bar{v}^{\hat{z}}}{\mathrm{d}y^2}\left|\tilde{v}'^{\hat{y}}\right|^2\mathrm{d}y,
\end{aligned}$$

where we used the boundary conditions (4.96) and have defined

$$I_0^2 =_{\mathrm{def}} \int_{-1}^{1}\left|\tilde{v}'^{\hat{y}}\right|^2\mathrm{d}y, \qquad I_1^2 =_{\mathrm{def}} \int_{-1}^{1}\left|\frac{\mathrm{d}\tilde{v}'^{\hat{y}}}{\mathrm{d}y}\right|^2\mathrm{d}y. \tag{4.98}$$

Since

$$\begin{aligned}
\frac{\mathrm{d}\tilde{v}'^{\hat{y}}}{\mathrm{d}y}\left(\tilde{v}'^{\hat{y}}\right)^* &= \frac{1}{2}\left(\frac{\mathrm{d}\tilde{v}'^{\hat{y}}}{\mathrm{d}y}\left(\tilde{v}'^{\hat{y}}\right)^* + \tilde{v}'^{\hat{y}}\frac{\mathrm{d}(\tilde{v}'^{\hat{y}})^*}{\mathrm{d}y}\right) + \mathrm{i}\frac{1}{2\mathrm{i}}\left(\frac{\mathrm{d}\tilde{v}'^{\hat{y}}}{\mathrm{d}y}\left(\tilde{v}'^{\hat{y}}\right)^* - \tilde{v}'^{\hat{y}}\frac{\mathrm{d}(\tilde{v}'^{\hat{y}})^*}{\mathrm{d}y}\right)\\
&= \frac{1}{2}\frac{\mathrm{d}|\tilde{v}'^{\hat{y}}|^2}{\mathrm{d}y} - \mathrm{i}\frac{\mathrm{i}}{2}\left(\frac{\mathrm{d}\tilde{v}'^{\hat{y}}}{\mathrm{d}y}\left(\tilde{v}'^{\hat{y}}\right)^* - \tilde{v}'^{\hat{y}}\frac{\mathrm{d}(\tilde{v}'^{\hat{y}})^*}{\mathrm{d}y}\right),
\end{aligned}$$

the first identity can be further rewritten as

$$\begin{aligned}
\int_{-1}^{1}\bar{v}^{\hat{z}}\frac{\mathrm{d}^2\tilde{v}'^{\hat{y}}}{\mathrm{d}y^2}\left(\tilde{v}'^{\hat{y}}\right)^*\mathrm{d}y &= -\int_{-1}^{1}\frac{\mathrm{d}\bar{v}^{\hat{z}}}{\mathrm{d}y}\frac{\mathrm{d}\tilde{v}'^{\hat{y}}}{\mathrm{d}y}\left(\tilde{v}'^{\hat{y}}\right)^*\mathrm{d}y - \int_{-1}^{1}\bar{v}^{\hat{z}}\left|\frac{\mathrm{d}\tilde{v}'^{\hat{y}}}{\mathrm{d}y}\right|^2\mathrm{d}y\\
&= -\mathrm{i}(Q - Q^*) - \frac{1}{2}\int_{-1}^{1}\frac{\mathrm{d}\bar{v}^{\hat{z}}}{\mathrm{d}y}\frac{\mathrm{d}|\tilde{v}'^{\hat{y}}|^2}{\mathrm{d}y}\mathrm{d}y - \int_{-1}^{1}\bar{v}^{\hat{z}}\left|\frac{\mathrm{d}\tilde{v}'^{\hat{y}}}{\mathrm{d}y}\right|^2\mathrm{d}y\\
&= -\mathrm{i}(Q - Q^*) + \frac{1}{2}\int_{-1}^{1}\frac{\mathrm{d}^2\bar{v}^{\hat{z}}}{\mathrm{d}y^2}\left|\tilde{v}'^{\hat{y}}\right|^2\mathrm{d}y - \int_{-1}^{1}\bar{v}^{\hat{z}}\left|\frac{\mathrm{d}\tilde{v}'^{\hat{y}}}{\mathrm{d}y}\right|^2\mathrm{d}y.
\end{aligned}$$

where

$$Q =_{\text{def}} \frac{\mathrm{i}}{2}\int_{-1}^{1}\frac{\mathrm{d}\bar{v}^{\hat{z}}}{\mathrm{d}y}\tilde{v}'^{\hat{y}}\frac{\mathrm{d}(\tilde{v}'^{\hat{y}})^{*}}{\mathrm{d}y}\,\mathrm{d}y.$$

Altogether, the left hand side of (4.97) leads to

$$c\left(I_1^2+\alpha^2 I_0^2\right)-\mathrm{i}(Q-Q^*)-\int_{-1}^{1}\left[\bar{v}^{\hat{z}}\left|\frac{\mathrm{d}\tilde{v}'^{\hat{y}}}{\mathrm{d}y}\right|^2+\left(\alpha^2\bar{v}^{\hat{z}}+\frac{1}{2}\frac{\mathrm{d}^2\bar{v}^{\hat{z}}}{\mathrm{d}y^2}\right)\left|\tilde{v}'^{\hat{y}}\right|^2\right]\mathrm{d}y. \tag{4.99}$$

Concerning the terms emerging from the right hand side of (4.97), after taking into account the boundary conditions (4.96), we have

$$\frac{2\mathrm{i}\alpha}{\mathcal{R}_1}\int_{-1}^{1}\frac{\mathrm{d}\tilde{\mathrm{T}}_{\delta}^{\prime\hat{y}\hat{y}}}{\mathrm{d}y}\left(\tilde{v}'^{\hat{y}}\right)^{*}\mathrm{d}y=-\frac{2\mathrm{i}\alpha}{\mathcal{R}_1}\int_{-1}^{1}\tilde{\mathrm{T}}_{\delta}^{\prime\hat{y}\hat{y}}\frac{\mathrm{d}(\tilde{v}'^{\hat{y}})^{*}}{\mathrm{d}y}\,\mathrm{d}y, \tag{4.100a}$$

$$-\frac{1}{\mathcal{R}_1}\int_{-1}^{1}\left(\frac{\mathrm{d}^2}{\mathrm{d}y^2}+\alpha^2\right)\tilde{\mathrm{T}}_{\delta}^{\prime\hat{y}\hat{z}}\left(\tilde{v}'^{\hat{y}}\right)^{*}\mathrm{d}y=-\frac{1}{\mathcal{R}_1}\int_{-1}^{1}\tilde{\mathrm{T}}_{\delta}^{\prime\hat{y}\hat{z}}\left(\frac{\mathrm{d}^2}{\mathrm{d}y^2}+\alpha^2\right)\left(\tilde{v}'^{\hat{y}}\right)^{*}\mathrm{d}y. \tag{4.100b}$$

4.5.1 Estimates of the propagation speed

As can be seen from (4.94b) and (4.94c), the terms (4.100) arising from the right hand side of (4.97) are imaginary. Therefore, from (4.99), we see that the real part of the eigenvalue (*propagation speed*) satisfies

$$c_r=\left\{\int_{-1}^{1}\left[\bar{v}^{\hat{z}}\left|\frac{\mathrm{d}\tilde{v}'^{\hat{y}}}{\mathrm{d}y}\right|^2+\left(\alpha^2\bar{v}^{\hat{z}}+\frac{1}{2}\frac{\mathrm{d}^2\bar{v}^{\hat{z}}}{\mathrm{d}y^2}\right)\left|\tilde{v}'^{\hat{y}}\right|^2\right]\mathrm{d}y\right\}\Big/\left(I_1^2+\alpha^2 I_0^2\right), \tag{4.101}$$

which is the same result as for the eigenvalues of the classical Orr–Sommerfeld equation, see for example Synge (1938). Under additional assumption on the constitutive function $f\in C^1(\mathbb{R}_0^+)$, all the estimates of the propagation speed c_r given by Joseph (1968)[9] are valid, i.e.,

1. if $\left(\frac{\mathrm{d}^2\bar{v}^{\hat{z}}}{\mathrm{d}y^2}\right)_{\min}\geq 0$, then

$$\bar{v}_{\min}^{\hat{z}}<c_r<\bar{v}_{\max}^{\hat{z}}+\frac{2}{\pi^2+4\alpha^2}\left(\frac{\mathrm{d}^2\bar{v}^{\hat{z}}}{\mathrm{d}y^2}\right)_{\max}, \tag{4.102a}$$

2. if $\left(\frac{\mathrm{d}^2\bar{v}^{\hat{z}}}{\mathrm{d}y^2}\right)_{\min}\leq 0\leq\left(\frac{\mathrm{d}^2\bar{v}^{\hat{z}}}{\mathrm{d}y^2}\right)_{\max}$, then

$$\bar{v}_{\min}^{\hat{z}}+\frac{2}{\pi^2+4\alpha^2}\left(\frac{\mathrm{d}^2\bar{v}^{\hat{z}}}{\mathrm{d}y^2}\right)_{\min}<c_r<\bar{v}_{\max}^{\hat{z}}+\frac{2}{\pi^2+4\alpha^2}\left(\frac{\mathrm{d}^2\bar{v}^{\hat{z}}}{\mathrm{d}y^2}\right)_{\max}, \tag{4.102b}$$

3. if $\left(\frac{\mathrm{d}^2\bar{v}^{\hat{z}}}{\mathrm{d}y^2}\right)_{\max}\leq 0$, then

$$\bar{v}_{\min}^{\hat{z}}+\frac{2}{\pi^2+4\alpha^2}\left(\frac{\mathrm{d}^2\bar{v}^{\hat{z}}}{\mathrm{d}y^2}\right)_{\min}<c_r<\bar{v}_{\max}^{\hat{z}}, \tag{4.102c}$$

[9]The formulas in the original paper are slightly different since Joseph derived them for the interval $[0,1]$.

where $\bar{v}^{\hat{z}}_{\min}$, $\bar{v}^{\hat{z}}_{\max}$, $\left(\frac{\mathrm{d}^2\bar{v}^{\hat{z}}}{\mathrm{d}y^2}\right)_{\min}$ and $\left(\frac{\mathrm{d}^2\bar{v}^{\hat{z}}}{\mathrm{d}y^2}\right)_{\max}$ are minimum and maximum values of $\bar{v}^{\hat{z}}(y)$ and $\frac{\mathrm{d}^2\bar{v}^{\hat{z}}}{\mathrm{d}y^2}(y)$ for $y \in [-1,1]$. In other words, the propagation speed c_r is restricted to an interval which is slightly larger than the range of the basic flow velocity $\bar{v}^{\hat{z}}$.

From (4.17a) and (4.17c), the requirement $f \in C^1(\mathbb{R}_0^+)$ implies the continuity of $\bar{v}^{\hat{z}}$ and $\frac{\mathrm{d}^2\bar{v}^{\hat{z}}}{\mathrm{d}y^2}$. In order to proof the results, we can then express (4.101) using the mean value theorem as

$$c_r = \left[\bar{v}^{\hat{z}}(\xi_1)\left(I_1^2+\alpha^2 I_0^2\right)+\frac{1}{2}\frac{\mathrm{d}^2\bar{v}^{\hat{z}}}{\mathrm{d}y^2}(\xi_2)I_0^2\right]\Big/\left(I_1^2+\alpha^2 I_0^2\right) = \bar{v}^{\hat{z}}(\xi_1)+\frac{1}{2}\frac{\mathrm{d}^2\bar{v}^{\hat{z}}}{\mathrm{d}y^2}(\xi_2)\frac{1}{(I_1^2/I_0^2)+\alpha^2}, \quad (4.103)$$

where $\xi_1, \xi_2 \in (-1,1)$ are the mean values. Further, we employ the Wirtinger's inequality (4.72) from which follows that $I_1^2/I_0^2 \geq \frac{\pi^2}{4}$. In the particular cases of (4.102), we thus have

1. $\left(\frac{\mathrm{d}^2\bar{v}^{\hat{z}}}{\mathrm{d}y^2}\right)_{\min} \geq 0$:

$$0 < \frac{1}{2}\frac{\mathrm{d}^2\bar{v}^{\hat{z}}}{\mathrm{d}y^2}(\xi_2)\frac{1}{(I_1^2/I_0^2)+\alpha^2} < \frac{2}{\pi^2+4\alpha^2}\left(\frac{\mathrm{d}^2\bar{v}^{\hat{z}}}{\mathrm{d}y^2}\right)_{\max}, \quad (4.104a)$$

2. $\left(\frac{\mathrm{d}^2\bar{v}^{\hat{z}}}{\mathrm{d}y^2}\right)_{\min} \leq 0 \leq \left(\frac{\mathrm{d}^2\bar{v}^{\hat{z}}}{\mathrm{d}y^2}\right)_{\max}$:

$$\frac{2}{\pi^2+4\alpha^2}\left(\frac{\mathrm{d}^2\bar{v}^{\hat{z}}}{\mathrm{d}y^2}\right)_{\min} < \frac{1}{2}\frac{\mathrm{d}^2\bar{v}^{\hat{z}}}{\mathrm{d}y^2}(\xi_2)\frac{1}{(I_1^2/I_0^2)+\alpha^2} < \frac{2}{\pi^2+4\alpha^2}\left(\frac{\mathrm{d}^2\bar{v}^{\hat{z}}}{\mathrm{d}y^2}\right)_{\max}, \quad (4.104b)$$

3. $\left(\frac{\mathrm{d}^2\bar{v}^{\hat{z}}}{\mathrm{d}y^2}\right)_{\max} \leq 0$:

$$\frac{2}{\pi^2+4\alpha^2}\left(\frac{\mathrm{d}^2\bar{v}^{\hat{z}}}{\mathrm{d}y^2}\right)_{\min} < \frac{1}{2}\frac{\mathrm{d}^2\bar{v}^{\hat{z}}}{\mathrm{d}y^2}(\xi_2)\frac{1}{(I_1^2/I_0^2)+\alpha^2} < 0, \quad (4.104c)$$

and the estimates (4.102) immediately follow from (4.103) and (4.104).

Note that in both Drazin and Reid (2004) and Schmid and Henningson (2001), the upper bound of the estimate (4.102b) is missing the term $\bar{v}^{\hat{z}}_{\max}$. In the latter, also the lower bound is misspelled.

4.5.2 Estimates of the growth rate

To estimate the imaginary part of the eigenvalue (*growth rate*), we can express the relations for $\tilde{\mathrm{T}}_\delta^{\prime\hat{y}\hat{y}}$ and $\tilde{\mathrm{T}}_\delta^{\prime\hat{y}\hat{z}}$ from (4.94b) and (4.94c) as

$$\tilde{\mathrm{T}}_\delta^{\prime\hat{y}\hat{y}} = 2Cy\left(\frac{\mathrm{d}\bar{v}^{\hat{z}}}{\mathrm{d}y}\right)^{-1}\frac{\mathrm{d}\tilde{v}^{\prime\hat{y}}}{\mathrm{d}y},$$
$$\tilde{\mathrm{T}}_\delta^{\prime\hat{y}\hat{z}} = \mathrm{i}\frac{C}{\alpha}\left(\frac{\mathrm{d}^2\bar{v}^{\hat{z}}}{\mathrm{d}y^2}\right)^{-1}\left(\frac{\mathrm{d}}{\mathrm{d}y}+\alpha^2\right)\tilde{v}^{\prime\hat{y}},$$

and substitute them into (4.100)

$$\frac{2\mathrm{i}\alpha}{\mathcal{R}_1}\int_{-1}^{1}\tilde{\mathrm{T}}_{\delta}^{\prime\hat{y}\hat{y}}\frac{\mathrm{d}(\tilde{v}^{\prime\hat{y}})^*}{\mathrm{d}y}\,\mathrm{d}y=\mathrm{i}\frac{4C\alpha}{\mathcal{R}_1}\int_{-1}^{1}y\left(\frac{\mathrm{d}\bar{v}^{\hat{z}}}{\mathrm{d}y}\right)^{-1}\left|\frac{\mathrm{d}\tilde{v}^{\prime\hat{y}}}{\mathrm{d}y}\right|^2\mathrm{d}y, \tag{4.105a}$$

$$\begin{aligned}
&\frac{1}{\mathcal{R}_1}\int_{-1}^{1}\tilde{\mathrm{T}}_{\delta}^{\prime\hat{y}\hat{z}}\left(\frac{\mathrm{d}^2}{\mathrm{d}y^2}+\alpha^2\right)\left(\tilde{v}^{\prime\hat{y}}\right)^*\mathrm{d}y\\
&\quad=\mathrm{i}\frac{C}{\alpha\mathcal{R}_1}\int_{-1}^{1}\left(\frac{\mathrm{d}^2\bar{v}^{\hat{z}}}{\mathrm{d}y^2}\right)^{-1}\left(\frac{\mathrm{d}^2}{\mathrm{d}y^2}+\alpha^2\right)\tilde{v}^{\prime\hat{y}}\left(\frac{\mathrm{d}^2}{\mathrm{d}y^2}+\alpha^2\right)\left(\tilde{v}^{\prime\hat{y}}\right)^*\mathrm{d}y\\
&\quad=\mathrm{i}\frac{C}{\alpha\mathcal{R}_1}\int_{-1}^{1}\left(\frac{\mathrm{d}^2\bar{v}^{\hat{z}}}{\mathrm{d}y^2}\right)^{-1}\left[\left|\frac{\mathrm{d}^2\tilde{v}^{\prime\hat{y}}}{\mathrm{d}y^2}\right|^2+\alpha^4\left|\tilde{v}^{\prime\hat{y}}\right|^2+\alpha^2\left(\tilde{v}^{\prime\hat{y}}\frac{\mathrm{d}^2(\tilde{v}^{\prime\hat{y}})^*}{\mathrm{d}y^2}+\frac{\mathrm{d}^2\tilde{v}^{\prime\hat{y}}}{\mathrm{d}y^2}\left(\tilde{v}^{\prime\hat{y}}\right)^*\right)\right]\mathrm{d}y.
\end{aligned} \tag{4.105b}$$

From (4.17b), we further see that $y\left(\frac{\mathrm{d}\bar{v}^{\hat{z}}}{\mathrm{d}y}\right)^{-1}=\left[2Cf\left(2C^2y^2\right)\right]^{-1}$, and the growth rate is then obtained from (4.105) and (4.99) as

$$\begin{aligned}
c_i=\frac{Q-Q^*}{I_1^2+\alpha^2I_0^2}&-\frac{2\alpha}{\mathcal{R}_1\left(I_1^2+\alpha^2I_0^2\right)}\int_{-1}^{1}\frac{1}{f\left(2C^2y^2\right)}\left|\frac{\mathrm{d}\tilde{v}^{\prime\hat{y}}}{\mathrm{d}y}\right|^2\mathrm{d}y\\
&+\frac{|C|}{\alpha\mathcal{R}_1\left(I_1^2+\alpha^2I_0^2\right)}\times\\
\int_{-1}^{1}\left(\frac{\mathrm{d}^2\bar{v}^{\hat{z}}}{\mathrm{d}y^2}\right)^{-1}&\left[\left|\frac{\mathrm{d}^2\tilde{v}^{\prime\hat{y}}}{\mathrm{d}y^2}\right|^2+\alpha^4\left|\tilde{v}^{\prime\hat{y}}\right|^2+\alpha^2\left(\tilde{v}^{\prime\hat{y}}\frac{\mathrm{d}^2(\tilde{v}^{\prime\hat{y}})^*}{\mathrm{d}y^2}+\frac{\mathrm{d}^2\tilde{v}^{\prime\hat{y}}}{\mathrm{d}y^2}\left(\tilde{v}^{\prime\hat{y}}\right)^*\right)\right]\mathrm{d}y.
\end{aligned} \tag{4.106}$$

Here we have also used the fact that the pressure gradient C is negative. It is clear that the last integral diverges for base velocity profiles with inflection points, or equivalently for non-monotonous constitutive relations, see (4.17c). In other words, the growth rate is unbounded and the flow is unstable. This is a tantamount result to those concluded earlier in this chapter and in Chapter 3.

For parabolic-like velocity profiles when $\frac{\mathrm{d}^2\bar{v}^{\hat{z}}}{\mathrm{d}y^2}<0$, using the estimate

$$|Q-Q^*|\le qI_0I_1,\qquad q=_{\mathrm{def}}\max_{y\in[-1,1]}\left|\frac{\mathrm{d}\bar{v}^{\hat{z}}}{\mathrm{d}y}(y)\right|, \tag{4.107}$$

and the fact that f is positive, we can bound the growth rate as

$$\begin{aligned}
c_i\le\frac{qI_0I_1}{I_1^2+\alpha^2I_0^2}&-\frac{2\alpha I_1^2}{\mathcal{R}_1\left(I_1^2+\alpha^2I_0^2\right)\max f\left(2C^2y^2\right)}\\
&-\frac{|C|}{\alpha\mathcal{R}_1\left(I_1^2+\alpha^2I_0^2\right)\max\left|\frac{\mathrm{d}^2\bar{v}^{\hat{z}}}{\mathrm{d}y^2}\right|}\left(I_2^2-2\alpha^2I_1^2+\alpha^4I_0^2\right).
\end{aligned} \tag{4.108}$$

For the last term we have used integration by parts and the quantities I_0, I_1 and I_2 are given by (4.98) and by additional definition

$$I_2^2=_{\mathrm{def}}\int_{-1}^{1}\left|\frac{\mathrm{d}^2\tilde{v}^{\prime\hat{y}}}{\mathrm{d}y^2}\right|^2\mathrm{d}y. \tag{4.109}$$

From (4.17c) that connects the second derivative of the base flow and the constitutive relation

$$0 > \frac{\mathrm{d}^2\bar{v}^{\hat{z}}}{\mathrm{d}y^2} = 2C\left[f\left(2C^2y^2\right) + 4C^2y^2\left.\frac{\mathrm{d}f}{\mathrm{d}s}\right|_{s=2C^2y^2}\right], \tag{4.110}$$

we see that $f\left(2C^2y^2\right) + 4C^2y^2\left.\frac{\mathrm{d}f}{\mathrm{d}s}\right|_{s=2C^2y^2}$ is positive. Under a reasonable assumption that the function f is monotonous, we have to distinct between $\frac{\mathrm{d}f}{\mathrm{d}s}$ being non-negative or nonpositive.

For $\frac{\mathrm{d}f}{\mathrm{d}s} \geq 0$, the bound (4.108) can be further rewritten using $-\frac{1}{f(2C^2y^2)} \leq -\frac{1}{f(2C^2y^2)+4C^2y^2\left.\frac{\mathrm{d}f}{\mathrm{d}s}\right|_{s=2C^2y^2}}$ as

$$\begin{aligned} c_i \leq{}& \frac{qI_0I_1}{I_1^2+\alpha^2I_0^2} \\ &- \frac{1}{2\alpha\mathcal{R}_1\left(I_1^2+\alpha^2I_0^2\right)\max\left(f\left(2C^2y^2\right) + 4C^2y^2\left.\frac{\mathrm{d}f}{\mathrm{d}s}\right|_{s=2C^2y^2}\right)}\left(I_2^2+2\alpha^2I_1^2+\alpha^4I_0^2\right). \end{aligned} \tag{4.111}$$

Since $\mu \sim f^{-1}$, this situation corresponds to the shear-thinning fluids. On the contrary, for shear-thickening fluids when $\frac{\mathrm{d}f}{\mathrm{d}s} \leq 0$, we exploit $-\frac{1}{f(2C^2y^2)+4C^2y^2\left.\frac{\mathrm{d}f}{\mathrm{d}s}\right|_{s=2C^2y^2}} \leq -\frac{1}{f(2C^2y^2)}$ in (4.108) to obtain

$$c_i \leq \frac{qI_0I_1}{I_1^2+\alpha^2I_0^2} - \frac{1}{2\alpha\mathcal{R}_1\left(I_1^2+\alpha^2I_0^2\right)\max f\left(2C^2y^2\right)}\left(I_2^2+2\alpha^2I_1^2+\alpha^4I_0^2\right). \tag{4.112}$$

Both in (4.111) and (4.112), the second terms have clearly stabilizing effect as they diminish the growth rate for smaller Reynolds numbers.

The estimate for classical Newtonian fluid, $f \equiv 1$ and $\frac{\mathrm{d}^2\bar{v}^{\hat{z}}}{\mathrm{d}y^2} = 2C$, can be easily obtained from (4.108), (4.111) or (4.112) as

$$c_i \leq \frac{qI_0I_1 - \left(2\alpha\mathcal{R}_1\right)^{-1}\left(I_2^2+2\alpha^2I_1^2+\alpha^4I_0^2\right)}{I_1^2+\alpha^2I_0^2}. \tag{4.113}$$

This result was first given by Synge (1938) and later stated (though with a misspelled denominator) by Joseph (1968).

The first term in the estimates can be additionally bounded using the inequality

$$2\alpha I_0I_1 \leq I_1^2+\alpha^2I_0^2, \tag{4.114}$$

which follows from $0 \leq (a-b)^2 = a^2 - 2ab + b^2$ by setting $a = I_1$ and $b = \alpha I_0$, while the second term can be bounded as

$$\begin{aligned} -\left(I_2^2+2\alpha^2I_1^2+\alpha^4I_0^2\right) &= -\left(I_2^2+\alpha^2I_1^2\right) - \alpha^2\left(I_1^2+\alpha^2I_0^2\right) \\ &\leq -\left(\frac{\pi^2}{4}+\alpha^2\right)I_1^2 - \alpha^2\left(\frac{\pi^2}{4}+\alpha^2\right)I_0^2 \\ &= -\left(\frac{\pi^2}{4}+\alpha^2\right)\left(I_1^2+\alpha^2I_0^2\right). \end{aligned} \tag{4.115}$$

This is obtained from inequalities

$$I_0^2 \leq \frac{4}{\pi^2}I_1^2, \qquad I_1^2 \leq \frac{4}{\pi^2}I_2^2, \tag{4.116}$$

which are a consequence of the general Wirtinger's inequality (4.72). So, for example, the estimate for the Newtonian fluid (4.113) takes the form

$$c_i \leq \frac{q}{2\alpha} - (2\alpha\mathcal{R}_1)^{-1}\left(\frac{\pi^2}{4}+\alpha^2\right), \tag{4.117}$$

where the first term amounts to the inviscid result of Høiland (1953).

Stress representation

The integrals in (4.100) can be also expressed in an opposite manner, that is in terms of the stress. In this case, we take the complex conjugates of (4.94b) and (4.94c)

$$\begin{aligned}\frac{\mathrm{d}(\tilde{v}'^{\hat{y}})^*}{\mathrm{d}y} &= \frac{1}{2Cy}\frac{\mathrm{d}\bar{v}^{\hat{z}}}{\mathrm{d}y}\left(\tilde{\mathrm{T}}_\delta'^{\hat{y}\hat{y}}\right)^*,\\ \left(\frac{\mathrm{d}^2}{\mathrm{d}y^2}+\alpha^2\right)\left(\tilde{v}'^{\hat{y}}\right)^* &= \frac{\mathrm{i}\alpha}{C}\frac{\mathrm{d}^2\bar{v}^{\hat{z}}}{\mathrm{d}y^2}\left(\tilde{\mathrm{T}}_\delta'^{\hat{y}\hat{z}}\right)^*,\end{aligned}$$

and insert them into (4.100)

$$-\frac{2\mathrm{i}\alpha}{\mathcal{R}_1}\int_{-1}^{1}\tilde{\mathrm{T}}_\delta'^{\hat{y}\hat{y}}\frac{\mathrm{d}(\tilde{v}'^{\hat{y}})^*}{\mathrm{d}y}\,\mathrm{d}y = -\frac{\mathrm{i}\alpha}{\mathcal{R}_1 C}\int_{-1}^{1} y^{-1}\frac{\mathrm{d}\bar{v}^{\hat{z}}}{\mathrm{d}y}\left|\tilde{\mathrm{T}}_\delta'^{\hat{y}\hat{y}}\right|^2\mathrm{d}y, \tag{4.118a}$$

$$-\frac{1}{\mathcal{R}_1}\int_{-1}^{1}\tilde{\mathrm{T}}_\delta'^{\hat{y}\hat{z}}\left(\frac{\mathrm{d}^2}{\mathrm{d}y^2}+\alpha^2\right)\left(\tilde{v}'^{\hat{y}}\right)^*\mathrm{d}y = -\frac{\mathrm{i}\alpha}{\mathcal{R}_1 C}\int_{-1}^{1}\frac{\mathrm{d}^2\bar{v}^{\hat{z}}}{\mathrm{d}y^2}\left|\tilde{\mathrm{T}}_\delta'^{\hat{y}\hat{z}}\right|^2\mathrm{d}y. \tag{4.118b}$$

The growth rate then satisfies

$$c_i = \frac{Q-Q^*}{I_1^2+\alpha^2 I_0^2} - \frac{\alpha}{\mathcal{R}_1 C\left(I_1^2+\alpha^2 I_0^2\right)}\int_{-1}^{1}\left[y^{-1}\frac{\mathrm{d}\bar{v}^{\hat{z}}}{\mathrm{d}y}\left|\tilde{\mathrm{T}}_\delta'^{\hat{y}\hat{y}}\right|^2+\frac{\mathrm{d}^2\bar{v}^{\hat{z}}}{\mathrm{d}y^2}\left|\tilde{\mathrm{T}}_\delta'^{\hat{y}\hat{z}}\right|^2\right]\mathrm{d}y. \tag{4.119}$$

From (4.17b), we see that $y^{-1}\frac{\mathrm{d}\bar{v}^{\hat{z}}}{\mathrm{d}y} = 2Cf\left(2C^2y^2\right)$ and applying (4.107) gives us an estimate for c_i

$$\begin{aligned}c_i \leq \frac{qI_0I_1}{\left(I_1^2+\alpha^2I_0^2\right)} - \frac{2\alpha}{\mathcal{R}_1\left(I_1^2+\alpha^2I_0^2\right)}&\int_{-1}^{1} f\left(2C^2y^2\right)\left|\tilde{\mathrm{T}}_\delta'^{\hat{y}\hat{y}}\right|^2\mathrm{d}y\\ &+\frac{\alpha}{\mathcal{R}_1|C|\left(I_1^2+\alpha^2I_0^2\right)}\int_{-1}^{1}\frac{\mathrm{d}^2\bar{v}^{\hat{z}}}{\mathrm{d}y^2}\left|\tilde{\mathrm{T}}_\delta'^{\hat{y}\hat{z}}\right|^2\mathrm{d}y.\end{aligned} \tag{4.120}$$

The second term has obviously only stabilizing effect, while the third one can also play a destabilizing role. Since we assume the second derivative of the base flow to be continuous, we can express the last integral using the mean value theorem as

$$\int_{-1}^{1}\frac{\mathrm{d}^2\bar{v}^{\hat{z}}}{\mathrm{d}y^2}\left|\tilde{\mathrm{T}}_\delta'^{\hat{y}\hat{z}}\right|^2\mathrm{d}y = \frac{\mathrm{d}^2\bar{v}^{\hat{z}}}{\mathrm{d}y^2}(\xi)\int_{-1}^{1}\left|\tilde{\mathrm{T}}_\delta'^{\hat{y}\hat{z}}\right|^2\mathrm{d}y, \qquad \xi\in[-1,1]. \tag{4.121}$$

The eigenvalue bound thus mostly depends on the sign of $\frac{\mathrm{d}^2\bar{v}^{\hat{z}}}{\mathrm{d}y^2}(\xi)$ as the sole expression that can be both negative and positive.[10] Once again, this is related to the (non)existence of inflection points in the base flow velocity profile and the (non)monotonicity of the constitutive relation.

[10] In case of the classical Newtonian fluid, this term is negative as $\frac{\mathrm{d}^2\bar{v}^{\hat{z}}}{\mathrm{d}y^2} = 2C$.

4.6 Linearized stability of different constitutive relations

The goal of this section is to numerically verify the result of hydrodynamic instability of the decreasing part of the flow curve which was developed by different approaches in Chapter 3 and in Sections 4.2 and 4.5 of this chapter.

To this end, we numerically solve the generalized eigenvalue system (4.93) with boundary conditions (4.96). For the discretization of the equations, we use a variant of the spectral collocation method based on Chebyshev polynomials, see for example Trefethen (2000); Boyd (2001) or Canuto et al. (2006, 2007). The reason is that the spectral collocation methods are particularly effective and easy to implement in simple domains, and the expansion of Chebyshev polynomials have proven useful to the solution of hydrodynamic stability problems, see Orszag (1971).

As the system is solved on an interval $y \in [-1, 1]$, we use a discrete grid that consists of the Gauss–Lobatto–Chebyshev points

$$y_i = \cos\left(\frac{(i-1)\pi}{N-1}\right), \qquad i = 1, \ldots, N, \tag{4.122}$$

where N is the number of collocation points. These points are the extrema of the Chebyshev polynomial of the first kind $\mathrm{T}_{N-1}(y) =_{\mathrm{def}} \cos\left[(N-1)\cos^{-1} y\right]$ of degree $N-1$. Equations (4.93a) and (4.93b) are enforced at all inner collocation points ($2(N-2)$ equations) while equation (4.93c) is enforced at all the collocation points (N equations). We also explicitly supplement the system with the boundary conditions for the velocity derivative (2 equations). Since the values of $\tilde{v}'^{\hat{y}}$ are given at the boundary due to (4.96), the number of equations is consistent with the $(N-2) + 2N$ unknowns for $\tilde{v}'^{\hat{y}}$, $\mathrm{T}_{\delta}^{\prime\hat{y}\hat{y}}$ and $\mathrm{T}_{\delta}^{\prime\hat{y}\hat{z}}$. For differentiation, we use spectral differentiation matrices in the form given by Weideman and Reddy (2000) and the final generalized eigenvalue system is then solved using the function `eig` in MATLAB®, The MathWorks, Inc. (2014), see Appendix B for the particular implementation for the model (2.13).

Even though the system (4.93) could be also reformulated as a single equation, this would be somewhat cumbersome and could lead to singularities due to possible existence of inflection points in the base flow velocity profile. Another advantage of our approach is that it is free from spurious modes – two eigenvalues with large positive imaginary parts, whose magnitude increases roughly as $O(N^4)$, see Dawkins et al. (1998); Boyd (2001). This might be a consequence of having a lower-order system instead of one high-order differential equation as was noted by Lindsay and Ogden (1992) who, in fact, advocated for formulating the equations describing the particular problem as a system of first-order equations in order to get rid of the spurious eigenvalues. In this manner, all variables are assigned their own spectral expansions and derivatives are treated as independent variables – a technique similar to the one proposed by Huang and Sloan (1994).

4.6.1 Navier–Stokes model

To verify our approach and implementation, we first solve the problem of hydrodynamic stability for the classical Navier–Stokes model and compare it with the known results.

(Schmid and Henningson, 2001, Table 3.2) listed eigenvalues of two-dimensional plane Poiseuille flow for $\alpha = 1$ and $\mathrm{Re} = 2\mathcal{R}_1 = 5\ 000$. Using their code, (Schmid and Henningson, 2001, Appendix 6), we were able to reproduce their results.[11] With our method, we could compute all the values except for the third one. Therefore, we implemented the codes given by (Weideman and Reddy, 2000, Table XVII) and (Trefethen, 2000, Program 4) to test for this eigenvalue. Neither of the codes was able to compute this eigenvalue, see Table 4.1, hence we think there might be fault in the code by (Schmid and Henningson, 2001, Appendix 6). The computed spectrum is shown in Figure 4.3 with the letters corresponding to the APS-branches introduced by Mack (1976). Eigenvalues in Table 4.1 are also grouped with respect to these branches.

Schmid, Henningson	**Our code**	**Weideman, Reddy**	**Trefethen**
	A-branch		
0.26813 – 0.00175i	✓	✓	✓
0.50275 – 0.16921i	✓	✓	✓
0.42658 – 0.22346i	×	×	×
	P-branch		
0.94996 – 0.04961i	✓	✓	✓
0.82949 – 0.16797i	✓	✓	✓
0.71481 – 0.29109i	✓	✓	✓
	S-branch		
0.68368 – 0.34720i	✓	✓	✓
0.66889 – 0.84601i	✓	✓	✓
0.66858 – 0.97773i	✓	✓	✓

Table 4.1: Eigenvalues of two-dimensional plane Poiseuille flow of Newtonian fluid for $\alpha = 1$, $\mathrm{Re} = 2\mathcal{R}_1 = 5\ 000$ given by (Schmid and Henningson, 2001, Table 3.2) and consequent comparison of our approach and codes by (Weideman and Reddy, 2000, Table XVII) and (Trefethen, 2000, Program 4). Labeling of the particular branches is due to Mack (1976).

We also computed for the least stable eigenvalues of two-dimensional plane Poiseuille flow for $\alpha = 1$, $\mathrm{Re} = 10\ 000$ and compared them with (Orszag, 1971, Table 5), which is considered to be the exact solution. Not only were the computed eigenvalues in complete agreement, we were also able to recover the missing 18th least stable eigenvalue, first found by Dongarra et al. (1996). The 33 least stable eigenvalues are listed in Table 4.2 and the spectrum is shown in Figure 4.4. Note that in this case, particularly the asymptotic behavior of the S-branch is influenced by the numerical resolution, i.e., by the number of collocation points N, see also (Schmid and Henningson, 2001, Figure 3.16).

We were also able to accurately compute the least stable eigenvalue

$$c = \frac{\omega}{\alpha_c} = 0.26400174 - 0.000000003\mathrm{i},$$

[11] Schmid and Henningson (2001) falsely posted the first eigenvalue as $0.26813 - 0.0175\mathrm{i}$.

Mode number	Eigenvalue
1	0.23752649 + 0.00373967i
2	0.96463092 – 0.03516728i
3	0.96464251 – 0.03518658i
4	0.27720434 – 0.05089873i
5	0.93631654 – 0.06320150i
6	0.93635178 – 0.06325157i
7	0.90798305 – 0.09122274i
8	0.90805633 – 0.09131286i
9	0.87962729 – 0.11923285i
10	0.87975570 – 0.11937073i
11	0.34910682 – 0.12450198i
12	0.41635102 – 0.13822653i
13	0.85124584 – 0.14723393i
14	0.85144938 – 0.14742560i
15	0.82283504 – 0.17522868i
16	0.82313696 – 0.17547807i
17	0.19005925 – 0.18282193i
18	0.21272578 – 0.19936069i
19	0.79438838 – 0.20322066i
20	0.79481839 – 0.20352914i
21	0.53204521 – 0.20646522i
22	0.47490119 – 0.20873122i
23	0.76587681 – 0.23118599i
24	0.76649408 – 0.23158507i
25	0.36849848 – 0.23882483i
26	0.73741576 – 0.25871708i
27	0.73811501 – 0.25969188i
28	0.63671937 – 0.25988571i
29	0.38398761 – 0.26510650i
30	0.58721293 – 0.26716171i
31	0.71231586 – 0.28551474i
32	0.51291620 – 0.28662504i
33	0.70887464 – 0.28765536i

Table 4.2: Least stable eigenvalues of two-dimensional plane Poiseuille flow of Newtonian fluid for $\alpha = 1$, Re = $2\mathcal{R}_1 = 10\ 000$, $N = 100$. The shaded eigenvalue was absent in Orszag (1971) and was first found by Dongarra et al. (1996).

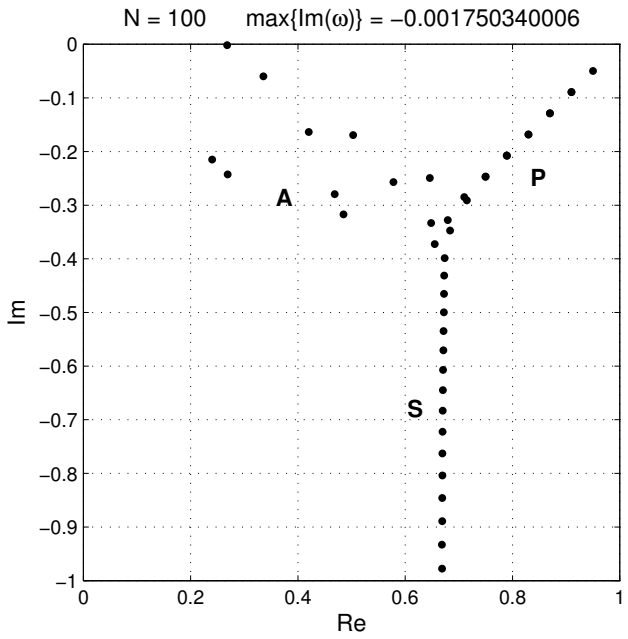

Figure 4.3: Spectrum of two-dimensional plane Poiseuille flow of Newtonian fluid for $\alpha = 1$, $\mathrm{Re} = 2\mathcal{R}_1 = 5\ 000$, $N = 100$. Labeling of the particular branches is due to Mack (1976).

for the critical Reynolds number $\mathrm{Re}_c = 5\ 772.22$ with the critical streamwise number $\alpha_c = 1.02056$, see Orszag (1971).

Since the formulation (4.94) and its numerical solution by means of the spectral collocation method gives for the Newtonian fluid the same results as the classical Orr–Sommerfeld equation, we shall consider it acceptable and exploit it even for the non-Newtonian fluid models of type (2.4).

4.6.2 Shear rate limiting model

Now, we shall study hydrodynamic stability of a model where for large (infinite) values of the stress, there is no change of the shear rate, i.e., the shear rate tends to some finite value. Such one-dimensional model might read

$$\dot{\gamma} = \left(1 + \sigma^a\right)^{-1/a} \sigma, \qquad a \geq 1, \tag{4.123}$$

with finite, non-zero limit

$$\dot{\gamma}_\infty = \lim_{\sigma \to \infty} \frac{\sigma}{\left(1 + \sigma^a\right)^{1/a}} = 1, \tag{4.124}$$

see Figure 4.5. As a three-dimensional counterpart of (4.123), we shall then consider

$$\mathbb{D} = \left(1 + |\mathbb{T}_\delta|^a\right)^{-1/a} \mathbb{T}_\delta. \tag{4.125}$$

In this case, we have $f(s) = \left(1 + s^{a/2}\right)^{-1/a}$, thus we can immediately obtain the relations for the first and second derivatives of the base flow velocity from (4.17b)

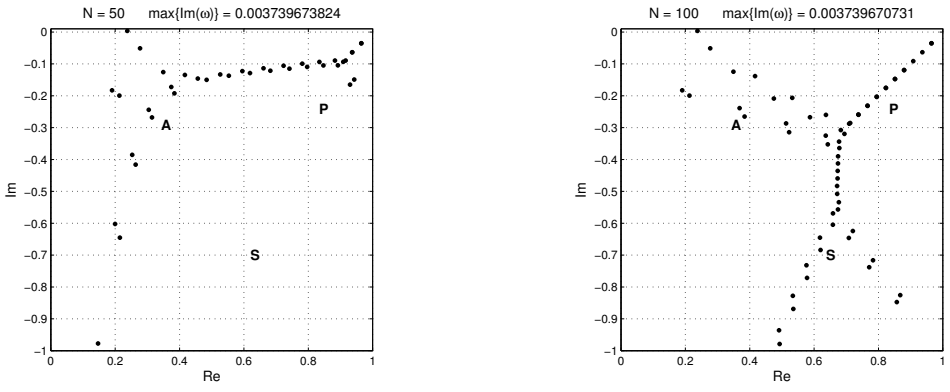

(a) $N = 50$ (b) $N = 100$

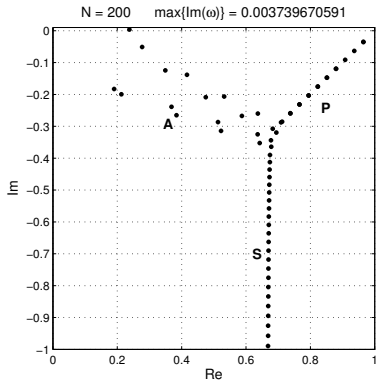

(c) $N = 200$

Figure 4.4: Spectra of two-dimensional plane Poiseuille flow of Newtonian fluid for $\alpha = 1$, $\mathrm{Re} = 2\mathcal{R}_1 = 10\ 000$ and different number of collocation points N. Labeling of the particular branches is due to Mack (1976).

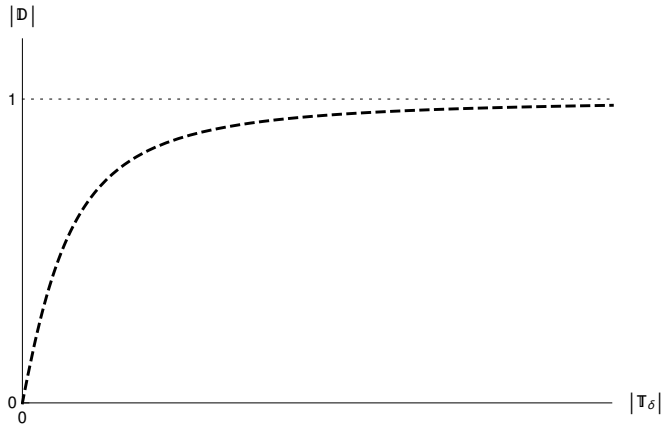

Figure 4.5: Qualitative behavior of the shear rate limiting model (4.125).

and (4.17c) as

$$\frac{\mathrm{d}\bar{v}^{\hat{z}}}{\mathrm{d}y} = 2Cy\left[1+\left(2C^2y^2\right)^{a/2}\right]^{-1/a}, \tag{4.126a}$$

$$\frac{\mathrm{d}^2\bar{v}^{\hat{z}}}{\mathrm{d}y^2} = 2C\left[1+\left(2C^2y^2\right)^{a/2}\right]^{-\frac{1+a}{a}}. \tag{4.126b}$$

Clearly, the second derivative of the base flow velocity doesn't vanish for any y, i.e., the velocity profile is without inflection points. The base flow velocity can be found as the solution to (4.126a) using

$$\begin{aligned}\mathcal{F}(s) &= \int \left(1+s^{a/2}\right)^{-1/a}\,\mathrm{d}s = \left|\eta = -s^{a/2}\right| \\ &= \frac{2}{a}(-1)^{2/a}\int \eta^{2/a-1}\left(1-\eta\right)^{-1/a}\,\mathrm{d}\eta = \frac{2}{a}(-1)^{2/a}\int \eta^{2/a-1}\mathrm{F}\left(\left[\frac{1}{a},\frac{2}{a}\right];\left[\frac{2}{a}\right];\eta\right)\mathrm{d}\eta \\ &= \frac{2}{a}(-1)^{2/a}\frac{a}{2}\eta^{2/a}\mathrm{F}\left(\left[\frac{1}{a},\frac{2}{a}\right];\left[\frac{2}{a}+1\right];\eta\right) = s\mathrm{F}\left(\left[\frac{1}{a},\frac{2}{a}\right];\left[\frac{2}{a}+1\right];-s^{a/2}\right),\end{aligned} \tag{4.127}$$

where $\mathrm{F}\left([\cdot,\cdot];[\cdot];\cdot\right)$ is the Gauss hypergeometric function. In (4.127), we used (Abramowitz and Stegun, 1964, Eq. 15.1.8) and (Gradshteyn and Ryzhik, 2014, Eq. 5.7.3). Having the function $\mathcal{F}$, we can recover the formula for the velocity from (4.17a) as

$$\begin{aligned}\bar{v}^{\hat{z}}(y) = C\Bigg[&y^2\mathrm{F}\left(\left[\frac{1}{a},\frac{2}{a}\right];\left[\frac{2}{a}+1\right];-\left(2C^2y^2\right)^{a/2}\right) \\ &-\mathrm{F}\left(\left[\frac{1}{a},\frac{2}{a}\right];\left[\frac{2}{a}+1\right];-\left(2C^2\right)^{a/2}\right)\Bigg].\end{aligned} \tag{4.128}$$

For $a = 1, 2$, (4.128) can be written in a simpler form

$$\bar{v}^{\hat{z}}(y) = \begin{cases}\frac{1}{C}\left[\left(\sqrt{2C^2y^2}-\sqrt{2C^2}\right)-\ln\left(\frac{1+\sqrt{2C^2y^2}}{1+\sqrt{2C^2}}\right)\right], & a=1,\\ \frac{1}{C}\left[\left(1+2C^2y^2\right)^{1/2}-\left(1+2C^2\right)^{1/2}\right], & a=2.\end{cases} \tag{4.129}$$

Note that the second expression is tantamount to (Málek et al., 2010, Eq. (2.12)) with $n = -\frac{1}{2}$,.

Solving numerically the generalized eigenvalue system (4.94), we have found that for the shear rate limiting model (4.125), it is always possible to find Reynolds number small enough that the flow is stable, see examples of stable flow spectra in Figure 4.6. In other words, stability of the flow depends only on the Reynolds number analogue $\mathcal{R}_1$ and the pressure gradient C, similarly as for the classical Newtonian fluid.

4.6.3 Stress power-law model

The stress power-law model

$$\mathbb{D} = \left(1+|\mathbb{T}_\delta|^2\right)^n\mathbb{T}_\delta, \tag{4.130}$$

where n is a real number, is a special case of the model (4.19) with $\mathcal{R}_3 = 0$ and it was studied by Málek et al. (2010). They showed that for $n < -\frac{1}{2}$ the velocity

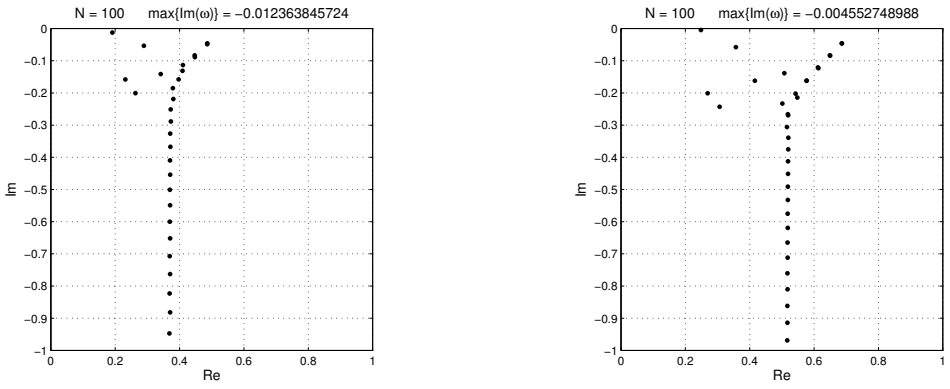

(a) Stable flow, $a = 1$. (b) Stable flow, $a = 2$.

Figure 4.6: Spectra of two-dimensional plane Poiseuille flow of the shear rate limiting model (4.125) for $\mathcal{R}_1 = 3\ 000$, $C = -1$, $N = 100$.

profile of the plane Poiseuille flow has inflection points. This can be immediately seen from (4.17c) which connects the existence of inflection points in the velocity profile with the existence of (local) extrema of the relation between $\mathbb{D}$ and $\mathbb{T}_\delta$. Indeed, inflection points occur in the velocity profile once the maximum stress is larger than the extremal point of the flow curve, i.e.,

$$\max_{y\in[-1,1]} |\mathbb{T}_\delta| > \frac{1}{\sqrt{-(1+2n)}}, \tag{4.131}$$

see Figure 4.7. Since $|\mathbb{T}_\delta| = \sqrt{2}\,|C|\,|y|$ for the two-dimensional plane Poiseuille flow, the condition for existence of inflection points can be rewritten in terms of the pressure gradient C as

$$|C| > \frac{1}{\sqrt{-2(1+2n)}}. \tag{4.132}$$

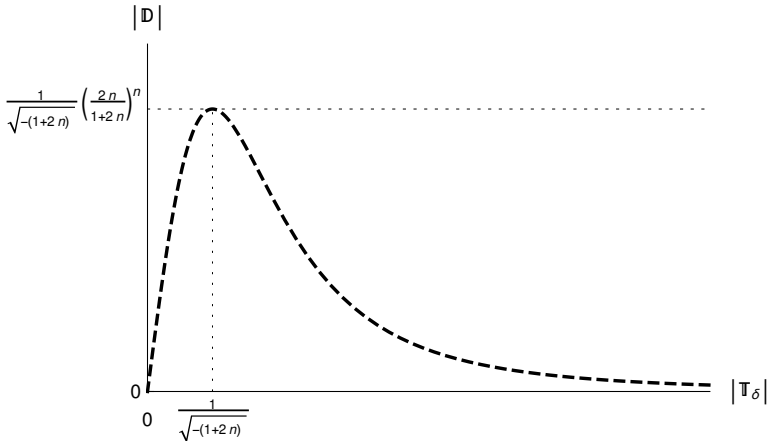

Figure 4.7: Qualitative behavior of the stress power-law model (4.130) for $n < -\frac{1}{2}$.

The base flow velocity can be obtained from (4.20) by setting $\mathcal{R}_3 = 0$ as

$$\bar{v}^{\hat{z}}(y) = \begin{cases} \frac{1}{2(n+1)C}\left[(1+2C^2y^2)^{n+1} - (1+2C^2)^{n+1}\right], & n \neq -1, \\ \frac{1}{2C}\left[\ln\left(1+2C^2y^2\right) - \ln\left(1+2C^2\right)\right], & n = -1. \end{cases} \tag{4.133}$$

In Figure 4.8, we have plotted examples of spectra for base flow velocities with and without inflection points for $n = -2$. In this case, the critical pressure gradient is $C = -\frac{1}{\sqrt{6}}$ from (4.132). For $C = -\frac{1}{\sqrt{7}}$, there are no inflection points in the base flow velocity profile as the fluid is restricted only to the increasing part of the curve in Figure 4.7. It is possible to find such Reynolds number that the flow is stable, see Figure 4.8a. On the other hand, for $C = -\frac{1}{2}$, parts of the fluid lie already on the decreasing part of the curve in Figure 4.7 and there are inflection points present in the base flow velocity profile. The spectrum is clearly distinct and the eigenvalues have practically unbounded positive imaginary parts for any Reynolds number, i.e., the flow is unconditionally unstable. This instability coincides with the decreasing part of the flow curve and thus goes hand in hand with the results derived in Chapter 3 and Sections 4.2 and 4.5 of this chapter.

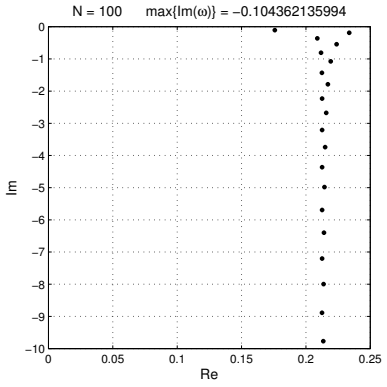

(a) Stable flow with no inflection points for $C = -\frac{1}{\sqrt{7}}$.

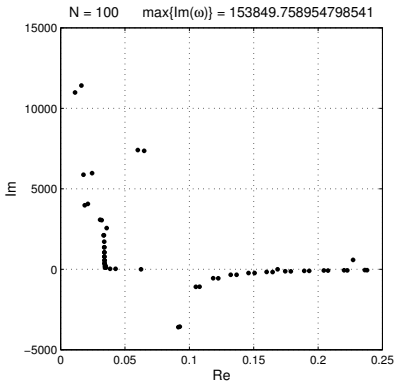

(b) Unstable flow with inflection points for $C = -\frac{1}{2}$.

Figure 4.8: Stable and unstable spectra of two-dimensional plane Poiseuille flow of the stress power-law model (4.130) for $\mathcal{R}_1 = 100$, $n = -2$, $N = 100$.

4.6.4 Non-monotone model

Le Roux and Rajagopal (2013) considered model (2.13) which is a generalization of (4.130). In its dimensionless form (4.19), it reads

$$\mathbb{D} = \left[\left(1 + |\mathbb{T}_\delta|^2\right)^n + \mathcal{R}_3\right]\mathbb{T}_\delta, \tag{4.134}$$

where $\mathcal{R}_3$ is a non-negative constant and n is a real number. They showed that if the condition

$$2\left(\frac{2n-2}{2n+1}\right)^{n-1} \leq \mathcal{R}_3, \tag{4.135}$$

holds, the flow curve is strictly increasing or, as follows from (4.17c), there are no inflection points in the velocity profile given by (4.20).

First, we shall consider a case when the relation (4.135) is satisfied as an equality. In this case, the flow curve is monotonically increasing and there is a plateau at σ_*. For example, the values $n = -2$ and $\mathcal{R}_3 = 0.25$ imply $\sigma_* = 1$, see Figure 4.9. The value $|\mathbb{T}_\delta| = 1$ corresponds to a pressure gradient $C = -\frac{1}{\sqrt{2}}$. As the curve in Figure 4.9 is increasing, there are no inflection points in the base

flow velocity profile. Both for low and high pressure gradients (with respect to $C = -\frac{1}{\sqrt{2}} \approx -0.707$), it is always possible to find such Reynolds number that the flow is stable, see Figure 4.10.

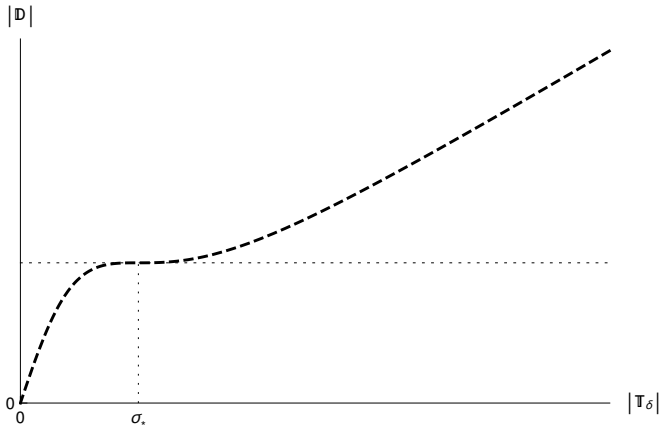

Figure 4.9: Qualitative behavior of the model (4.134) for $n = -2$, $\mathcal{R}_3 = 0.25$ with a plateau at $\sigma_* = 1$.

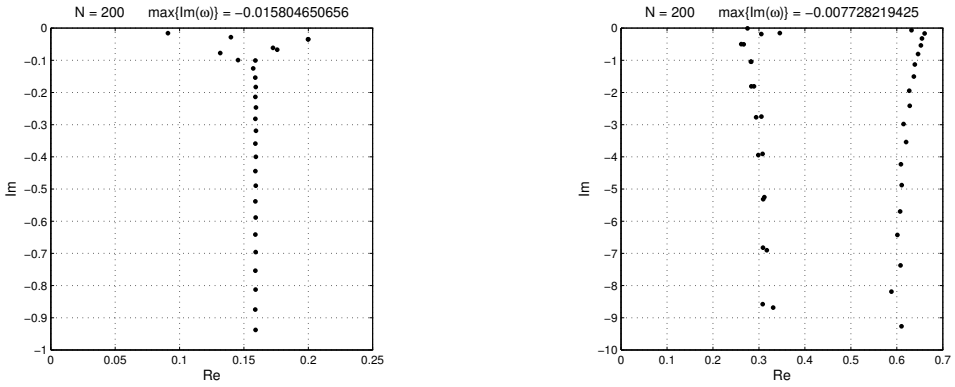

(a) Stable flow for $C = -0.2$.

(b) Stable flow for $C = -2$.

Figure 4.10: Spectra of two-dimensional plane Poiseuille flow of the model (4.134) for $\mathcal{R}_1 = 1000$, $n = -2$, $\mathcal{R}_3 = 0.25$, $N = 200$.

Leaving n unchanged but slightly adjusting $\mathcal{R}_3$ to 0.24 violates the flow curve monotonicity condition (4.135) and there is now a region that the curve in Figure 4.9 is decreasing. Then, for values of the pressure gradient C such that parts of the fluid are confined within the decreasing part of the flow curve, there are inflection points in the base flow velocity profile and the flow is unconditionally unstable, see Figure 4.11. This is analogical to the behavior of the stress power-law model (4.130).

4.7 Conclusion

We have discussed hydrodynamic stability of flows of fluids described by implicit constitutive relation of the particular form (2.12). Models of this type were developed in a thermodynamically sound way in Chapter 2 by means of the entropy

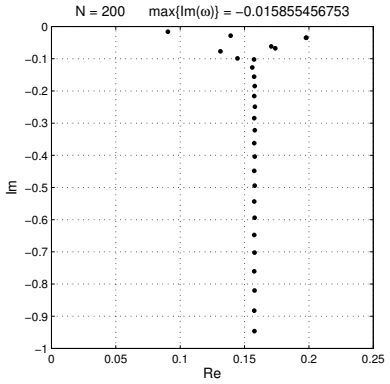

(a) Stable flow with no inflection points for $C = -0.2$.

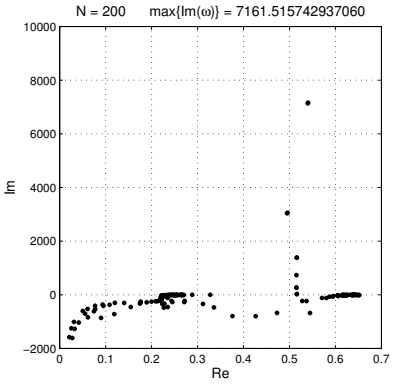

(b) Unstable flow with inflection points for $C = -2$.

Figure 4.11: Spectra of two-dimensional plane Poiseuille flow of the model (4.134) for $\mathcal{R}_1 = 1000$, $n = -2$, $\mathcal{R}_3 = 0.24$, $N = 200$.

production maximization and in Chapter 3 by means of non-convex dissipation potential within gradient dynamics.

First, we have derived the solution to the stationary two-dimensional plane Poiseuille flow in Section 4.1. This solution later served as the base flow that is disturbed with an imposed perturbation. From the kinetic energy of the perturbation, we have derived a generalized version of the Reynolds–Orr equation (4.45) in Section 4.3. Using this equation we were able to determine the exponential decrease of the kinetic energy of a disturbance imposed onto a fluid at rest and deduce stability criteria for the Poiseuille flow in a channel.

Linearizing the governing equation for the wave-like disturbance, we derived the generalized Orr–Sommerfeld–Squire system (4.84) in Section 4.4. Proving that it is sufficient to consider only two-dimensional disturbances, we obtained estimates of both the propagation speed and the growth rate of the disturbance in Section 4.5. We were able to conclude that once the constitutive relation is not monotone, there are inflection points in the velocity profile, the flow is unconditionally unstable. This is analogous to the results derived in Section 4.2 and Chapter 3. This was also numerically verified in Section 4.6 for several constitutive models.

Particularly the instability of the flow of a fluid described by the constitutive relation (2.13) considered by Le Roux and Rajagopal (2013), can be viewed yet from another perspective. Flow of such fluid can be understood as a flow of two fluids with different viscosities as the constitutive relation has two distinct stable and one unstable branches, see Chapter 3. It is well known that such flow is unstable due to the viscosity stratification, see Yih (1967).

5. Taylor–Couette flow

One of the classical flow problems is the Taylor–Couette flow, see Donnelly (1991), where the investigated fluid is confined between two infinite concentric cylinders Γ_1 and Γ_2 of radii R_1 and R_2 respectively, $R_1 < R_2$, see Figure 5.1 for its two-dimensional representation. At the walls, one can assume several boundary conditions. Here, we shall consider the inner cylinder to be at rest and the outer one to rotate with some prescribed velocity. This setting is the so-called *shear rate controlled experiment*. As the name suggests, we want to control the shear rate of the fluid (through the prescribed velocity). The goal is then to measure the corresponding shear stress exerted by the fluid.

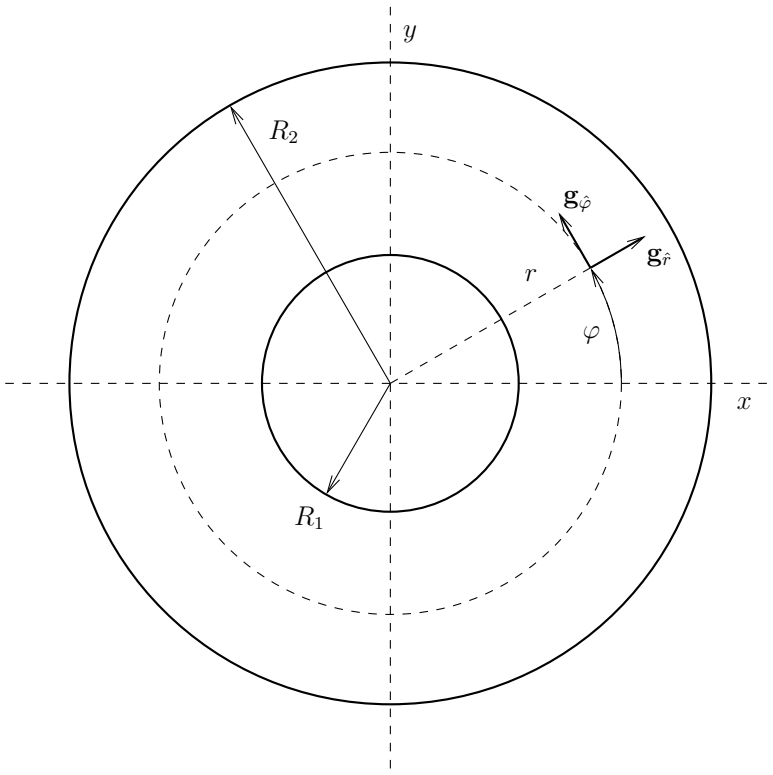

Figure 5.1: Taylor–Couette flow geometry and the normed base vectors in the polar coordinate system.

First, we derive the classical analytical solution for the steady Navier–Stokes equations in the two-dimensional Taylor–Couette flow in Section 5.1. This may also serve as a benchmark to validate our finite element implementation. Then, we focus on the solution of the flow of the Le Roux–Rajagopal model (2.13). Since the constitutive relation is non-monotone, the stress might be multivalued and we cannot use the standard formulation. To this end, in Section 5.3, we reformulate the governing equations as a system for the pressure–velocity–apparent viscosity triple $(p, \boldsymbol{v}, \mu)$ and in Section 5.4, we propose a numerical scheme for the solution of the resulting governing equations.

In order to study the dynamical behavior implied by the non-monotone constitutive relations, we introduce a reduced version of the problem in Section 5.5. In the reduced problem we neglect the contributions from other effects like pressure

or convection, and we focus solely on the constitutive relation. We introduce a variant of the proposed numerical scheme for the reduced problem and we present the simulation results to illustrate the behavior of the reduced system. Numerical results of the simulations are reported in Section 5.6 where we comment on the behavior of the system.

The main idea behind using the non-monotone constitutive relation specifically in the Taylor–Couette geometry is to reproduce the experimentally observed shear banding behavior portrayed in Figure 5.2.

This chapter is a subject of a future publication Janečka et al. (2018) currently being in preparation.

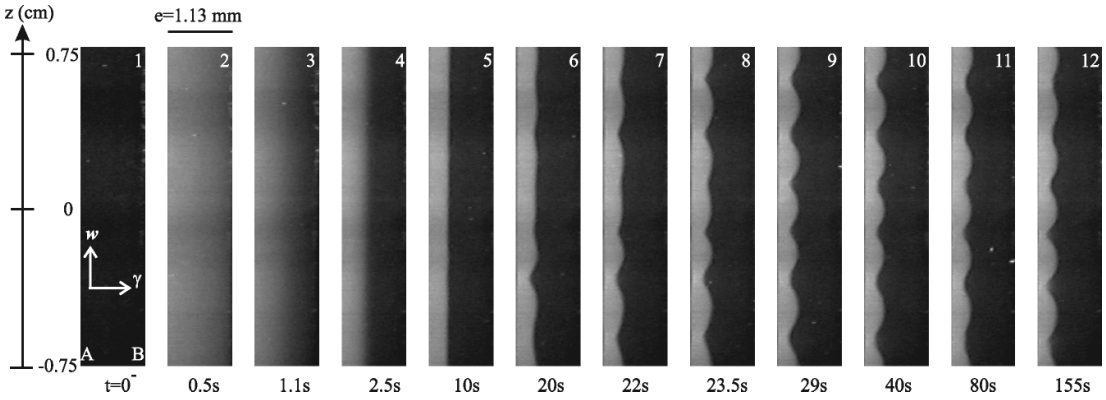

(a) Formation of induced gradient bands in the velocity gradient/vorticity plane. Recording of the scattered intensity in the the gap between the inner (A) and the outer (B) cylinder of the Couette device subjected to a shear rate of $30\,\mathrm{s}^{-1}$. Reprinted from Lerouge et al. (2006).

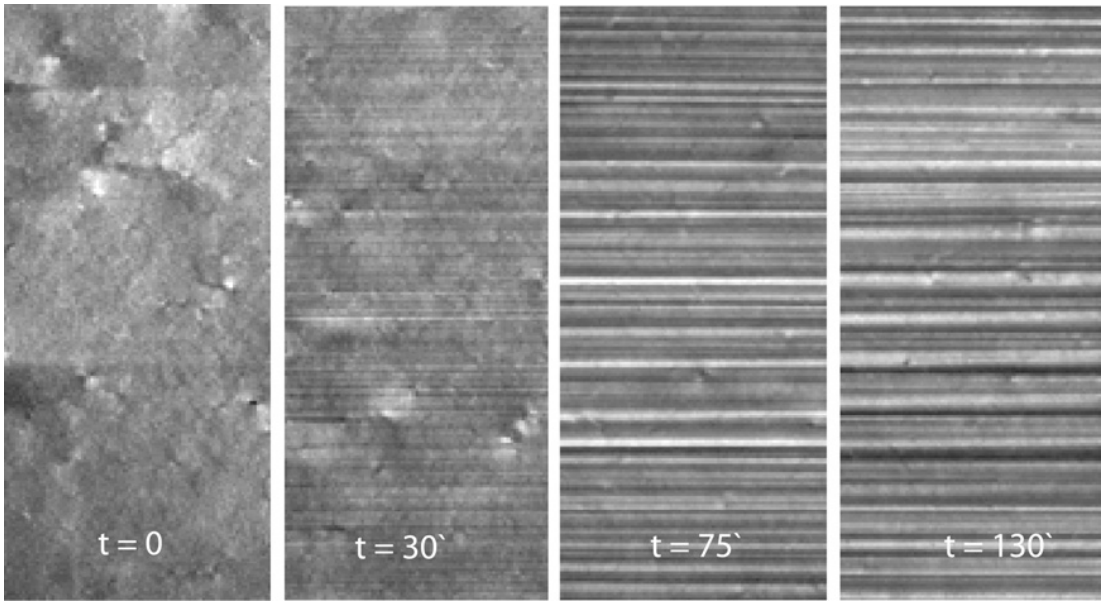

(b) Cross-polarized CCD-images from side of a cylindrical shear-cell under a shear-rate $\dot{\gamma} = 0.3\,\mathrm{s}^{-1}$ during vorticity bands formation over 2 hours time span. Reprinted from Dhont et al. (2003).

Figure 5.2: Experimental observations of gradient and vorticity banding.

5.1 Steady flow of Navier–Stokes fluid

The dimensional steady Navier–Stokes equations for the incompressible fluid read

$$[\nabla \boldsymbol{v}]\boldsymbol{v} = -\nabla p + \mu \operatorname{div} 2\mathbb{D}, \tag{5.1a}$$

$$\operatorname{div} \boldsymbol{v} = 0. \tag{5.1b}$$

In the Taylor–Couette geometry it is natural to seek the solution in polar coordinates with the normed basis $\{\boldsymbol{g}_{\hat{r}}, \boldsymbol{g}_{\hat{\varphi}}\}$, see Appendix C for details. Due to the symmetry of the problem, we can assume the quantities to depend only on the radial coordinate r and the velocity to have only the angular component $v^{\hat{\varphi}}$

$$\boldsymbol{v} = v^{\hat{\varphi}}(r)\boldsymbol{g}_{\hat{\varphi}}, \qquad p = p(r). \tag{5.2}$$

With this assumption, the incompressibility constraint (5.1a) is automatically satisfied and the momentum equation (5.1b) expressed in the polar coordinates reads

$$-\frac{(v^{\hat{\varphi}})^2}{r} = -\frac{\mathrm{d}p}{\mathrm{d}r}, \tag{5.3a}$$

$$0 = \mu\left(\frac{\mathrm{d}^2 v^{\hat{\varphi}}}{\mathrm{d}r^2} + \frac{1}{r}\frac{\mathrm{d}v^{\hat{\varphi}}}{\mathrm{d}r} - \frac{v^{\hat{\varphi}}}{r^2}\right). \tag{5.3b}$$

Equation (5.3b) is the Euler ordinary differential equation with solution

$$v^{\hat{\varphi}}(r) = Ar + \frac{B}{r}, \tag{5.4}$$

where A and B are constants to be determined from boundary conditions. The pressure can be easily reconstructed (up to a constant) from (5.3a).[1]

As we consider the inner cylinder to be at rest and the outer one to rotate with a prescribed velocity V, the corresponding boundary conditions are

$$\boldsymbol{v}|_{r=R_1} = \boldsymbol{0}, \qquad \boldsymbol{v}|_{r=R_2} = V\boldsymbol{g}_{\hat{\varphi}}. \tag{5.5}$$

These boundary conditions are fulfilled for $A = V\frac{R_2}{R_2^2 - R_1^2}$ and $B = -AR_1^2$, thus the velocity takes the form

$$v^{\hat{\varphi}}(r) = V\frac{R_2}{R_2^2 - R_1^2}\left(r - \frac{R_1^2}{r}\right). \tag{5.6}$$

Controlling the velocities of the individual cylinders, we can effectively control the shear-rate of the fluid. Indeed, if the gap between cylinders is relatively small, shear-rate can be well approximated by the velocity difference between the cylinders, i.e., $|\mathbb{D}| \sim \frac{v^{\hat{\varphi}}(R_2) - v^{\hat{\varphi}}(R_1)}{R_2 - R_1}$. Then, the common experimentally measured quantity closely related to the shear-stress is the torque at the outer cylinder

$$\begin{aligned}\boldsymbol{\tau} &=_{\mathrm{def}} \int_{\Gamma_2} R_2\boldsymbol{g}_{\hat{r}} \times \mathbb{T}\boldsymbol{g}_{\hat{r}}\,\mathrm{d}l = R_2\int_{\Gamma_2} \boldsymbol{g}_{\hat{r}} \times \left[(\boldsymbol{g}_{\hat{r}}\cdot\mathbb{T}\boldsymbol{g}_{\hat{r}})\,\boldsymbol{g}_{\hat{r}} + (\boldsymbol{g}_{\hat{\varphi}}\cdot\mathbb{T}\boldsymbol{g}_{\hat{r}})\,\boldsymbol{g}_{\hat{\varphi}}\right]\mathrm{d}l \\ &= R_2\int_{\Gamma_2} (\boldsymbol{g}_{\hat{\varphi}}\cdot\mathbb{T}\boldsymbol{g}_{\hat{r}})\,(\boldsymbol{g}_{\hat{r}}\times\boldsymbol{g}_{\hat{\varphi}})\,\mathrm{d}l = \left(R_2\int_{\Gamma_2} \mathrm{T}_{\hat{\varphi}\hat{r}}\,\mathrm{d}l\right)\boldsymbol{g}_{\hat{z}},\end{aligned} \tag{5.7}$$

[1] In case of the Stokes flow where the inertial terms can be neglected, we would obtain the same velocity field but the pressure would be constant since the left-hand side of (5.3a) would be zero.

where $\mathrm{d}l$ is the line element. From the velocity solution (5.6), we can get an explicit formula for the torque. Since the corresponding component of the stress is

$$\mathrm{T}_{\hat{\varphi}\hat{r}} = \frac{2}{\mathrm{Re}}\mathrm{D}_{\hat{\varphi}\hat{r}} = \frac{1}{\mathrm{Re}} r \frac{\mathrm{d}}{\mathrm{d}r}\left(\frac{v^{\hat{\varphi}}}{r}\right) = V \frac{2}{\mathrm{Re}} \frac{R_2}{R_2^2 - R_1^2}\left(\frac{R_1}{r}\right)^2,$$

the torque is

$$\boldsymbol{\tau} = 2\pi R_2 V \frac{2}{\mathrm{Re}} \frac{R_1^2}{R_2^2 - R_1^2} \boldsymbol{g}_{\hat{z}}. \tag{5.8}$$

Finally, unsteady flow of the Navier–Stokes fluid in the Taylor–Couette flow geometry can be resolved by means of the finite Hankel transforms introduced by Sneddon (1946) and then extended by Cinelli (1965). The resulting formulas are in the form of infinite series expansion of the Bessel functions, see Tranter (1951).

5.2 Non-monotone constitutive relation

The corresponding system of governing equations for an incompressible non-Newtonian fluid specified by constitutive relation (2.13) reads

$$\operatorname{div} \boldsymbol{v} = 0, \tag{5.9a}$$

$$\rho \frac{\mathrm{d}\boldsymbol{v}}{\mathrm{d}t} = -\nabla p + \operatorname{div} \mathbb{T}_\delta + \rho \boldsymbol{b}, \tag{5.9b}$$

$$\mathbb{D} = \left[a\left(1 + b\left|\mathbb{T}_\delta\right|^2\right)^n + c\right]\mathbb{T}_\delta. \tag{5.9c}$$

The main difficulty in solving (5.9) for $n < -\frac{1}{2}$ is the fact that (5.9c) is non-monotone, therefore cannot be inverted and $\mathbb{T}_\delta$ cannot be expressed as a function of $\mathbb{D}$. Consequently, system (5.9) cannot be formulated as a system for the pressure–velocity pair $(p, \boldsymbol{v})$. However, this is just a matter of a reformulation of the problem as a problem for the pressure–velocity–stress triple $(p, \boldsymbol{v}, \mathbb{T}_\delta)$. The key conceptual difficulty is the treatment of the constitutive relation (5.9c). The reason is that (5.9c) admits for $n < -\frac{1}{2}$ multiple values of $\mathbb{T}_\delta$ to be associated with the same value of the symmetric part of the velocity gradient $\mathbb{D}$.

Unfortunately, this issue prevents one from using most of the already available results concerning the systems of the type

$$\operatorname{div} \boldsymbol{v} = 0, \tag{5.10a}$$

$$\rho \frac{\mathrm{d}\boldsymbol{v}}{\mathrm{d}t} = -\nabla p + \operatorname{div} \mathbb{T}_\delta + \rho \boldsymbol{b}, \tag{5.10b}$$

$$\mathfrak{h}(\mathbb{T}_\delta, \mathbb{D}) = \mathbb{0}, \tag{5.10c}$$

where $\mathfrak{h}(\mathbb{T}_\delta, \mathbb{D})$ is an implicit tensorial function. The available results, see Bulíček et al. (2009, 2012) for the proof of long-time and large-data existence of weak solution to (5.10), and Stebel (2016) and Diening et al. (2013) for the results concerning the discretized counterparts of (5.10), are based on the fact that the equation $\mathfrak{h}(\mathbb{T}_\delta, \mathbb{D}) = \mathbb{0}$ defines a *maximal monotone graph*. Although the maximal *monotone* graph defined by $\mathfrak{h}$ can be possibly multivalued, systems of the type (5.9) with *non-monotone* response, that is (5.9c) with $n < -\frac{1}{2}$, are not covered by the otherwise very general theory by Bulíček et al. (2009, 2012).

The numerical scheme for solution of (5.9) introduced below represents the first attempt to study systems of this type. The proposed scheme does not fully answer the question on the existence of a solution to (5.9), yet an important step can be made. Namely, a discrete finite-dimensional nonlinear system that arises in the time-stepping of system (5.9) can be shown to be solvable, see Janečka et al. (2018).

In Section 5.3, we reformulate the system (5.9) as a nonlinear system for the pressure–velocity–apparent viscosity triple $(p, \boldsymbol{v}, \mu)$. This is the key step in the derivation of the numerical scheme. The tensorial constitutive relation (5.9c) is effectively replaced by a scalar implicit relation for the apparent viscosity. The arising system shares some similarities with the standard Navier–Stokes system.

Then in Section 5.4, we present an iterative implicit nonlinear numerical scheme. The proposed numerical scheme is then employed for the Taylor–Couette flow. The results of the simulations are reported in Section 5.6.

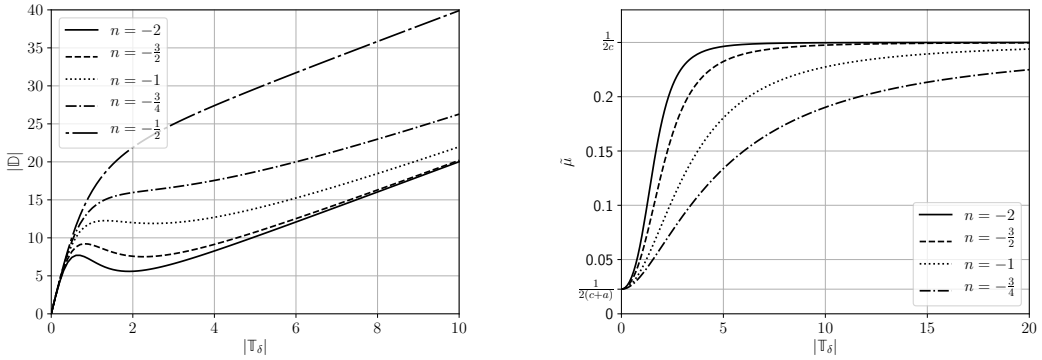

(a) Relation between $|\mathbb{D}|$ and $|\mathbb{T}_\delta|$.

(b) Apparent viscosity $\tilde{\mu}$.

Figure 5.3: Constitutive relation $\mathbb{D} = \left[a\left(1 + b\,|\mathbb{T}_\delta|^2\right)^n + c\right]\mathbb{T}_\delta$. Parameter values set to $a = 20$, $b = 1$, $c = 2$. The exponent n takes values $n \in \left\{-2, -\frac{3}{2}, -1, -\frac{3}{4}, -\frac{1}{2}\right\}$.

5.3 Reformulation of the problem in terms of apparent viscosity

Let us consider a bounded domain $\Omega \subset \mathbb{R}^d$, $d = \{2, 3\}$. For the sake of simplicity we shall further assume that no external body force is present, i.e., $\boldsymbol{b} = \boldsymbol{0}$, and the density ρ is equal to one. System (5.9) then reads

$$\operatorname{div} \boldsymbol{v} = 0, \tag{5.11a}$$

$$\frac{\mathrm{d}\boldsymbol{v}}{\mathrm{d}t} = -\nabla p + \operatorname{div} \mathbb{T}_\delta, \tag{5.11b}$$

$$\mathbb{D} = \left[a\left(1 + b\,|\mathbb{T}_\delta|^2\right)^n + c\right]\mathbb{T}_\delta. \tag{5.11c}$$

Since the trace of $\mathbb{T}_\delta$ is by definition equal to zero, constitutive relation (5.11c) in fact already enforces the incompressibility constraint (5.11a). We shall however keep (5.11a) in the system in an explicit way as the constitutive relation (5.11c) will be reformulated. Keeping (5.11a) is the price to be paid for the reformulation.

The aim is to find the triple $(p, \boldsymbol{v}, \mathbb{T}_\delta)$ such that it solves (5.11) subject to suitable initial and boundary conditions.

Introducing the apparent viscosity μ as

$$\mu(\boldsymbol{x}, t) =_{\text{def}} \frac{1}{2} \frac{|\mathbb{T}_\delta(\boldsymbol{x}, t)|}{|\mathbb{D}(\boldsymbol{x}, t)|}, \tag{5.12}$$

we see that it can be rewritten as a function $\tilde{\mu}$ of the traceless part of the Cauchy stress tensor, $\mu(\boldsymbol{x}, t) = \tilde{\mu}\left(|\mathbb{T}_\delta(\boldsymbol{x}, t)|\right)$, where

$$\tilde{\mu}(u) =_{\text{def}} \frac{1}{2}\left[a\left(1 + bu^2\right)^n + c\right]^{-1}.^2 \tag{5.13}$$

Note that if $n < -\frac{1}{2}$, then the apparent viscosity $\tilde{\mu}$ introduced in (5.13) is a positive *increasing and bounded function* of u satisfying for all $u \in [0, +\infty)$

$$\frac{1}{2(c+a)} \leq \tilde{\mu}(u) \leq \frac{1}{2c}, \tag{5.14}$$

see Figure 5.3b. Furthermore, constitutive relation (5.11c) can be rewritten as $\mathbb{T}_\delta = \tilde{\mu}(|\mathbb{T}_\delta|)\mathbb{D}$, which implies that system (5.11) can be reformulated as a system

$$\operatorname{div} \boldsymbol{v} = 0, \tag{5.15a}$$

$$\frac{\mathrm{d}\boldsymbol{v}}{\mathrm{d}t} = -\nabla p + \operatorname{div}\left(2\mu\mathbb{D}\right), \tag{5.15b}$$

$$\mu = \frac{1}{2}\left[a\left(1 + 4b\mu^2\,|\mathbb{D}|^2\right)^n + c\right]^{-1} \tag{5.15c}$$

for the triple $(p, \boldsymbol{v}, \mu)$. Note that the last equation is an implicit equation for the apparent viscosity μ in terms of $\mathbb{D}$.

5.4 Numerical scheme

Our goal is to design a numerical scheme to approximate the system (5.15). The system shall be discretized in space using the finite element method and using finite differences for the temporal discretization. The implicit scalar equation (5.15c) for the strictly monotone and bounded apparent viscosity μ takes the place of the non-monotone constitutive relation (5.11c) between the symmetric part of the velocity gradient $\mathbb{D}$ and the deviatoric part of the stress tensor $\mathbb{T}_\delta$. As we focus on the influence of the non-monotone constitutive relation on the behavior of the system, for the sake of simplicity, we neglect the convective effects in the presentation of the numerical algorithm.

We assume a uniform partition of the time interval $t_n = n\Delta t$, where $\Delta t > 0$ represents a fixed time step. Further, let $(p^n, \boldsymbol{v}^n, \mu^n) \in P_h \times \boldsymbol{V}_h \times M_h$ be known, where P_h, $\boldsymbol{V}_h$ and M_h denote appropriate finite element function spaces related to a regular triangulation $\mathcal{T}_h$ of Ω. Then, we compute $(p^{n+1}, \boldsymbol{v}^{n+1}, \mu^{n+1})$ as the

[2] For general constitutive relations of the type (4.1), we would have $\tilde{\mu}(u) = \frac{1}{2f(u^2)}$.

solution of the nonlinear discrete system

$$\left(\operatorname{div} \boldsymbol{v}^{n+1}, \bar{p}\right) = 0, \tag{5.16a}$$

$$\left(\frac{\boldsymbol{v}^{n+1} - \boldsymbol{v}^{n}}{\Delta t}, \bar{\boldsymbol{v}}\right) + \left(2\mu^{n+1}\mathbb{D}^{n+1}, \bar{\mathbb{D}}\right) + \left(\nabla p^{n+1}, \bar{\boldsymbol{v}}\right) = 0, \tag{5.16b}$$

$$\left(\mu^{n+1}, \bar{\mu}\right) - \left(\frac{1}{2}\left[a\left(1 + 4b\left(\mu^{n+1}\right)^2 \left|\mathbb{D}^{n+1}\right|^2\right)^n + c\right]^{-1}, \bar{\mu}\right) = 0, \tag{5.16c}$$

for test functions $(\bar{p}, \bar{\boldsymbol{v}}, \bar{\mu}) \in P_h \times \boldsymbol{V}_h \times M_h$.

5.4.1 Iterative algorithm

In order to approximate the nonlinear scheme (5.16), we propose the following iterative algorithm:

Initialization:
Define $\boldsymbol{v}^n \equiv \boldsymbol{v}^\ell =_{\text{def}} \boldsymbol{v}^0$ and $(p^\ell, \mu^\ell) =_{\text{def}} (p^0, \mu^0)$.

Step 1:
From $(p^\ell, \boldsymbol{v}^\ell, \mu^\ell)$, find $(p^{\ell+1}, \boldsymbol{v}^{\ell+1})$ such that

$$\left(\operatorname{div} \boldsymbol{v}^{\ell+1}, \bar{p}\right) = 0, \tag{5.17a}$$

$$\left(\frac{\boldsymbol{v}^{\ell+1} - \boldsymbol{v}^{n}}{\Delta t}, \bar{\boldsymbol{v}}\right) + \left(2\mu^{\ell}\mathbb{D}^{\ell+1}, \bar{\mathbb{D}}\right) + \left(\nabla p^{\ell+1}, \bar{\boldsymbol{v}}\right) = 0, \tag{5.17b}$$

$\forall (\bar{p}, \bar{\boldsymbol{v}}) \in P_h \times \boldsymbol{V}_h$.

Step 2:
Compute

$$\mu^{\ell+1} = \frac{1}{2}\left[a\left(1 + 4b\left(\mu^{\ell}\right)^2 \left|\mathbb{D}^{\ell+1}\right|^2\right)^n + c\right]^{-1}. \tag{5.18}$$

Step 3:
Compute

$$\eta = \left\|p^{\ell+1} - p^{\ell}\right\|_{L^2(\Omega)} + \left\|\boldsymbol{v}^{\ell+1} - \boldsymbol{v}^{\ell}\right\|_{L^2(\Omega)} + \left\|\mu^{\ell+1} - \mu^{\ell}\right\|_{L^2(\Omega)}, \tag{5.19}$$

update $(p^\ell, \boldsymbol{v}^\ell, \mu^\ell) =_{\text{def}} (p^{\ell+1}, \boldsymbol{v}^{\ell+1}, \mu^{\ell+1})$ and then check if

$$\begin{cases} \eta > \text{tol} \Rightarrow \text{go to } \textbf{Step 1} \text{ and iterate again,} \\ \eta \leq \text{tol} \Rightarrow \text{move to new time step, define } (p^n, \boldsymbol{v}^n, \mu^n) =_{\text{def}} (p^{\ell+1}, \boldsymbol{v}^{\ell+1}, \mu^{\ell+1}) \\ \qquad\qquad \text{and go to } \textbf{Step 1}, \end{cases} \tag{5.20}$$

where $\text{tol} > 0$ represents a tolerance parameter.

5.5 Reduced problem

5.5.1 The model and numerical scheme

In order to investigate qualitative features of models based on the implicit non-monotone constitutive relations, we present a reduced version of the system (5.11)

and introduce a numerical scheme analogous to the scheme proposed in Section 5.4. The idea is to design a reduced model that would allow us to see the *qualitative behavior that is induced by the non-monotone constitutive relation* without the unnecessary complications such as the convective nonlinearity and the incompressibility condition.

In particular, instead of the vector–tensor variables $(\boldsymbol{v}, \mathbb{T}_\delta)$, we consider scalar–vector variables $(u, \boldsymbol{q})$ whose evolution is governed by the system

$$\frac{\partial u}{\partial t} = \operatorname{div} \boldsymbol{q}, \tag{5.21a}$$

$$\nabla u = \left[a \left(1 + b \left| \boldsymbol{q} \right|^2 \right)^n + c \right] \boldsymbol{q}. \tag{5.21b}$$

This system is with respect to the relation between the flux $\boldsymbol{q}$ and the affinity ∇u structurally similar to (5.11), where the flux is the Cauchy stress tensor $\mathbb{T}_\delta$ and the affinity (thermodynamic force) is the symmetric part of the velocity gradient $\mathbb{D}$. Note that if we interpret $\boldsymbol{q}$ as the heat flux and u as the temperature, (5.21b) then corresponds to an implicit variant of Fourier's law, (3.72) being its counterpart.

If $n < -\frac{1}{2}$, the flux–affinity (force) constitutive relation is non-monotone and the relation between the norms qualitatively corresponds to that shown in Figure 5.4.

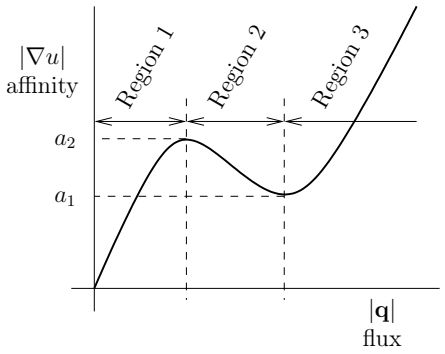

Figure 5.4: Different regions in the non-monotone constitutive relation.

Following the idea exploited in (5.13), we define the quantity $\tilde{\mu}$ as

$$\tilde{\mu}(\boldsymbol{q}) =_{\text{def}} \left[a \left(1 + b \left| \boldsymbol{q} \right|^2 \right)^n + c \right]^{-1}, \tag{5.22}$$

and the problem (5.21) can be rewritten as a system for $(u, \tilde{\mu})$ as

$$\frac{\partial u}{\partial t} = \operatorname{div} \left(\tilde{\mu} \nabla u \right), \tag{5.23a}$$

$$\tilde{\mu} = \left[a \left(1 + b \tilde{\mu}^2 \left| \nabla u \right|^2 \right)^n + c \right]^{-1}. \tag{5.23b}$$

Using the same arguments as in Section 5.4, we propose the following iterative algorithm:

Initialization:

Define $u^n \equiv u^\ell =_{\text{def}} u^0$ and $\tilde{\mu}^\ell =_{\text{def}} \tilde{\mu}^0$.

Step 1:

From $(u^\ell, \tilde{\mu}^\ell)$, find $u^{\ell+1}$ such that

$$\left(\frac{u^{\ell+1} - u^n}{\Delta t}, \bar{u}\right) + \left(\tilde{\mu}^\ell \nabla u^{\ell+1}, \nabla \bar{u}\right) = 0, \qquad \forall \bar{u} \in U_h. \tag{5.24}$$

Step 2:

Compute

$$\tilde{\mu}^{\ell+1} = \left[a\left(1 + b\left(\tilde{\mu}^\ell\right)^2 \left|\nabla u^{\ell+1}\right|^2\right)^s + c\right]^{-1}. \tag{5.25}$$

Step 3:

Compute

$$\eta = \left\|u^{\ell+1} - u^\ell\right\|_{L^2(\Omega)} + \left\|\tilde{\mu}^{\ell+1} - \tilde{\mu}^\ell\right\|_{L^2(\Omega)}, \tag{5.26}$$

update $(u^\ell, \tilde{\mu}^\ell) =_{\text{def}} (u^{\ell+1}, \tilde{\mu}^{\ell+1})$ and then check if

$$\begin{cases} \eta > \text{tol} \Rightarrow \text{go to } \textbf{Step 1} \text{ and iterate again,} \\ \eta \leq \text{tol} \Rightarrow \text{move to new time step, define } (u^n, \tilde{\mu}^n) =_{\text{def}} (u^{\ell+1}, \tilde{\mu}^{\ell+1}) \\ \qquad\qquad \text{and go to } \textbf{Step 1}, \end{cases} \tag{5.27}$$

where $\text{tol} > 0$ represents a tolerance parameter.

5.5.2 Numerical results

Here, we present results of several simulations using the numerical scheme (5.24)–(5.27). We consider a unit square domain $\Omega =_{\text{def}} [0,1]^2$ with 50×50 triangular mesh. To goal is to determine the behavior of the system depending on the initial and boundary conditions. Initial conditions are chosen so that the constitutive relation is satisfied identically in the whole domain with values corresponding to one of the three regions of the non-monotone constitutive relation, see Figure 5.4.

We consider two types of *boundary conditions*. First we consider zero Dirichlet boundary condition $u|_{\partial\Omega} = 0$ (Type A) and then the non-homogeneous Dirichlet boundary condition $u|_{x=0} = y(1-y)$, $u|_{\partial\Omega\setminus\{x=0\}} = 0$ (Type B).

We consider three different *initial conditions*. The particular *initial condition* is always specified only by the constant initial vector of the form $\boldsymbol{q}^0 = q^0_{\hat{x}} \boldsymbol{e}_{\hat{x}}$. The initial value of u is then given by

$$\tilde{\mu}^0 u^0 = q^0_{\hat{x}} x, \tag{5.28}$$

with the initial quantity $\tilde{\mu}$ given by

$$\tilde{\mu}^0 = \left[a\left(1 + b\left|\boldsymbol{q}^0\right|^2\right)^n + c\right]^{-1}. \tag{5.29}$$

Various choices of $\boldsymbol{q}^0$ always lead to flux–affinity pairs that are consistent with the constitutive relation 5.21b and using different values of $\boldsymbol{q}^0$ one can start with different locations of the initial flux–affinity pair at the constitutive curve, see Figure 5.4.

The problem is solved using a finite element approximation in space and the backward Euler method in time in the FEniCS Project software, Logg et al.

(2012); Alnæs et al. (2015). Unknown u is approximated by the finite element space $\mathcal{P}_1 =_{\text{def}} \left\{v \in C\left(\overline{\Omega}\right) : v|_T \in P_1(T), \forall T \in \mathcal{T}_h\right\}$, whereas the apparent viscosity $\tilde{\mu}$ is approximated by the piecewise constant finite element space $d\mathcal{P}_0 =_{\text{def}} \{v \in L^2(\Omega) : v|_T \in P_0(T), \forall T \in \mathcal{T}_h\}$.[3] The idea is to iterate one time step from $t = 0$ to $t = \Delta t$ to understand the dynamics of the constitutive relation. The used parameters are listed in Table 5.1.

Δt	a	b	c	n	tol
10^{-10}	1.0	0.1	10^{-3}	−0.75	10^{-10}

Table 5.1: Simulation parameters for the reduced problem.

Case 1: Initial condition in Region 1 and Type B boundary conditions

Considering $q^0_{\hat{x}} = 3$, all the points are initially in Region 1 of the constitutive curve, see Figure 5.5a. The points move along the constitutive curve in such a manner that there is no overlap between Region 1 and Region 3. (Meaning that all the points where the value of the affinity ∇u allows multiple associated fluxes $\boldsymbol{q}$ are located in Region 1. None of the actual flux–affinity pairs is in this presumably ambiguous case located in Region 3.) Moreover, none of the flux–affinity pairs can be found in Region 2 (the decreasing part of the constitutive curve) see Figure 5.5b.

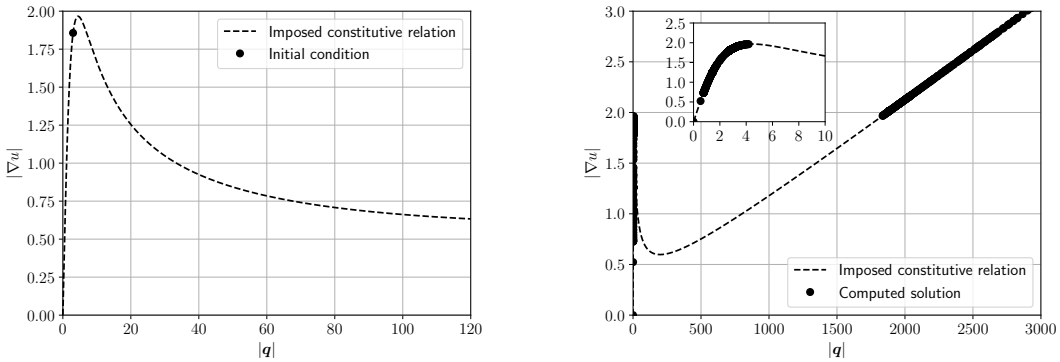

(a) Initial condition. All initial flux–affinity pairs are located in Region 1.

(b) Computed solution at time $t = \Delta t$.

Figure 5.5: Case 1. Initial condition and computed solution at $t = \Delta t$, $q^0_{\hat{x}} = 3$, non-homogeneous Dirichlet boundary condition.

Case 2: Initial condition in Region 3 and Type A boundary conditions

For $q^0_{\hat{x}} = 1000$, all the points are initially in Region 3 of the constitutive curve, see Figure 5.6a. Again, after one time step, there is no overlapping between Region 1 and Region 3 and no actual flux–affinity pair is located in Region 2 of the constitutive curve, see Figure 5.6b. In order to resolve all flux-affinity pairs for small values of $|\boldsymbol{q}|$, we had to use 8× denser mesh than in Case 1.

[3] See Section 5.6 for the justification of this particular finite element space choice.

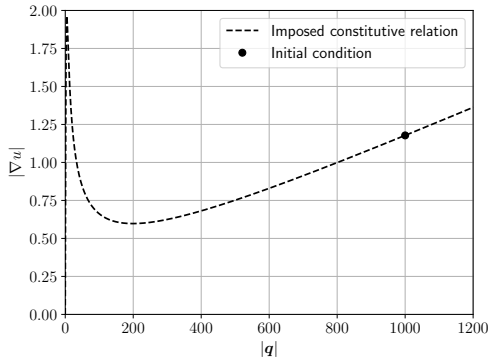

(a) Initial condition. All initial flux–affinity pairs are located in Region 3.

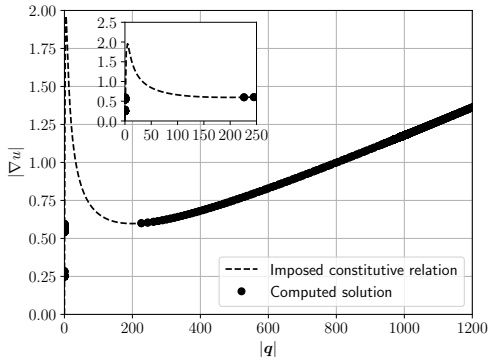

(b) Computed solution at time $t = \Delta t$.

Figure 5.6: Case 2. Initial condition and computed solution at $t = \Delta t$, $q^0_{\hat{x}} = 1000$, homogeneous Dirichlet boundary condition.

Case 3: Initial condition in Region 2 and Type A boundary conditions

Here, $q^0_{\hat{x}} = 25$, hence all the flux-affinity pairs are initially located in Region 2, see Figure 5.7a. As the time evolves, the flux–affinity pairs move from Region 2 to Region 1 and Region 3. Again there is no overlap between these two regions, see Figure 5.7b.

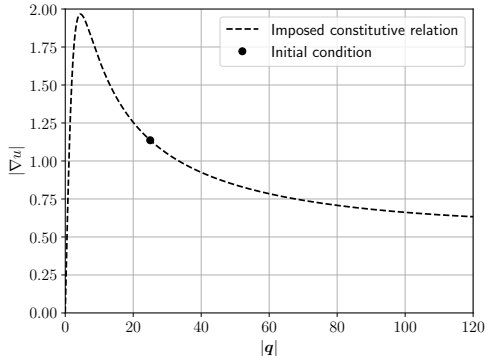

(a) Initial condition. All initial flux–affinity pairs are located in Region 2.

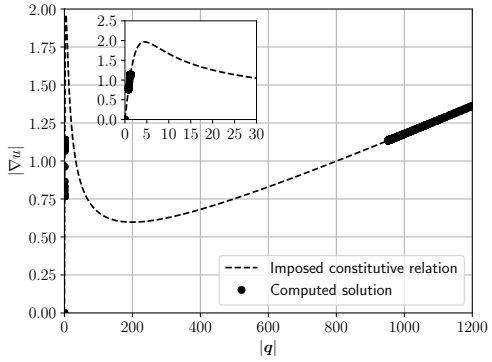

(b) Computed solution at time $t = \Delta t$.

Figure 5.7: Case 3. Initial condition and computed solution at $t = \Delta t$, $q^0_{\hat{x}} = 25$, homogeneous Dirichlet boundary condition.

Case 4: Initial condition in Region 3 and Type B boundary conditions

Now, the initial condition is the same as in Case 3, that is $q^0_{\hat{x}} = 25$, hence all the flux-affinity pairs are again initially located in Region 2, see Figure 5.8a. On the other hand, the boundary condition is now the non-homogeneous Dirichlet boundary condition. The qualitative behavior is however identical to Case 3, while the only difference is higher number of points in Region 1, see Figure 5.8b.

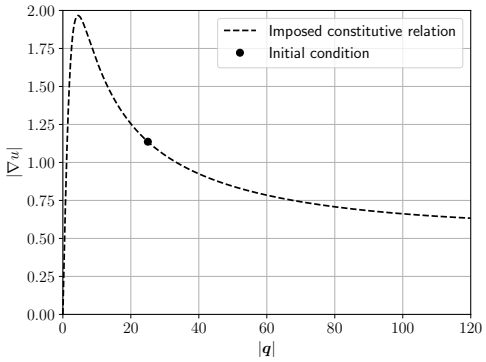

(a) Initial condition. All initial flux–affinity pairs are located in Region 2.

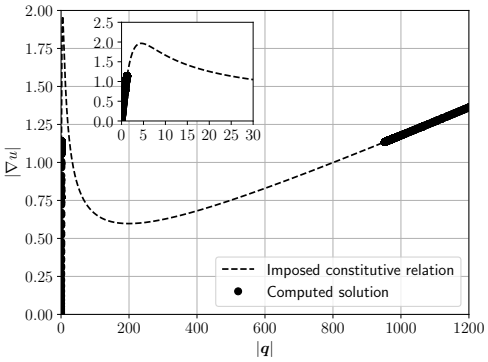

(b) Computed solution at time $t = \Delta t$.

Figure 5.8: Case 4. Initial condition and computed solution at $t = \Delta t$, $q_x^0 = 25$, non-homogeneous Dirichlet boundary condition.

Conclusion

We have designed a simple numerical experiment that allowed us to investigate quantitative and qualitative behavior of a system whose response is described by an implicit non-monotone constitutive relation (5.21b). The chosen constitutive relation predicts, see Figure 5.4, that once the affinity ∇u reaches the range (a_1, a_2), then there exist several fluxes $\boldsymbol{q}$ such that the corresponding flux–affinity pair lies on the constitutive curve. This behavior qualitatively corresponds to the behavior of relation between the Cauchy stress tensor $\mathbb{T}_\delta$ (flux) and the symmetric part of the velocity gradient $\mathbb{D}$ (affinity) in the case of more complex constitutive relation (5.9c). Apparently, such a behavior should lead to ambiguous specification of actual flux–affinity pairs.

The numerical simulations however indicate that once the problem is solved as an evolution problem, then no ambiguity arises. The position of actual flux–affinity pairs is fully determined by the initial conditions, boundary conditions and the evolution equation for the linear momentum. In particular, it seems that no actual flux–affinity pair can occupy Region 2, which corresponds to unstable flux–affinity pairs. This is in a perfect agreement with the thermodynamical stability analysis given in Chapter 3.

5.6 Numerical simulations

After demonstrating the numerical scheme presented in Section 5.4 to solve the reduced problem (5.21) in the previous section, we now numerically study the flow of a fluid described by the non-monotone constitutive relation (2.13) in the Taylor–Couette geometry. Again, all the simulations were carried out using the FEniCS Project software, Logg et al. (2012); Alnæs et al. (2015). The pressure-velocity pair $(p, \boldsymbol{v})$ was approximated by the standard lowest order Taylor–Hood elements $(\mathcal{P}_1, \boldsymbol{\mathcal{P}}_2)$, where $\mathcal{P}_k =_{\text{def}} \left\{ v \in C\left(\overline{\Omega}\right) : v|_T \in P_k(T), \forall T \in \mathcal{T}_h \right\}$ is the Lagrange element of order k and $\boldsymbol{\mathcal{P}}_k$ is its vectorial counterpart. For the viscosity, it is not clear how to choose the appropriate finite element function space. Since it is computed as

a function of the discontinuous velocity gradient from (5.18), we used piecewise constant approximation $d\mathcal{P}_0$ as the lowest order discontinuous Lagrange element $d\mathcal{P}_k =_{\text{def}} \{v \in L^2(\Omega) : v|_T \in P_k(T), \forall T \in \mathcal{T}_h\}$. For the temporal discretization, we used the Crank–Nicolson method.

As in the steady case, the inner cylinder is at rest. However, the outer one is now considered to rotate with prescribed time-dependent velocity $V(t) = \omega(t)R_2$, $\omega(t)$ being the angular velocity. The corresponding boundary conditions then read

$$\boldsymbol{v}|_{r=R_1} = \mathbf{0}, \qquad \boldsymbol{v}|_{r=R_2} = \omega(t)R_2\boldsymbol{g}_{\hat{\varphi}}, \tag{5.30}$$

where $\boldsymbol{g}_{\hat{\varphi}}$ is the azimuthal base vector in the polar coordinate system. The second boundary condition can be expressed in the Cartesian coordinate system as

$$\boldsymbol{v}|_{r=R_2} = \omega(t)\left(-y\boldsymbol{e}_{\hat{x}} + x\boldsymbol{e}_{\hat{y}}\right), \tag{5.31}$$

$\boldsymbol{e}_{\hat{x}}$ and $\boldsymbol{e}_{\hat{y}}$ being the Cartesian basis. We shall consider the time-dependent angular velocity $\omega(t)$ in the form

$$\omega(t) = \begin{cases} \omega_0 \sin\left(\pi \frac{t}{t_0}\right), & t \le t_0, \\ 0, & t > t_0, \end{cases} \tag{5.32}$$

with $\omega_0 = 0.2$ and $t_0 = 2 \times 10^{-8}$, see Figure 5.9a. Other material and geometrical parameters used in the numerical simulations are listed in Table 5.2. The maximal value of the angular velocity is chosen in such a way that the shear-rate is expected, in certain time interval, to enter the region where the S-shaped constitutive curve formally allows multiple flux–affinity (stress–shear rate) pairs.

Since the convergence of the parameter η in the numerical scheme was very poor, we had to limit its evaluation to 200 iterations. Otherwise, the computation would be extremely lengthy. If large enough, the iteration limit had only little effect on the results. For the complete implementation, see Appendix D.

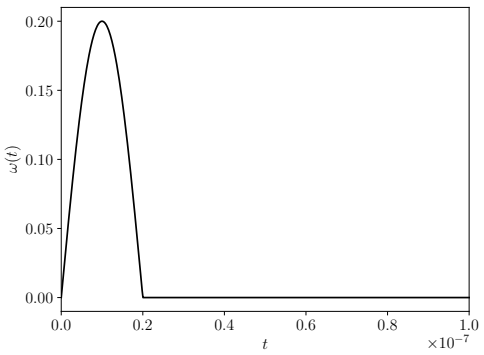

(a) Time dependence of the imposed angular velocity $\omega(t)$.

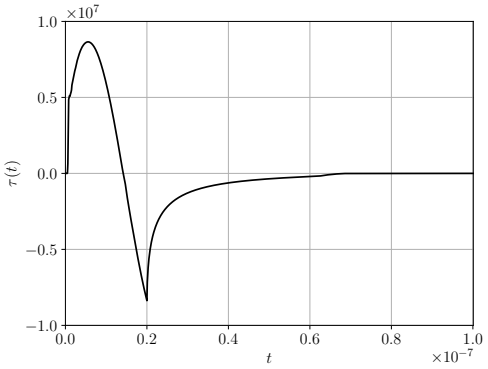

(b) Time dependence of the computed torque $\tau(t)$.

Figure 5.9: Taylor–Couette flow. Imposed angular velocity and computed torque.

Again, we are interested in the torque at the outer cylinder $\boldsymbol{\tau}$ given by (5.7). In the Cartesian coordinate system, it reads

$$\boldsymbol{\tau} = \left\{ \frac{1}{R_2} \int_{\Gamma_2} \left[\left(\mathrm{T}_{\hat{y}\hat{y}} - \mathrm{T}_{\hat{x}\hat{x}}\right) xy + \mathrm{T}_{\hat{x}\hat{y}}(x^2 - y^2) \right] \mathrm{d}l \right\} \boldsymbol{e}_{\hat{z}}, \tag{5.33}$$

R_1	R_2	a	b	c	n	Δt	T	tol
0.3	1.0	1.0	0.1	10^{-6}	−0.75	10^{-10}	10^{-7}	10^{-5}

Table 5.2: Parameters used in the Taylor–Couette flow simulations.

see Appendix C. For the prescribed angular velocity (5.32), the computed torque is shown in Figure 5.9b.

Time evolution of the apparent viscosity is then depicted in Figure 5.10. Increasing the angular velocity of the outer cylinder, a high viscosity region emerges at the outer wall and penetrates the domain towards the inner cylinder. At this point, the boundary between the low and high viscosity regions is rather distinct. The high viscosity region is present in the domain even after the outer cylinder comes to a stop but with the boundary between the two viscosity regions considerably distorted. Then, the fluid slowly returns to the original state when the whole domain is occupied only with low viscosity region. We believe that the scattered boundary between the viscosity regions when the fluid is slowing down can be attributed to computational complexity and poor convergence on one hand and the possible underlying physical instability, see Yih (1967), on the other hand.

A snapshot of the computed constitutive curve at time $t = 2 \times 10^{-8}$, i.e., when the angular velocity of the outer cylinder is brought back to zero, is presented in Figure 5.11. Since the poor convergence of the parameter η in numerical scheme, especially for high shear stresses, the constitutive relation is not perfectly satisfied. As in the case of the reduced problem in Section 5.5, there are no shear stress–shear rate pairs on the decreasing part of the constitutive curve.

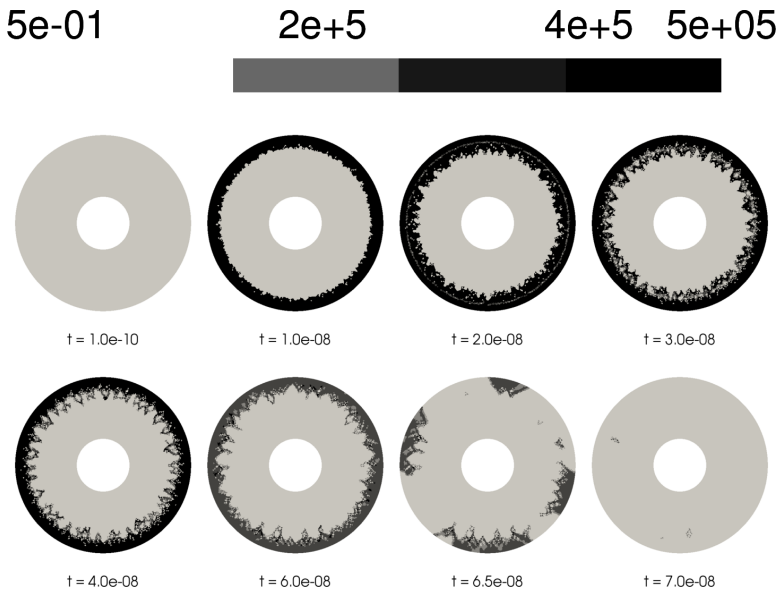

Figure 5.10: Time evolution of the apparent viscosity μ in the Taylor–Couette flow.

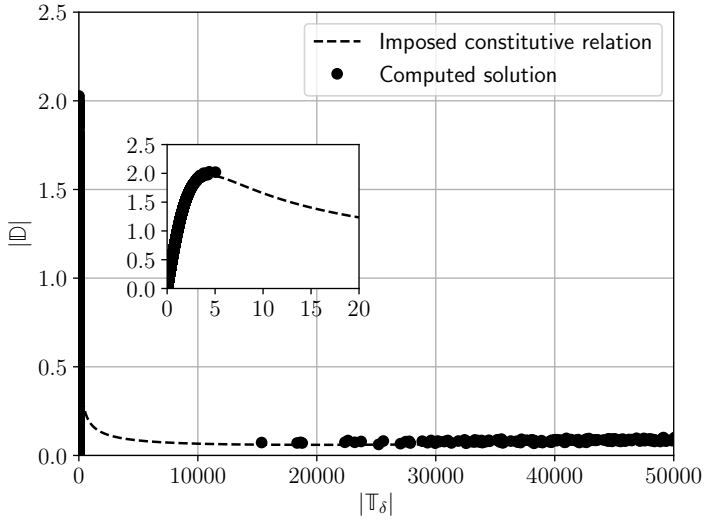

Figure 5.11: Taylor–Couette flow. Computed solution at time $t = 2 \times 10^{-8}$.

5.7 Conclusion

We proposed a numerical scheme for simulation of transient flows of incompressible non-Newtonian fluids characterized by the non-monotone constitutive relation (2.13).

Even though we have demonstrated the numerical scheme only for one particular type of flow, it is a general finite element scheme, therefore it is not problem related. Of particular interest are extensional flows as noted by Fielding (2016): "[...] interplay of shear and extensional effects in shear banding fluids has been underexplored in the literature to date." To this end, we have also employed the scheme in a flow through a channel with sinusoidal contraction, where the distinct regimes of the flow were controlled by the magnitude of the inflow velocity on the left boundary, see Figure 5.12.

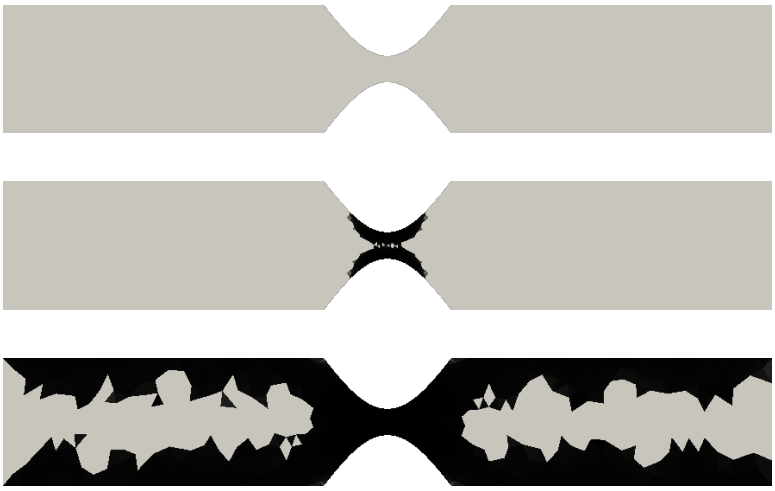

Figure 5.12: Apparent viscosity μ for different inflow velocity magnitudes, low (top) to high (bottom), in the narrowing channel (extensional) flow. Gray color corresponds to the low viscosity regime, black to the high viscosity one.

The numerical experiments have shown that only a portion of the S-shaped curve in the Cauchy stress–symmetric part of the velocity gradient plot is actually active in the complex flows. It has been observed that the flow domain usually splits into multiple regions while different branches of the constitutive curve are active in the particular regions, see Section 5.5 and Section 5.6 for details. It is known that such a behavior might be tantamount to morphological changes in the microscopic constituents of the fluid, see for example Boltenhagen et al. (1997) and Hu et al. (1998). Interestingly, such morphological changes can be visualized by various experimental techniques, see for example the references in Divoux et al. (2016) and Fardin et al. (2015), hence the predicted flow induced morphological heterogeneity of the fluid is potentially verifiable in experiments.

Most of the arguments used in the development of the numerical scheme can be also applied to general constitutive relations of the type $\mathbb{D} = f(|\mathbb{T}_\delta|)\mathbb{T}_\delta$, where f is a suitable scalar function. Conceptually, constitutive relation (2.13) belongs to the class of *implicit constitutive relations*, see Rajagopal (2003, 2006), Průša and Rajagopal (2012) and Perlácová and Průša (2015). The presented study opens the possibility to investigate the flows of fluids characterized by more complex implicit constitutive relations in complicated geometries.

6. Other models for non-monotonous shear stress/rate relation

In the thesis, we are particularly interested in investigating viscoelastic materials with S-shaped type response in the shear stress/shear rate dependence in the simple steady shear flow. There are only couple of models we are aware of, that are able to capture the desired S-shaped response. On the other hand, there are several models demonstrating its inverse, i.e., S-shaped response in the shear rate/shear stress dependence. They could serve as a motivation for similar constructions in the shear stress/shear rate models we are interested in.

In this chapter, we summarize several models capable of capturing either a non-monotone response of the shear rate as a function of the shear stress or a non-monotone response of the shear stress as a function of the shear rate.

6.1 Shear rate as a function of shear stress

6.1.1 Algebraic model

The model introduced by Le Roux and Rajagopal (2013)

$$\mathbb{D} = \left[a\left(1 + b\left|\mathbb{T}_\delta\right|^2\right)^n + c\right]\mathbb{T}_\delta, \tag{6.1}$$

is a competent model for capturing the S-shaped response and it is the central model of the thesis. It can be consistently derived using both the entropy production maximization and the gradient dynamics, as we have shown in Chapter 2 and in Chapter 3, respectively.

6.1.2 Viscoelastic model

Model (6.1) can be further generalized as a viscoelastic (rate type) model

$$\mathbb{T} = -p\mathbb{I} + \mathbb{S}, \tag{6.2a}$$

$$\left[a\left(1 + b\left|\mathbb{S}\right|^2\right)^n + c\right]\mathbb{S} + \lambda\overset{\triangledown}{\mathbb{S}} = 2\mu\mathbb{D}, \tag{6.2b}$$

recently studied by Fusi and Farina (2017); Fusi et al. (2018). It can be also derived using the extended hydrodynamics within the gradient dynamics formalism, as can be seen from (3.62).

6.2 Shear stress as a function of shear rate

6.2.1 Johnson–Segalman model

In the *Johnson–Segalman model*, see Johnson and Segalman (1977), the total stress $\mathbb{T}$ is assumed to consist of the pressure p, the standard Newtonian contri-

bution $2\mu\mathbb{D}$ and the viscoelastic contribution $\mathbb{\Sigma}$ that has its own dynamics

$$\mathbb{T} = -p\mathbb{I} + 2\mu\mathbb{D} + \mathbb{\Sigma}, \tag{6.3a}$$

$$\mathbb{\Sigma} + \tau\overset{\diamond}{\mathbb{\Sigma}} = 2\eta\mathbb{D}. \tag{6.3b}$$

Here, η is the viscoelastic viscosity, τ is the relaxation time and $\overset{\diamond}{\mathbb{\Sigma}} =_{\text{def}} \frac{\mathrm{d}\mathbb{\Sigma}}{\mathrm{d}t} + (\mathbb{\Sigma}\mathbb{W} - \mathbb{W}\mathbb{\Sigma}) - a(\mathbb{\Sigma}\mathbb{D} + \mathbb{D}\mathbb{\Sigma})$ the Gordon–Schowalter time derivative of $\mathbb{\Sigma}$ where $\mathbb{W} =_{\text{def}} \frac{1}{2}(\nabla\boldsymbol{v} - \nabla\boldsymbol{v}^{\mathsf{T}})$ is the skew-symmetric part of the velocity gradient and $|a| \leq 1$ is the slip parameter, see Gordon and Schowalter (1972).

For a unidirectional steady simple shear flow in the Cartesian coordinate system with velocity of the form $\boldsymbol{v}(x, y, z) = v^{\hat{z}}(y)\boldsymbol{e}_{\hat{z}}$, we can reconstruct the one-dimensional constitutive relation for the corresponding component of (6.3a)

$$\sigma = \mu\dot{\gamma} + \Sigma^{\hat{y}\hat{z}}, \tag{6.4}$$

where we have denoted $\sigma =_{\text{def}} \mathrm{T}^{\hat{y}\hat{z}}$ the shear stress and $\dot{\gamma} =_{\text{def}} 2\mathrm{D}^{\hat{y}\hat{z}} = \frac{\mathrm{d}v^{\hat{z}}}{\mathrm{d}y}$ the shear rate. From the relevant components of (6.3b)

$$\Sigma^{\hat{y}\hat{z}} - \left(\frac{a+1}{2}\Sigma^{\hat{y}\hat{y}} + \frac{a-1}{2}\Sigma^{\hat{z}\hat{z}}\right)\tau\dot{\gamma} = \eta\dot{\gamma}, \tag{6.5a}$$

$$\Sigma^{\hat{y}\hat{y}} - (a-1)\tau\dot{\gamma}\Sigma^{\hat{y}\hat{z}} = 0, \tag{6.5b}$$

$$\Sigma^{\hat{z}\hat{z}} - (a+1)\tau\dot{\gamma}\Sigma^{\hat{y}\hat{z}} = 0, \tag{6.5c}$$

we can obtain $\Sigma^{\hat{y}\hat{z}}$, so the one-dimensional constitutive relation reads

$$\sigma = \mu\dot{\gamma} + \frac{\eta\dot{\gamma}}{1 + (1-a^2)(\tau\dot{\gamma})^2}. \tag{6.6}$$

For $|a| < 1$ and the ratio μ/η sufficiently small, (6.6) is a S-shaped curve in the shear rate/shear stress dependence. The same relation was derived for the cylindrical Taylor–Couette geometry by Greco and Ball (1997).

Although the Johnson–Segalman model (6.3) is commonly used as a simple model to describe the shear banding, it cannot uniquely predict the selection of the stress at which the banding occurs. This is resolved by the addition of a nonlocal diffusive term to the evolution equation (6.3b). For example, Yuan (1999) introduced a model with the shear rate diffusion $-\mathcal{D}\Delta\mathbb{D}$, while Olmsted et al. (2000) argued for the viscoelastic stress diffusion $\mathcal{D}\Delta\mathbb{\Sigma}$. The stresses selected by the resulting diffusive (modified) Johnson–Segalman models differ but are independent of the positive diffusion coefficient $\mathcal{D}$, see Olmsted (2008).

6.2.2 Bautista–Manero model

The *Bautista–Manero model*, see Bautista et al. (1999, 2000), is commonly used to describe rheological behavior of wormlike micellar systems, see for example López-Aguilar et al. (2014). It consists of the upper convected Maxwell constitutive relation and an additional kinetic equation for the fluidity (reciprocal viscosity) $\varphi =_{\text{def}} \mu^{-1}$ due to Fredrickson (1970)

$$\mathbb{T} = -p\mathbb{I} + \mathbb{S}, \tag{6.7a}$$

$$\mathbb{S} + \frac{1}{G_0\varphi}\overset{\triangledown}{\mathbb{S}} = \frac{2}{\varphi}\mathbb{D}, \tag{6.7b}$$

$$\frac{\mathrm{d}\varphi}{\mathrm{d}t} = -\frac{\varphi - \varphi_0}{\lambda} + k(\varphi_\infty - \varphi)\mathbb{S} : \mathbb{D}, \tag{6.7c}$$

where G_0 is the plateau shear modulus, φ_0 and φ_∞ are the fluidities at zero and very high (infinite) shear rates, λ is the relaxation time and $k = k(\dot\gamma)$ is the shear rate dependent destruction function.

Assuming again the steady simple shear flow of the form $\boldsymbol{v}(x,y,z) = v^{\hat z}(y)\boldsymbol{e}_{\hat z}$, the yz-component of (6.7b) reads

$$\sigma = \frac{1}{\varphi}\dot\gamma, \tag{6.8}$$

where $\sigma =_{\text{def}} \mathrm{T}^{\hat y\hat z} \equiv \mathrm{S}^{\hat y\hat z}$ is the shear stress and $\dot\gamma =_{\text{def}} 2\mathrm{D}^{\hat y\hat z} = \frac{\mathrm{d}v^{\hat z}}{\mathrm{d}y}$ the shear rate. Then, from (6.7c), $\mathbb{S}{:}\mathbb{D} = \dot\gamma\sigma$ and (6.8) follows a quadratic equation for the fluidity

$$\varphi^2 - \varphi_0\varphi - k\lambda(\varphi_\infty - \varphi)\dot\gamma^2 = 0, \tag{6.9}$$

with a non-negative root

$$\varphi = \frac{1}{2}\left[-\left(k\lambda\dot\gamma^2 - \varphi_0\right) + \sqrt{\left(k\lambda\dot\gamma^2 - \varphi_0\right)^2 + 4k\lambda\dot\gamma^2\varphi_\infty}\right]. \tag{6.10}$$

For linear destruction function $k(\dot\gamma) = k_0(1+\mu_1\dot\gamma)$, (6.8) together with (6.10) gives a S-shaped relation for the shear rate/shear stress dependence, see Bautista et al. (2000).

6.2.3 Giesekus model

Another generalization of the upper convected Maxwell model is the *Giesekus model* with additional quadratic term of the extra stress $\mathbb{S}$, see Giesekus (1982),

$$\mathbb{T} = -p\mathbb{I} + \mathbb{S}, \tag{6.11a}$$

$$\mathbb{S} + \lambda\overset{\triangledown}{\mathbb{S}} + \frac{\alpha\lambda}{\mu}\mathbb{S}^2 = 2\mu\mathbb{D}, \tag{6.11b}$$

where λ is the relaxation time and $\alpha \in [0,1]$. For $\alpha = 0$, the model apparently reduces to the standard upper convected Maxwell model.

For the steady simple shear flow, the nonzero components of (6.11b) read

$$\mathrm{S}^{\hat y\hat y} + \frac{\alpha\lambda}{\mu}\left[\left(\mathrm{S}^{\hat y\hat y}\right)^2 + \sigma^2\right] = 0, \tag{6.12a}$$

$$\mathrm{S}^{\hat z\hat z} + \frac{\alpha\lambda}{\mu}\left[\left(\mathrm{S}^{\hat z\hat z}\right)^2 + \sigma^2\right] = 2\lambda\dot\gamma\sigma, \tag{6.12b}$$

$$\frac{\alpha\lambda}{\mu}\left(\mathrm{S}^{\hat y\hat y} + \mathrm{S}^{\hat z\hat z}\right)\sigma + \sigma - \lambda\dot\gamma\mathrm{S}^{\hat y\hat y} = \mu\dot\gamma. \tag{6.12c}$$

From (6.12a), we immediately see that $\mathrm{S}^{\hat y\hat y} \le 0$ with equality for $\alpha = 0$. Subtracting the first equation from the second one and rewriting the third equation leads to

$$\left[\frac{\alpha\lambda}{\mu}\left(\mathrm{S}^{\hat y\hat y} + \mathrm{S}^{\hat z\hat z}\right) + 1\right]\left(\mathrm{S}^{\hat z\hat z} - \mathrm{S}^{\hat y\hat y}\right) = 2\lambda\dot\gamma\sigma, \tag{6.13a}$$

$$\left[\frac{\alpha\lambda}{\mu}\left(\mathrm{S}^{\hat y\hat y} + \mathrm{S}^{\hat z\hat z}\right) + 1\right]\sigma = \dot\gamma\left(\mu + \lambda\mathrm{S}^{\hat y\hat y}\right). \tag{6.13b}$$

The formula for the shear stress σ as a function of $S^{\hat{y}\hat{y}}$ and $S^{\hat{z}\hat{z}}$ follows from the division of (6.13b) by (6.13a)

$$\sigma^2 = \frac{S^{\hat{z}\hat{z}} - S^{\hat{y}\hat{y}}}{2\lambda}\left(\mu + \lambda S^{\hat{y}\hat{y}}\right). \tag{6.14}$$

Substituting this into (6.12a), we can express the difference $S^{\hat{z}\hat{z}} - S^{\hat{y}\hat{y}}$ as a function of $S^{\hat{y}\hat{y}}$

$$S^{\hat{z}\hat{z}} - S^{\hat{y}\hat{y}} = -\frac{2S^{\hat{y}\hat{y}}\left(\mu + \alpha\lambda S^{\hat{y}\hat{y}}\right)}{\alpha\left(\mu + \lambda S^{\hat{y}\hat{y}}\right)}. \tag{6.15}$$

which, in return, enables us to reformulate the shear stress σ as a function of $S^{\hat{y}\hat{y}}$ only

$$\sigma^2 = -\frac{S^{\hat{y}\hat{y}}}{\alpha\lambda}\left(\mu + \alpha\lambda S^{\hat{y}\hat{y}}\right). \tag{6.16}$$

This relation can be also obtained immediately from (6.12a) and in addition, it yields the lower bound $S^{\hat{y}\hat{y}} \geq -\frac{\mu}{\lambda}$ for $\alpha = 1$.

Multiplying (6.13a) with (6.13b) results in

$$\left[\frac{\alpha\lambda}{\mu}\left(S^{\hat{y}\hat{y}} + S^{\hat{z}\hat{z}}\right) + 1\right]^2 \left(S^{\hat{z}\hat{z}} - S^{\hat{y}\hat{y}}\right) = 2\lambda\dot{\gamma}^2\left(\mu + \lambda S^{\hat{y}\hat{y}}\right), \tag{6.17}$$

and together with (6.15), it enables us to formulate $\dot{\gamma}$ as a function of $S^{\hat{y}\hat{y}}$

$$\dot{\gamma}^2 = -\frac{S^{\hat{y}\hat{y}}(\mu + \alpha\lambda S^{\hat{y}\hat{y}})}{\alpha\lambda(\mu + \lambda S^{\hat{y}\hat{y}})^4}\left[\mu - (1-2\alpha)\lambda S^{\hat{y}\hat{y}}\right]^2 \tag{6.18}$$

Introducing the substitution

$$S^{\hat{y}\hat{y}} = -\frac{1}{\lambda}\frac{\mu(1-\Lambda)}{1 + (1-2\alpha)\Lambda}, \tag{6.19}$$

the relation for $\dot{\gamma}$ can be rewritten as a biquadratic equation

$$\dot{\gamma}^2 = \frac{1 - \Lambda^2}{4\alpha(1-\alpha)\lambda^2\Lambda^4}, \tag{6.20}$$

with a non-negative solution

$$\Lambda^2 = \frac{1}{8\alpha(1-\alpha)\lambda^2\dot{\gamma}^2}\left[\sqrt{1 + 16\alpha(1-\alpha)\lambda^2\dot{\gamma}^2} - 1\right]. \tag{6.21}$$

From (6.19) also follows that $\Lambda \in [0, 1]$ since $S^{\hat{y}\hat{y}} \in \left[-\frac{\mu}{\lambda}, 0\right]$.

Substituting for Λ from (6.21) into (6.19) provides the relation for $S^{\hat{y}\hat{y}}$. With this we can obtain the formula for the shear stress σ from (6.16) as

$$\sigma = \frac{\mu}{\alpha\lambda}\frac{\sqrt{\alpha(1-\alpha)\left[\sqrt{1 + 16\alpha(1-\alpha)\lambda^2\dot{\gamma}^2} - 1\right]}}{\sqrt{2}(1-2\alpha) + \sqrt{\sqrt{1 + 16\alpha(1-\alpha)\lambda^2\dot{\gamma}^2} + 1}}. \tag{6.22}$$

Even though this relation cannot demonstrate an S-shaped curve, for $\alpha > \frac{1}{2}$, the one-dimensional constitutive relation has a maximum and qualitatively resembles the model by Málek et al. (2010). Specially for $\alpha = 1$, the shear stress has a simple form

$$\sigma = \frac{\mu\dot{\gamma}}{1 + \lambda^2\dot{\gamma}^2}. \tag{6.23}$$

6.2.4 Grmela model

Within the GENERIC framework (see Chapter 3), Grmela et al. (2010) derived a rheological model of fluids composed of wormlike micelles

$$\mathbb{T} = -p\mathbb{I} + \mathbb{S}, \tag{6.24a}$$

$$\mathbb{S} = 2H\mathbb{c} - k_{\mathrm{B}}T\mathbb{I} + 2(1-\zeta)\frac{G\mu}{1-\mu^2}\mathbb{c}, \tag{6.24b}$$

$$\overset{\triangledown}{\mathbb{c}} = -\Lambda\left(H\mathbb{c} - \frac{k_{\mathrm{B}}T}{2}\mathbb{I}\right), \tag{6.24c}$$

$$\frac{\mathrm{d}\mu}{\mathrm{d}t} = 2(1-\zeta)\mathbb{c} : \mathbb{D} - \lambda\frac{G\mu}{1-\mu^2}, \tag{6.24d}$$

where $\mathbb{c}$ is a symmetric conformation tensor, $\mu \in [0,1]$ is a dimensionless scalar structural variable, H and G are two elastic moduli, ζ is a slip coefficient, k_{B} is the Boltzmann constant, T is constant temperature and Λ and λ are positive kinetic coefficients. The coefficients ζ, Λ and λ can all depend on the structural variable μ. Note that in the absence of μ, the model reduces to the classical Maxwell model for the extra stress $\mathbb{S}$ with relaxation time $\frac{1}{\lambda H}$ and viscosity $\frac{k_{\mathrm{B}}T}{\lambda H}$.

In the steady unidirectional simple shear flow, we then have

$$\sigma = 2\mathrm{c}^{\hat{y}\hat{z}}\left[H + (1-\zeta)\frac{G\mu}{1-\mu^2}\right], \tag{6.25a}$$

$$0 = \Lambda\left(H\mathrm{c}^{\hat{x}\hat{x}} - \frac{k_{\mathrm{B}}T}{2}\right), \tag{6.25b}$$

$$0 = \Lambda\left(H\mathrm{c}^{\hat{y}\hat{y}} - \frac{k_{\mathrm{B}}T}{2}\right), \tag{6.25c}$$

$$2\dot{\gamma}\mathrm{c}^{\hat{y}\hat{z}} = \Lambda\left(H\mathrm{c}^{\hat{z}\hat{z}} - \frac{k_{\mathrm{B}}T}{2}\right), \tag{6.25d}$$

$$\dot{\gamma}\mathrm{c}^{\hat{y}\hat{y}} = \Lambda H\mathrm{c}^{\hat{y}\hat{z}}, \tag{6.25e}$$

$$\mathrm{c}^{\hat{x}\hat{y}} = \mathrm{c}^{\hat{x}\hat{z}} = 0, \tag{6.25f}$$

$$2\dot{\gamma}(1-\zeta)\mathrm{c}^{\hat{y}\hat{z}} = \lambda\frac{G\mu}{1-\mu^2}, \tag{6.25g}$$

which further simplifies to

$$\dot{\gamma}^2\frac{k_{\mathrm{B}}T}{H^2}\frac{1-\zeta}{\Lambda} = \lambda\frac{G\mu}{1-\mu^2}, \tag{6.26}$$

and

$$\sigma = \dot{\gamma}\frac{k_{\mathrm{B}}T}{H^2}\frac{1}{\Lambda}\left[H + G(1-\zeta)\frac{\mu}{1-\mu^2}\right]. \tag{6.27}$$

For given functions $\Lambda(\mu)$, $\lambda(\mu)$ and $\zeta(\mu)$, we can solve (6.26) for μ and insert it into (6.27) to obtain the one-dimensional constitutive relation. With a particular choice $\Lambda = 0.01 + \mu^2$, $\lambda = 1$ and $\zeta = 0.98$, Grmela et al. (2010) illustrated that this relation might be an S-shaped curve.

Conclusion

We have studied behavior and properties of a special class of incompressible non-Newtonian fluids. Since the rheological response of these fluids cannot be described using the classical phenomenological theory of constitutive relations, we have introduced the **implicit constitutive theory** and we have discussed its possible benefits in modeling the responses of this kind.

Together with the idea of implicit constitutive relations, we have presented two desirable approaches for developing mathematical models for this type of non-Newtonian fluids. Namely, in Chapter 2, the framework of entropy production maximization, Rajagopal and Srinivasa (2004), and in Chapter 3, gradient dynamics in the GENERIC formalism, Grmela and Öttinger (1997); Öttinger and Grmela (1997).

In Chapter 3, we have used the non-monotone model (6.1) to fit particular experimental data in the shear flow experiment. The data are of great interest as varying the shear rate generates jumps in the response, even though the variation of the shear stress leads to a continuous response. The discontinuities can lead to a hysteretic behavior between different branches of the non-monotone constitutive relation. To understand this phenomenon, we were able to reformulate the non-monotone constitutive relation in the GENERIC structure as the derivative of a **non-convex dissipation potential**. Though being convex near equilibrium, the dissipation potential loses convexity for higher stresses. Due to the loss of convexity the Legendre-like conjugate dissipation potential is multivalued which corresponds to the fact that the shear stress response might be equivocal. We have also shown that the phenomenon of critical heat flux can be addressed analogically. The effects resulting from non-convex dissipation potentials are somewhat similar to those arising from non-convex energy. Nevertheless, it is a different physical process since the non-convexity is not in the dissipative part of the evolution as in our case.

Elevating the classical hydrodynamics to the extended hydrodynamics level, we have introduced the concept of **CR-stability** explaining various regimes of the dynamics with respect to perturbations of the constitutive relation. It enables us to identify CR-stability, CR-metastability and CR-instability of different branches of the constitutive relation. Moreover, it is also possible to determine the discontinuous behavior of the shear stress. Our findings are compatible with the experimental data and we are not aware of such analysis being conducted before.

In Chapter 4, we have discussed **hydrodynamic stability** of flows of incompressible fluids described by implicit constitutive relation of the particular form $\mathbb{D} = \mathfrak{f}(\mathbb{T}_\delta)$. First, we have derived the base flow as the solution to the stationary two-dimensional plane Poiseuille flow. To study stability, the base flow is then disturbed and we observe the behavior of the imposed perturbation. In a simple setting, we have also demonstrated that flows within a regime of decreasing constitutive relations as functions of either the shear rate or the shear stress are unconditionally unstable.

From the kinetic energy of the perturbation, we have derived a generalized version of the Reynolds–Orr equation. Using this equation we were able to deter-

mine the exponential decrease of the kinetic energy of a disturbance imposed onto a fluid at rest and deduce stability criteria for the Poiseuille flow in a channel.

Linearizing the governing equations for the Poiseuille flow in a channel and assuming a wave-like disturbance, we have derived the generalized Orr–Sommerfeld–Squire system, which can be seen as a generalized eigenvalue problem. We have proved that it is sufficient to consider only two-dimensional disturbances and we have obtained estimates for both the propagation speed and the growth rate of the disturbance. We have concluded that once the constitutive relation is not monotone and the external forcing is strong enough, there are inflection points in the velocity profile and the flow is unconditionally unstable. This result confirms the instability of the decreasing branch of the constitutive relation stated beforehand.

Then, for several constitutive models, we have numerically solved the generalized eigenvalue problem by means of pseudospectral collocation method and have once again validated the instability of the decreasing branch of a non-monotone constitutive relation. Particularly the instability of the flow of a fluid described by the constitutive relation (6.1) can be understood as a flow of two fluids with different viscosities as the constitutive relation has two distinct stable and one unstable branch. Due to the viscosity stratification, flow of this type is unstable, see Yih (1967).

In Chapter 5, we have proposed a **numerical scheme** for simulation of transient flows of incompressible non-Newtonian fluids characterized by a particular implicit type model (6.1). The numerical scheme is based on reformulation of the governing equations as a system for the triple pressure–velocity–apparent viscosity, where the apparent viscosity is given by a scalar implicit equation. Then, we have numerically studied flow of a fluid characterized by this non-monotone constitutive relation in two-dimensional Taylor–Couette geometry.

In order to investigate the dynamical behavior implied by the non-monotone constitutive relations, we have also presented a reduced problem that can be understood as an implicit variant of Fourier's law of heat conduction. In the numerical experiments, we have observed that the flow domain usually splits into multiple regions corresponding to different branches of the constitutive curve. We have confirmed that only a portion of the S-shaped curve in the Cauchy stress–symmetric part of the velocity gradient plot is attainable with the decreasing part being omitted once again.

Finally in Chapter 6, we have mention several other models that are also able to describe non-monotone response between the shear stress and the shear rate in the simple steady shear flow. In the future, these models could provide a motivation for the construction of models with non-monotone shear rate/shear stress response.

Bibliography

Abramowitz, M. and I. A. Stegun (Eds.) (1964). *Handbook of mathematical functions with formulas, graphs, and mathematical tables*. Number 55 in Applied Mathematics Series. Washington D.C.: United States Dept. of Commerce, National Bureau of Standards.

Alnæs, M., J. Blechta, J. Hake, A. Johansson, B. Kehlet, A. Logg, C. Richardson, J. Ring, M. Rognes, and G. Wells (2015). The FEniCS project version 1.5. *Archive of Numerical Software 3*(100).

Arnold, V. (1966). Sur la géometrie différentielle des groupes de lie de dimension infini et ses applications dans l'hydrodynamique des fluides parfaits. *Annales de l'institut Fourier 16*(1), 319–361.

Asszonyi, C., T. Fülöp, and P. Ván (2015, Nov). Distinguished rheological models for solids in the framework of a thermodynamical internal variable theory. *Continuum Mechanics and Thermodynamics 27*(6), 971–986.

Barus, C. (1893). Isotherms, isopiestics and isometrics relative to viscosity. *Amer. J. Sci. 45*, 87–96.

Bauschke, H. and Y. Lucet (2012). What is a Fenchel conjugate? *Notices of the AMS 59*(1), 44–46.

Bautista, F., J. M. de Santos, J. E. Puig, and O. Manero (1999). Understanding thixotropic and antithixotropic behavior of viscoelastic micellar solutions and liquid crystalline dispersions. I. The model. *J. Non-Newton. Fluid Mech. 80*(2–3), 93–113.

Bautista, F., J. F. A. Soltero, J. H. Pérez-López, J. E. Puig, and O. Manero (2000). On the shear banding flow of elongated micellar solutions. *J. Non-Newton. Fluid Mech. 94*(1), 57–66.

Beretta, G. P. (2014, Oct). Steepest entropy ascent model for far-nonequilibrium thermodynamics: Unified implementation of the maximum entropy production principle. *Phys. Rev. E 90*, 042113.

Berezovski, A. and P. Ván (2017). *Internal Variables in Thermoelasticity*, Volume 243 of *Solid Mechanics and Its Applications*. Springer International Publishing.

Bergman, T. L., A. S. Lavine, F. P. Incropera, and D. P. DeWitt (2011). *Fundamentals of Heat and Mass Transfer* (7th ed.). John Wiley & Sons, Inc.

Bi, D., J. Zhang, B. Chakraborty, and R. P. Behringer (2011). Jamming by shear. *Nature 480*(7377), 355–358.

Bingham, C. E. (1922). *Fluidity and plasticity*. New York: McGraw–Hill.

Böhme, G. (1987). *Non-newtonian fluid mechanics*. North-Holland.

Boltenhagen, P., Y. Hu, E. F. Matthys, and D. J. Pine (1997, Sep). Observation of bulk phase separation and coexistence in a sheared micellar solution. *Phys. Rev. Lett. 79*, 2359–2362.

Boyd, J. P. (2001). *Chebyshev and Fourier spectral methods* (Second ed.). Mineola, NY: Dover Publications Inc.

Bulíček, M., P. Gwiazda, J. Málek, and A. Świerczewska-Gwiazda (2009). On steady flows of incompressible fluids with implicit power-law-like rheology. *Adv. Calc. Var. 2*(2), 109–136.

Bulíček, M., P. Gwiazda, J. Málek, and A. Świerczewska-Gwiazda (2012). On unsteady flows of implicitly constituted incompressible fluids. *SIAM J. Math. Anal. 44*(4), 2756–2801.

Bulíček, M., M. Pokorný, and N. Zamponi (2017). Existence analysis for incompressible fluid model of electrically charged chemically reacting and heat conducting mixtures. *SIAM Journal on Mathematical Analysis 49*(5), 3776–3830.

Callen, H. B. (1985). *Thermodynamics and an introduction to thermostatistics* (Revised ed.). John Wiley & Sons.

Canuto, C., M. Y. Hussaini, A. Quarteroni, and T. A. Zang (2006). *Spectral methods: Fundamentals in single domains*. Scientific Computation. Berlin: Springer-Verlag.

Canuto, C., M. Y. Hussaini, A. Quarteroni, and T. A. Zang (2007). *Spectral methods: Evolution to complex geometries and applications to fluid dynamics*. Scientific Computation. Berlin: Springer.

Carreau, P. J. (1972). Rheological equations from molecular network theories. *J. Rheol. 16*(1), 99–127.

Casimir, H. B. G. (1945, Apr). On Onsager's principle of microscopic reversibility. *Rev. Mod. Phys. 17*, 343–350.

Chandrasekhar, S. (1961). *Hydrodynamic and hydromagnetic stability*. The International Series of Monographs on Physics. Clarendon Press, Oxford.

Cinelli, G. (1965). An extension of the finite Hankel transform and applications. *International Journal of Engineering Science 3*(5), 539–559.

Clausius, R. (1879). *The Mechanical Theory of Heat*. London: MacMillan.

Coleman, B. D., H. Markovitz, and W. Noll (1966). *Viscometric flows of non-newtonian fluids. Theory and experiment*. Berlin: Springer-Verlag.

Coleman, B. D. and W. Noll (1960). An approximation theorem for functionals, with applications in continuum mechanics. *Arch. Ration. Mech. Anal. 6*, 355–370.

Dawkins, P. T., S. R. Dunbar, and R. W. Douglass (1998). The origin and nature of spurious eigenvalues in the spectral tau method. *Journal of Computational Physics 147*(2), 441–462.

de Gennes, P. G. (1974). Coil-stretch transition of dilute flexible polymers under ultrahigh velocity gradients. *J. Chem. Phys. 60*(12), 5030–5042.

de Groot, S. R. and P. Mazur (1984). *Non-equilibrium thermodynamics*. New York: Dover Publications. Reprint of the 1962 original.

de Waele, A. (1923). Viscometry and plastometry. *J. Oil Colour Chem. Assoc. 6*, 33–69.

Desvillettes, L. and C. Villani (2005, Feb). On the trend to global equilibrium for spatially inhomogeneous kinetic systems: The Boltzmann equation. *Inventiones mathematicae 159*(2), 245–316.

Dhont, J. K. G., M. P. Lettinga, Z. Dogic, T. A. J. Lenstra, H. Wang, S. Rathgeber, P. Carletto, L. Willner, H. Frielinghaus, and P. Lindner (2003). Shear-banding and microstructure of colloids in shear flow. *Faraday Discuss. 123*, 157–172.

Diening, L., C. Kreuzer, and E. Süli (2013). Finite element approximation of steady flows of incompressible fluids with implicit power-law-like rheology. *SIAM J. Numer. Anal. 51*(2), 984–1015.

DiPerna, R. J. and P. L. Lions (1991, Mar). Global solutions of Boltzmann's equation and the entropy inequality. *Archive for Rational Mechanics and Analysis 114*(1), 47–55.

Divoux, T., M. A. Fardin, S. Manneville, and S. Lerouge (2016). Shear banding of complex fluids. *Annu. Rev. Fluid Mech. 48*(1), 81–103.

Dongarra, J., B. Straughan, and D. Walker (1996). Chebyshev tau-QZ algorithm methods for calculating spectra of hydrodynamic stability problems. *Applied Numerical Mathematics 22*(4), 399–434.

Donnelly, R. J. (1991, NOV). Taylor–Couette flow: the early days. *Phys. Today 44*(11), 32–39.

Dorst, L. and R. Van den Boomgaard (1993). An analytical theory of mathematical morphology. In *Mathematical Morphology and its Applications to Signal Processing*, Barcelona, pp. 245–250.

Dorst, L. and R. Van den Boomgaard (1994). Morphological signal processing and the slope transform. *Signal Processing 38*(1), 79–98.

Drazin, P. and L. Howard (1966). Hydrodynamic stability of parallel flow of inviscid fluid. *Adv. Appl. Mech. 9*, 1–89.

Drazin, P. G. and W. H. Reid (2004). *Hydrodynamic stability* (Second ed.). Cambridge Mathematical Library. Cambridge: Cambridge University Press. With a foreword by John Miles.

Drew, T. B. and A. C. Mueller (1937). Boiling. *Trans. Am. Inst. Chem. Eng. 33*, 449–473.

Fan, X.-J., R. B. Bird, and M. Renardy (1985). Configuration-dependent friction coefficients and elastic dumbbell rheology. *J. Non-Newtonian Fluid Mech. 18*(3), 255–272.

Fardin, M.-A., O. Radulescu, A. Morozov, O. Cardoso, J. Browaeys, and S. Lerouge (2015). Stress diffusion in shear banding wormlike micelles. *J. Rheol. 59*(6), 1335–1362.

Fielding, S. M. (2007). Complex dynamics of shear banded flows. *Soft Matter 3*, 1262–1279.

Fielding, S. M. (2016). Editor's preface to the special issue: Shear banding in complex fluids. *Journal of Rheology 60*(5), 819–820.

Fjørtoft, R. (1950). Application of integral theorems in deriving criteria for instability for laminar flows and for the baroclinic circular vortex. *Geofys. Publ., Oslo 17*(6), 1–52.

François, N., Y. Amarouchene, B. Lounis, and H. Kellay (2009). Polymer conformations and hysteretic stresses in nonstationary flows of polymer solutions. *EPL (Europhysics Letters) 86*(3), 34002.

Fredrickson, A. G. (1970). A model for the thixotropy of suspensions. *AIChE J. 16*(3), 436–441.

Fusi, L. and A. Farina (2017). Flow of a class of fluids defined via implicit constitutive equation down an inclined plane: Analysis of the quasi-steady regime. *Eur. J. Mech. B Fluids 61*, 200–208.

Fusi, L., A. Farina, G. Saccomandi, and K. Rajagopal (2018). Lubrication approximation of flows of a special class of non-Newtonian fluids defined by rate type constitutive equations. *Applied Mathematical Modelling 60*, 508–525.

Germann, N., L. P. Cook, and A. N. Beris (2013). Nonequilibrium thermodynamic modeling of the structure and rheology of concentrated wormlike micellar solutions. *J. Non-Newtonian Fluid Mech. 196*(0), 51–57.

Gibbs, J. W. (1876). On the equilibrium of heterogeneous substances. *Trans. Conn. Acad. Arts Sci. 3*, 108–248.

Gibbs, J. W. (1878). On the equilibrium of heterogeneous substances. *Trans. Conn. Acad. Arts Sci. 3*, 343–524.

Giesekus, H. (1982). A simple constitutive equation for polymer fluids based on the concept of deformation-dependent tensorial mobility. *J. Non-Newton. Fluid Mech. 11*(1-2), 69–109.

Gordon, R. J. and W. R. Schowalter (1972). Anisotropic fluid theory: A different approach to the dumbbell theory of dilute polymer solutions. *Transactions of the Society of Rheology 16*(1), 79–97.

Gradshteyn, I. S. and I. M. Ryzhik (2014). *Table of Integrals, Series, and Products* (Eight ed.). Academic Press.

Greco, F. and R. C. Ball (1997). Shear-band formation in a non-Newtonian fluid model with a constitutive instability. *Journal of Non-Newtonian Fluid Mechanics 69*(2), 195–206.

Grmela, M. (1993, Jan). Weakly nonlocal hydrodynamics. *Phys. Rev. E 47*, 351–365.

Grmela, M. (2010). Why GENERIC? *J. Non-Newton. Fluid Mech. 165*(17-18), 980–986. Proceedings of the 5th International Workshop on Non-Equilibrium Thermodynamics IWNET 2009.

Grmela, M. (2012). Fluctuations in extended mass-action-law dynamics. *Physica D: Nonlinear Phenomena 241*(10), 976–986.

Grmela, M. (2017). Externally driven macroscopic systems: Dynamics versus thermodynamics. *J. Stat. Phys. 166*(2), 282–316.

Grmela, M., F. Chinesta, and A. Ammar (2010, May). Mesoscopic tube model of fluids composed of worm-like micelles. *Rheologica Acta 49*(5), 495–506.

Grmela, M., D. Jou, J. Casas-Vazquez, M. Bousmina, and G. Lebon (2004). Ensemble averaging in turbulence modelling. *Physics Letters A 330*(1), 54–64.

Grmela, M., V. Klika, and M. Pavelka (2015, Sep). Reductions and extensions in mesoscopic dynamics. *Phys. Rev. E 92*, 032111.

Grmela, M. and H. C. Öttinger (1997). Dynamics and thermodynamics of complex fluids. I. Development of a general formalism. *Phys. Rev. E 56*(6), 6620–6632.

Grob, M., C. Heussinger, and A. Zippelius (2014, May). Jamming of frictional particles: A nonequilibrium first-order phase transition. *Phys. Rev. E 89*, 050201.

Grosch, C. and H. Salwen (1968). The stability of steady and time-dependent plane Poiseuille flow. *J. Fluid Mech. 34*, 177–205.

Hardy, G., J. Littlewood, and G. Pólya (1952). *Inequalities* (Second ed.). Cambridge University Press.

Haupt, P. (2000). *Continuum mechanics and theory of materials*. Advanced Texts in Physics. Springer-Verlag, Berlin. Translated from the German by Joan A. Kurth.

Hébraud, P. (2009). Normal and tangential stress fluctuations during jamming. *Rheologica Acta 48*(8), 845–853.

Herschel, W. H. and R. Bulkley (1926, August). Konsistenzmessungen von Gummi-Benzollösungen. *Colloid Polym. Sci. 39*(4), 291–300.

Hinch, E. J. (1974). Mechanical models of dilute polymer solutions for strong flows with large polymer deformations. In *Colloques Internationaux du CNRS*, Volume 233 of *Polymères et Lubrification*, CNRS, Paris, pp. 241.

Hinch, E. J. (1977). Mechanical models of dilute polymer solutions in strong flows. *Phys. Fluids 20*(10), S22–S30.

Høiland, E. (1953). On two-dimensional perturbation of linear flow. *Geofys. Publ. 18*(9), 3–12.

Holmes, C. B., M. E. Cates, M. Fuchs, and P. Sollich (2005). Glass transitions and shear thickening suspension rheology. *J. Rheol. 49*(1), 237–269.

Horgan, C. O. (1995). Korn's inequalities and their applications in continuum mechanics. *SIAM Rev. 37*(4), 491–511.

Howard, L. N. (1961). Note on a paper of John W. Miles. *Journal of Fluid Mechanics 10*(4), 509–512.

Hron, J., J. Málek, J. Stebel, and K. Touška (2017). A novel view on computations of steady flows of Bingham fluids using implicit constitutive relations. Journal of Non-Newtonian Fluid Mechanics (submitted).

Hu, Y. T., P. Boltenhagen, and D. J. Pine (1998). Shear thickening in low-concentration solutions of wormlike micelles. I. Direct visualization of transient behavior and phase transitions. *J. Rheol. 42*, 1185–1208.

Huang, W. and D. M. Sloan (1994). The pseudospectral method for solving differential eigenvalue problems. *Journal of Computational Physics 111*(2), 399–409.

Hutter, K. and K. Jöhnk (2004). *Continuum methods of physical modeling*. Berlin: Springer-Verlag.

Hütter, M. and B. Svendsen (2013, Nov). Quasi-linear versus potential-based formulations of force–flux relations and the GENERIC for irreversible processes: comparisons and examples. *Continuum Mechanics and Thermodynamics 25*(6), 803–816.

Janečka, A., J. Málek, V. Průša, and G. Tierra (2018). Numerical scheme for simulation of transient flows of non-Newtonian fluids characterised by a non-monotone relation between the symmetric part of the velocity gradient and the Cauchy stress tensor. In preparation.

Janečka, A. and M. Pavelka (2018a). Gradient dynamics and entropy production maximization. *J. Non-Equilib. Thermodyn. 43*(1), 1–19.

Janečka, A. and M. Pavelka (2018b). Non-convex dissipation potentials in multiscale non-equilibrium thermodynamics. *Continuum Mech. Therm.* (online).

Janečka, A. and V. Průša (2015). Perspectives on using implicit type constitutive relations in the modelling of the behaviour of non-newtonian fluids. *AIP Conference Proceedings 1662*, –.

Janečka, A., V. Průša, and K. R. Rajagopal (2016). Euler–Bernoulli type beam theory for elastic bodies with nonlinear response in the small strain range. *Arch. Mech. 68*, 3–25.

Johnson, M. W. and D. Segalman (1977). A model for viscoelastic fluid behavior which allows non-affine deformation. *J. Non-Newton. Fluid Mech. 2*(3), 255–270.

Joseph, D. D. (1968, 9). Eigenvalue bounds for the Orr–Sommerfeld equation. *Journal of Fluid Mechanics 33*, 617–621.

Jou, D., J. Casas-Vázquez, and G. Lebon (2010). *Extended Irreversible Thermodynamics* (4th ed.). Springer Netherlands.

Junker, P., J. Makowski, and K. Hackl (2014, May). The principle of the minimum of the dissipation potential for non-isothermal processes. *Continuum Mechanics and Thermodynamics 26*(3), 259–268.

Kampé de Fériet, J. (1949). Sur la decroissance de l'énergie cinétique d'un fluide visqueux incompressible occupant un domaine borné ayant pour frontière des parois solides fixes. *Ann. Soc. Sci. Bruxelles 63*, 35–46.

Kannan, K. and K. R. Rajagopal (2011). A thermodynamical framework for chemically reacting systems. *Z. angew. Math. Phys. 62*(2), 331–363.

Kröger, M. and M. Hütter (2010). Automated symbolic calculations in nonequilibrium thermodynamics. *Computer Physics Communications 181*(12), 2149–2157.

Kubin, L. P. and J.-P. Poirier (1988). Relaxation oscillations and stick-slip of materials. *Solid State Phenomena 3–4*, 473–481.

Kulvait, V., J. Málek, and K. R. Rajagopal (2013). Anti-plane stress state of a plate with a V-notch for a new class of elastic solids. *Int. J. Frac. 179*(1–2), 59–73.

Landau, L. D. and E. M. Lifshitz (1968). *Course of theoretical physics. Vol. 5: Statistical physics*. Translated from the Russian by J. B. Sykes and M. J. Kearsley. Second revised and enlarged edition. Oxford: Pergamon Press.

Laun, H. M. (1994). Normal stresses in extremely shear thickening polymer dispersions. *J. Non-Newton. Fluid Mech. 54*, 87–108.

Le Roux, C. and K. R. Rajagopal (2013). Shear flows of a new class of power-law fluids. *Appl. Math. 58*(2), 153–177.

Lerouge, S., M. Argentina, and J. P. Decruppe (2006, Feb). Interface instability in shear-banding flow. *Phys. Rev. Lett. 96*, 088301.

Lin, C. C. (1955). *The Theory of Hydrodynamic Stability*. Cambridge monographs on mechanics and applied mathematics. Cambridge [Eng.]: University Press.

Lindsay, K. A. and R. R. Ogden (1992). A practical implementation of spectral methods resistant to the generation of spurious eigenvalues. *International Journal for Numerical Methods in Fluids 15*(11), 1277–1294.

Logg, A., K.-A. Mardal, G. N. Wells, et al. (2012). *Automated Solution of Differential Equations by the Finite Element Method*. Springer.

López-Aguilar, J. E., M. F. Webster, H. R. Tamaddon-Jahromi, and O. Manero (2014). A new constitutive model for worm-like micellar systems – Numerical simulation of confined contraction–expansion flows. *Journal of Non-Newtonian Fluid Mechanics 204*, 7–21.

Mack, L. M. (1976). A numerical study of the temporal eigenvalue spectrum of the Blasius boundary layer. *Journal of Fluid Mechanics 73*(3), 497–520.

Málek, J. and V. Průša (2017). Derivation of equations for continuum mechanics and thermodynamics of fluids. In Y. Giga and A. Novotný (Eds.), *Handbook of Mathematical Analysis in Mechanics of Viscous Fluids*, pp. 1–70. Springer.

Málek, J., V. Průša, and K. R. Rajagopal (2010). Generalizations of the Navier–Stokes fluid from a new perspective. *Int. J. Eng. Sci. 48*(12), 1907–1924.

Málek, J., K. R. Rajagopal, and K. Tůma (2015). A thermodynamically compatible model for describing the response of asphalt binders. *Int. J. Pavement Eng. 16*(4), 297–314.

Maragos, P. (1995, Apr). Slope transforms: theory and application to nonlinear signal processing. *IEEE Transactions on Signal Processing 43*(4), 864–877.

Matolcsi, T. (1992). Dynamical laws in thermodynamics. *Physics Essays 5*(3), 320–327.

Mielke, A. (2003, Aug). Energetic formulation of multiplicative elasto-plasticity using dissipation distances. *Continuum Mechanics and Thermodynamics 15*(4), 351–382.

Mielke, A., D. R. M. Renger, and M. A. Peletier (2016). A generalization of Onsager's reciprocity relations to gradient flows with nonlinear mobility. *Journal of Non-Equilibrium Thermodynamics 41*(2), 141–149.

Müller, I. (1985). *Thermodynamics*. Interaction of Mechanics and Mathematics. London: Pitman Publishing Limited.

Narayan, S. P. A. and K. R. Rajagopal (2013). Unsteady flows of a class of novel generalizations of the Navier–Stokes fluid. *Appl. Math. Comput. 219*(19), 9935–9946.

Nečas, J. (2012). *Direct Methods in the Theory of Elliptic Equations*. Springer Monographs in Mathematics. Springer–Verlag Berlin Heidelberg.

Nukiyama, S. (1934). The maximum and minimum values of the heat Q transmitted from metal to boiling water under atmospheric pressure. *Journal Japan Soc. Mech. Engrs. 37*, 367–374. Translation: *International Journal of Heat and Mass Transfer 9*(12), pp. 1419–1433, 1966.

Oldroyd, J. G. (1947). A rational formulation of the equations of plastic flow for a Bingham solid. *Math. Proc. Camb. Philos. Soc. 43*(01), 100–105.

Oldroyd, J. G. (1950). On the formulation of rheological equations of state. *Proc. R. Soc. A-Math. Phys. Eng. Sci. 200*(1063), 523–541.

Olmsted, P. D. (2008). Perspectives on shear banding in complex fluids. *Rheol. Acta 47*(3), 283–300.

Olmsted, P. D., O. Radulescu, and C.-Y. D. Lu (2000). Johnson–Segalman model with a diffusion term in cylindrical Couette flow. *J. Rheol. 44*(2), 257–275.

Onsager, L. (1931a, FEB). Reciprocal relations in irreversible processes I. *Phys. Rev. 37*(4), 405–426.

Onsager, L. (1931b, DEC). Reciprocal relations in irreversible processes II. *Phys. Rev. 38*(12), 2265–2279.

Orr, W. (1907a). The stability or instability of the steady motions of a perfect liquid and of a viscous liquid. Part I: A perfect liquid. *Proceedings of the Royal Irish Academy. Section A: Mathematical and Physical Sciences 27*, 9–68.

Orr, W. (1907b). The stability or instability of the steady motions of a perfect liquid and of a viscous liquid. Part II: A viscous liquid. *Proceedings of the Royal Irish Academy. Section A: Mathematical and Physical Sciences 27*, 69–138.

Orszag, S. A. (1971). Accurate solution of the Orr-Sommerfeld stability equation. *J. Fluid Mech. 50*, 689–703.

Ostwald, W. (1925). Über die Geschwindigkeitsfunktion der Viskosität disperser Systeme. I. *Colloid Polym. Sci. 36*, 99–117.

Öttinger, H. C. (2005). *Beyond equilibrium thermodynamics*. Hoboken, New Jersey: John Wiley & Sons.

Öttinger, H. C. and M. Grmela (1997, Dec). Dynamics and thermodynamics of complex fluids. II. Illustrations of a general formalism. *Phys. Rev. E 56*(6), 6633–6655.

Pavelka, M. and M. Grmela (2016). Braun-Le Chatelier principle in dissipative thermodynamics. Submitted.

Pavelka, M., V. Klika, O. Esen, and M. Grmela (2016). A hierarchy of Poisson brackets in non-equilibrium thermodynamics. *Physica D: Nonlinear Phenomena 335*(Supplement C), 54–69.

Pavelka, M., V. Klika, and M. Grmela (2014, Dec). Time reversal in nonequilibrium thermodynamics. *Phys. Rev. E 90*, 062131.

Perlácová, T. and V. Průša (2015). Tensorial implicit constitutive relations in mechanics of incompressible non-Newtonian fluids. *J. Non-Newton. Fluid Mech. 216*, 13–21.

Prakash, J. R. (2009). Micro and macro in the dynamics of dilute polymer solutions: Convergence of theory with experiment. *Korea-Australia Rheology Journal 21*(4), 245–268.

Průša, V. and K. R. Rajagopal (2012). On implicit constitutive relations for materials with fading memory. *J. Non-Newton. Fluid Mech. 181–182*, 22–29.

Radulescu, O., P. D. Olmsted, and C.-Y. D. Lu (1999, Dec). Shear banding in reaction-diffusion models. *Rheologica Acta 38*(6), 606–613.

Rajabian, M., C. Dubois, and M. Grmela (2005, Jul). Suspensions of semi-flexible fibers in polymeric fluids: Rheology and thermodynamics. *Rheologica Acta 44*(5), 521–535.

Rajagopal, K. (2013). On the nonlinear elastic response of bodies in the small strain range. *Acta Mech.*, 1–9.

Rajagopal, K. R. (2003). On implicit constitutive theories. *Appl. Math. 48*(4), 279–319.

Rajagopal, K. R. (2006). On implicit constitutive theories for fluids. *J. Fluid Mech. 550*, 243–249.

Rajagopal, K. R. (2010). On a new class of models in elasticity. *Mathematical and Computational Applications 15*(4).

Rajagopal, K. R. (2015). Remarks on the notion of "pressure". *Int. J. Non-Linear Mech. 71*(0), 165–172.

Rajagopal, K. R. and A. R. Srinivasa (2000). A thermodynamic frame work for rate type fluid models. *J. Non-Newton. Fluid Mech. 88*(3), 207–227.

Rajagopal, K. R. and A. R. Srinivasa (2004). On thermomechanical restrictions of continua. *Proc. R. Soc. Lond., Ser. A, Math. Phys. Eng. Sci. 460*(2042), 631–651.

Rajagopal, K. R. and A. R. Srinivasa (2008). On the thermodynamics of fluids defined by implicit constitutive relations. *Z. angew. Math. Phys. 59*(4), 715–729.

Rajagopal, K. R. and A. R. Srinivasa (2011). A Gibbs-potential-based formulation for obtaining the response functions for a class of viscoelastic materials. *Proc. R. Soc. A-Math. Phys. Eng. Sci. 467*(2125), 39–58.

Rayleigh, L. (1879). On the stability, or instability, of certain fluid motions. *Proceedings of the London Mathematical Society 11*(1), 57–72.

Rayleigh, L. (1887). On the stability or instability of certain fluid motions, ii. *Proceedings of the London Mathematical Society 19*(1), 67–75.

Reynolds, O. (1883). An experimental investigation of the circumstances which determine whether the motion of water shall be direct or sinuous, and of the law of resistance in parallel channels. *Proc. R. Soc. Lond. 25*, 84–99.

Reynolds, O. (1895). On the dynamical theory of incompressible viscous fluids and the determination of the criterion. *Philos. Trans. R. Soc. 186*, 123–164.

Roubíček, T. (2005). *Nonlinear Partial Differential Equations with Applications*. Birkhäuser.

Rummler, B. (1997). The eigenfunctions of the Stokes operator in special domains. *Z. angew. Math. Mech. 77*(8), 619–627.

Salwen, H. and C. E. Grosch (1972). The stability of Poiseuille flow in a pipe of circular cross section. *J. Fluid Mech. 54*, 93–112.

Sarti, G. and G. Marrucci (1973). Thermomechanics of dilute polymer solutions: multiple bead-spring model. *Chemical Engineering Science 28*(4), 1053–1059.

Schmid, P. J. and D. S. Henningson (2001). *Stability and transition in shear flows*. Number 142 in Applied Mathematical Sciences. New York: Springer.

Schmitt, V., C. M. Marques, and F. Lequeux (1995, Oct). Shear-induced phase separation of complex fluids: The role of flow-concentration coupling. *Phys. Rev. E 52*, 4009–4015.

Schroeder, C. M., H. P. Babcock, E. S. G. Shaqfeh, and S. Chu (2003). Observation of polymer conformation hysteresis in extensional flow. *Science 301*(5639), 1515–1519.

Serrin, J. (1959). On the stability of viscous fluid motions. *Arch. Ration. Mech. Anal. 3*, 1–13.

Sneddon, I. N. (1946). III. Finite Hankel transforms. *The London, Edinburgh, and Dublin Philosophical Magazine and Journal of Science 37*(264), 17–25.

Sommerfeld, A. (1908). Ein beitrag zur hydrodynamischen erklärung der turbulenten flüssigkeitbewegungen. In *Atti. del 4. Congr. Inrnat. dei Mat. III*, pp. 116–124. Rome.

Spencer, A. J. M. (1971). Theory of invariants. In A. C. Eringen (Ed.), *Continuum Physics*, Volume I, pp. 239–353. New York: Academic Press.

Squire, H. B. (1933). On the stability of three dimensional disturbances of viscous fluid between parallel walls. *Proc. Roy. Soc. Lond. Ser. A 142*, 621–628.

Sridhar, T., D. A. Nguyen, R. Prabhakar, and J. R. Prakash (2007, Apr). Rheological observation of glassy dynamics of dilute polymer solutions near the coil-stretch transition in elongational flows. *Phys. Rev. Lett. 98*, 167801.

Srinivasan, S. and S. Karra (2015). Flow of "stress power-law" fluids between parallel rotating discs with distinct axes. *Int. J. Non-Linear Mech. 74*, 73–83.

Stebel, J. (2016). Finite element approximation of Stokes-like systems with implicit constitutive relation. In A. Handlovičová, Z. Minarechova, and D. Ševčovič (Eds.), *Proceedings of the Conference ALGORITMY*, Bratislava,

pp. 291–300. Publishing House of Slovak University of Technology. 19th Conference on Scientific Computing, Vysoké Tatry - Podbanské, Slovakia, September 9 - 14, 2012.

Stosic, Z. V. (2005, September). On the frontier of boiling curve and beyond design of its origin. In B. Mavko and I. Kljenak (Eds.), *Nuclear Energy for New Europe 2005*, Bled, Slovenia. Nuclear Society of Slovenia.

Süli, E. and T. Tscherpel (2018, April). Fully discrete finite element approximation of unsteady flows of implicitly constituted incompressible fluids. *ArXiv e-prints*.

Synge, J. L. (1938). Hydrodynamical stability. *Semicentenn. Publ. Amer. Math. Soc 2*, 227–269.

Tanner, R. and K. Walters (1998). *Rheology: an historical perspective*, Volume 7 of *Rheology Series*. Amsterdam: Elsevier.

Tanner, R. I. (1975). Stresses in dilute-solutions of bead-nonlinear-spring macromolecules. 3. Friction coefficient varying with dumbbell extension. *Trans. Soc. Rheol. 19*(4), 557–582.

The MathWorks, Inc. (2014). MATLAB R2014a (8.3.0.532). Natick, Massachusetts, United States.

Tranter, C. J. (1951). *Integral Transforms in Mathematical Physics*. New York: John Wiley and Sons.

Trefethen, L. N. (2000). *Spectral methods in MATLAB*, Volume 10 of *Software, Environments, and Tools*. Philadelphia, PA: Society for Industrial and Applied Mathematics (SIAM).

Trefethen, L. N., A. E. Trefethen, S. C. Reddy, and T. A. Driscoll (1993, July). Hydrodynamic stability without eigenvalues. *Science 261*(5121), 578–584.

Truesdell, C. and W. Noll (1965). The non-linear field theories of mechanics. In S. Flüge (Ed.), *Handbuch der Physik*, Volume III/3. Berlin: Springer.

Truesdell, C. and W. Noll (2004). *The non-linear field theories of mechanics* (3rd ed.). Berlin: Springer.

Verhás, J. (1997). *Thermodynamics and Rheology*. Fluid Mechanics and Its Applications. Springer Netherlands.

Waldram, J. (1985). *The Theory of Thermodynamics*. Cambridge University Press.

Weideman, J. A. and S. C. Reddy (2000). A MATLAB differentiation matrix suite. *ACM Trans. Math. Softw. 26*(4), 465–519.

Yerushalmi, J., S. Katz, and R. Shinnar (1970). The stability of steady shear flows of some viscoelastic fluids. *Chemical Engineering Science 25*(12), 1891–1902.

Yih, C.-S. (1967). Instability due to viscosity stratification. *J. Fluid Mech. 27*, 337–352.

Yuan, X.-F. (1999). Dynamics of a mechanical interface in shear-banded flow. *Europhys. Lett. 46*(4), 542–548.

Zia, R. K. P., E. F. Redish, and S. R. McKay (2009). Making sense of the Legendre transform. *American Journal of Physics 77*(7), 614–622.

A. Generalizations of the Legendre transformation

For a smooth, strictly convex (with positive second derivative) real function $f(x)$, the *Legendre transform*, see Callen (1985), is defined as

$$f_L^*(u) =_{\text{def}} f(x) - ux, \tag{A.1}$$

where x satisfies $f'(x) = u$. Since the function f is strictly convex, its derivative is monotonic and thus invertible, i.e., $x = (f')^{-1}(u)$. Then we can write

$$f_L^*(u) = f\left[(f')^{-1}(u)\right] - u\,(f')^{-1}(u). \tag{A.2}$$

The Legendre transform of a convex function is concave which can be immediately seen from

$$\frac{\mathrm{d}f_L^*}{\mathrm{d}u} = \frac{\mathrm{d}f}{\mathrm{d}x}\frac{\mathrm{d}x}{\mathrm{d}u} - x - u\frac{\mathrm{d}x}{\mathrm{d}u} = -x, \qquad \text{and} \qquad \frac{\mathrm{d}^2 f_L^*}{\mathrm{d}u^2} = -\frac{\mathrm{d}x}{\mathrm{d}u} = -\left(\frac{\mathrm{d}^2 f}{\mathrm{d}x^2}\right)^{-1}. \tag{A.3}$$

Zia et al. (2009) advocated for a definition with the opposite sign

$$f_L^*(u) =_{\text{def}} ux - f(x), \tag{A.4}$$

which is a symmetric representation of the Legendre transform, $f_L^*(u) + f(x) = ux$, and converses convexity. Both versions are invertible and the biconjugate is the original function $f^{**} = f$. In the second version, the formula for the inverse transform is identical to the primal transform.

The generalization of the Legendre transform to arbitrary functions is the *Fenchel transform* (also called the Fenchel–Legendre transform or the Young–Fenchel conjugate)

$$f_F^*(u) =_{\text{def}} \sup_x \left[ux - f(x)\right]. \tag{A.5}$$

The Fenchel transform is not invertible, the inversion of the conjugate yields the convex hull of the original function

$$f_F^{**}(x) = \left(\overline{\text{conv}} f\right)(x) \le f(x), \tag{A.6}$$

thus some information is lost in the process.

The Fenchel transform can be defined in the same manner for functionals, see Bauschke and Lucet (2012); Roubíček (2005). Let V be a real Hilbert space and $f : V \to \mathbb{R}$, then the Fenchel transform f_F^* at $u \in V^*$ is

$$f_F^*(u) =_{\text{def}} \sup_{v \in V} \left[\langle u, v\rangle - f(v)\right], \tag{A.7}$$

where $\langle \bullet, \bullet \rangle$ is the corresponding inner product. The conjugate f_F^* is always convex and lower semicontinuous and $f_F^{**} = f$ if and only if f is convex and lower semicontinuous.

For arbitrary differentiable functions, Dorst and Van den Boomgaard (1993, 1994) introduced the invertible multivalued *slope transform*

$$f_S^*(u) =_{\text{def}} \text{stat}_x \left[ux - f(x)\right], \tag{A.8}$$

where $\operatorname{stat}_x f(x)$ is the set of all stationary values of $f(x)$ with respect to x

$$\operatorname{stat}_x f(x) =_{\text{def}} \{f(x) : f'(x) = 0\}. \tag{A.9}$$

Then, the inverse slope transform is

$$f(x) =_{\text{def}} \operatorname{stat}_u [ux - f_S^*(u)]. \tag{A.10}$$

In Chapter 3, we use this general definition of the Legendre-like conjugation for it is invertible and no information is lost. For functions with consecutively variating convex and concave parts, each with an invertible derivative (as in our case), the slope transform corresponds to application of the classical Legendre transform to each part. Then, the number of different functions in the multivalued Legendre transform agrees to the number of convex/concave parts of the original function, see Maragos (1995). For functionals in general, we believe that the slope transform should be invertible as well, unfortunately we could not find any relevant mathematical reference.

B. Code for linearized hydrodynamic stabilty calculation

```
function generalized_orr_sommerfeld(N, alpha, R1, R3, n, C)

%
%  Computes the eigenvalues of the generalized Orr-Sommerfeld
%  equation using NxN Chebyshev differentiation matrices.
%
%  INPUT
%  N     - number of collocation points
%  alpha - streamwise wave number
%  R1    - Reynolds number analoque
%  R3    - material parameter
%  n     - material parameter
%  C     - dimensionless pressure gradient
%

close all;

% Load the package by Weideman, Reddy (2000)
addpath('./dmsuite');

%% Differentation matrices

% Get collocation points and derivative (sub)matrices
[y, D] = chebdif(N, 2);
D1 = D(:, :, 1);
D2 = D(:, :, 2);

D1bar = D1(:, 2:end-1);
D2bar = D2(:, 2:end-1);

D1hat = D1(2:end-1, :);
D2hat = D2(2:end-1, :);

D2tilde = D2(2:end-1, 2:end-1);

% Identity matrix and its submatrices
I      = eye(N);
Ibar   = I(:, 2:end-1);
Ihat   = I(2:end-1, :);
Itilde = I(2:end-1, 2:end-1);

%% Le Roux--Rajagopal constitutive relation

T  = C*y;
s  = 2*C^2*y.^2;

f    = diag((1 + s).^n + R3);
dfds = diag(n*(1 + s).^(n-1));


```

```
% Base flow velocity
switch n
    case -1
        V = diag(1/(2*C)*log((1+2*C^2*y.^2)/(1+2*C^2)) + ...
            C*R3*(y.^2-1));
    otherwise
        V = diag(1/(2*C*(n+1))*((1+2*C^2*y.^2).^(n+1) - ...
            (1+2*C^2)^(n+1)) + C*R3*(y.^2 - 1));
end

ddVddy = diag(2*C*(1 + 2*C^2*y.^2).^(n-1).*(1 + ...
    2*(1+2*n)*C^2*y.^2) + 2*C*R3);

%% Set up A and B matrices

A11 = 1i*alpha*(V(2:end-1, 2:end-1)*(D2tilde-alpha^2*Itilde) - ...
    ddVddy(2:end-1, 2:end-1));
A12 = 2*alpha^2*D1hat/R1;
A13 = 1i*alpha*(D2hat + alpha^2*Ihat)/R1;

A21 = D1bar;
A22 = [zeros(1, N); -f(2:end-1, :); zeros(1, N)];
A23 = zeros(N);

A31 = 1i/(2*alpha)*(D2bar + alpha^2*Ibar);
A32 = zeros(N);
A33 = -(f + 4*diag(T.^2)*dfds);

A = [A11 A12 A13; ...
    A21 A22 A23; ...
    A31 A32 A33];

B = [1i*(D2tilde - alpha^2*Itilde) zeros(N-2, N) zeros(N-2, N); ...
    zeros(N, N-2) zeros(N) zeros(N); ...
    zeros(N, N-2) zeros(N) zeros(N)];

%% Compute eigenvalues

[~, e] = eig(A, B);
e = diag(e);
e = e./alpha;

%% Plot the eigenvalues

figure(1), plot(e, 'k.', 'MarkerSize', 12);
set(1, 'Name', 'Eigenvalues', 'NumberTitle', 'Off');
title(['N = ' int2str(N) '      max\{Im(\omega)\} = ' ...
    num2str(max(imag(e).*isfinite(imag(e))), '%16.12f')], ...
    'FontSize', 12);
xlabel('Re', 'FontSize', 12);
ylabel('Im', 'FontSize', 12);
axis([0 1 -1 0]);
grid on, axis square;

%% Find and print the eigenvalue with the largest imaginary part

[~, l] = max(imag(e).*isfinite(imag(e)));
```

```
fprintf('\nEigenvalue with largest imaginary part (most unstable ...
    mode): %12.10f %12.10fi\n\n', real(e(l)), imag(e(l)));

%% List the k least stable modes

k = 33;

finite_e = e(isfinite(e));
[~, sort_index] = sort(imag(finite_e), 'descend');
fprintf('Least stable eigenvalues:\n\n');
fprintf('%i\t %12.8f %12.8fi\n', [(1:k)' ...
    real(finite_e(sort_index(1:k))) ...
    imag(finite_e(sort_index(1:k)))]');

end
```

Listing B.1: MATLAB® script, file `generalized_orr_sommerfeld.m`.

C. Polar coordinates

The relation between the Cartesian coordinates $[x, y]$ in the standard two-dimensional Euclidean space $\mathbb{R}^2$ and the polar coordinates $[r, \varphi]$ of a point $\boldsymbol{x} \in \mathbb{R}^2$ is given by

$$x = r\cos\varphi, \qquad y = r\sin\varphi, \tag{C.1}$$

where $r > 0$ is the radial and $\varphi \in [0, 2\pi)$ the angular coordinate. The local curvilinear covariant basis $\{\boldsymbol{g}_i\}_{i=1}^2$ is given by

$$\boldsymbol{g}_i =_{\text{def}} \frac{\partial x^j}{\partial \xi^i}\boldsymbol{e}_j, \tag{C.2}$$

where $\boldsymbol{x} = [x^1, x^2] = [x, y]$ and $\boldsymbol{\xi} = [\xi^1, \xi^2] = [r, \varphi]$, and we have

$$\boldsymbol{g}_r = \begin{bmatrix}\cos\varphi \\ \sin\varphi\end{bmatrix}, \qquad \boldsymbol{g}_\varphi = \begin{bmatrix}-r\sin\varphi \\ r\cos\varphi\end{bmatrix}. \tag{C.3}$$

From $\|\boldsymbol{g}_r\| = 1$ and $\|\boldsymbol{g}_\varphi\| = r$, we can introduce the normed basis

$$\boldsymbol{g}_{\hat{r}} =_{\text{def}} \frac{\boldsymbol{g}_r}{\|\boldsymbol{g}_r\|} = \begin{bmatrix}\cos\varphi \\ \sin\varphi\end{bmatrix}, \qquad \boldsymbol{g}_{\hat{\varphi}} =_{\text{def}} \frac{\boldsymbol{g}_\varphi}{\|\boldsymbol{g}_\varphi\|} = \begin{bmatrix}-\sin\varphi \\ \cos\varphi\end{bmatrix}. \tag{C.4}$$

We can also define the dual contravariant basis $\{\boldsymbol{g}^i\}_{i=1}^2$ as

$$\boldsymbol{g}^i =_{\text{def}} \frac{\partial \xi^i}{\partial x^j}\boldsymbol{e}^j. \tag{C.5}$$

From the inverse relation between the Cartesian and polar coordinates

$$r = \sqrt{x^2 + y^2}, \qquad \varphi = \arctan\left(\frac{y}{x}\right), \tag{C.6}$$

we get the contravariant base vectors

$$\boldsymbol{g}^r = \begin{bmatrix}\cos\varphi \\ \sin\varphi\end{bmatrix}, \qquad \boldsymbol{g}^\varphi = \begin{bmatrix}-\frac{1}{r}\sin\varphi \\ \frac{1}{r}\cos\varphi\end{bmatrix}. \tag{C.7}$$

Again, we can normalize the basis with $\|\boldsymbol{g}^r\| = 1$ and $\|\boldsymbol{g}^\varphi\| = \frac{1}{r}$

$$\boldsymbol{g}^{\hat{r}} =_{\text{def}} \frac{\boldsymbol{g}^r}{\|\boldsymbol{g}^r\|} = \begin{bmatrix}\cos\varphi \\ \sin\varphi\end{bmatrix}, \qquad \boldsymbol{g}^{\hat{\varphi}} =_{\text{def}} \frac{\boldsymbol{g}^\varphi}{\|\boldsymbol{g}^\varphi\|} = \begin{bmatrix}-\sin\varphi \\ \cos\varphi\end{bmatrix}, \tag{C.8}$$

and the normed covariant and contravariant bases coincide, i.e., $\boldsymbol{g}_{\hat{r}} = \boldsymbol{g}^{\hat{r}}$ and $\boldsymbol{g}_{\hat{\varphi}} = \boldsymbol{g}^{\hat{\varphi}}$.

We can also express the Cartesian basis in terms of the normed polar basis as

$$\boldsymbol{e}_{\hat{x}} = \frac{1}{\sqrt{x^2 + y^2}}\left(x\boldsymbol{g}_{\hat{r}} - y\boldsymbol{g}_{\hat{\varphi}}\right), \qquad \boldsymbol{e}_{\hat{y}} = \frac{1}{\sqrt{x^2 + y^2}}\left(y\boldsymbol{g}_{\hat{r}} + x\boldsymbol{g}_{\hat{\varphi}}\right). \tag{C.9}$$

Since we know all the basis transformation rules, it is now easy to derive the relations between vector and tensor components in each coordinate system. In the polar coordinate system, a vector $\boldsymbol{v}$ is written in components as

$$\boldsymbol{v} = v^{\hat{r}}\boldsymbol{g}_{\hat{r}} + v^{\hat{\varphi}}\boldsymbol{g}_{\hat{\varphi}} = \left(v^{\hat{r}}\cos\varphi - v^{\hat{\varphi}}\sin\varphi\right)\boldsymbol{e}_{\hat{x}} + \left(v^{\hat{r}}\sin\varphi + v^{\hat{\varphi}}\cos\varphi\right)\boldsymbol{e}_{\hat{y}}, \tag{C.10}$$

from which we can immediately see the relations for the Cartesian components

$$v^{\hat{x}} = \frac{1}{\sqrt{x^2+y^2}}\left(v^{\hat{r}}x - v^{\hat{\varphi}}y\right), \qquad v^{\hat{y}} = \frac{1}{\sqrt{x^2+y^2}}\left(v^{\hat{r}}y + v^{\hat{\varphi}}x\right). \tag{C.11}$$

We can proceed in the same way for a tensor $\mathbb{T}$. As we only need to know the expression in Cartesian coordinates for the $\hat{\varphi}\hat{r}$-component (since it figures in the definition of torque in Chapter 5), we derive only this one

$$\mathbb{T} = \mathrm{T}^{\hat{x}}{}_{\hat{x}}\boldsymbol{e}_{\hat{x}} \otimes \boldsymbol{e}^{\hat{x}} + \mathrm{T}^{\hat{x}}{}_{\hat{y}}\boldsymbol{e}_{\hat{x}} \otimes \boldsymbol{e}^{\hat{y}} + \mathrm{T}^{\hat{y}}{}_{\hat{x}}\boldsymbol{e}_{\hat{y}} \otimes \boldsymbol{e}^{\hat{x}} + \mathrm{T}^{\hat{y}}{}_{\hat{y}}\boldsymbol{e}_{\hat{y}} \otimes \boldsymbol{e}^{\hat{y}} \tag{C.12}$$

$$= \frac{1}{x^2+y^2}\left[\left(\mathrm{T}^{\hat{y}}{}_{\hat{y}} - \mathrm{T}^{\hat{x}}{}_{\hat{x}}\right)xy + \mathrm{T}^{\hat{x}}{}_{\hat{y}}x^2 - \mathrm{T}^{\hat{y}}{}_{\hat{x}}y^2\right]\boldsymbol{g}_{\hat{\varphi}} \otimes \boldsymbol{g}^{\hat{r}} + \text{other terms}. \tag{C.13}$$

If tensor $\mathbb{T}$ is symmetric, i.e., $\mathrm{T}^{\hat{x}}{}_{\hat{y}} = \mathrm{T}^{\hat{y}}{}_{\hat{x}}$, the corresponding component is expressed in Cartesian coordinates as

$$\mathrm{T}^{\hat{\varphi}}{}_{\hat{r}} = \frac{1}{x^2+y^2}\left[\left(\mathrm{T}^{\hat{y}}{}_{\hat{y}} - \mathrm{T}^{\hat{x}}{}_{\hat{x}}\right)xy + \mathrm{T}^{\hat{x}}{}_{\hat{y}}\left(x^2-y^2\right)\right]. \tag{C.14}$$

Further, gradient of a vector field $\boldsymbol{v}$ is defined as

$$\nabla\boldsymbol{v} =_{\mathrm{def}} v^{\hat{i}}\Big|_{\hat{j}}\,\boldsymbol{g}_{\hat{i}} \otimes \boldsymbol{g}^{\hat{j}}, \tag{C.15}$$

where

$$v^{\hat{i}}\Big|_{\hat{j}} = \|\boldsymbol{g}_i\|\,\|\boldsymbol{g}^j\|\left[\frac{\partial}{\partial\xi^j}\left(\frac{v^{\hat{i}}}{\|\boldsymbol{g}_i\|}\right) + \Gamma^i{}_{jl}\frac{v^{\hat{l}}}{\|\boldsymbol{g}_l\|}\right], \tag{C.16}$$

is the physical (normed) covariant derivative of the i-th component with respect to the j-th coordinate and $\Gamma^i{}_{jl}$ are the Christoffel symbols given by

$$\Gamma^{\varphi}{}_{r\varphi} = \Gamma^{\varphi}{}_{\varphi r} = \frac{1}{r},$$
$$\Gamma^{r}{}_{\varphi\varphi} = -r.$$

If the vector field $\boldsymbol{v}$ has the specific form

$$\boldsymbol{v} = v^{\hat{\varphi}}(r)\boldsymbol{g}_{\hat{\varphi}}, \tag{C.17}$$

its gradient is given by

$$\nabla\boldsymbol{v} = \begin{bmatrix} 0 & -\frac{v^{\hat{\varphi}}}{r} \\ r\frac{\mathrm{d}}{\mathrm{d}r}\left(\frac{v^{\hat{\varphi}}}{r}\right) + \frac{v^{\hat{\varphi}}}{r} & 0 \end{bmatrix}, \tag{C.18}$$

and the symmetric part of the gradient of $\boldsymbol{v}$ is then

$$\mathbb{D} = \frac{1}{2}\begin{bmatrix} 0 & r\frac{\mathrm{d}}{\mathrm{d}r}\left(\frac{v^{\hat{\varphi}}}{r}\right) \\ r\frac{\mathrm{d}}{\mathrm{d}r}\left(\frac{v^{\hat{\varphi}}}{r}\right) & 0 \end{bmatrix}. \tag{C.19}$$

It can be also shown that the following holds

$$\operatorname{div} 2\mathbb{D} = \left\{\frac{\mathrm{d}}{\mathrm{d}r}\left[r\frac{\mathrm{d}}{\mathrm{d}r}\left(\frac{v^{\hat{\varphi}}}{r}\right)\right] + 2\frac{\mathrm{d}}{\mathrm{d}r}\left(\frac{v^{\hat{\varphi}}}{r}\right)\right\}\boldsymbol{g}_{\hat{\varphi}} = \left(\frac{\mathrm{d}^2v^{\hat{\varphi}}}{\mathrm{d}r^2} + \frac{1}{r}\frac{\mathrm{d}v^{\hat{\varphi}}}{\mathrm{d}r} - \frac{v^{\hat{\varphi}}}{r^2}\right)\boldsymbol{g}_{\hat{\varphi}}. \tag{C.20}$$

D. Code for Taylor–Couette flow

```
"""
Two-dimensional Taylor--Couette flow for incompressible
Le Roux--Rajagopal model

 du/dt + [grad(u)]u = div(T) + f
             div(u) = 0
                  D = f(T)
"""

from __future__ import print_function, division

from fenics import *
from math import hypot
import numpy as np
import matplotlib
matplotlib.use('pdf')
import matplotlib.pyplot as plt
plt.rcParams['font.size'] = 14
import os

from TaylorCouetteParam import ProblemParam

rank = MPI.rank(mpi_comm_world())
set_log_level(WARNING if rank==0 else WARNING+1)

parameters['form_compiler']['representation'] = 'uflacs'
parameters['form_compiler']['optimize'] = True

problem_name = 'taylor-couette-2d'

### Problem Parameters
param = ProblemParam()

r1, r2  = param.radii()
a       = param.a()
b       = param.b()
c       = param.c()
n       = param.n()
omega_0 = param.anglr_vlct()
dt      = param.dt()
T       = param.T()
t0      = param.t0()

### Mesh
(mesh, bndry_mrkrs) = param.mesh()
x  = SpatialCoordinate(mesh)
ds = Measure('ds', domain=mesh, subdomain_data=bndry_mrkrs)

### Function Spaces Definition
V  = VectorElement('P', mesh.ufl_cell(), 2)
P  = FiniteElement('P', mesh.ufl_cell(), 1)
TH = MixedElement([V, P])
W  = FunctionSpace(mesh, TH)
M  = FunctionSpace(mesh, 'DG', 0)

```

```
### Boundary Conditions
inner_vlct = DirichletBC(W.sub(0), Constant((0.0, 0.0)),
    bndry_mrkrs, 1)

anglr_vlct = 'omega_0*sin(pi*t/t0)'
bndry_vlct = Expression(('-{}*x[1]*(t<=t0)'.format(anglr_vlct),
    '{}*x[0]*(t<=t0)'.format(anglr_vlct)), omega_0=omega_0, t0=t0,
    t=0.0, degree=2)
outer_vlct = DirichletBC(W.sub(0), bndry_vlct, bndry_mrkrs, 2)

prssr_fix  = DirichletBC(W.sub(1), Constant(0.0), bndry_mrkrs, 2)

bcs = [inner_vlct, outer_vlct, prssr_fix]

'''
Weak formulation

 (u-u_n)/dt + inner([grad(u)]u, v)*dx + inner(T, grad(v))*dx =
     inner(f, v)*dx
                                                  q*div(u)*dx = 0
'''

### Steady Part of the Momentum Equation
def steady(u):
    return ( inner(grad(u)*u, v) - p*div(v) +
        inner(2.0*mu_l*sym(grad(u)), grad(v)) ) * dx

### Unknown and Test Functions
w  = Function(W)
(u, p) = split(w)

(v, q) = TestFunctions(W)

### Functions for Solutions at Previous Time Step
w_n = Function(W)
(u_n, _) = split(w_n)

mu_l = interpolate(Expression('1.0/(2.0*a)', a=a, degree=0), M)

w_l = Function(W)
(u_l, p_l) = w_l.split()

### Temporal Part of the Equation
theta = Constant(0.5)
F = (1.0/dt)*inner(u-u_n, v)*dx + (1-theta)*steady(u_n) +
    theta*steady(u) + q*div(u)*dx

### Problem Definition
J = derivative(F, w)
problem = NonlinearVariationalProblem(F, w, bcs, J)
solver  = NonlinearVariationalSolver(problem)

### Solver Parameters
prm = solver.parameters
prm['newton_solver']['absolute_tolerance'] = 1.0E-8
prm['newton_solver']['relative_tolerance'] = 1.0E-8
prm['newton_solver']['maximum_iterations'] = 20
prm['newton_solver']['error_on_nonconvergence'] = False
```

```
108
109 ### Create Files for Storing the Solution
110 if not os.path.exists('results/' + problem_name):
111     os.makedirs('results/' + problem_name)
112
113 ufile  = XDMFFile('results/{}/u.xdmf'.format(problem_name))
114 ufile.parameters['flush_output'] = True
115 ufile.parameters['rewrite_function_mesh'] = False
116
117 pfile  = XDMFFile('results/{}/p.xdmf'.format(problem_name))
118 pfile.parameters['flush_output'] = True
119 pfile.parameters['rewrite_function_mesh'] = False
120
121 mufile = XDMFFile('results/{}/mu.xdmf'.format(problem_name))
122 mufile.parameters['flush_output']= True
123 mufile.parameters['rewrite_function_mesh'] = False
124
125 if not os.path.exists('figures/' + problem_name):
126     os.makedirs('figures/' + problem_name)
127
128 tol = 1.0E-9
129 torque_series = [0] # 0 due to initial condition
130 t  = 0
131 it = 0
132 while t < T:
133     # Update Current Time
134     t +=  float(dt)
135     it += 1
136     begin(CRITICAL, 't = ' + str(t))
137
138     ### Update Boundary Condition
139     bndry_vlct.t = t
140
141     eta = 1.0
142     loc_it = 0
143     while eta > tol and loc_it < 200:
144         loc_it += 1
145
146         ### Solve the Nonlinear System
147         solver.solve()
148
149         ### Extract Solutions
150         (u, p) = w.split()
151
152         ### Update the Viscosity
153         mu = project(0.5 * pow(a * pow(1.0 + 4.0 * b * pow(mu_l,
                2.0) * inner(sym(grad(u)), sym(grad(u))), n) + c, -1.0),
                M)
154
155         ### Compute the Residual
156         eta = errornorm(p, p_l, degree_rise=0) + errornorm(u, u_l,
                degree_rise=0) + errornorm(mu, mu_l, degree_rise=0)
157         log(30, 'eta = ' + str(eta))
158         begin(30, 'Particular Terms:')
159         log(30, str(errornorm(p, p_l, degree_rise=0)))
160         log(30, str(errornorm(u, u_l, degree_rise=0)))
161         log(30, str(errornorm(mu, mu_l, degree_rise=0)))
162         end()
```

```
163
164         # Update the Functions
165         w_l.vector()[:]  = w.vector()
166         mu_l.vector()[:] = mu.vector()
167
168     ### Save the Solution
169     u.rename('u', 'velocity')
170     p.rename('p', 'pressure')
171     mu.rename('mu', 'viscosity')
172     ufile.write(u, t)
173     pfile.write(p, t)
174     mufile.write(mu, t)
175
176     ### Plot the Constitutive Curve with Computed Values
177     if (it % 200 == 0):
178         gradsym_norm_squared = project(inner(sym(grad(u)),
                sym(grad(u))), M)
179         gradsym_norm_loc =
                np.sqrt(gradsym_norm_squared.vector().get_local())
180         cstress_norm_loc = 2*np.multiply(mu.vector().get_local(),
                gradsym_norm_loc)
181
182         gradsym_len = len(gradsym_norm_loc)
183         cstress_len = len(cstress_norm_loc)
184         gradsym_counts =
                np.array(mpi4py.MPI.COMM_WORLD.gather(gradsym_len, 0))
185         cstress_counts =
                np.array(mpi4py.MPI.COMM_WORLD.gather(cstress_len, 0))
186         assert np.array_equal(gradsym_counts, cstress_counts)
187
188         if rank == 0:
189             gradsym_norm = np.empty(M.dim(), dtype='float64')
190             cstress_norm = np.empty(M.dim(), dtype='float64')
191         else:
192             gradsym_norm = None
193             cstress_norm = None
194
195         mpi4py.MPI.COMM_WORLD.Gatherv(sendbuf=gradsym_norm_loc,
                recvbuf=(gradsym_norm, gradsym_counts), root=0)
196         mpi4py.MPI.COMM_WORLD.Gatherv(sendbuf=cstress_norm_loc,
                recvbuf=(cstress_norm, cstress_counts), root=0)
197
198         if rank == 0:
199             assert len(gradsym_norm) == M.dim()
200             assert len(cstress_norm) == M.dim()
201             np.savetxt('results/' + problem_name +
                    '/const-curve-t-' + str(t) + '.txt',
                    np.c_[cstress_norm, gradsym_norm])
202
203     ### Compute the Torque
204     torque = assemble((1.0/r2)*(2*mu*(sym(grad(u))[1, 1] -
            sym(grad(u))[0, 0])*x[0]*x[1] + 2*mu*sym(grad(u))[0,
            1]*(pow(x[0], 2.0) - pow(x[1], 2.0)))*ds(2))
205     log(30, 'Torque: ' + str(torque))
206     torque_series.append(torque)
207
208
209
```

```
210     ### Plot the Torque Series
211     plt.figure()
212     plt.plot(np.linspace(0.0, t, len(torque_series)),
            torque_series, 'k-')
213     plt.xlabel(r"$t$")
214     plt.ylabel(r'$\tau (t)$')
215     plt.savefig('figures/{}/torque.pdf'.format(problem_name))
216
217     ### Update Previous Solution
218     w_n.vector()[:] = w.vector()
219     end()
220
221 ### Save the Torque Series
222 np.savez('results/{}/torque'.format(problem_name), np.linspace(0.0,
        t, len(torque_series)), torque_series)
```

Listing D.1: FEniCS (Python) script, file `taylor-couette-2d.py`.

```
__all__ = ['ProblemParam']

from fenics import Point, Mesh, CompiledSubDomain, MeshFunction,
    Constant
from math import hypot
import argparse

class ProblemParam(object):

    def __init__(self):
        parser = argparse.ArgumentParser(
            formatter_class=argparse.ArgumentDefaultsHelpFormatter,
            description='Solves the 2D cylindrical Couette flow for
                incompressible Le-Roux--Rajagopal model.')

        parser.add_argument('--r1', metavar='float', type=float,
            default=0.3,
                            help='radius of the inner cylinder')

        parser.add_argument('--r2', metavar='float', type=float,
            default=1.0,
                            help='radius of the outer cylinder')

        parser.add_argument('--a', metavar='float', type=float,
            default=1.0,
                            help='coefficient a')

        parser.add_argument('--b', metavar='float', type=float,
            default=0.1,
                            help='coefficient b')

        parser.add_argument('--c', metavar='float', type=float,
            default=1.0e-6,
                            help='coefficient c')

        parser.add_argument('--n', metavar='float', type=float,
            default=-0.75,
                            help='coefficient n')

        parser.add_argument('--omega', metavar='float', type=float,
            default=0.2,
                            help='angular velocity')

        parser.add_argument('--dt', metavar='float', type=float,
            default=1.0e-10,
                            help='time step')

        parser.add_argument('--T', metavar='float', type=float,
            default=1.0e-7,
                            help='end time')

        parser.add_argument('--t0', metavar='float', type=float,
            default=2.0e-8,
                            help='central time of loading')

        self._args = parser.parse_args()

```

```
46          center = Point(0.0, 0.0)
47          self._mesh = Mesh('taylor-couette-2d.xml')
48
49          r = 'hypot(x[0]-c0, x[1]-c1)'
50          inner_bndry = CompiledSubDomain('on_boundary && {} < (r1 +
                r2)/2.0'.format(r), r1=self._args.r1, r2=self._args.r2,
                c0=center[0], c1=center[1])
51          outer_bndry = CompiledSubDomain('on_boundary && {} > (r1 +
                r2)/2.0'.format(r), r1=self._args.r1, r2=self._args.r2,
                c0=center[0], c1=center[1])
52          bndry_mrkrs = MeshFunction('size_t', self._mesh,
                self._mesh.topology().dim() - 1, 0)
53          inner_bndry.mark(bndry_mrkrs, 1)
54          outer_bndry.mark(bndry_mrkrs, 2)
55          self._bndry_mrkrs = bndry_mrkrs
56
57      def radii(self):
58          return self._args.r1, self._args.r2
59
60      def a(self):
61          return Constant(self._args.a)
62
63      def b(self):
64          return Constant(self._args.b)
65
66      def c(self):
67          return Constant(self._args.c)
68
69      def n(self):
70          return Constant(self._args.n)
71
72      def anglr_vlct(self):
73          return Constant(self._args.omega)
74
75      def dt(self):
76          return Constant(self._args.dt)
77
78      def T(self):
79          return self._args.T
80
81      def t0(self):
82          return self._args.t0
83
84      def mesh(self):
85          return self._mesh, self._bndry_mrkrs
```

Listing D.2: Problem parameters script (Python), file `TaylorCouetteParam.py`.

List of notations

Notation	Description
$\langle \bullet, \bullet \rangle$, $(\bullet, \bullet)$	L^2 scalar product
$\{\bullet, \bullet\}$	Poisson bracket
a, b, c, n	material parameters of the model (2.13)
$\boldsymbol{a} \cdot \boldsymbol{b}$	vector scalar product
$(\boldsymbol{a} \otimes \boldsymbol{b})_{ij} =_{\text{def}} a_i b_j$	tensor product
$\mathbb{A} : \mathbb{B} =_{\text{def}} \operatorname{Tr}(\mathbb{A}\mathbb{B}^\top)$	tensorial scalar product
$\lvert\mathbb{A}\rvert =_{\text{def}} (\mathbb{A} : \mathbb{A})^{\frac{1}{2}}$	tensorial norm
$\mathbb{A}_\delta =_{\text{def}} \mathbb{A} - \left(\frac{1}{3}\operatorname{Tr}\mathbb{A}\right)\mathbb{I}$	traceless (deviatoric) part of a tensor
$\overset{\triangledown}{\mathbb{A}} =_{\text{def}} \frac{\mathrm{d}\mathbb{A}}{\mathrm{d}t} - \mathbb{L}\mathbb{A} - \mathbb{A}\mathbb{L}^\top$	upper convected (Oldroyd) time derivative
α	streamwise wave number
$\boldsymbol{b}$	specific body force
β	spanwise wave number
$c = c_r + \mathrm{i}c_i$	complex phase speed
$\mathbb{c}$, $\mathbb{c}^*$	conformation tensor and its conjugate
C	dimensionless pressure gradient
C_F	Friedrichs' constant
$\mathbb{C}_t$	relative right Cauchy–Green tensor
$\mathbb{D} =_{\text{def}} \frac{1}{2}(\nabla \boldsymbol{v} + \nabla \boldsymbol{v}^\top)$	symmetric part of the velocity gradient
$\mathrm{d}a$	surface element
$\frac{\mathrm{d}}{\mathrm{d}t} =_{\text{def}} \frac{\partial}{\partial t} + \boldsymbol{v} \cdot \nabla$	convective derivative
Δ	Laplace operator
div	divergence operator
$\mathrm{d}l$	line element
$\mathrm{d}v$	volume element
$\{\boldsymbol{e}_{\hat{x}}, \boldsymbol{e}_{\hat{y}}, \boldsymbol{e}_{\hat{z}}\}$	Cartesian basis
E	total energy of the system; disturbance energy
e	specific internal energy
$e_{\text{tot}} =_{\text{def}} e + \frac{1}{2}\boldsymbol{v} \cdot \boldsymbol{v}$	specific total energy
η	specific entropy
$\eta^{\hat{y}}$	normal vorticity of the disturbance
f, f_{char}	positive scalar function and its characteristic value
$\mathcal{F}$	primitive function of f
$\mathfrak{f}$, $\mathfrak{g}$, $\mathfrak{h}$	tensorial functions
$\{\boldsymbol{g}_{\hat{r}}, \boldsymbol{g}_{\hat{\varphi}}, \boldsymbol{g}_{\hat{z}}\}$	cylindrical basis
$\dot{\gamma}$	shear rate
Γ	general operator
Γ_1, Γ_2	inner and outer cylinders
$I_0^2 =_{\text{def}} \int_{-1}^{1} \lvert\tilde{v}'^{\hat{y}}\rvert^2 \,\mathrm{d}y$	
$I_1^2 =_{\text{def}} \int_{-1}^{1} \left\lvert\frac{\mathrm{d}\tilde{v}'^{\hat{y}}}{\mathrm{d}y}\right\rvert^2 \mathrm{d}y$	
$I_2^2 =_{\text{def}} \int_{-1}^{1} \left\lvert\frac{\mathrm{d}^2\tilde{v}'^{\hat{y}}}{\mathrm{d}y^2}\right\rvert^2 \mathrm{d}y$	

Notation	Description
$\mathbb{I}$	identity tensor
$\mathbf{J}$	thermodynamic fluxes
$\boldsymbol{j}_q$	heat flux
$k^2 =_{\text{def}} \alpha^2 + \beta^2$	wave number
L	channel half-width (characteristic linear dimension)
$\mathbb{L} =_{\text{def}} \nabla \boldsymbol{v}$	velocity gradient
$\mathbf{L}$	Poisson bivector
λ, λ_1, λ_2	Lagrange multipliers
M	total mass of the system
M_h	finite element space for the apparent viscosity
μ	dynamic viscosity
μ_0	equilibrium chemical potential
$\boldsymbol{n}$	unit outward normal
N_1, N_2	normal stress differences
∇	gradient operator
$\omega = \alpha c$	complex frequency
$\omega(t)$	time dependent angular velocity
p	pressure (mean normal stress)
P_h	finite element space for the pressure
$\mathcal{P}_k$, $\boldsymbol{\mathcal{P}}_k$	scalar and vectorial Lagrange elements of order k
$\Psi^{(\bullet\to\bullet)}$	multiscale thermodynamic Lyapunov (MTL) function
$q =_{\text{def}} \max_{y\in[-1,1]} \left\lvert \frac{\mathrm{d}\bar{v}^{\hat{z}}}{\mathrm{d}y}(y) \right\rvert$	
$Q =_{\text{def}} \frac{\mathrm{i}}{2} \int_{-1}^{1} \frac{\mathrm{d}\bar{v}^{\hat{z}}}{\mathrm{d}y} \tilde{v}'^{\hat{y}} \frac{\mathrm{d}(\tilde{v}'^{\hat{y}})^*}{\mathrm{d}y} \mathrm{d}y$	
$\mathbb{Q}$	orthogonal tensor
$\boldsymbol{r}$	position vector
R_1, R_2	inner/outer cylinder radius
$\mathcal{R}_1 =_{\text{def}} f_{\text{char}} \rho V L$	Reynolds number analoque
$\mathcal{R}_2 =_{\text{def}} \frac{bV^2}{a^2L^2}$, $\mathcal{R}_3 =_{\text{def}} \frac{c}{a}$	dimensionless quantities of the model (4.19)
Re	Reynolds number
ρ	density
(r, φ, z)	cylindrical coordinates
s	entropy density
S	total entropy of the system
σ	shear stress
t	time
Δt	time step
$\mathbb{T}$	Cauchy stress tensor
$\boldsymbol{\tau}$	torque at the outer cylinder
$T_{\text{char}} =_{\text{def}} \frac{V}{f_{\text{char}} L}$	characteristic stress
$\mathbb{T}_\delta =_{\text{def}} \mathbb{T} - \left(\frac{1}{3}\operatorname{Tr}\mathbb{T}\right)\mathbb{I}$, $\mathbb{T}_\delta^*$	deviatoric part of the Cauchy stress tensor and its conjugate
$\mathcal{T}_h$	regular triangulation of Ω

Notation	Description
T, $\theta =_{\text{def}} \frac{\mathrm{d}e}{\mathrm{d}\eta}$	thermodynamic temperature
T_0	equilibrium temperature
Tr	trace operator
$(\bullet)^\top$	transpose operator
$\boldsymbol{u}$, $\boldsymbol{u}^*$	momentum density and its conjugate
$\boldsymbol{v}$	velocity
$v^{\hat{x}}$, $v^{\hat{y}}$, $v^{\hat{z}}$	Cartesian velocity components
$\left(\bar{\boldsymbol{v}}, \bar{\mathbb{T}}_\delta\right)$	base flow
$\left(\boldsymbol{v}', \mathbb{T}'_\delta\right)$	flow disturbance
V	characteristic velocity
$\boldsymbol{V}_h$	finite element space for the velocity
$\boldsymbol{x}$, $\boldsymbol{x}^*$	state variables and their conjugates
$\mathbf{X}$	thermodynamic forces
ξ	entropy production per unit volume
Ξ, Ξ^*	dissipation potential and its conjugate
(x, y, z)	Cartesian coordinates